UNIVERSITÉ DE LORRAINE

Ecole doctorale C2MP

THÈSE

Pour l'obtention du titre de :

DOCTEUR de L'UNIVERSITÉ DE LORRAINE

Spécialité : Sciences des Matériaux

Présentée par :

Wassim JRAD

Dynamic behavior of thin-walled beams: Analytical, numerical and experimental approaches

---

Présentée et soutenue publiquement le 05 Décembre 2019 à l'UFR MIN Metz devant le jury composé de :

M. Eric JACQUELIN, Professeur, Université Claude Bernard, Lyon1, France	Rapporteur
M. Mustapha TAAZOUNT, Professeur, Université de Blaise Pascal, France	Rapporteur
Mme Laetitia DUIGOU, MCF, Université de Bretagne Sud, France	Examinateur
M. Salim BELOUETTAR, Professeur, LIST, Luxembourg	Examinateur
M. Erasmo CARRERA, Professeur, Université de Politecnico di Torino, Italie	Examinateur
M. Guillaume ROBIN, IGR., Université de Lorraine, France	Examinateur
M. Foudil MOHRI, MCF-HDR, Université de Lorraine, France	Directeur
M. El Mostafa DAYA, Professeur, Université de Lorraine, France	Co-Directeur
M. Jihad AL-HAJJAR, Professeur, Université Libanaise, Liban	Co-Directeur

---

**Laboratoire d'Etude des Microstructures et de Mécanique des Matériaux (LEM3), CNRS UMR 7239. Université de Lorraine 7 rue Félix Savart, 57073 METZ (France)*

Université de Lorraine – Pôle M4 : matière, matériaux, métallurgie, mécanique

Abstract

Thin-walled beams with open section constitute main elements in engineering applications fields as in civil engineering, automotive and aerospace construction. They are widely adopted for their lightness and realization simplicity. Due to their particular section shapes, these elements are very sensitive to torsion and instabilities, present in both statics and dynamics. In statics, overall stability as buckling, and flexural-torsional buckling are common and often important in design criteria. In dynamics, the torsional and flexural-torsional modes of vibration are often lower frequencies compared to the classical plane pure bending modes. Thus, planar failures of such structures are known to be an exception rather than a rule. In torsion, warping is important and governs the behavior (non-uniform torsion). The static behavior of thin-walled beams in non-uniform torsion is well known (Vlasov's model), but the dynamic behavior remains open for investigations and especially in the presence of arbitrary open-section beams.

In this thesis work, we are interested with the dynamic behavior of thin-walled beams with arbitrary open cross sections. Based on the Vlasov's model, the 3D motion equations are derived from the Hamilton's principle. Original analytical solutions for different boundary conditions are derived for higher free vibration modes in 3D context. In these solutions, the effects of the inertial rotation terms in bending and torsion are taken into account. These solutions are limited to simple cases. For general cases, a 3D beam finite element model is described and implemented. Compared to conventional 3D beams, warping is considered as an additional **D**egree **O**f **F**reedom (**DOF**). As a result, 3D beams with 7 DOF are adopted in the mesh process. The mass and stiffness matrices are obtained by numerical integration (Gauss method). In the model, free and forced vibration analyses are possible. In forced vibration, the response is derived in the frequency field. The Rayleigh damping model is adopted. The model is validated by comparison with benchmark solutions found in the literature and other numerical results obtained by new simulations and recent experimental tests. Additional numerical simulations are performed using some available commercial codes.

In order to validate the theoretical and numerical models, laboratory test campaign is undertaken at the Laboratoire d'Etude des Microstructures et de Mécanique des Matériaux (LEM3, Metz). Tests were carried out on thin-walled beams with different boundary conditions at the beam ends and intermediate supports (braces). Tests with shaker and a hammer are performed. In the analysis, the response spectra and vibration modes are searched in the range (1-400 Hz). The dynamic response curves of the beams are measured using accelerometers. In the presence of arbitrary sections, flexural-torsional vibration modes are observed. The analytical, the numerical and the experimental solutions are compared and validated. Moreover, the numerical and experimental

dynamic response spectra are compared. A good agreement between the various solutions is remarked.

The model is extended to 3D beams in presence of lateral supports (braces) as in bridge structures. 3D elastic and viscous springs are added in the finite element model. The beam behavior in presence of elastic and rigid springs becomes possible in statics and dynamic. The effect of the springs is studied in order to improve the behavior of thin-walled beams against undesirable lateral bending and torsion modes.

Keywords: Thin-walled beam, Arbitrary cross-section, Torsion, Warping, Coupled modes, Free vibration, Forced vibration, Finite element method, Bracing, Dynamic, 3D Open section beam, Experimental test, Elastic spring, Dashpot, vibration control.

Résumé

Les poutres à parois minces à sections ouvertes sont les éléments de base des ouvrages courants en génie civil, de l'automobile et de l'aéronautique. Elles sont abondamment adoptées pour leur légèreté et la simplicité de mise en service. En raison de leurs formes particulières, ces sections sont très sensibles à la torsion et aux instabilités, qui peuvent être présentes en statique et dynamique. En statique, le flambage, le déversement et le voilement sont courants et souvent déterminant dans le dimensionnement. En dynamique, les modes de vibration en torsion et flexion-torsion sont plus dominants par rapport au modes de flexion couramment utilisés dans l'hypothèse d'un comportement plan. Ainsi, les défaillances planaires de telles structures sont connues pour être une exception plutôt qu'une règle. En torsion, le gauchissement est important (torsion non uniforme). Le comportement statique des poutres à parois minces en torsion non uniforme (modèle de Vlasov) est maîtrisé, mais le comportement dynamique et vibratoire reste ouvert et surtout en présence des poutres à sections ouvertes arbitraires.

Dans ce travail de thèse, on s'intéresse au comportement dynamique de poutres à parois minces et à section ouvertes arbitraires. En se basant sur le modèle de Vlasov, les équations de mouvement 3D sont dérivées à partir du principe d'Hamilton. Des solutions analytiques originales pour différentes conditions aux limites sont dérivées pour des modes supérieurs en vibration libre dans le contexte 3D. Dans ces solutions, les effets des termes de rotation inertiels en flexion et torsion sont pris en compte. Ces solutions sont limitées à des cas simples. Pour des cas généraux, un modèle élément fini de poutre 3D est décrit et implémenté. Par rapport aux poutres 3D classiques, le gauchissement est considéré comme degré de liberté (ddl) supplémentaire. De ce fait des poutres 3D à 7 ddl sont adoptées dans le processus de maillage. Toutes les matrices de rigidité masse de base sont calculées par intégration numérique (intégration de Gauss). Dans le modèle, les calculs en vibrations libres et forcées sont possibles. En vibration forcée, la réponse est donnée dans le domaine fréquentiel. L'amortissement type de Rayleigh est adopté. Le modèle est validé par comparaison aux solutions de référence trouvées dans la littérature et à d'autres résultats numériques obtenu par des nouvelles simulations et des tests expérimentaux récents. Des simulations supplémentaires par éléments finis sont effectuées à l'aide de codes commerciaux.

Afin de valider le modèle théorique et numérique utilisé, une campagne d'essais a été suivie au LEM3. Des essais ont été réalisés sur des poutres à parois minces avec différentes conditions aux limites aux bords et intermédiaires (entretoises). Des essais avec pot vibrant et marteau de choc sont effectués. Dans l'analyse, les spectres de réponse et les modes de vibration sont recherchés dans le domaine 1-400 Hz. Les courbes de réponse dynamique des poutres sont mesurées à l'aide des accéléromètres. En présence des sections arbitraires, des modes de vibration couplés en torsion et flexion sont

observés. Les solutions analytiques, numériques et les mesures expérimentales sont comparées et validées. De mêmes les courbes de réponse en vibration forcée numériques sont comparées aux courbes expérimentales. Un bon accord entre les différentes solutions est constaté.

Le modèle est étendu aux poutres 3D retenues latéralement par des entretoises comme dans les ponts. Des ressorts élastiques et visqueux 3D sont ajoutés dans le modèle numérique. Cela permet de modéliser le comportement statique et dynamique des poutres avec entretoises souples ou rigides. L'effet des entretoises est étudié dans le but d'améliorer le comportement des poutres à parois minces vis-à-vis des modes indésirables de type flexion latérale et torsion.

Mots-clés : Poutre à parois minces, Section ouverte, Torsion, Gauchissement, vibration libre, vibration forcée, éléments finis, modes couplés, entretoises, amortissement.

Acknowledgment

It is hard to come up with a list of every person who had supported me to finish this work. Nevertheless, some are merited to be recognized for all of their efforts and assistance.

I would like to begin by thanking my PhD supervisor Mr. Foudil Mohri, for having welcomed me and for having trusted me and giving me this thesis subject. During thesis period, he made me discover the exciting field of vibration behavior and control of thin-walled beams. I would like to express my deep gratitude to him for his availability, his scientific rigor and the friendly working atmosphere that prevailed during thesis work progress.

I would like to express my thankfulness to my co-supervisor Pr. El Mostafa Daya for his follow up, motivation, patience, and immense knowledge. His expert advices and guidance have been invaluable throughout all the phases of the work.

My sincere thanks also goes to my second co-supervisor Pr. Jihad Al-Hajjar for his supervision especially when in Lebanon. I am gratefully indebted to his valuable help. Also, I take pride in acknowledging the insightful guidance of Mr. Guillaume Robin. The door to his office was always open for any help needed. Without his expertise and input, the work and the experiments could not have been successfully conducted.

The PHD defense has been possible after a positive opinion of Mr. Eric Jacquelin (Professor, Claude Bernard, Lyon1 University, France) and Mr. Mustapha Taazount (Professor, Blaise Pascal University, France). They are acknowledged for their comments. They read carefully the manuscript and suggested important remarks. Their comments helped to improve the quality of the manuscript.

I can’t forget Pr. Erasmo Carrera (Politecnico di Torino University, Italy) who accepted to be jury member and chairman of the commission defense. My thanks also go to Pr. Salim Beloauttar (Professor, Luxembourg Institute of Science and Technology, Luxembourg) and Mrs. Laetitia Duigou (MCF, Bretagne Sud University, France).

I also extend my sincere thanks to the jury members for having accepted to review my thesis, and for evaluating the presented work. Allow me to express them here deep gratitude.

Nobody has been more important to me in the pursuit of this work than the members of my family. I must express my deep gratitude to my mom, brother, sisters and my fiancé, for supporting me spiritually and for providing me continuous encouragement throughout my studies. This accomplishment would not have been possible without them.

Finally, my warm thanks to all my friends and colleagues for their moral support and help.

Table of Contents

Figures list

Tables list

Nomenclature and abbreviations

A: cross section area

E: Young's modulus

f: eigenfrequency

G: shear modulus

I_0: polar moment of inertia about shear center

I_y, I_z: strong and weak bending inertia

I_ω: warping constant

I_t: Saint-Venant torsion constant

L: beam slenderness

N: axial stress force

M_y, M_z: bending moments about the strong and weak axes

B_ω: warping stress force 'bimoment'

M_{sv}: De Saint-Venant torsion moment (called st-Venant)

q_x, q_y, q_z: distributed loads in the x, y, z directions

m_x: distributed torsion moment

U: beam total strain energy

U_b: strain energy of the classical beam

U_s: strain energy of the additional elastic 3D springs

T: kinetic energy

Γ: total damping of the beam

Γ_b: classical viscous damping of the beam

Γ_d: damping of dashpots

W: applied load work

u: axial displacement.

v, w: lateral and vertical displacement components

u_M, v_M, w_M: displacement components of point M on the cross section contour

y_C, z_C: shear center co-ordinates in the Gyz reference

α, β: Rayleigh's mass and stiffness damping coefficients

ε_{xx}, ε_{xy}, ε_{xz}: axial and shear strain components

ω: Vlassov's warping co-ordinate (sectorial coordinate)

Ω: angular velocities (eigenvalue)

ϖ: excitation frequency

θ_x: twist angle

σ_{xx}, σ_{xy} , σ_{xz}: axial and shear stress components

k_u, k_v, k_w, $k_{\theta x}$: springs stiffness components

c_u, c_v, c_w, c_{θ_x}: dashpot damping components

C_u, C_v, C_w, C_{θ_x}: beam damping components

$k_{\max}$: required stiffness to provide full support

Vectors and Matrices

$\{f\}$: distributed force vector

$\{F\}$: finite element force vector

$\{d\}$: finite element displacement vector

$\{q\}$: displacement vector in continuous media

$\{\gamma\}$: strain vector

$\{\Sigma\}$: stress vector

$\{\varphi\}$: gradient vector

$\{\phi\}$: free vibration eigenvector

[C]: total damping matrix

$[C_b]$: beam damping matrix

$[C_d]$: dashpots damping matrix

$[D]$: behavior matrix

$[G]$: gradient matrix

$[N]$: shape function matrix

$[K]$: total stiffness matrix

$[K_b]$ beam stiffness matrix

$[K_s]$ springs stiffness matrix

$[M_1]$, $[M_2]$, $[M]$: basic and global mass matrices

$[\Phi]$: mode shape matrix

General introduction

The construction sector uses thousands millions tons of material each year, this excessive use of materials has an adverse impact on the environment, due to the extraction of raw materials that cause emissions of high quantities of CO2. Legislators work to create rigorous regulations surrounding construction, to enforce standards for limiting the environmental impacts of construction projects. In consequence, designers are stepping to find new sustainable methods by reducing costs and as well as the environmental impact of construction projects. To this aim, research for better methods, impose to find new solutions in construction projects that consist intelligent uses and material savings by weight reduction. Slender thin-walled elements are a good compromise. All current materials from steel, concrete wood and glass are concerned by this opportunity. Optimization of section shapes in presence of bending loads leads to cross sections with web and two flanges.

Most of the thin-walled beams have a good bending resistance with respect to the first principal axis, but a low bending resistance with respect to the second principal axis and also a low resistance in torsion. This is why an element bent with respect to its strong axis exhibits an instability leading to a sudden flexural-torsional behavior (lateral buckling stability). So, the planar failures of such structures are known to be an exception rather than a rule (Figure 1).

Figure 1: Out of plan failures of structures composed by thin-walled beams elements.

The behavior of open thin-walled cross section beams is predominated by torsion. For such beams, the torsion behavior exhibits warping. The classical Saint-Venant model is no longer valid. Other models accounting for warping are more efficient (Vlasov's model). Under static loads, torsion occurs in presence of instabilities under axial forces (buckling instability) and bending forces (lateral buckling stability). In vibration and dynamic loads, torsion modes are frequent.

Motivations and objectives of the research work

After assessing the instability phenomena, the main focus of the work is on vibration and dynamic behavior in both theory, finite element approach and experimental tests on the vibration behavior. In order to improve the structure strength against vibration effects and to save materials by getting optimum sections, one possible solution is the increase of stiffness by adding discrete or distributed elastic springs (elastic supports). The elastic spring contribute in the elastic stiffness matrix of the structure. By increasing the stiffness constant of the elastic support, the vibration behavior (frequencies and modes) vary accordingly.

It is important to remind that in civil engineering recourse to this solution is frequent. This is the case in braced beams and columns in buildings or lateral bracing in bridges (Figure 2). These solutions are adopted in practice, but only empirical procedure is known. It is known that without these secondary elements the full strength of the building is not guaranteed and risk of failure due to out of plane deformations is present. Other solution is using discrete viscous dampers (dashpots) in parallel with elastic springs to control displacements of structure when it is subjected to dynamic forces, in this case modes, frequencies and structure displacements are controlled.
The important points to be studied are the number, distribution, and required stiffness and damping factor to reach the optimal design.

Figure 2: Structures composed by thin-walled elements with intermediate lateral braces.

For vibration control, the engineer is asked for improved solutions for vibration behavior. The lower eigenfrequencies can be removed by adequate elastic supports. The followings solutions can be adopted if we are interested by a particular mode. when the spring stiffness is sufficient, one can remove the first mode and goes directly to mode 2 where the eigenfrequency is 4 times higher than the first. In presence of 3 elastic supports, we obtain directly to the third mode with an eigenfrequency 9 times higher than the first.
This procedure can be followed in the case of thin-walled in presence in 3D vibration modes when bending and torsion modes are present and can be strengthened by adequate

elastic supports. Moreover, under forced vibrations, viscous springs can be adopted in order to reduce displacements structures near the resonance.
The work is followed by analytical and numerical simulations using a home-made code and commercial codes: Abaqus, Adina…. etc. Finally, test setup is also adopted in this study to validate theoretical and numerical solutions.

Thesis organization

The work carried out during this thesis is presented in this report and is entitled in five chapters:
In chapter 1, literature review to understand the mechanical behavior of thin walled beams. First, the 3D flexural-torsional behavior of thin-walled open sections beams is discussed. It is shown that torsion exhibit with warping effect, so Saint-Venant theorem is not adequate to solve torsion problem in case of thin-walled section. Thus, the requirement of non-uniform torsion theory for this type of beams. Otherwise, the former works for thin-walled beams dynamics are reviewed. References that treat the linear free and forced vibrations are well studied and summarized in this chapter. Also, damping types are stated and used in forced vibration model. On the other hand, Fourier Transformation method is detailed and used later on to convert signals from time to frequency domain. Adding to this, literature review on vibration control and modeling linear vibrations of thin-walled beams are presented in this chapter. All the studied points mentioned below, help us to perform a good assessment of subject positioning. Then, by analyzing this bibliographic review, we can define well the problematic, the framework and the means to use in the present study. Finally, the objectives of research topic are clearly illustrated at the end of this chapter.
In chapter 2, Analytical method for vibrations of thin-walled beams is investigated. Based on present beam model and on the Galerkin's approach, dynamic equations of motion are formulated. Using Hamilton’s principle, dynamic equations of motions are derived. In the first step, a model for free and forced vibrations is introduced. The kinematic of the model is detailed, then the variational formulation of motion equations are developed. After that, in free vibration context original analytical solutions for higher modes are derived. These solutions for arbitrary sections and different boundary conditions. In Forced vibration framework, solutions in frequency domain (steady state modal) are adopted. In the model, passive damping is taken into account, (Rayleigh type was chosen). Finally, some benchmark numerical examples are considered for model validation, then the conclusion is drawn.

In chapter 3, A finite element method for vibrations of thin-walled beams based on the model showed in chapter 2 is detailed. First, an introduction of finite element method is presented, then finite element formulation of thin-walled structures is demonstrated. Then, finite element discretization is illustrated. After that, element matrices are derived followed by the assembly procedure to obtain the global matrices for whole structure. Hereafter, generic solutions of thin-walled structures are detailed. In free vibrations eigenvalues and eigenvectors are investigated. Otherwise, in forced vibration, steady state modal analysis method was adopted to obtain dynamic response spectrum in frequency domain. In this method, damping is taken in account, by (Rayleigh type). Also, the FEM

can be used to study base motion effect, (earthquakes), vibration excitation with random signal (harmonic). Finally, numerical applications from literature and commercial codes are used for model validation process, then the conclusion.

In chapter 4, experimental tests on free and forced vibrations are performed to validate the developed theoretical-numerical method. Firstly, in the introduction, some references in experimental studies are reviewed. Secondly, Experimental setup and procedures are detailed. Thirdly, specimen's properties are given. Thereafter, tests results are presented in details and discussed. These results are natural frequencies, mode type, dynamic response spectrums, loss factors and damping values for each mode. After collection tests data, it is used to validate the numerical model in free and forced vibration context. Otherwise, some tests are performed after introducing of intermediate bracings to the specimens. Subsequently, the presented theoretical-numerical methods are validated by comparing results of the 3D vibration of arbitrary thin-walled open sections beams with benchmark, commercial codes and experimental results, then the conclusion.

In chapter 5, the effect of intermediate braces in vibration control is studied. First, in the introduction different type of braces are showed and summary of existing works is delivered. Furthermore, braces types elastic, viscous are introduced in the model. Kinematic of the model with intermediate braces is then offered. After that, motion equations are derived in presence of braces. Analytically, some particular solutions in case of doubly symmetric sections with lateral and torsional elastic springs are possible. Finite element formulation for thin-walled beams with intermediate braces in free and forced vibrations with intermediate viscoelastic braces are detailed and used to study vibration control of thin-walled beams. Numerical applications of beams with intermediate elastic springs in free vibration, and viscoelastic springs in forced vibration context are well studied. Finally, a new concept is concluded in vibration control can be used to optimize sections.

Finally, general remarks are settled and conclusions are displayed and some perspectives are suggested for possible future research based on the study results.

Chapter 1 Thin-walled beams, State of art. Motivation and Interest

1.1 Introduction

Thin-walled beams with open sections constitute basic parts of many complex structures in civil constructions, automotive and aeronautic fields. They are extensively used in engineering applications when requirements of weight saving are of primary importance. Due to their particular shapes, these structures are highly sensitive to torsion and instabilities, under both static and dynamic loads. Then, buckling study in statics and free vibration in dynamics are the most important phenomena that must be considered in the first steps of the design procedure.

In the analysis of thin-walled beams, the classical planar behavior Heyliger [1] is not sufficient to prevent the sudden unexpected flexural-torsional instabilities frequently present in these structures. In presence of the torsion some models are formulated according to Saint-Venant theory in both statics and dynamics [2,3]. In Gere and Lin [4], Rayleigh-Ritz method has been used to study the coupled bending-torsional free vibration of uniform beams with various boundary conditions. Moreover, in the case of thin-walled structures with open cross sections, the torsion is predominated by warping and flexural-torsional coupling especially in the case of arbitrary cross sections. To our knowledge, Vlasov's model is one the first models that include the warping phenomena in the behavior of thin-walled beams, in the 1930's [5]. Later on, Timoshenko et al. [6] presented a model for vibration of thin walled beams using Euler-Bernoulli theory and including flexural-torsional coupling effect. Furthermore, Bishop [7] extended the Bernoulli-Euler theory of beam flexure combined with the Saint-Venant theory with warping to investigate the free vibration of beams in torsion. Then, Bishop demonstrated that the errors which can be made in computing the natural frequencies of beams of open section under the assumption of uniform torsion can be very large to models with warping included. Some other reference works in this field can be found in [8-11]. In Banerjee [12], the dynamic behavior of beams in the context of bending torsion coupling was investigated. The classical Euler-Bernoulli and Saint-Venant theories were adopted and the dynamic stiffness matrix is implemented in the study. Banerjee [13] extended the previous model and derived an exact explicit formulation for the natural frequencies and mode shapes of cantilever beams in presence of flexural-torsional couplings (warping ignored).

It is well known that the analytical solutions are limited to some simple cases according to classical boundary conditions. Nowadays, the recourse to numerical models is important, since it permits to generalize the study to more general cases where the analytical solutions become cumbersome. Many models have been developed for the vibration analysis of thin-walled elements. The first attempts at applying the Finite Element Method (FEM) to coupled vibrations of thin-walled beams have been investigated in [14,15]. Friberg [16] derived the stiffness and mass matrices of open thin-walled beam in presence of initial axial stress forces. In solution of the eigenvalue

problem, Wittrick-Williams algorithm was adopted in solution. Ohga *et al.* [17] investigated the free vibration of thin-walled members with open and closed sections by the transfer matrix method. Lee [18,19] presented an analytical approach of linear vibrations of composite I and channel open sections. Pestel and Leckie [20] presented a method for the determination of natural frequencies of continuous beams and shafts, and illustrated the dynamic response under harmonic excitation. The steady state vibration with damping effect was studied by Ebner and Billington [21]. Using the finite element method, Chen and Hsiao [22] analysed the coupled vibration of thin walled beams with a generic open section induced by the boundary conditions. Fernanda de Borbon et al. [23] developed a finite element method based on Vlasov's theory to investigate free vibration of thin walled beams with arbitrary cross sections under axial loads. The presented method includes shear deformations and rotary inertia. Numerical examples from literature without/with axial loads were used in the validation. The free vibration of beams with arbitrary cross sections have been studied in [24,25]. Later on, Chen [26] and Cortinez *et al.* [27] applied the differential quadrature method to Vlasov's model for the vibration of thin-walled elements. A modified Vlasov's model was used by Ambrosini *et al.* [28], for linear dynamic analysis. The nonlinear dynamic behavior of doubly-symmetric I section in torsion has been investigated by Rozmarynowski and Szymczak [29] using FEM. More recently, a model for nonlinear dynamics has been formulated by Egidio *et al.* [30]. The multiple scale method has been applied for the steady-state motions and stability of beams with mono-symmetric sections.

In the literature, many extensive works investigated the free vibration of thin-walled beams. Yaman [31] solved the triply coupled vibrations of beams by a wave propagation approach. Gendy and Saleeb [32] developed a finite element method for the free vibration behavior analysis. Based on energy method, Prokić [33] derived the differential motion equations of the flexural-torsional thin-walled beams with arbitrary cross and studied the triply free coupled vibrations. Prokić [34] derived the system of equations for fivefold coupled vibrations of Timoshenko model for thin-walled beams with arbitrary open cross sections using the principal of virtual displacements. He also studied the effect of shear deformation over the natural frequencies. In his model the effect of rotary inertia and warping are included. A semi-analytical method is investigated for simply supported beams. A substantial research work is presented by Carrera [35, 36] on buckling and postbuckling of multilayered structures, in non-linear analysis and stability behavior. Moreover, the development of efficient and reliable FE formulations 'Carrera Unified Formulation (CUF)' for thin-walled beams, layered structures and smart structures. More recently, Carrera applied the (CUF) the behavior of beams under static and dynamic loads [37, 38]. By the help of this method, the classical Euler–Bernoulli and Timoshenko beam theories are viewed as particular cases of these variable kinematic models. According to higher order expansion, it permits the detection of in-plane cross-section deformation obtained by shell-like elements. Applications of the method in civil engineering applications were studied. Free vibration modes of thin-walled beams in presence of overall, local and distortional modes can be investigated. Other applications to frames, 3D trusses and industrial buildings are made possible by the help of CUF method. In [39], the method has been applied successfully in post-buckling of beams and struts in presence of large displacements and rotations. Changes in mode buckling along the equilibrium curves are demonstrated. Other applications of the method in mechanical engineering

were investigated in [40]. Mohri *et al.* [41] investigated the vibration behavior of pre-buckled and post-buckled thin-walled beams with open sections according to a non-linear model which accounts for flexural-torsional coupling and warping effects and interaction of buckling and vibration behavior. Most of the previous works treated the vibration problem from an analytical or a numerical point of view. The effect of rotational terms in bending and torsion are always omitted. Arpaci demonstrated in [42] that rotational terms cannot be neglected. When they are accounted for semi analytical procedures or simulations on commercial codes are followed [25, 28, 42, 43]. Forced vibrations under periodic or random loads are available in [11, 44]. Eslimy and Banerjee [45] investigated the free and forced dynamic behavior of beams in flexural-torsional coupling. Deterministic and random loads were considered and the normal mode method was adopted in solution strategy. Hashemi and Richard [46] studied the free vibration behavior of beams according to the classical Euler-Bernoulli and Saint-Venant theories. The dynamic finite element method was used in solution of the free vibration problem of thin walled beams with arbitrary cross sections. Jun et al. [47, 48] adopted the Vlasov's model and derived the dynamic transfer matrix in free vibration analysis of beams with singly symmetric cross sections. In the study, the effect of initial axial stress forces on the natural frequencies was considered. Comparisons to Friberg [16] solutions were undertaken in the validation. Gokdag and Kopmaz [49] studied the coupled flexural-torsional free and forced vibrations of a beam with singly symmetric open cross section. In the model, the mass and stiffness properties are included in the dynamic stiffness matrix derived from the principle of virtual work. Using Benscoter's theory, Prokic and Lukic [50] derived the differential motion equations of thin-walled beams with closed sections and investigated the free vibration behavior of simply supported beams. Burlon et al. [51] proposed an exact approach for the free vibration analysis of beams with mono-symmetric cross section including the flexural-torsional and the presence of arbitrary number of in-span elastic supports and additional masses. More recently, the model has been extended the viscoelastic dampers in Burlon et al. [52]. Thin-walled composite beams vibration behavior were extensively studied in Librescu and Song [53].

Analytical theories and numerical studies on vibration behavior of thin walled beams with open sections are frequently studied in literature. However, the number of experimental tests presented in previous work are still rare, especially experimental tests that studied unsymmetrical cross sections. For these cross sections, the investigation of vibration dominant modes is difficult due to the effect of three coupled flexural-torsional modes.

Experimentally some of the works that treated vibration behavior of thin-walled beams are presented in what follows. Klausbruckner [54] investigated the behavior of beams with channel sections using analytical Timoshenko approach, FEM and the experimental data from Electro-Optic Holography and Heterodyne Hologram Interferometry, he proved that Timoshenko theory unrealistic for increasing flange width and higher modes. Ambrosini [55], Demonstrated the equations of motion for non-symmetrical open thin-walled cross-section beams within state variables approach in the frequency domain taking into account for the shear flexibility and rotatory inertias. Moreover, Ambrosini presented a set of experimental free vibration tests to prove the theoretical results accuracy. Ambrosini [56], presented an experimental free vibration study of doubly unsymmetrical open sections thin walled beams. Test results verified the exactitude of developed theoretical-numerical model. Ribeiro [57], using experimental test explored

the non-linear vibration of a hinged–hinged beam excited by sinusoidal forces. First and higher modes was analyzed to detect the modes involved in the motions, and proved the existence of internal resonance between modes.
Recently, Piana et al. [58] based on experimental test, extracted the natural frequencies of aluminum slightly non-symmetric crucify section thin-walled beam. Doubly clamped ends boundary condition was adopted using a universal machine with suitable end constraints for warping displacement. The beam was excited by a non-instrumental hammer impulse. To extract the natural frequencies, they used PZT detectors, and laser sensors. The experimental results were compared with numerical results and an in-house code taking in consideration the effects of non-symmetric cross-sections and warping. Another comparison of the experimental tests with the numerical natural frequencies and buckling loads of aluminum non-symmetric thin-walled beams under axial forces has been performed. Jingwei Zhou et al. [59] analyzed coupled bending torsional vibrations of uniform and non-uniform thin walled beams numerically using transfer differential transform method. Then, numerical results were validated in free vibration context experimentally using the hammer test procedure. The natural frequencies were investigated for cantilevers beams with uniform and non-uniform channels section. Furthermore, forced vibration study was performed numerically by mode expansion method. The frequency response curves were compared to experimental test ones to prove method accuracy.

In the present contribution, a model is developed for the dynamic behavior of thin-walled beams with arbitrary cross sections. In the study, the effects of warping and rotational terms are included. The finite element approach of the model (B3Dw) is described and implemented for free and forced vibration analyses in Matlab Toolbox. Additionally, analytical solutions for the higher free vibration modes of thin-walled beams with arbitrary cross sections are investigated in the same context. These solutions seem to be original and important in design. The present model is validated according to benchmark solutions available in literature and to finite element simulations on a commercial code. The accuracy of the present model is then outlined. Beams with arbitrary cross sections and any boundary conditions from rigid to elastic supports are possible. The present model is for straight beams. In presence of curved and 3D frame structures, 3D rotation matrice must be adopted in the matrix assembly. In the stage, a particular attention should be done to warping and bimoment transmission, since these components are not vectorial quantities. Warping transmission in 3D frames depend on the joint geometry the cross section shape and the presence of stiffeners. There are many papers that deal with this problem Bazant [60], Yang and McGuire [61], Morrell et al [62], Basaglia and al [63]. Moreover, the present model is extended to solve thin-walled beams with intermediate elastic and viscoelastic supports. Original analytical solutions were developed for simply supported beams with doubly symmetric cross-sections with intermediate lateral elastic braces. For other cases of sections and boundary conditions the analytical solutions become cumbersome and the finite element approach is more powerful. For this reason, the present FE beam element is also extended to take in consideration of the additional elastic and viscoelastic braces. After that, this FEM is used to study many cases of beams with intermediate elastic and viscoelastic braces in free and forced vibration context respectively.

Otherwise, experimental tests study about free and forced vibration of thin walled arbitrary cross sections used to provide experimental data that can be used for checking the accuracy of the finite element method for free and forced vibration (B3Dw). The procedure of the experimental tests are detailed, specimens with different unsymmetrical cross sections, materials and dimensions was tested. To obtain natural frequencies and dynamic response spectrum in frequency domain, two type of tests are performed respectively, Hammer test and shaker machine test. Experimental data are then compared among (B3Dw) results and commercial code Abaqus [64] to verify the reliability and to prove the accuracy of values obtained by code. In what follows, thin-walled beams with open section as described in terms of fabrication, uses and behavior. In the mechanical behavior a particular attention is devoted to torsion. The warping phenomenon is then defined and described.

1.2 Thin-walled beams elements

Thin-walled sections beams are used extensively in civil engineering constructions, mechanical, aeronautical engineering in many types structures. His importance is due to the following features: Lightweight, fabrication techniques, possibilities of standardization and agreement with the requirements of industrial buildings. According to manufacturing process [65], these elements types are divided to three categories:

- Rolled sections
- Formed sections
- Welded built-up sections

Rolled sections

Rolling is a process in which metal stock is passed through one or more pairs of rolls to reduce the thickness and to make the thickness uniform (Figure 1.1). The concept is similar to the rolling of dough. Rolling is classified according to the temperature of the metal rolled. If the temperature of the metal is above its recrystallization temperature, then the process is known as hot rolling. If the temperature of the metal is below its recrystallization temperature, the process is known as cold rolling. Roll stands holding pairs of rolls are grouped together into rolling mills that can quickly process metal, typically steel, into products such as structural steel profiles (I-beams, angle, channel, H-beams and so on) see Figure 1.2.

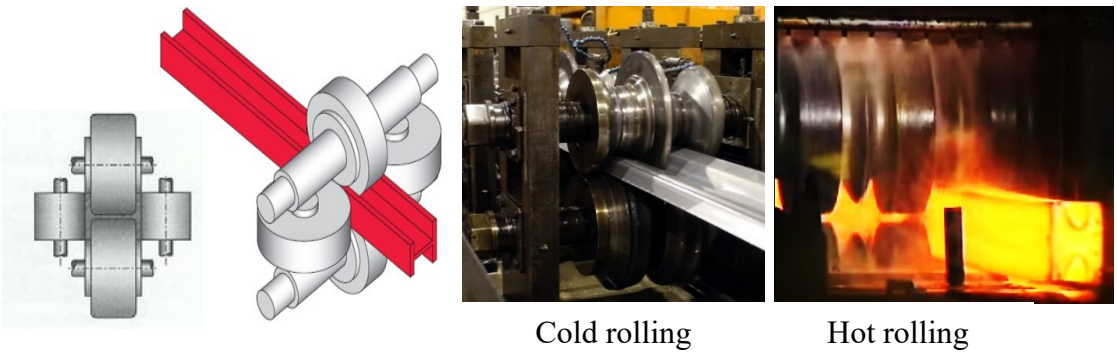

Cold rolling Hot rolling

Figure 1.1: Rolling beams processes.
(https://www.steelconstruction.info and https://www.cmrp.com)

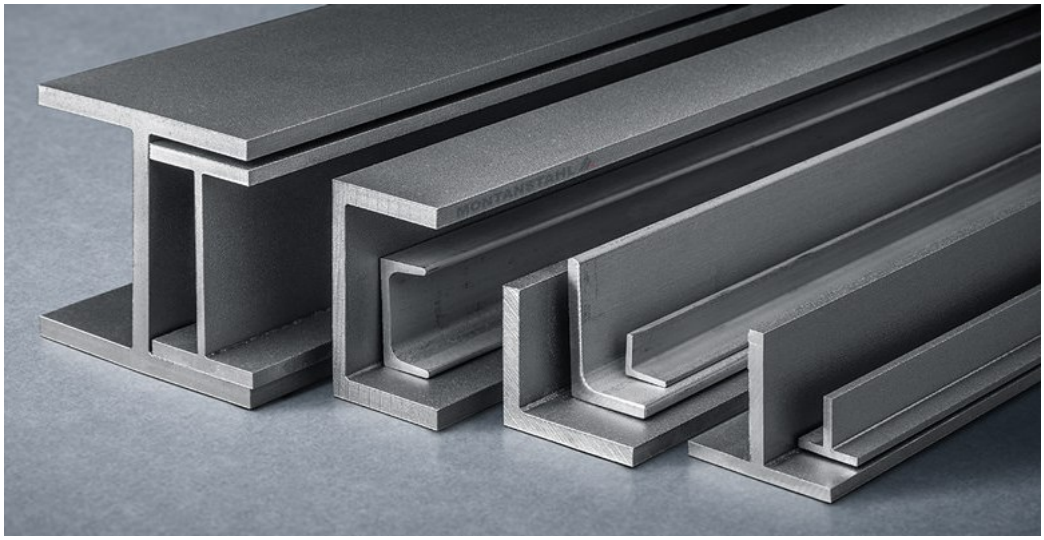

Figure 1.2: Type of sections obtained by hot rolling process.
(http://www.colonybuildings.com)

Cold Formed sections

The thin-walled open section profiles are formed using different techniques and procedures, see Figure 1.3. The metal forming can be under different temperatures: cold, warm and hot.

Metal forming: Large set of manufacturing processes in which the material is deformed plastically to take the shape of the die geometry. The tools used for such deformation are called die, punch etc. depending on the type of process, see Figures 1.4-1.5.

In this manufacturing process the plastic deformation (when the stresses exceed the yield strength of the workpiece material so a permanent shape changes occurs) is used to change the shape of the workpiece. Categories: Bulk metal forming, Sheet metal forming.

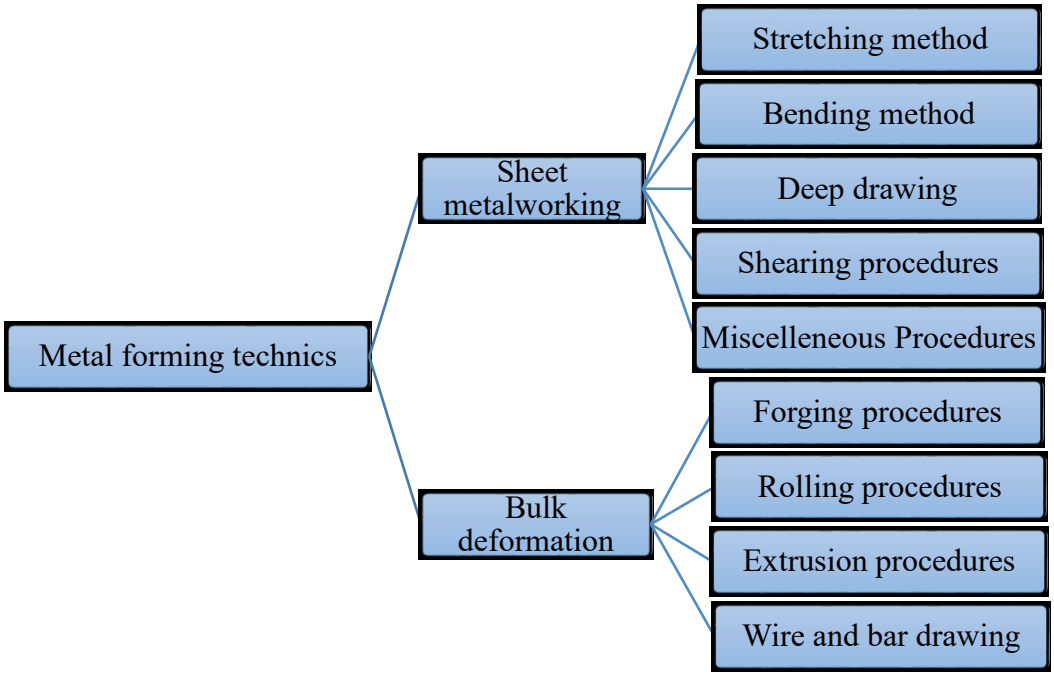

Figure 1.3: General classification of metal forming procedures.

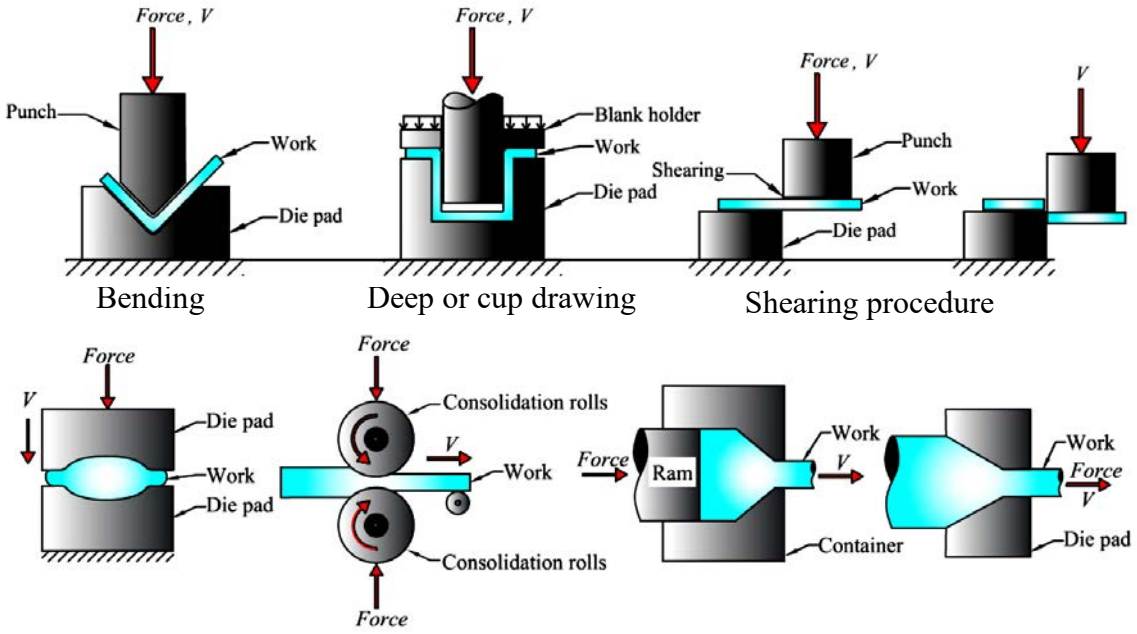

Figure 1.4: Metal forming processes details.

Cold working: Generally done at room temperature or slightly above RT. The cold forming process has many advantages compared to hot forming: (1) closer tolerances can be achieved; (2) good surface finish; (3) because of strain hardening, higher strength and hardness is seen in part; (4) grain flow during deformation provides the opportunity for desirable directional properties; (5) since no heating of the work is involved, furnace, fuel, electricity costs are minimized, (6) Machining requirements are minimum resulting in possibility of near net shaped forming.

On the other side, the technique presents some disadvantages as: (1) higher forces and power are required; (2) strain hardening of the work metal limit the amount of forming that can be done, (3) sometimes cold forming-annealing-cold forming cycle should be followed, (4) the work piece is not ductile enough to be cold worked.

Warm working: In this case, forming is performed at temperatures just above room temperature but below the recrystallization temperature. The working temperature is taken to be 0.3 Tm where Tm is the melting point of the workpiece. The warm forming process has the following advantages: (1) enhanced plastic deformation properties, (2) lower forces required, (3) intricate work geometries possible, (4) annealing stages can be reduced.

Hot working: Involves deformation above recrystallization temperature, between 0.5Tm to 0.75Tm. The advantages of the hot working process are the followings: (1) significant plastic deformation can be given to the sample, (2) significant change in workpiece shape, (3) lower forces are required, (4) materials with premature failure can be hot formed, (5) absence of strengthening due to work hardening. Nevertheless, there are some disadvantages of this method like: (1) shorter tool life, (2) poor surface finish, (3) lower dimensional accuracy, (4) sample surface oxidation.

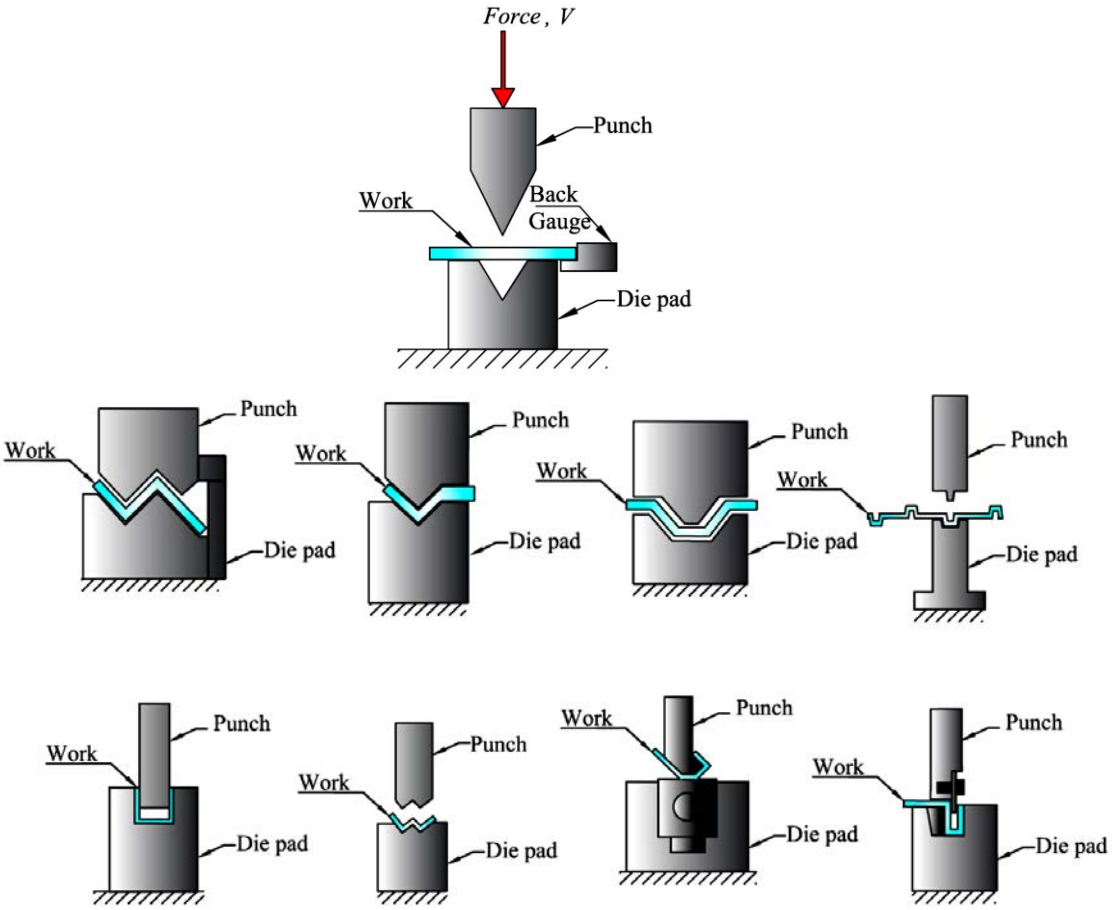

Figure 1.5: Forming profiles.

Welded built-up sections

Built up steel sections are comprised of other smaller members. Built-up shapes can be bolted or welded. The welding or punching for bolt holes creates significant residual stresses in the member, weakening its capacity.

Manufacturing of built-up sections is more simple than other forming technics. The built-up sections are formed by the assembly of thin-wall plates by welding or bolts. This type of sections is more economical than other types of sections.

These elements are useful in metal construction, because they permit to obtain sections with any needed dimensions and inertia of web and flanges, or variable inertia and non-prismatic sections if needed. Otherwise, by reducing thickness of web or flanges this permits to save weigh and obtain just the needed inertia and bending stiffness. A comparative study between hot rolled and welded built-up sections is shown in Figure1.6. In this figure the importance of welled built-up sections is illustrated. The most important inconvenience, that the designers should consider is that welded built-up sections are highly sensitive to lateral bending, torsion, warping and instabilities.

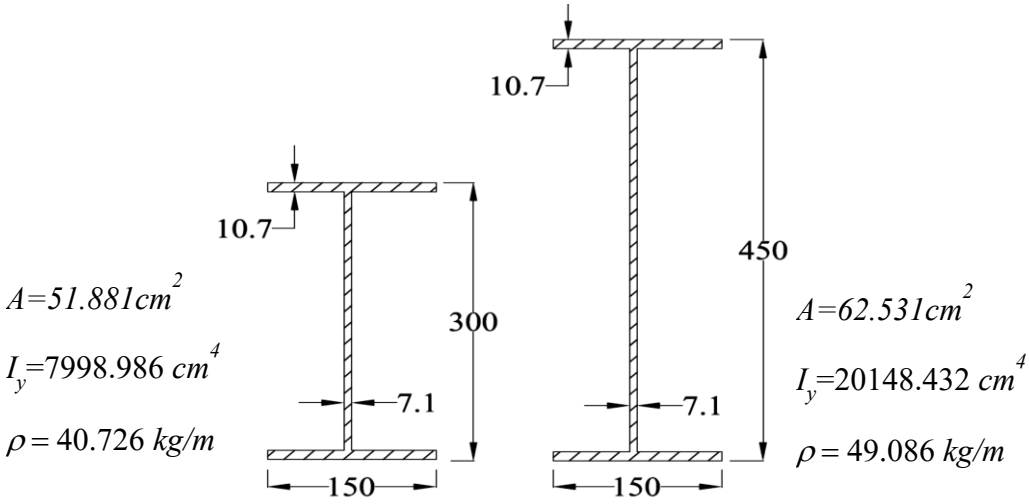

Figure 1.6: Comparison of mass and inertia between hot rolled and welded built-up sections.

1.3 Torsion and warping of thin-walled beams

1.3.1 Origin of the phenomenon

As shown in Figure 1.7, let us consider a bi-symmetric I-section beam, for this section the center of symmetry coincides with both the center of gravity and the torsional center. When, on the one hand, the line of action of transverse loads is perpendicular to the longitudinal axis of the beam, and on the other hand, the plane of loading coincides with a plane of symmetry of the cross section (Figure 1.7-a), the beam is not subjected to axial force nor torsion. The only internal forces are therefore a bending moment and a shear force. Otherwise, when the loading plan passes through the center of symmetry of the section without coinciding with one of the principal plans, a deviated simple bending of beam (Figure 1.7-b) appears. The non-coincidence of the loading plane with a plane of symmetry of the section causes an eccentricity of the transverse loads with respect to the torsional center of the section. Hence, the beam is subjected to either a simple monoaxial or biaxial bending and twisting (Figure 1.7-c and d).

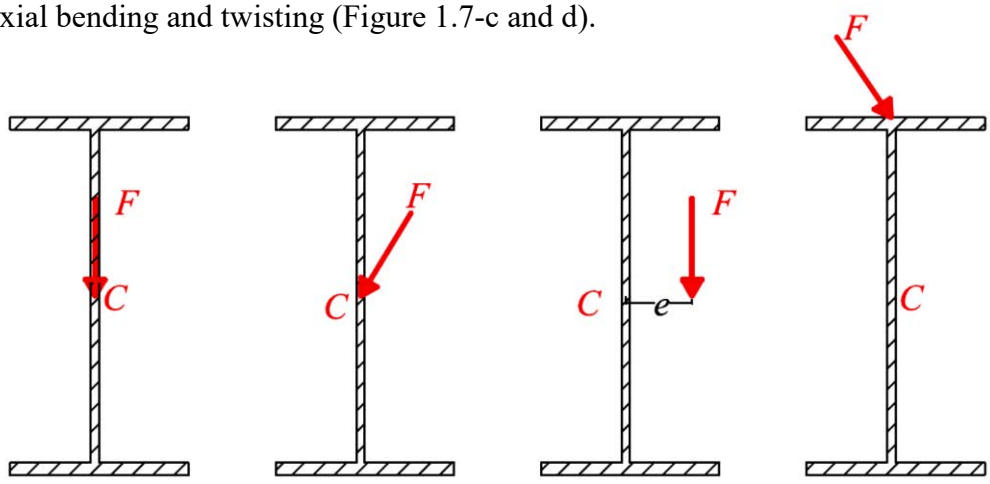

Figure 1.7: Beam internal forces as function of loading types.

An additional axial force appears especially when the beam axis is not perpendicular to the direction of transverse forces. Therefore, the beam is subjected to mono axial bending, bi-axial bending (1st and 2nd cases) and flexural-torsional behavior in the last two cases of Fig. 1.7.

1.3.2 Uniform torsion (De Saint-Venant theory)

In general, solid-section beams are distinguished from thin-walled ones and, for the latter, closed sections are distinguished from open sections.

The theory of torsion for solid sections was developed by Saint-Venant in 1855. This model is the generalization of the torsion problem of beams with circular cross sections. In the model, the torsion moment applied to the shaft leads to a twist angle and its rate along the axial coordinate. The Torsion moment is equilibrated by shear in the section and no additional axial stresses occur (Figure 1.8).

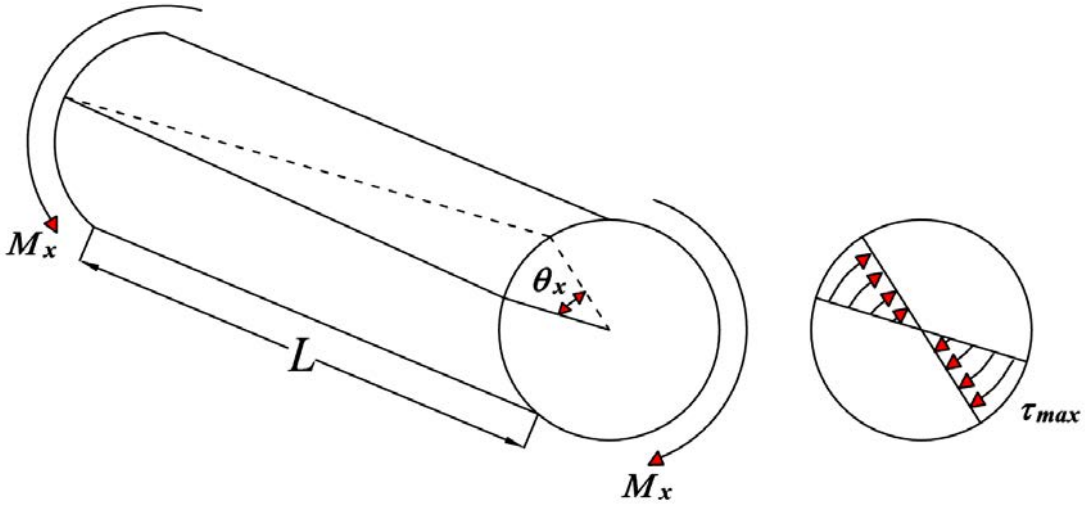

Figure 1.8: Saint-Venant torsion for solid beams.

According to this theory, the equation used to compute the torsion angle θ_x as function of torsion moment $M_x$is given by:

$$\theta_x' = \frac{M_x}{\mathrm{GI}_t} \tag{1.1}$$

With:

G: Shear modulus.

I_t: Torsion inertia constant.

G I_t: Uniform torsion stiffness.

The solution of equation (1.1) gives a linear twist angle along the beam.

The tangential stress distribution in solid-section beams can be done using membrane analogy. These constraints vary proportionally from zero to the center of the section, up to the maximum value at the extreme fiber in the case of circular section (Figure 1.8). According to Zbirohowski-Koscia [119], for a rectangular section (Figure 1.9), the variation of the stresses is considered based on the shear stress contours lines.

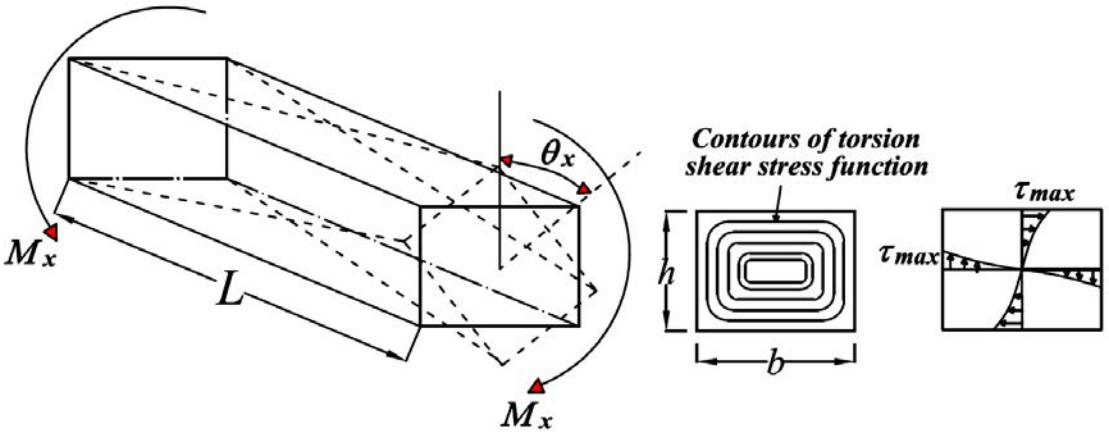

Figure 1.9: Torsion of beams with rectangular solid sections and distribution of shear stresses in the section.

The maximum shear stresses, has the following expression [119]:

$$\tau_{max} = M_x \frac{b}{\alpha \frac{hb^3}{3}} = M_x \frac{3}{\alpha h b^2} \quad (1.2)$$

Where:

b, h: cross section dimensions

α: Geometric coefficient. It depends on the ratio h/b

The value of α varies from $\alpha = 0.624$ for $h/b = 1$ to $\alpha = 1$ for $h/b > 10$.

The equation (1.2) can also be used for any cross-section and especially for thin-walled open sections (Figure 1.10).

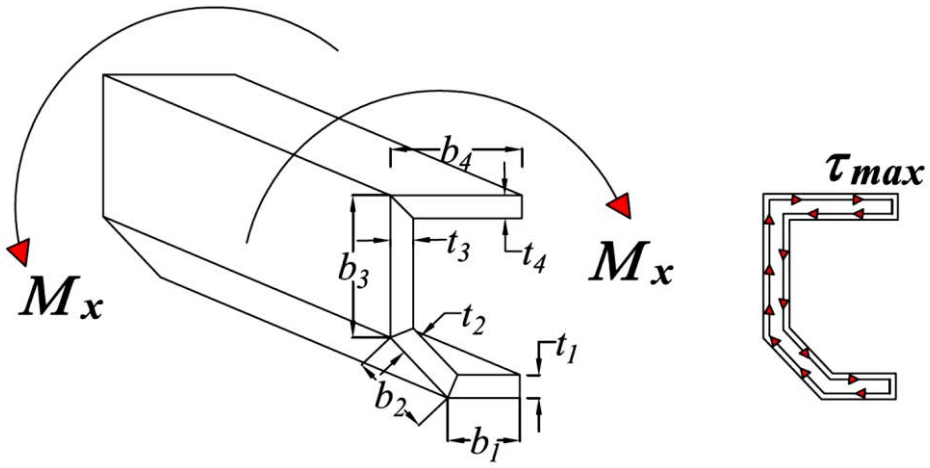

Figure 1.10: Beam with arbitrary thin-walled cross-sections.

The generalized form of the equation (1.2) is written as follows:

$$\tau_{max} = \frac{M_x t}{I_t} \tag{1.3}$$

$$\text{With: } \mathrm{I_t} = \alpha \sum_{\mathrm{k=1}}^{n} \frac{b_k t_k^3}{3} \tag{1.4}$$

and

n: number of segments, b_k, t_k: length and thickness of the k^{th} segment.

In case of thin-walled open sections $\alpha = 1$.

1.3.3 Non-uniform torsion (Vlasov's theory)

In the classical beam theory, the internal stresses in beams result from axial and shear stresses. These stresses are carried out from the reduction of the existing subjected forces and momentums to the beam centroidal axis: (*N, F_y, F_z, M_y, M_z, M_x).* These components are defined as the followings N is the normal force perpendicular to the cross section. F_y and F_z shear forces about the principle axis *Y, Z*. The bending moments about Y and Z are noted M_y, M_z. M_x is the torsion moment. Consequently, *N, M_y and M_z* causes the normal stresses and shear stresses are due to shear forces and torsion moment F_y, F_z and M_x.

Moreover, in thin-walled open sections beams the different points of the section may have, in addition to displacements governed by the uniform torsion, additional longitudinal displacements what is known as the warping effect of the beam cross-sections. Due to this, thin-walled beams cross sections are subjected to non-uniform torsion. Since the torsion of these elements are predominated with warping effect, torsional stiffness of the element has two components: the first is the classical Saint-Venant torsional stiffness, proportional to the shear modulus G. The second contribution is due to the warping of the cross sections.

Consequently, when thin-walled beams are subjected to torsion with a variable rate of twist different type of stresses occurred in the section: the uniform torsion shear stresses

M_{sv} known as Saint-Venant torsion and the warping stresses composed by the normal stresses in the longitudinal direction of the cross section and shear stresses in the cross sections plans. Hence warping stresses can be significant in relation to other stresses like the bending, and so they cannot be omitted.

Because of the warping on the beam cross section a longitudinal load differently to transverse load cannot be replaced by a statically equivalent longitudinal forces system.

Moreover, the non-uniform warping of the cross sections in the longitudinal direction results moments in some locations of the beam section what is named in literature [5] bimoment B_ω.

To illustrate this problem let us consider a cantilever beam with I cross section carrying an eccentric load $4F$ acting at the free end of the beam on the extremity of the bottom flange and parallel to the longitudinal axis. The force eccentricity about the beam principle axis are noted $e_y=b/2$ and $e_z=h/2$ as shown in Figure 1.11. According to the classical beam theory, this load can be decomposed into the equivalent system involving normal force and two bending moments M_y, M_z at the centroid as shown in Figure 1.11. Each of these charges can be replaced by the equivalent forces applied in the four flange tip ends of the section as depicted in Figure 1.12a-c. However, the superposition of the loads presented in Figures 1.12a,b,c leads to the loads depicted in Figure 1.12d which does not correspond to the initial load presented in 1.6a. So there is additional load for thin-walled beams defined in 1.12e as the warping effect (bimoments). The warping effect is presented initially by Vlasov and defined by two equal moments M_0 having equal magnitude and opposite sign acting on the flanges subjecting flexions in opposite orientation and separated by a distance equal to the height of the beam h see Figure 1.12d.

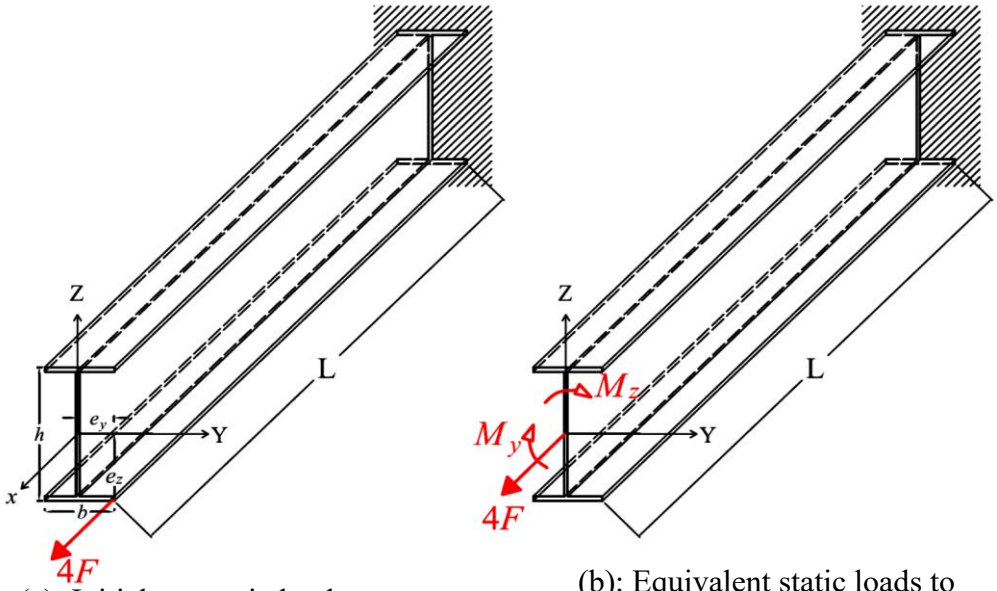

(a): Initial eccentric load

(b): Equivalent static loads to

Figure 1.11: Equivalent axial and bending loads due to eccentric load applied at the flange tip. (according to classical beam theory).

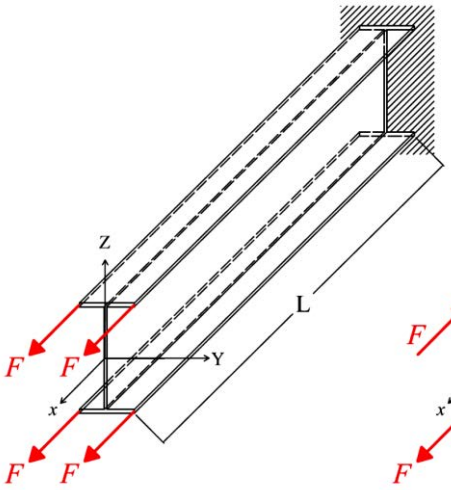

(a): axial load (traction)

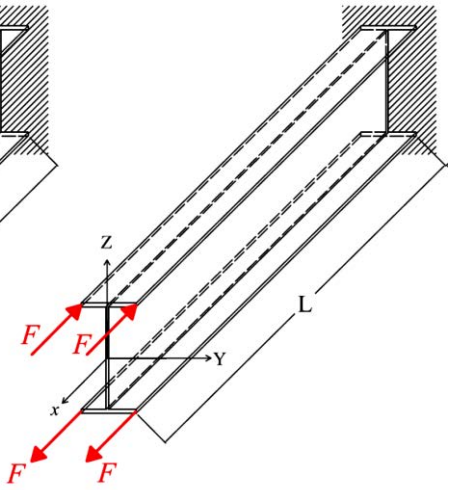

(b): y axis bending

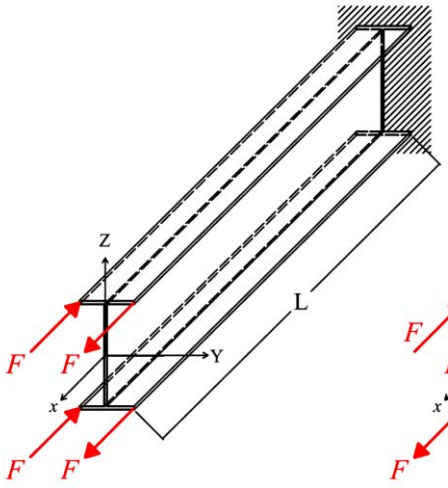

(c): z axis bending

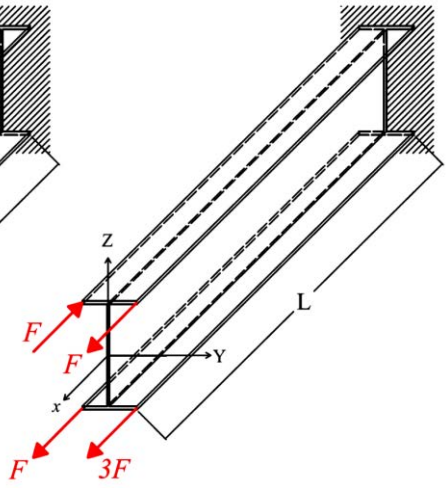

(d): superposition of (a,b,c)

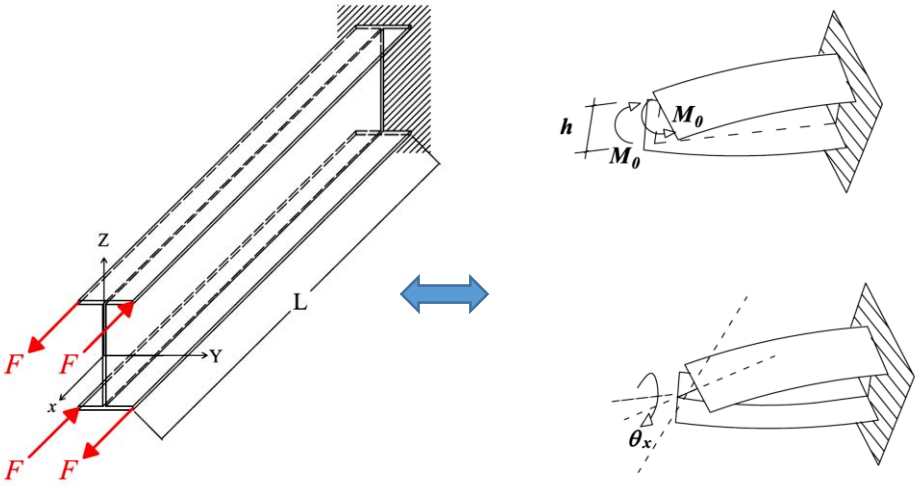

(e): Warping force, (Bimoment) defined according to Vlasov theory

Figure 1.12: Equivalent axial forces due to eccentric load 4*F* applied at the flange tip of Figure 1.11. (according to Vlasov theory).

From the analysis of Figure 1.12e, we can interpret that if the flanges and the web are separated, and the free end of the beam is loaded by two moments M_0, each flange will bend separately. Otherwise, to restore the reliability of the beam, both flanges and web have to be twisted. This can be obtained by setting a Saint-Venant torsion moment M_{sv} or a rotation θ_x. Thus, as the web is flexible in torsion, the cross section is permitted to exhibit out-of-plane displacements, and the Euler-Bernoulli hypothesis of plane cross sections after deformation is no longer valid. This implies that the moment vectors M_0 cannot be added vectorially and their effects must be considered in the kinematical description of a thin-walled beam.

This problem was solved by [5] who gives as extension to the Euler-Bernoulli beam theory by introducing the non-uniform torsion theory for thin walled-beams with open cross section including the warping effect. However, Vlasov assumed that the section is rigid in-plane and no distortion in the section middle surface.

Consequentially, for the thin-walled open sections the classical theory is not sufficient and the warping effort (bimoment) must be calculated as additional effort. Thus, according to the general theory for this type of elements, the reduction of forces and momentums to the beam has number of seven internal efforts: (N, F_y, F_z, M_y, M_z, M_x and B_ω).

1.3.3.1 Torsion equation

In thin-walled open sections beams (like I sections) subjected to torsion moments, it is remarkable that in addition to torsional angle there is a transversal displacement v that occur and causes flexural and shear stresses in the flanges (Figure 1.13). The torsional moment for these types of sections is equivalent to Saint-Venant tangential shear stresses and momentum result of shear stresses T_y at the flanges. This gives the following relationship:

$$M_x = M_{SV} + M_\omega = GI_t \frac{d\theta_x}{dx} + T_y h \tag{1.5}$$

Where:

M_{SV}: Twisting moment of Saint-Venant, given by equation (1.1)

M_ω: Warping torsion moment

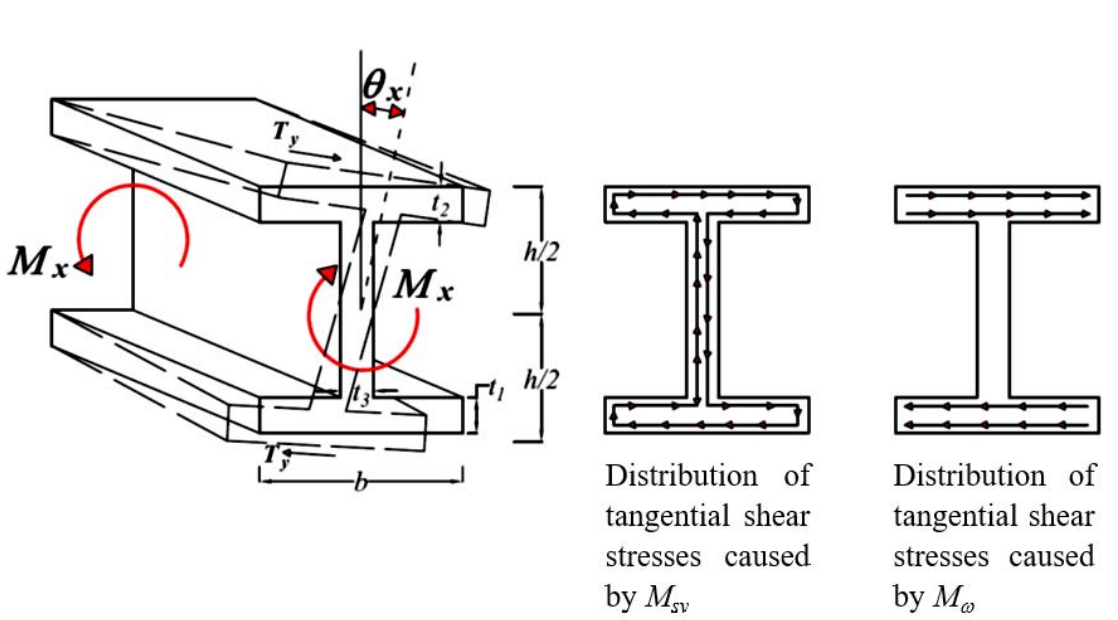

Figure 1.13: Warping of the I beam cross-section.

For small displacements, v in function of θ_x is denoted by the following relation:

$$v = \theta_x \, h/2 \tag{1.6}$$

The lateral displacement of the flange v and the bending moment M_z have the following relation:

$$M_z = -EI_z \frac{d^2v}{dx^2} \tag{1.7}$$

Where:

I_z: quadratic moment of inertia of the flange about z axis.

The shear force T_y is defined as the first derivative of M_z; therefore:

$$T_y = \frac{dM_z}{dx} \tag{1.8}$$

While considering the equations (1.6) and (1.7), (1.8) becomes:

$$T_y = -EI_z \frac{h}{2} \frac{d^3\theta_x}{dx^3} \tag{1.9}$$

The warping torsion moment developed in the flanges is denoted by:

$$M_\omega = T_y h \tag{1.10}$$

Therefore, M_ω becomes:

$$M_\omega = T_y h = -EI_z \frac{h^2}{2} \frac{d^3\theta_x}{dx^3} \tag{1.11}$$

By guttering (grouping) the geometric terms together, one defines a warping constant as:

$$I_\omega = \frac{I_z h^2}{2} = \frac{I_{zz} h^2}{4} \tag{1.12}$$

Where I_{zz} is the weak bending inertia of the I section (I_{zz}=2I_z). By replacing injecting (1.12) in the equation (1.11), the warping torsion moment becomes:

$$M_\omega = -EI_\omega \frac{d^3\theta_x}{dx^3} \tag{1.13}$$

Finally, the differential equation given the relation between the torsion moment and the torsion angle is denoted by:

$$M_x = M_{SV} + M_\omega = GI_t \frac{d\theta_x}{dx} - EI_\omega \frac{d^3\theta_x}{dx^3} \tag{1.14}$$

Where:

GI_t is the Saint-Venant torsion stiffness and EI_ω is the warping stiffness.

Hence, M_{SV} involves the appearance of the distribution of tangential stresses, following the theory of Saint-Venant and the warping section M_ω. The solution of the equation (1.14) gives a nonlinear torsion angle along the beam.

After, introducing the thin-walled elements properties and behavior in statics let us move to the vibration behavior of these elements. Firstly, let us introduce linear vibration behavior in general then we move to detail the case of thin-walled beams.

1.4 Vibration analysis

In the study of vibration phenomenon, engineers, and designers are interested by the behavior of structures in presence of dynamic loads where the forces are time dependent. The displacement amplitudes increase when the load frequency excitation coincide with the eigenfrequencies of the structures. This lead to resonance phenomenon. Thus, in the first step of the dynamic analysis procedure the natural frequencies (eigenvalues) and the mode shapes (eigenvectors) of the structures are carried out by adopting the free vibration analysis. Then, the response spectra, loss factors and modal damping are investigated in presence of dynamic loads by following the forced vibration analysis. In literature, existing works can be classified according to two types of approaches: analytical methods and numerical models. A vibratory system is composed of a spring, mass and damper. If all the components of a vibratory system behave linearly, the resulting vibration is known as linear vibration. But if any of the basic components behave nonlinearly, the vibration become nonlinear. In linear vibration the differential equations that govern the behavior are linear, the principle of superposition holds, and the mathematical techniques of analysis are well developed. For nonlinear systems differential equations are nonlinear. For nonlinear vibration, the superposition principle is not valid, and techniques of analysis are less well known. Vibratory systems tend to behave nonlinearly with increasing amplitude of oscillation.

The linear vibration theory is applied when a small amplitude vibrations of long, slender beams like long bridges are modelled, aero plane wings and helicopter blades. Nonlinear systems can display behaviors includes the followings: with the same excitation multiple steady state solutions are gotten, some stable and other unstable response. Jump phenomena, involving discontinuous and significant changes in the response of the system as some forcing parameter is slowly varied. Response at frequencies other than the forcing frequency. Internal resonances, involving different parts of the system vibrating at different frequencies, all with steady amplitudes. Self-sustained oscillations in the absence of explicit external periodic forcing, and complex, irregular motions that are extremely sensitive to initial conditions (chaos).

1.4.1 Free vibration

Free vibration occurs when a system is left to vibrate on its own after an initial excitation. In free vibration, there no external forces acting on the system. As example of free vibration it can be taken a simple pendulum in oscillation or a rotating system, see Figure 1.14.

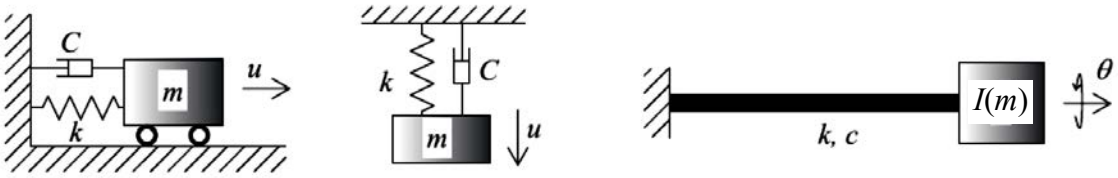

Translation Rotation (Torsion)

Figure 1.14: Free vibration systems models.

The vibration parameters of systems presented in Figure 1.14 can be summarized in the following table.

Table 1.1: Vibration systems parameters.

Parameter	Translation system	Rotating system
Movement type	Longitudinal displacement: u	Torsion angle: θ
Inertia	Masse: m	Mass moment of inertia: $I(m)$
Stiffness	Elongation resistance: k	Torsion resistance: k
Damping	Viscous damping: c	Viscous damping: c

The motion equations of a vibration system can be formulated from type of vibration systems parameters presented in Table 1.1 as a combination of translation and/or rotation movements. Thus, the motion equation of translation vibrating system can be expressed as function of systems parameters using one of the following methods: the balance of applied forces on the mass m or the law of energy conservation of the system.

Second Newton's law	Conservation of energy
Excitation force: F (=0 for free vibration)	Strain energy: $U = \frac{1}{2}ku^2$
Resistant force: $-ku$	Kinetic energy: $T = \frac{1}{2}m\dot{u}^2$
Damping force: $-c\dot{u}$	Dissipated power (due to damping): $P_D = c\dot{u}^2$
($\sum F = m\ddot{u}$)	External loads power: $P_W = F\dot{u}$
$F - c\dot{u} - ku = m\ddot{u}$ (1.15)	$\frac{d(U+T)}{dt} + P_D = P_W$ (1.16)

The second newton's law: the sum of the forces applied on an object in an inertial frame of reference, is equal to the mass m of that object multiplied by the acceleration $\ddot{u}$ of the object: $\sum F = m\ddot{u}$. (1.17)

The law of conservation of energy for a system states that the total energy of an isolated system is conserved over time.
Thus, the motion equation of the mass system is given as follows:

$m\ddot{u} + c\dot{u} + ku = F$ (F=0 for free vibration) (1.18)

Otherwise, for a rotational system subjected to a torsional moment M the motion equation becomes:

$I\ddot{\theta} + c\dot{\theta} + k\theta = M$ (M =0 for free vibration) (1.19)

The undamped free vibration problem consists to solve the motion equations (1.18) of a structure after vanishing the external load terms and damping terms.

$m\ddot{u} + ku = 0$ (1.20)

This leads to the known eigenvalue problem. By solving the eigenvalue problem, the natural frequencies and the corresponding vibration modes are carried out.

In presence of multi degrees of freedom system, the eigenvalue problem can be expressed according to the matrix system, given by:

$$([K] - \Omega_i^2[M])\phi_i = 0 \tag{1.21}$$

Where $[K]$ and $[K]$ are the stiffness and mass matrices. Ω and ϕ_i are the eigenvalues and eigenvectors of the system. By Solving the equations (1.21) above for *n*-degree-of-freedom system, one gets the required vibration modes with eigenvalues (angular velocities) and eigenvectors.

There are 2 types of free vibration, the first one is the non-damped vibration and the other is the damped free vibration. If the undamped free vibration is considered with a harmonic movement this leads to natural frequencies. For the other case a pseudo harmonic damped movement is obtained.

The eigenvalue solution methods are divided to five categories: methods based on the development of the system equation, methods that consist to transform the initial problem to diagonal or tridiagonal using successive transformations, iterative methods, subspace methods. Choosing one of these methods is based on the number of degree-of-freedom. In case of a system with a small number of DOF we can proceed directly to the development of the characteristic equations and solve them semi-analytically. But in general the eigenvalue problem is solved using the FEM. In this case the solution consists to transform the problem in sequence of statically problem of form (K*U=F) because of the most of the solution methods based in the power algorithms are based in this principle. So, to solve the eigenvalue problem the most known solution methods are: the eigenvector Iteration Methods (power iteration algorithm, inverse iteration method, inverse iteration with spectral shifting, Rayleigh quotients), Subspace Construction Methods (Subspace iteration method, Lanczos method. Therefore, one of the solution methods mentioned above can be adopted after calculation of the mass matrix [M], and the stiffness matrix [K]. The choice of the useful solution method is based on the matrices size (structure type, and DOF, and needed researched modes).

1.4.2 Forced vibration

Forced vibration takes place, when a system is subjected to an external time dependent loads. A forced vibration example is the oscillation that takes place in some vehicles engines. When the frequency of the external force coincides with one of the eigenvalues of the system, the resonance phenomenon happens, and the system exhibits large oscillations around the resonance frequency domain. Resonance phenomenon is the reason of failures of several structures such as bridges, buildings and airplane wings. Different methods of solutions for forced vibrations exist in the literature [11, 48], the most known methods are the steady state direct method and the modal analysis. The modal analysis is more efficient to carry out the dynamic response of structures subjected to dynamic excitation specially when there is large number of DOF. The efficiency reason is due to the method principle to carry out the response as a linear combination of a specific number of modes, otherwise of the direct method when we have a large number of DOF. Because that reduce the number of equations of the system when taking in consideration the orthogonality of the vibration modes calculated before.

To demonstrate the forced vibration solution method, let us take the conventional vibration system composed of a mass *m* connected to a spring with stiffness *k* and viscous damping *c* and subjected to a load *F.* The system is presented in Figure 1.15

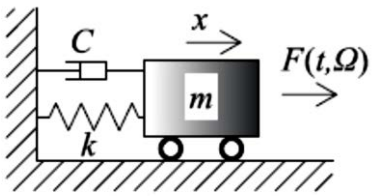

Figure 1.15: Model of forced vibration system.

The procedure of modal analysis is detailed herein. Let the harmonic arbitrary external forcing function be represented in complex form as $F(t) = F_0 e^{i\Omega t}$ so that the motion equation (1.18) becomes:

$$m\ddot{x} + c\dot{x} + kx = F_0 e^{i\Omega t} \tag{1.22}$$

Let us assume the following particular solution for the motion equation:

$$x_p(t) = Xe^{i\Omega t} \tag{1.23}$$

By substituting equation (1.23) with equation (1.22), the motion equation becomes:

$$-mX\omega^2 e^{i\Omega t} + iXc\Omega e^{i\Omega t} + kXe^{i\Omega t} = F_0 e^{i\Omega t}$$

$$-mX\Omega^2 + iXc\Omega + kX = F_0$$

The solution of the motion equation is given as follows:

$$X(\Omega) = \frac{F_0}{(k-\Omega^2 m)+ic\Omega} \tag{1.24}$$

By multiplying the numerator and denominator on the right side of equation (1.24) by $[(k-\Omega^2 m)-ic\Omega]$ and separating the real and imaginary parts, the following expression is gotten:

$$X(\Omega)=F_0\left[\frac{(k-\Omega^2 m)}{(k-\Omega^2 m)^2+c^2\omega^2}-i\frac{c\Omega}{(k-\Omega^2 m)^2+c^2\Omega^2}\right] \tag{1.25}$$

Using the relation $A+iB=C\ e^{i\emptyset}$ (1.26)

Where $C=\sqrt{A^2+B^2}$ and $\tan\emptyset=\frac{A}{B}$ (1.27 a, b)

The equation (1.25) can be expressed as:

$$X(\Omega,t)=\frac{F_0}{\left[(k-\Omega^2 m)^2+c^2\Omega^2\right]^{1/2}}e^{-i\emptyset} \tag{1.28}$$

Thus, the steady-state solution, equation (1.23), becomes:

$$x_p(\Omega,t)=\frac{F_0}{\left[(k-\Omega^2 m)^2+c^2\Omega^2\right]^{1/2}}e^{i(\Omega t-\emptyset)} \tag{1.29}$$

It should be noted that, when *F* (t) is a random excitation signal and cannot be expressed as a linear combination of harmonic functions, it become necessary to move into the complex form of signal using Laplace transform. Otherwise, if the excitation signal is given in time domain, this signal can be transformed into frequency domain by means of Fourier transform method. This transformation procedure is detailed in what follows.

1.4.3 Time domain, frequency domain and Fourier Transform

For modal testing, either time domain and frequency domain analysis is widely adopted in signal processing. Moreover, in vibration analysis under harmonic conditions, the frequency domain is widely adopted in the study. We can cover all range of frequencies which is impossible in time domain. Vibrational systems can be characterized by their inherent frequency components. But, some signals are given in time domain like earthquakes spectrograms. So the importance to convert signals from time into frequency domain. This process becomes easy due to the modern computational power. The most familiar method to transform signal from time to frequency domain is the Fourier transformation (FT). The importance of the Fourier transformation method is that it permits to decompose a complex signal into simpler parts witch facilitate analysis. Otherwise, it helps to transform the differential, difference equations and complex operations in the time domain to algebraic operations in the frequency domain.

In this paragraph, the Fourier transformation is presented. Let's consider a signal $x(t)$ given in time domain, this signal can be periodic or non-periodic. This signal can be written in the following form:

$$x(t) = \frac{1}{2\pi}\int_{-\infty}^{+\infty} X(\Omega)e^{i\Omega t}\, d\Omega \tag{1.30}$$

Where $X(\Omega)$ is the Fourier transformation of the time signal $x(t)$

In this case $X(\Omega)$ can be obtained by the following expression:

$$X(\Omega) = \int_{-\infty}^{+\infty} x(t)e^{-i\Omega t}\, \mathrm{dt} \tag{1.31}$$

The time signal $x(t)$ is the inverse Fourier transformation $X(\Omega)$. It should be noteed that an important condition for the existence of the Fourier transform is:

$\int_{-\infty}^{+\infty}|x(t)|dx =$finite number.

Hereafter, by introducing : $f=\Omega/2\pi$, the equations above becomes:

$$x(t) = \frac{1}{2\pi}\int_{-\infty}^{+\infty} X(f)e^{i2\pi ft}\, d\Omega \tag{1.32}$$

And

$$X(f) = \int_{-\infty}^{+\infty} x(t)e^{-i2\pi ft}\, \mathrm{dt} \tag{1.33}$$

Since the integral is general time varying involving complex variables, it is not easy to solve it manually, so numerical integration is needed here to do FT. A powerful algorithm called Discrete Fourier transform is used in solution process. A finite number of summations at discrete points adopted to drive integration.

If there are N sampled values as:

$x_k = x(t_k);\ t_k = k\Delta t\ ;\ \ k = 0,1,2, \ldots\ldots N-1$

Based on the sample data points, we assume that the time domain data project into the corresponding frequency data. The N discrete frequency points (f_1,……,f_N) define Fourier transformation. Where the frequency points should be in the range of Nyquist critical frequency (defined as: the half of the sampling rate of a discrete signal processing system)

$$f_c = \frac{1}{2\Delta t} \tag{1.34}$$

The sampling period Δt should be at least half of the period of signal to sufficiently represent signal.

Finally, the Discrete Fourier Transformation (DFT) is written as follow:

$$X(f_n) = \int_{-\infty}^{+\infty} x(t) e^{i2\pi f_n t}\, dt \sim \sum_{k=0}^{N-1} x_k\, e^{i2\pi f_n t_k} \Delta t \tag{1.35}$$

It should be noted that the discrete Fourier transformation (DFT) has the symmetry property with respect to the impute frequency (f_n):

$$X(f_n) = X(f_{N-n});\ f_n = \frac{n}{N\Delta t}\ \ , n = -\frac{N}{2}, \ldots\ldots, \frac{N}{2} \tag{1.36}$$

So half of the transform is needed to represent all frequency components, and the frequency range is given by:

$$0 < f < \frac{1}{2\Delta t} \tag{1.37}$$

A refined version of the DFT called Fast Fourier transform FFT which improves computational efficiency significantly. It turns out that the $e^{i2\pi f_n t_k}$ term in the above equation repeats over the frequency range, and the FFT makes use of this property. FFT algorithm is implemented in Matlab software. The number of operations for FFT is $\left(\frac{N}{2}\right) log_2 N$ when compared to N^2 for DFT.

By using Fourier Transform the signals with different time-domain characteristics gives spectra in frequency-domain with dissimilar characteristics. Hence, a continues-time a periodic signal gives a discrete non-periodic spectrum. For example, the FFT result of sinusoidal wave is shown in Figure 1.16. From this figure it can be seems that the frequencies between the harmonics can be thought of as having a value of zero, or simply not existing. Otherwise, a continues-time non-periodic signal gives continues non-periodic spectrum. The discrete non-periodic periodic signal becomes continues periodic spectrum. The discrete periodic signal is converted to discrete periodic spectrum.

The last transformation between time-domain and frequency is most useful. The reason that discrete is associated with both time-domain and frequency domain is because computers can only take finite discrete time signals.

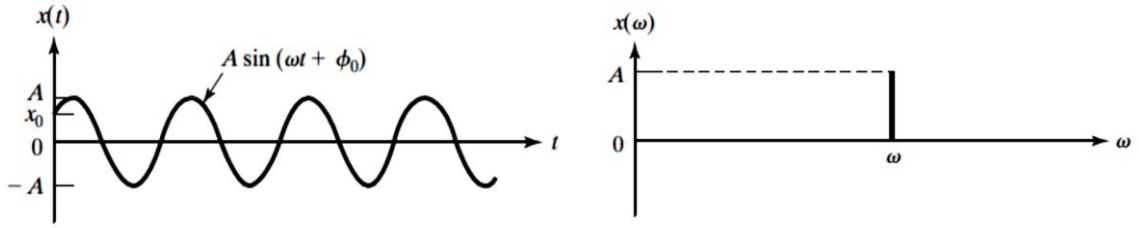

Figure 1.16: FFT result of sinusoidal wave (Harmonic function).

As example to demonstrate the FFT in the case of discrete non-periodic signals, A Matlab file is written to transform Elcentro recorded earthquake signal table from time domain (time-acceleration) to frequency domain (frequency-|Fourier Transform of acceleration|). The input file includes both accelerations and time interval. The time interval is transformed into the corresponding frequency scale based on the Nyquist critical frequency. The number of data points in the FFT should be power of 2, otherwise Matlab built in function fft fills the discrepancy with blank data. Figure 1.17 illustrate the time domain impulse and the corresponding FFT results. It should be noted that a harmonic function given by in time domain can be represented by the amplitude and the frequency in the frequency domain.

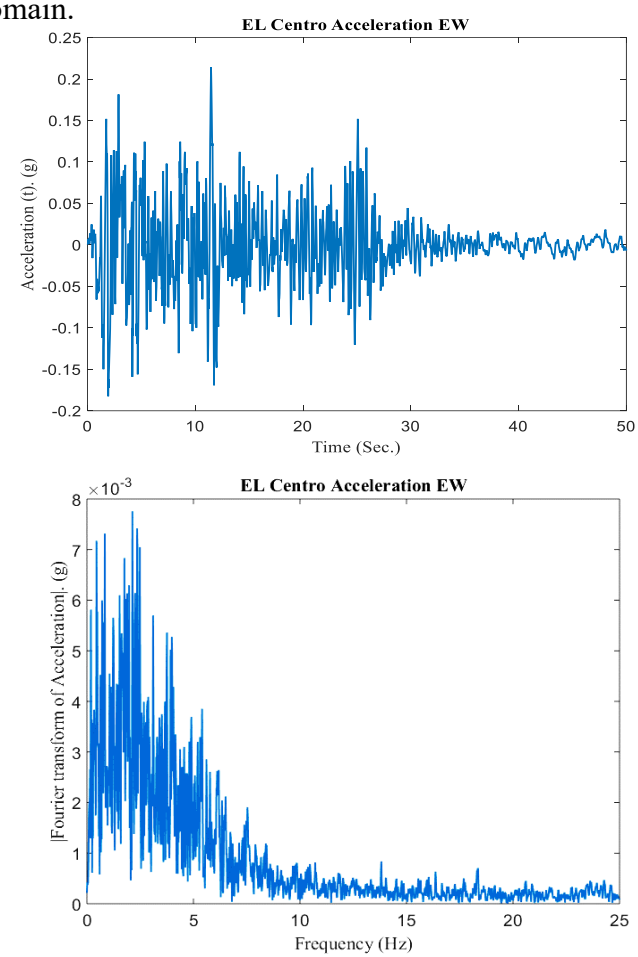

Figure 1.17: Transformation of El Centro EW earthquake signal from time domain to frequency domain using FFT.

1.4.4 Damping

The movement of structures subject to forces or imposed movements function of time, depends in damping properties, in other words, dissipation of energy in the materials of the structure and in the connections of the various elements of structure between each other's and with the surrounding environment.

The physical phenomena involved in this dissipation of energy are numerous friction, fluid-structure interaction in a fluid slide, shocks, viscosity and plasticity.

The models used to represent damping on the structures are:

• viscous damping: dissipated energy proportional to the velocity of the movement,

• structural damping dissipated energy proportional to the displacement such that the damping force is of opposite sign to that of the velocity.

Damping characteristics:

1.4.4.1. Loss factor

The loss factor η is a dimensionless coefficient characteristic of the damping effect defined to be the ratio of the energy dissipated during a cycle to the maximum strain energy in cycle $E_{p\,max}$ multiplied by 2π:

$$\eta = \frac{E_{d\,per\,cycle}}{2\pi E_{p\,max}} \tag{1.38}$$

The loss factor η is carried out experimentally from the obtained response spectrum using the bandwidth method -3 dB. It should be noted that this method is valid in case of $\eta \ll 1$. For an experimental response spectrum as presented in Figure 1.18 the loss factor can be computed as follows.

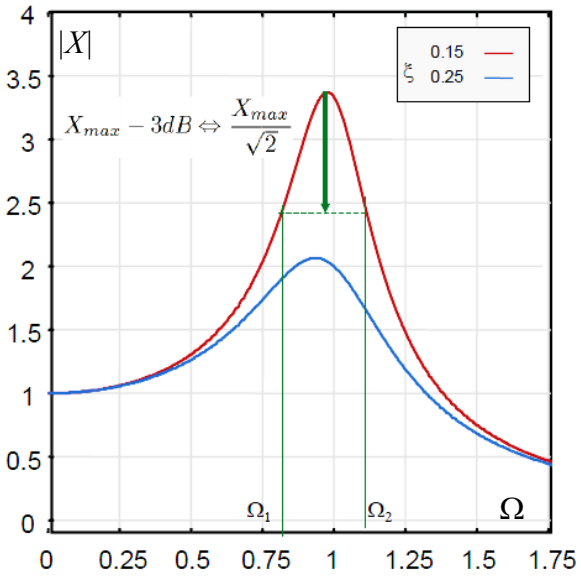

Figure 1.18: Computing loss factor from response spectrum using bandwidth method.

Thus, from Figure 1.18 the loss factor coefficient is computed by using the following equation:

$$\eta = \frac{\Delta\Omega_{3dB}}{2\Omega_{max}} = \frac{\Omega_2 - \Omega_1}{2\Omega_0} \tag{1.39}$$

It should be noted that several references [66-68] gave the loss factors ranges for the most of materials. Based on these references the typical loss factor for various materials adopted in this study are summarized in Table 1.2. These reference values have been obtained experimentally, and it can be used as reference to compute Rayleigh damping factors α, β for each vibration mode.

Table 1.2: Typical loss factor η for basic materials.

Material	Aluminum	Steel	Wood/concrete	Sand	Plastics
Loss factor	0.0001	0.0005-0.001	0.01	0.1	1

It should be noted that the relationship between the loss factor η and the viscous damping ratio ξ is given by:

$$\xi = \frac{\eta}{2} \tag{1.40}$$

1.4.4.2 Viscous damping model

1.4.4.2.1 Physical definition of viscous damping

Conventional damping devices (the crossing of a viscous fluid through the piston orifices driven by a vibratory movement) deliver forces proportional to the speed of the movement with opposite sign. During a cycle, the work of these forces is positive.

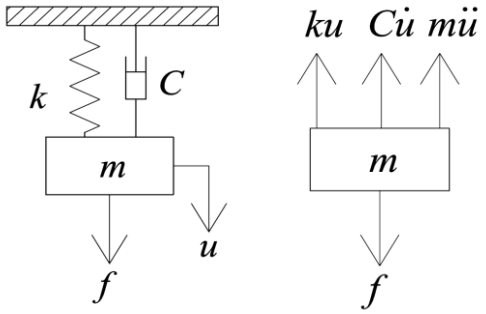

(a): Mass spring damper system (b): Free body diagram

Figure 1.19: Mass spring damping system.

For a simple oscillator presented in Figure 1.19a, composed of spring with stiffness *k*, mass *m* and viscous damping *C*, the external force *f* acting on the mass. The forces acting on the mass are: elastic restoring force *ku*, damping force due to viscous damper $C\dot{u}$, inertia of force $m\ddot{u}$ and the applied external force *f* see the free body diagram Figure

1.19b. Using Newton's second law of motion, which states that 'the rate of change of momentum of a mass is equal to the force acting on it'.

Hence, the dynamic motion equation:

$$m\ddot{u} + C\dot{u} + ku = f \tag{1.41}$$

For this viscous damping model, the energy dissipated during a pulsation cycle ω is proportional to the vibratory velocity $-\omega u_0 \sin(\omega t)$ associated with displacement $u_0 \cos(\omega t)$:

$$E_{d\ per\ cycle} = \int_0^{2\pi} -C\omega u_0 \sin(\omega t) d\,(u_0 \cos(\omega t)) = \pi C \omega u_0^2 \tag{1.42}$$

and the potential energy for sinusoidal displacement $u_0 \cos(\omega t)$ is :

$$E_{p\ max} = \int_{\pi/2}^{0} k u_0 \cos(\omega t)\, d(u_0 \cos(\omega t)) = \frac{1}{2}\pi k u_0^2 \tag{1.43}$$

For a pulsation cycle ω and sinusoidal displacement $u_0 \cos(\omega t)$, the loss factor is proportional to the movement frequency:

$$\eta = \frac{C\omega}{k} \tag{1.44}$$

1.4.4.2.2 Harmonic oscillator with viscous damping

The classical analysis of the free vibration undamped model is deduced from the equation (1.41) as follow:

$$m\ddot{u} + ku = 0 \tag{1.45}$$

As the oscillation is harmonic, the displacement *u* can be written as:

$$u(x,t)=u(x)\, e^{i\Omega t} \tag{1.46}$$

The insertion of the second derivative about time of equation (1.46) into the equation (1.45) gives:

$$(k - m\Omega^2)u = 0 \tag{1.47}$$

The solution of equation (1.47) gives the angular frequency:

$$\Omega_0 = \sqrt{\frac{k}{m}} \tag{1.48}$$

The critical damping from which the differential equation (1.41) has no oscillating solution is written as follows:

$$c_{critical} = 2\sqrt{km} = 2m\Omega_0 = \frac{2k}{\Omega_0} \tag{1.49}$$

This gives a numerical interpretation of reduced damping ratio, which is often expressed as a percentage of critical damping:

$$\xi = \frac{\eta}{2} = \frac{c}{c_{critical}} = \frac{c}{2m\Omega_0} \tag{1.50}$$

By putting equations (1.48, 1.50) in equation (1.27), the following relationship is obtained:

$$X(\Omega) = \frac{F_0}{m\left[\left({\Omega_0}^2 - \Omega^2\right)^2 + 4(\xi\Omega\,\Omega_0)^2\right]^{1/2}} \tag{1.51}$$

$$\text{And } \emptyset(\Omega) = Arctg\left(\frac{2\xi\Omega_0\Omega}{{\Omega_0}^2 - \Omega^2}\right) \tag{1.52}$$

The displacement response spectra X and phase angle $\emptyset$ are than plotted in terms of angular velocity Ω and damping ratio ξ as shown in Figure 1.20 depicted below.

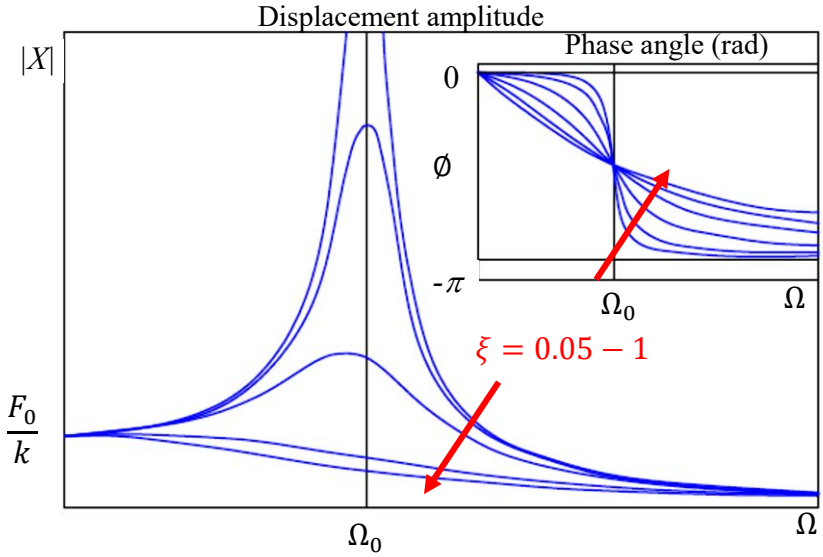

Figure 1.20: Displacement amplitude and phase angle in terms of damping ratio (in the frequency domain).

1.4.5 Effect of elastic and viscous springs on the dynamic behavior of structures

The elastic springs elements are used to introduce additional stiffness in some points of the structure. By adding stiffness to the structure, the natural frequencies increase. Accordingly, the dynamic behavior of the structure is improved against low vibration frequencies. The viscous springs are a power-dissipation mechanism called also dashpots. They are used to dissipate the energy of the structures subjected to a moving force. Thus, the role of these element is to reduce the displacement amplitude of the structure near to resonance. The elastic and viscous springs can be used in parallel as shown in Figure 1.21.

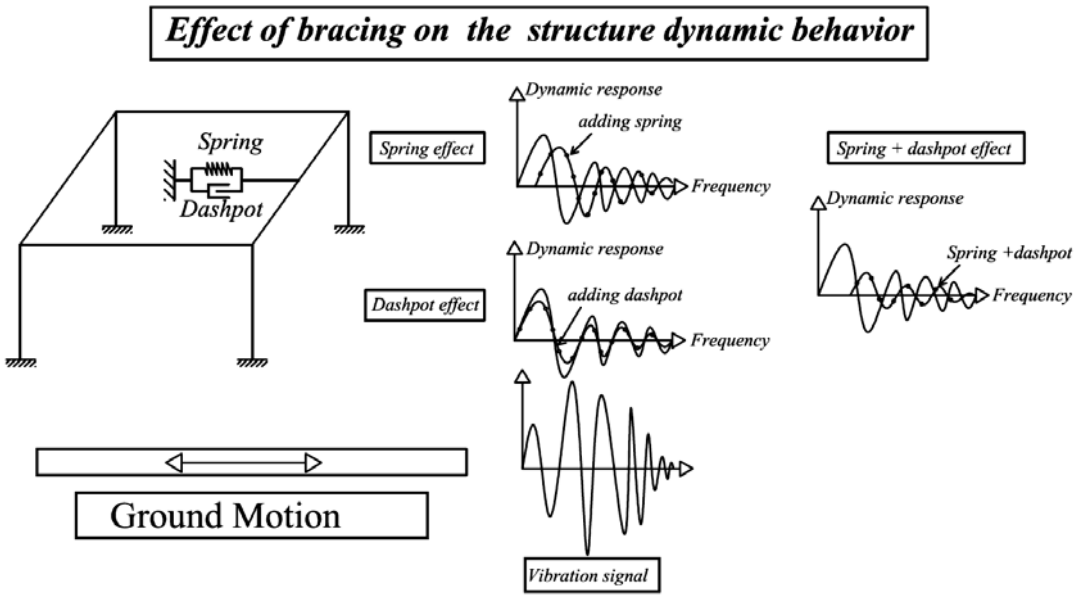

Figure 1.21: Effect of springs and dashpots on vibration behavior.

Thus, the viscous and elastic springs influence the response of the structure. A beam that is perfectly rigid will have a zero period. When the beam is subjected to dynamic loads an acceleration is induced in the structure. A beam that is perfectly flexible will have an infinite period. By adding elastic and viscous braces the dynamic response of the beam is modified as shown in Figure 1.21 that lead to control the vibration of such structure. In what follows let us introduce the effect of different types of braces.

Effect of elastic spring

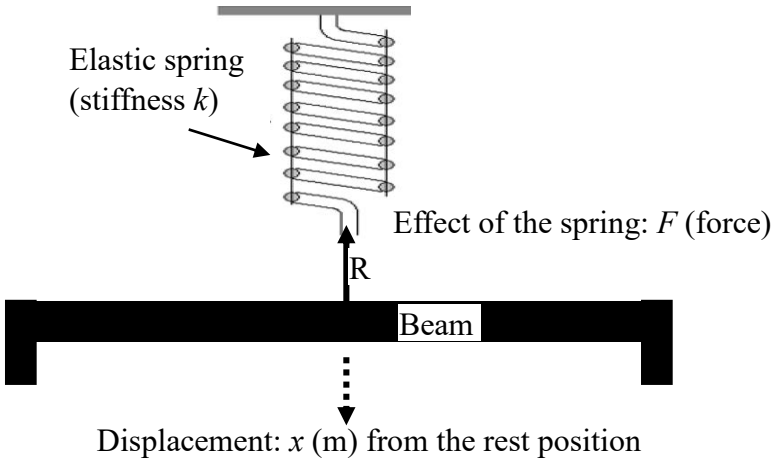

Figure 1.22: Effect of an elastic spring on the beam dynamic behavior.

To explain the effect of springs on the dynamic behavior of the beam. Let us take as example a simply supported beam with a lateral spring connected to point R and acting in x direction. See Figure 1.22.

When the beam is subjected to any type of dynamic loads in *x* direction, every point of the beam other than the points connected to supports move in *x* direction. At the point R attached to the spring with stiffness *k* the value of the displacement is given by *x*. In this case the effect of the spring attached to the point R on the beam is a resistant force *F*.
The spring resistant force is given by:

$$F = kx \tag{1.53}$$

In term of energy the spring effect can be expressed as additional strain energy *Us* to the energy produced by the motion of the system. This additional energy produced by the spring can be defined as follows:

$$Us = \frac{1}{2}kx^2 \tag{1.54}$$

Effect of dashpot

As mentioned before the dashpot is used to dissipate the kinetic energy of a mechanical system. Otherwise, the dashpot is a passive device that is means it has no force output. Thus, it is a device used to reduce the velocity of a dynamic structure by motion damping effect. By this way, a dashpot is a shock absorber. The effects of the dashpot on structures are summarized in the following points: it provides a protection of the structure against damage and violent or unexpected response caused by shock and vibration, reduce the impact of vibration on structures, improve the stability of the structures against noise without increasing the elements dimensions and using extra materials. So it improves the structures dynamic behavior with low cost.
In motion, the dashpot generate a resisting force which rises to equal the force of the acting load subjected to the structure, reaching a zero net force. This leads to zero acceleration and constant velocity.

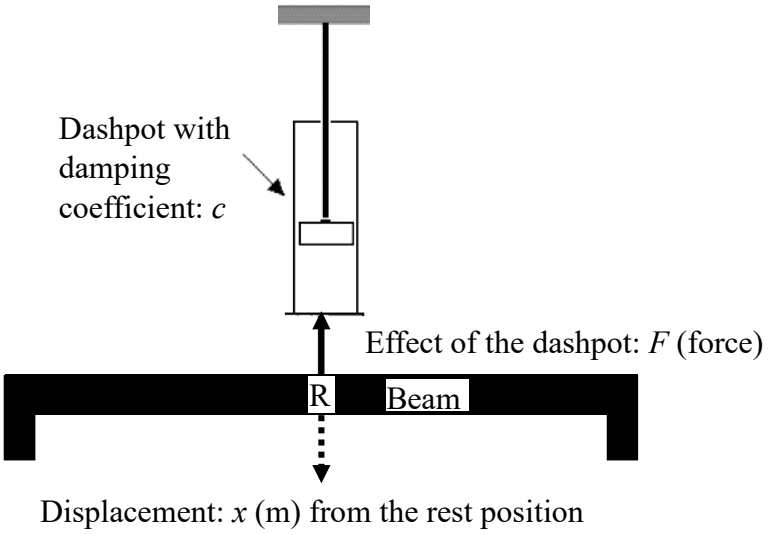

Figure 1.23: Effect of a dashpot on the beam dynamic behavior.

To clarify the effect of dashpot on the dynamic behavior of the beam. Let us take as example a simply supported beam with a lateral dashpot connected to point R and acting in *x* direction. See Figure 1.23.
When the beam is subjected to any type of dynamic loads in *x* direction, every point of the beam other than the points connected to supports move in *x* direction. At the point R attached to the dashpot with damping coefficient *c* the value of the displacement is given by *x*. In this case the effect of the dashpot attached to the point R on the beam is a resistant force *F*.
The dashpot resistant force is given by:

$$F = c\frac{dx}{dt} \tag{1.55}$$

In term of energy the dashpot effect can be expressed as additional strain energy Γ_d to the energy produced by the motion of the system. This additional energy produced by the dashpot can be defined as follows:

$$\Gamma_d = c\left(\frac{dx}{dt}\right)^2 \tag{1.56}$$

Superposition

In dynamics, the benefits of using braces in 3D steel structures design is for vibration control. By using these elements, the structures become less sensitive to uncertainties in vibrations or ground motion. Minor damage at the design level event means immediate reoccupation. The performance of the braces is highly predictable, so they are much more reliable than conventional structural components. Even in case of larger-than-expected seismic events, damage will concentrate in the bracing system, where elements can be easily substituted to restore the complete functionality of the structure. Otherwise, bracing system minimize the need for strengthening measures of the beams, like increasing sections dimensions to resist against the dynamic loads.
Bracing system leads to a structures with high performance and help to optimize sections in the same time when they are subjected to dynamic loads. This is the feasible solution for structural design of the 3D steel structures resistible against vibrations.

1.5 Modeling linear vibrations of thin-walled beams

From the literature review it is well known that the linear vibration of thin-walled beams with arbitrary cross-sections exhibits with flexural-torsional coupled modes. otherwise, it is shown in the section 1.3 that the torsion for this types of sections is predominated with the warping effect. For this reason, it is necessary in for this types of beams to investigate a linear vibration model that take in consideration of these two important points. Thus, we decided to develop a beam model based on the Galerkin's approach, to formulate the dynamic equations of motion. Using Hamilton's principle, the finite element approach of the model is established. For more precision in the model, the effects of rotational inertial kinematic terms are considered. In the FE procedure the efficient model with minimum cost of calculation and that gives high precision solutions is based on the beam element with seven degree of freedom. In the model the 7^{th} degree of freedom is related to warping effect in the thin-walled beams sections that is indispensable in torsion computation for these types of sections.

1.6 Assessment of subject positioning

The understanding of the mechanical behavior of thin walled beam is essential to avoid planar failures of structures due to flexural-torsional behavior (lateral buckling stability). Mohri et al. [69] have developed a numerical method based on a non-linear stability model to calculate bar buckling and lateral buckling of unrestrained thin-walled open sections beams. The obtained lateral buckling loads or equivalent buckling moments are compared to the solutions of the eigenvalue problem obtained with Abaqus software. Then Mohri et al [70], settle analytical solutions that are derived for simply supported beam-column elements with bi-symmetric I sections under combined bending and axial forces using Vlasov's model for non-uniform torsion to determine lateral buckling of thin-walled beam-column elements. They found that the Saint-Venant theorem is not adequate in case of thin-walled section to solve torsion problem. Mohri et al [71] and [72] improved the model to take account of large torsion and warping effects is checked.

To study complex problem Mohri et al [70], used the finite element method. they implement a new beam element taking account of valsov's theorem and large torsion observed with thin walled beams. The results obtained with this element are compared to results calculated with beam and shell elements of Abaqus code. To study dynamics problems, Mohri et al [41], develop the basics of the free vibration behavior of pre-buckled and post-buckled thin-walled beams with open sections.

In our work we are interested in free and forced vibrations of thin walled beam and to introduce damping. The finite element method was used to solve this problem. Jacob and Belytschko [73], Liu and Quek [74] applied Hamilton's principle to develop the finite element equations. Direct Analysis method presented by Petyt [11] will be adopted in solutions.

Also Petyt [11] developed the general structure of motion equation, then he introduced 2 types of damping forces: structural, Rayleigh… (viscous damping). He has also formulated equations for steady state forced and free vibration. He used FEM for flexural vibration in beam and solving free vibration problem. Adding to this I refer to some subjects treated by Petyt [11] related to the present work like: solution methods for eigenvalue problem, harmonic response, modal analysis, response to periodic excitation, transient response, modal analysis.

Rao et. al [44] work on fundamental concept of vibration, outline of the history type of vibration and harmonic, different methods to derive equation of motion in free vibration case: newton 2nd law of motion, method d'Alembert principle, principle of virtual displacement, principle of conservation of energy and their solutions.

In relation to our studies we also benefit from these subjects treated by Rao [44]:

-harmonically excited vibration aspect of resonance, beats, amplitude ratio, phase angle, steady state vibration.

-Determination of natural frequency and mode shapes using eigenvalue (natural frequencies) and eigenvectors (mode shape) for multi degree of freedom different methods: Rayleigh, Holzer's, matrix iteration method, Jacobi's method.

-Study the methods of deriving the equation of motion for continues systems (beam) using boundary conditions.

-Vibration control using vibration monographs and vibration criteria to determine acceptable levels of vibration, and some methods to vibration control changing stiffness K, mass M, or adding damping C.

-Numerical integration methods of motion equations in time domain. The most adopted methods are Runge-Kutta, Houbolt, Wilson and Newmark, see the reference [75].

It is important to note that Newmark method is widely used in the research of structural dynamics and nonlinear dynamics. The advantages of this method are first that when solving structural dynamic equations Newmark method is for solving second-order ODEs directly while Runge-Kutta methods are for solving first-order ODEs. Adding to this, the order of accuracy for Newmark method is second-order. There are several variants of Runge-Kutta method with different orders of accuracy, up to fourth-order. So with Newmark method one can solve second-order ODEs directly without having to convert them into state-space which is a must for Runge-Kutta methods. This means fewer DOFs, hence lower computational cost, when compared to the other methods.

1.7 Objectives of research topic

Many objectives can be dressed for this PHD work. They are listed below:

- The vibration behavior (free and forced vibration) of beams is limited to 2D pure bending according to the classical beam theory. The effects of rotary inertia are neglected. For design, analytical solutions in this case are available in [1, 76].

- In presence of torsion, the vibration behavior is limited to shaft vibration according to the Saint-Venant theory. Again, analytical solutions exist in literature [2, 3, 12]

- The bending and torsion vibration are uncoupled.

However, the behavior of unrestrained beams is in 3D context. This means that the strong and weak bending modes should be present with torsion modes. Again, warping is important and can control the behavior of torsion modes. Moreover, in presence of arbitrary cross sections, coupling is present. 3D flexural-torsional vibration modes are frequent. Thus, planar behavior of such structures is known to be an exception rather than a rule. The analytical solutions are rather scant and limited to some simply design cases.

The first objective of the present work is to assess the vibration behavior of thin-walled beams with open sections. The analysis is undertaken in 3D context with no assumption

on the cross section geometry. When possible analytical solutions are carried out for the flexural-torsional vibration modes in presence of flexural-torsional coupling, warping and rotary inertia effects. These solutions seem to be more general, since the 2D case can be straightforward when the additional terms are disregarded.

Analytical solutions for the flexural-torsional free vibration of 3D beams with open sections are limited to some representative boundary conditions. In more general cases, numerical procedures are believed. The 3D beam elements implemented in the commercial codes are not accurate and fail in presence of torsion warping, and arbitrary cross sections. After testing a large number of models using Abaqus and Adina, it is proven that Abaqus code fails in presence lateral buckling and nonlinear behavior of beams with arbitrary cross sections. The warping DOF is not available. Recourse to shell elements is always followed in literature. See [69, 70]. In Adina code, arbitrary cross sections are possible but it is difficult to apply loads on top or bottom flanges. Otherwise, in the developed FEM it is easy to access to the mass and stiffness matrices by adding terms related to bracing elements. Investigation of accurate models for the flexural-torsional behavior of thin-walled beams is then necessary.

In the present study, the finite element approach is followed in the study. For this aim, 3D beams allowing warping are adopted in the free and forced vibration analyses. In forced vibration, damping is considered according to Rayleigh approach.

In engineering applications, the analytical and numerical models need to be checked according to test research and experimental benchmark solutions. Extensive research is devoted to the static behavior of thin-walled beams. In free and forced vibration, scant results were published and always limited to free vibration analysis. In the present work a large part is devoted to the experimental dynamic flexural-torsional behavior of thin-walled beams. The experimental setup is described and test results are compared to the analytical and numerical results derived in the analytical and numerical parts.

In order to improve the structure strength against lateral and torsion vibration modes and to save materials by getting optimum sections, one possible solution is the increase of stiffness by adding discrete or distributed elastic springs (elastic supports). The elastic spring contribute in the elastic stiffness matrix of the structure. By increasing the stiffness constant of the elastic support, the vibration behavior (frequencies and modes) vary accordingly. Other solution can be used is adding viscoelastic braces to control vibration. One gets then the case of braced structures commonly encountered in design of real structures. To illustrate the effect of elastic springs on the vibration behavior of thin-walled beams let us present the following example for a simply supported beam under rigid supports (Figure 1.24). For this beam vibration modes for n=1 to 3 are depicted in the same figure.

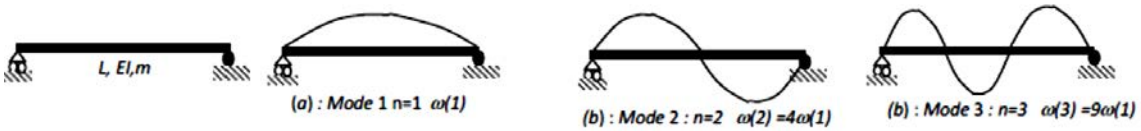

Figure 1.24: Free vibration modes of simply supported beam with rigid supports.

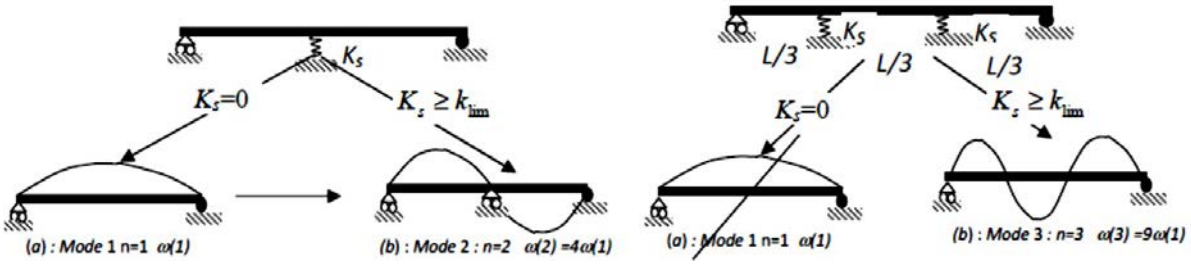

Figure 1.25: Free vibration modes for Simply supported beam with intermediate elastic springs.

For vibration control, the engineer is asked for improved solutions for vibration behavior. The lower eigenfrequencies can be removed by adequate elastic supports. The followings solutions can be adopted if we are interested by a particular mode (Figure 1.25). In Figure 1.25a, when the stiffness K_s is sufficient, one can remove the first mode and goes directly to mode 2 where the eigenfrequency is 4 times higher than the first. In presence of 3 elastic supports, we get directly to the third mode with natural frequency 9 times higher than the first.

This procedure can be followed in the case of thin-walled in presence in 3D vibration modes when bending and torsion modes are present and can be strengthened by adequate elastic supports. Moreover, under forced vibrations, viscous springs can be adopted in order to reduce displacements structures near the resonance.

The work is followed by analytical and numerical simulations using a home-made code (implemented on Matlab) and commercial code (Abaqus, Adina) to study the effect of viscoelastic intermediate braces and to carry out the optimum solutions for different cases of sections and boundary conditions. Validation by test setup of beams with intermediate braces is also achieved.

'The finite element model investigated for the behavior of unrestrained 3D beams is extended to braced beams. For this aim, elastic springs are incorporated in the 3D beam element developed on Mohri [70].'
It is important to remind that in civil engineering recourse to this solution is frequent. This is the case in braced beams and columns in buildings or lateral bracing in bridges (Figure 1.26).

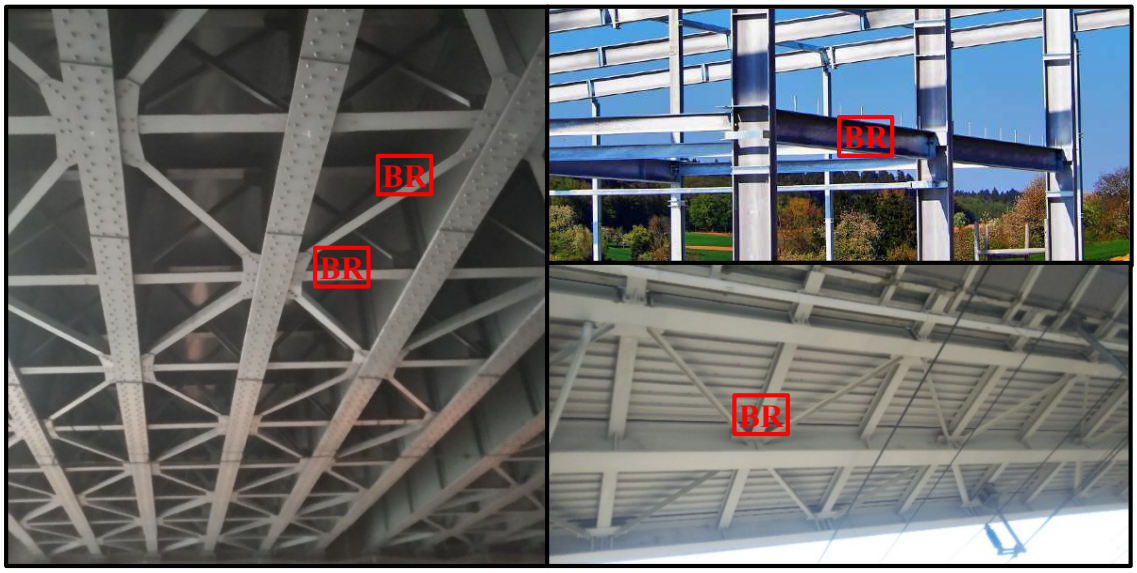

BR : Braces

Figure 1.26: Practical example of using braces in bridges and buildings.

These solutions are adopted in practice, but only empirical procedure is known. It is known that without these secondary elements the full strength of the building is not guaranteed and risk of failure due to out of plane deformations should be dominant.
Other solution is using discrete viscous dampers (dashpots) in parallel with elastic springs to control displacements of structure when it is subjected to dynamic forces, in this case modes, frequencies and structure displacements are controlled.
The important points to be studied are the number, distribution, and required stiffness and damping factor to reach the optimal design.
For vibration control, the engineer is asked for improved solutions for vibration behavior. The lower eigenfrequencies can be removed by adequate elastic supports. The followings solutions can be adopted if we are interested by a particular mode. when the spring stiffness is sufficient, one can remove the first mode and goes directly to mode 2 where the eigenfrequency is 4 times higher than the first. In presence of 3 elastic supports, one gets directly to the third mode with natural frequency 9 times higher than the first.
This procedure can be followed in the case of thin-walled in presence in 3D vibration modes when undesirable lateral bending and torsion modes are present and; can be strengthened by adequate elastic supports. Moreover, under forced vibrations, viscous springs can be adopted in order to reduce displacements structures near the resonance.
The work is followed by analytical and numerical simulations using a home-made code and commercial codes: Abaqus, Adina…. etc. Finally, test setup is also adopted in this study to validate theoretical and numerical solutions.
In the present work assessing Thin-walled structures and beams is performed using the followings items of the 3D behavior of thin-walled beams:

- Flexural-torsional linear behavior.
- Flexural-torsional free vibration.
- Forced vibration of under 3D loadings.

In these items, analytical solutions are investigated for beams under classical boundary conditions. The finite element approach is followed in presence of arbitrary loads and boundary conditions. The free and force vibration behaviors are studied by test campaign where some beams are tested in free and forced vibration at the LEM3 laboratory.

The previous models applied for unrestrained 3D beams, are extended to restrained beams in presence of discrete or continuous springs in 3D context. For the purpose, the FEM investigated in Mohri [70], is extended by adding flexural-torsional springs. The static and dynamic behavior of braced beams becomes possible.

Moreover, in forced vibration, effects of elastic springs viscous dashpots are included. The work contains the following parts.

1.7.1 Free vibration of beams in flexural-torsional behavior

In the present study, the free vibration of thin-walled beams is studied by analytical, numerical and experimental approaches. Analytical solutions for free vibration problem are carried out taking in consideration the rotary inertia terms. So, the natural frequencies for *n* modes are computed with high accuracy. The analytical solution developed in the cases of simply supported beams, cantilever beams, clamped-clamped beams, with different sections types: doubly symmetric like IPE section, singly symmetric cross sections and arbitrary sections.

Analytical solutions are limited to simple cases. To be more general, the finite element approach of the present model is implemented. The vibration modes (eigenfrequencies and vibration modes) are obtained by solutions classical eigenvalue problem.

Scant experimental works on the vibration behavior of thin-walled beams in free or forced vibration of thin-walled beams. For this aim, an extensive campaign has been adopted by the laboratory team in order to assess the vibration behavior of beams with arbitrary cross sections and boundary conditions.

All the solutions carried out in the present study are validated by comparisons to other simulations obtained from some commercial codes and some benchmark solutions available in the literature.

1.7.2. Forced vibration analysis of thin-walled beams

Carrying out the dynamic response spectra (displacements, accelerations for any point of the beam) using the modal analysis method. The response spectra are carried out in the frequency domain. Harmonic excitation force or moment or random can be applied to this beam in any chosen point. Base motion excitation is also treated using the present FEM. The maximum values of displacement ‘resonance’ are observed near the eigenfrequencies.

The same procedure used previously is applied to solve forced vibration problem:

-Analytical method: Presenting the existing problem solution formulation.

-Numerical part: the FEM is developed to solve forced vibration problem. Some examples with our code are compared to Abaqus and Adina commercial codes to validate results.

- Experimental part:

Tests on beams with different boundary conditions and a non-symmetric section. To do this, we propose to study a specimen of thin-walled beams with arbitrary cross-sections. In this part the electrodynamic shaker machine is used to carry out the acceleration and displacement response spectra of some chosen points. Acceleration sensor are used to record the spectra and to control the vibration frequencies and the load.

1.7.3. Effect of the elastic and viscous springs on vibration control

The elastic springs added to structures increase their natural frequency. Otherwise, the displacement amplitude of the structures near to resonance can be reduced by introducing a power-dissipation mechanism (dashpots).

Therefore, by introducing elastic springs the vibration of the structure can be controlled by eliminating the undesirable vibration modes. Moreover, by adding dashpots in some points of the beams, the displacement of the structure near to the natural frequencies is controlled.

Consequently, this procedure can be followed for thin-walled beams in presence of 3D vibration modes. When bending and torsion modes are present, lateral and torsion viscoelastic springs should be used to improve the dynamic behavior of the structures. The optimal positions of the additional viscoelastic springs and their properties should be studied in order to obtain an optimal vibration control. The effect of adding lateral elastic springs to the beam is demonstrated in Figure 1.25.

The work is followed by analytical and numerical simulations using a home-made code (implemented on Matlab) and commercial code (Abaqus, Adina) to study the effect of viscoelastic intermediate braces and to carry out the optimum solutions for different cases of sections and boundary conditions. Validation by test setup of beams with intermediate braces is also achieved.

1.8 Conclusion

Chapter 1 provided an overview about thin-walled beams. The principle manufacturing processes of these elements have been detailed. The importance of these structural elements in different engineering domains has been illustrated. Moreover, the features and the mechanical characteristics of thin-walled beams has been also detailed. Next, a literature review was conducted to explore the available information about static and dynamic behavior of thin walled beams. Afterward, an analysis study was made to the existing studies in the literature. Based on that, different interpretations have been endorsed. The first one is that in literature the tin-walled beams have been studied in both static and dynamic using analytical and semi-analytical methods. But only simple cases of sections and boundary conditions have been investigated, especially in free vibration. The most of works treated the simply supported boundary conditions with bi-symmetric or mono-symmetric sections. The kinetic rotary terms were always neglected in the previous studies also the warping effect sometime was not taken in consideration. Otherwise, the finite element approach has been adopted in free vibration using commercial codes and some developed elements. However, in this case it is remarkable that commercial codes are always based on shell elements, which lead to a long calculation time. Some other studies adopted the beam element in commercial code to investigate the thin-walled beams. However, the warping effect is not taken in consideration in the boundary conditions in some commercial codes and the beam element fails in some cases of sections or boundary condition which lead to singular results. In-house codes based on a beam elements have been also adopted in the literature, nevertheless there are inaccessible and limited to some types of sections and used for free vibration only.

Otherwise, damping types stated in this chapter and the Rayleigh viscous model was adopted later in the forced vibration in the present study. On the other hand, Fourier Transformation method has been detailed and used later on to convert signals from time to frequency domain. The effect of elastic springs and viscous springs has been also introduced. Then the effect superposition of these elements has been detailed. Based on these studies the model of vibration of thin-walled beams, objectives of research work and topics have been defined. Based on the literature analysis the objectives of the present study are proposed. First, the 3D flexural-torsional behavior of thin-walled open sections beams is discussed. It is shown that torsion exhibit with warping effect, so Saint-Venant theorem is not adequate to solve torsion problem in case of thin-walled section. Thus, the requirement of non-uniform torsion theory for this type of beams. Otherwise, it is necessary to develop an adequate model for thin-walled beams with open cross sections to investigate the dynamic behavior of these elements. A 3D beam model for flexural-torsional coupling has been proposed. Then, based on the developed model the analytical solutions will be carried out and the finite element approach will be developed in the next chapters. After that, the validation of these solutions will be by comparing to benchmark results and using experimental study. Adding to this, literature review on vibration control and modeling linear vibrations of thin-walled beams are presented in this chapter. Then, by analyzing this bibliographic review, we decided to go further by using the developed finite element approach to study the dynamic behavior of braced beams. These proposed braces elements can be used to improve the dynamic behavior of 3D thin-walled beams.

Thus, in this chapter the problematic, the framework and the means to use in the present study have been defined well. Finally, the objectives of research topic have been clearly illustrated at the end of this chapter.

Chapter 2 Analytical method for the vibration behavior of thin-walled beams

2.1 Introduction

In this chapter, a beam model is developed for the dynamic behavior, especially for vibration, of thin-walled beams with arbitrary cross sections. Vibration behaviors of flexural-torsional and lateral pre-buckled thin-walled beams with open sections are investigated. Based on present beam model and on the Galerkin's approach, dynamic equations of motion are formulated for linear vibration analysis. Using Hamilton's principle, the finite element approach of the model is established. In the model, the effects of rotational inertial kinematic terms are considered. Analytical formations of natural frequencies are given, closed form solutions of the eigenvalues for doubly symmetric, singly symmetric, and arbitrary cross sections are developed for some practical cases used in design. Fundamental eigenfrequencies are given for simply supported beams, cantilever beams and double fixed beams.

2.2 Free and forced vibration analyses

2.2.1 Kinematics of the model

A straight element with thin-walled open section shown in Figure 2.1 is inspected in the following work. The rectangular system of coordination (*G,x,y,z*) is used, with *G* is the cross section center. The x-axis is parallel to the length of the beam, *y* and *z* axis are assumed as the principle axis of beam cross-section. The shear center was noted *C*, its co-ordinates in *Gyz* are (y_c, z_c). A point *M* on the section contour have the following co-ordinates (y, z, ω), where ω is the sectorial co-ordinate of the point used in Vlasov's model for non-uniform torsion [5]. Based on the usual assumptions of the theory of thin-walled elements, the displacements components of *M* can be derived from those of the shear center and centroid points. Moreover, in the presented model it considered that:

- No distortion deformation of the section, which denote that the cross section contour is rigid in its plane.

- No shear deformation in the section mean surface.

Therefore, the transversal displacements v_M and w_M components of point *M* are the following:

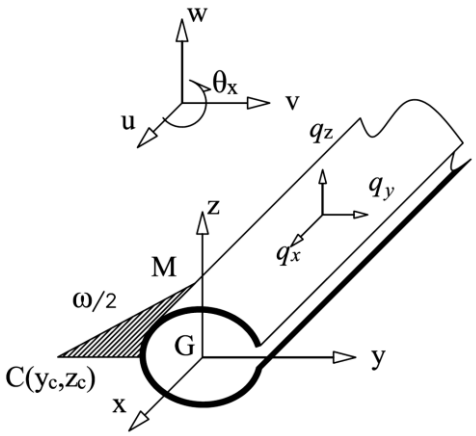

Figure 2.1: Thin-walled open section element.

$$v_M = v - (z - z_c)\sin\theta_x - (y - y_c)(1 - \cos\theta_x) \tag{2.1}$$

$$w_M = w + (y - y_c)\sin\theta_x - (z - z_c)(1 - \cos\theta_x) \tag{2.2}$$

In these relationships, *v, w* and θ_x are respectively the bending displacement in the *y* and *z* directions and the torsion angle of the shear point.

The axial displacement u_M is derived from the hypothesis that shear deformation is null in the mean surface. Let us introduce at a point *M* of the section, a curvilinear reference *Mtn*, having curvilinear co-ordinate *s*. Let us denote v_t and w_t the displacement components of *M* in the curvilinear reference presented in Figure 2.2. By taking in consideration the second assumption, the Green shear deformation along the contour verifies the following condition:

$$\varepsilon_{xs} = \frac{\partial u_M}{\partial s} + \frac{\partial v_t}{\partial x} + \frac{\partial v_t}{\partial x}\frac{\partial v_t}{\partial s} + \frac{\partial w_t}{\partial x}\frac{\partial w_t}{\partial s} = 0 \tag{2.3}$$

Otherwise, the displacements v_t and w_t can be deduced from equations (2.1,2):

$$v_t = v\cos\alpha + w\sin\alpha + h\sin\theta_x + r(\cos\theta_x - 1) \tag{2.4}$$

$$w_t = -v\sin\alpha + w\cos\alpha + r\sin\theta_x - h(\cos\theta_x - 1) \tag{2.5}$$

In the equations above, α denotes the angle between the *y* axis and the tangent *Mt. h*(*s*) *and r*(*s*) are the co-ordinates of the shear center *C* in *Mtn*. Otherwise, we have:

$$\frac{\partial h}{\partial s} = 0; \frac{\partial r}{\partial s} = 1; dy = ds\ \cos\alpha\ ; dz = ds\ \sin\alpha; \omega = \int_s h\ ds \tag{2.6a-e}$$

Therefore, u_M is gotten by integration of equation (2.3) with respect to the variable *s* and using relationships equations. (2.6a-e) as follows:

$$u_M = u - y(v'\cos\theta_x + w'\sin\theta_x) - z(w'\cos\theta_x + v'\sin\theta_x) - \omega\theta_x' \tag{2.7}$$

In this formulation (.)' denotes the *x*-derivate and *u* is the axial displacement of the centroid, in *x* direction.

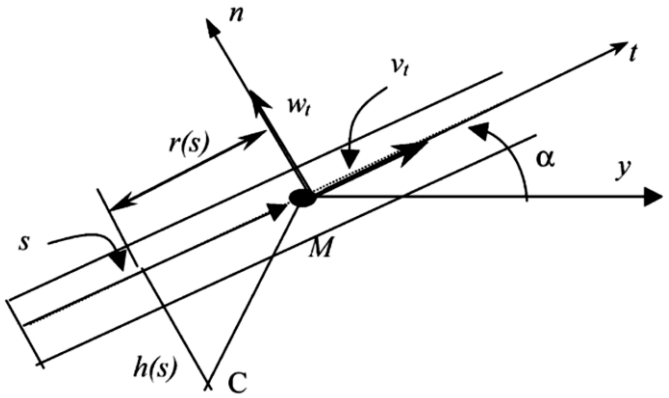

Figure 2.2: Section contour with tangential and normal axis.

Then, the expressions of displacements of point M are given by the equations (2.1), (2.2) and (2.7). Considering small torsion, using the approximation (*cos* $\theta_x = 1$) and (*sin* $\theta_x = \theta_x$) and disregarding the resulting nonlinear terms, the classical relationships used in Vlasov's model are straightforward:

$$u_M = u - yv' - zw' - \omega\theta_x' \tag{2.8}$$

$$v_M = v - (z - z_c)\theta_x \tag{2.9}$$

$$w_M = w + (y - y_c)\theta_x \tag{2.10}$$

Based on the kinematics equations (2.1-3) a finite element model has been derived under static loads for the nonlinear behaviour, for buckling and lateral buckling analyses [78, 79]. In the present work attention is for the behaviour under dynamic loads. In the framework of free vibration and linear dynamics, the relationships equations. (2.8-10) are sufficient. They are adopted in this study. Furthermore, the Green strain tensor which integrates large displacements is the following:

$$\varepsilon_{ij} = \frac{1}{2}\left(\frac{\partial u_i}{\partial x_j} + \frac{\partial u_j}{\partial x_i} + \frac{\partial u_k}{\partial x_i}\frac{\partial u_k}{\partial x_j}\right),\ i, j, k = 1,2,3 \tag{2.11}$$

Therefore, the strain tensor components for thin-walled beams are given by:

$$\varepsilon_{xx} = u_M' + \frac{1}{2}\left((v_M')^2 + (w_M')^2\right) \tag{2.12}$$

$$\varepsilon_{xy} = \frac{1}{2}\left(\frac{\partial u_M}{\partial y} + \frac{\partial v_M}{\partial x} + \frac{\partial v_M}{\partial x}\frac{\partial v_M}{\partial y} + \frac{\partial w_M}{\partial x}\frac{\partial w_M}{\partial y}\right) \tag{2.13}$$

$$\varepsilon_{xz} = \frac{1}{2}\left(\frac{\partial u_M}{\partial z} + \frac{\partial w_M}{\partial x} + \frac{\partial v_M}{\partial x}\frac{\partial v_M}{\partial z} + \frac{\partial w_M}{\partial x}\frac{\partial w_M}{\partial z}\right) \tag{2.14}$$

The insertion of equations (2.1), (2.2) and (2.3) into equations (2.12) to (2.14), gives:

$$\varepsilon_{xx} = \varepsilon_1 + \varepsilon_2 \tag{2.15}$$

In which:

$$\varepsilon_1 = u' - y(v''\cos\theta_x + w''sin\,\theta_x) - z(w''\cos\theta_x + v''sin\,\theta_x) - w\theta_x'' \tag{2.16}$$

$$\varepsilon_2 = \frac{1}{2}\left(v'^2 + w'^2 + R^2\,\theta_x'^2\right) - y_c\theta_x'(w'\cos\theta_x - v'\sin\theta_x) + z_c\theta_x'(v'cos\,\theta_x + w'sin\,\theta_x) \tag{2.17}$$

$$\varepsilon_{xy} = -\frac{1}{2}(z - z_c + \frac{\partial\omega}{\partial y})\theta_x' \tag{2.18}$$

$$\varepsilon_{xz} = \frac{1}{2}(y - y_c - \frac{\partial\omega}{\partial z})\theta_x' \tag{2.19}$$

$$R^2 = (y - y_c)^2 + (z - z_c)^2 \tag{2.20}$$

In the equations (2.15) the strains components depend nonlinearly on the displacements (u, v and w) and torsion angle θ_x. However, using Vlasov's approximations equations (2.8) to (2.10) the following relationships are retained for the deformation components:

$$\varepsilon_{xx} = u' - yv'' - zw'' - \omega\theta_x'' \tag{2.21a}$$

$$\varepsilon_{xy} = -\frac{1}{2}(z - z_c + \frac{\partial\omega}{\partial y})\theta_x' \tag{2.21b}$$

$$\varepsilon_{xz} = \frac{1}{2}(y - y_c - \frac{\partial\omega}{\partial z})\theta_x' \tag{2.21c}$$

For this aim, the derivation of strain, the kinetic energies followed with the external loads work are needed in derivation of the motion equations.

2.2.2 Variational formulation of motion equations

In order to derive the dynamic motion equations, Hamilton's principle is applied, based on the variational principle for dynamical systems defined by:

$$\begin{cases} \int_{t_1}^{t_2} \delta(U - T - W)\mathrm{d}t = 0 \\ \delta q(t_1) = \delta q(t_2) \end{cases} \tag{2.22}$$

Where U, T and W define respectively the strain energy, the kinetic energy and the external load work.

In what follow and in the highlight of the finite element approach, the matrix formulation is adopted. For this aim, let us introduce the following trial vectors needed for the different parts of equation system (2.22):

$$\{q\}^t = \{u\ v\ w\ \theta_x\}$$

$$\{\varphi\}^t = \{u'\ v'\ w'\ \theta_x'\ v''\ w''\ \theta_x''\ \theta_x\}$$

$$\{\gamma\}^t = \{u'\ v''\ w''\ \theta_x\ \theta_x''\}$$

$$\{\Sigma\}^t = \{N\ M_z\ M_y\ M_{sv}\ B_\omega\}$$

$$\{f\}^t = \{q_x\ q_y\ q_z\ m_x\} \tag{2.23a-e}$$

where $\{\ \}^t$ denotes the transpose operator. The strain energy variation δU is given by:

$$\delta U = \int_L \int_A (\sigma_{xx}\,\delta\varepsilon_{xx} + 2\sigma_{xy}\,\delta\varepsilon_{xy} + 2\sigma_{xz}\,\delta\varepsilon_{xz})\,dAdx \tag{2.24}$$

Where (σ_{xx}, σ_{xy} , σ_{xz}) are the beam stress (Piola-Kirchhoff stress tensor) components and (ε_{xx}, ε_{xy}, ε_{xz}) are the strain components defined in equations (2.21).

The strain energy variation can be expressed as function of the stress resultants acting on cross-section A of the thin-walled element in the deformed state as the followings:

$$N = \int_A \sigma_{xx} dA\,; \qquad M_y = \int_A \sigma_{xx} z dA\,; \qquad M_z = -\int_A \sigma_{xx} y dA\,;$$

$$B_\omega = -\int_A \sigma_{xx}\omega dA\,; \qquad M_{sv} = \int_A \left(\sigma_{xz}\left(y - y_c - \frac{\partial\omega}{\partial z}\right) - \sigma_{xy}\left(z - z_c + \frac{\partial\omega}{\partial y}\right)\right) dA \tag{2.25}$$

In these equations, N is the axial force, M_y and M_z are the bending moments, B_ω is the bimoment and M_{sv} is the Saint-Venant torsion moment presented in Figure 2.3.

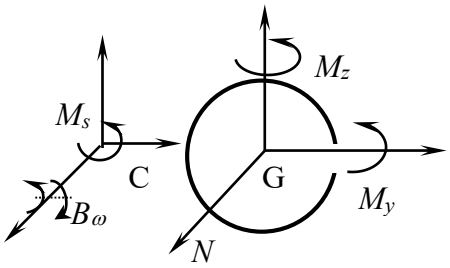

Figure 2.3: Section stress resultants.

Based on equation (2.25) and after integration over the cross section, the strain energy can be expressed as:

$$\delta U = \int_L \left(N\delta u' + M_z\delta v'' - M_y\delta w'' + B_\omega\delta\theta_x'' + M_{sv}\delta\theta_x'\right) dx \tag{2.26}$$

The inertial moments I_y and I_z about principle axes y and z, the Saint-Venant torsion and warping constants I_t and I_ω are derived from the following relationships:

$$I_y = \int_A z^2 dA;\; I_z = \int_A y^2 dA;\; I_\omega = \int_A \omega^2 dA;\; I_t = \int_A r^2 dA \tag{2.27}$$

Under linear and elastic behavior assumption, the stress resultants expressed in the principal axes are derived from relationships equation (2.25) and lead to:

$$N = EA(u');\; M_y = -EI_y(w'');\; M_z = EI_z(v'');\; B_\omega = EI_\omega(\theta_x'');\; M_{sv} = GI_t(\theta_x') \tag{2.28}$$

Where E and G are respectively the Young's and shear modulus. A denotes the cross section area. According to the vector definition equation (23), the strain energy variation and the material behavior relations written in matrix shape form are the following:

$$\begin{cases} \delta U = \int_L \{\delta\gamma\}^t \{\Sigma\} dx \\ \{\Sigma\} = [D]\{\gamma\} \end{cases} \tag{2.29}$$

$\{\Sigma\}$ and $\{\gamma\}$ define the stress and the strain vectors. Their components have been defined in equations (20c,d). $[D]$ is the matrix behavior. It includes the material constants and the cross section characteristics.

The kinetic energy T of a straight thin-walled element with constant mass density ρ is given by:

$$T = \frac{1}{2}\int_L \int_A \rho\left[\left(\frac{\partial u_M}{\partial t}\right)^2 + \left(\frac{\partial v_M}{\partial t}\right)^2 + \left(\frac{\partial w_M}{\partial t}\right)^2\right] dA dx \tag{2.30}$$

After integration over the cross section and putting ($m=\rho A$), one gets the following expression for T:

$$T = \int_L m\left[\left(\frac{\partial u_M}{\partial t}\right)^2 + \left(\frac{\partial v_M}{\partial t}\right)^2 + \left(\frac{\partial w_M}{\partial t}\right)^2\right] dx \tag{2.31}$$

In the following, the time derivation is adopted by $\left(\frac{\partial X}{\partial t} = \dot{X}\right)$, the kinetic energy variation (δT) is given by:

$$\begin{aligned} \delta T = \int_L m\left(\dot{u}\delta\dot{u} + \dot{v}\delta\dot{v} + \dot{w}\delta\dot{w} + I_0\dot{\theta}_x\delta\dot{\theta}_x\right)dx + \int_L m\left(z_c\left(\delta\dot{v}\dot{\theta}_x + \dot{v}\delta\dot{\theta}_x\right) - \right. \\ \left. y_c\left(\delta\dot{w}\dot{\theta}_x + \dot{w}\delta\dot{\theta}_x\right)\right)dx + \int_L \left(m\frac{I_z}{A}\left(\dot{v}'\delta\dot{v}'\right) + m\frac{I_y}{A}\left(\dot{w}'\delta\dot{w}'\right) + \right. \\ \left. m\frac{I_\omega}{A}\left(\dot{\theta}_x{}'\delta\dot{\theta}_x{}'\right)\right)dx \end{aligned} \tag{2.32}$$

Based on trial vectors defined in equation (2.23), kinetic energy variation δT becomes:

$$\delta T = \int_L \{\delta\dot{q}\}^t [M_1]\{\dot{q}\}dx + \int_L \{\delta\dot{\varphi}\}^t [M_2]\{\dot{\varphi}\}dx \tag{2.33}$$

$\{q\}$ and $\{\varphi\}$ are displacements and gradient vectors, defined in equations (2.23a, b).

$[M_1]$ and $[M_2]$ are mass matrices defined by:

$$[M_1] = m\begin{bmatrix} 1 & 0 & 0 & 0 \\ 0 & 1 & 0 & z_c \\ 0 & 0 & 1 & -y_c \\ 0 & z_c & -y_c & I_0 \end{bmatrix} \tag{2.34}$$

I_0 is the polar moment of inertia about shear center:

$$I_0 = \frac{I_y + I_z}{A} + y_c^2 + z_c^2 \tag{2.35}$$

$[M_2]$ is an 8x8 matrix. It includes the rotational terms effects in the kinetic energy. The non-vanished terms of this matrix are the following:

$$M_2(2,2) = \frac{mI_z}{A},\ M_2(3,3) = \frac{mI_y}{A},\ M_2(4,4) = \frac{mI_\omega}{A} \tag{2.36a-c}$$

In the present study, we admit that 3D loads (q_x q_y, q_z). The axial load q_x is applied on centroid axis and the bending (q_y, q_z) are on the cross section contour with eccentricities (e_y, e_z) from the shear point Figure 2.4a. These loads are similar to q_x applied on centroid axis and (q_y, q_z) moved to shear centre with an additional torsional moment m_x due to load eccentricities from *C*, Figure 2.4b. Then, the variation of external load work δW is given by:

$$\delta W = \int_L \left(q_x \delta u + q_y \delta v + q_z \delta w + m_x \delta\theta_x\right) dx \tag{2.37}$$

Based on vector definition equations (2.23a) and (2.23e), the matrix formulation of δW is:

$$\delta W = \int_L \{\delta q\}^t \{f\} dx \tag{2.38}$$

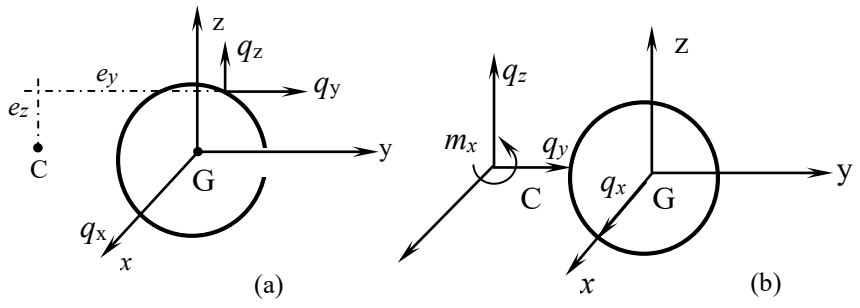

Figure 2.4: Applied loads components and equivalent load resultants.

The finite element formulation of δU, δT *and* δW derived in equations (2.29), (2.33) and (2.38) is undertaken hereafter.

2.2.3 Free vibration analysis

Vibration behaviors of flexural-torsional and lateral pre-buckled thin-walled beams with open sections are investigated in this part based on this model and on the Galerkin's approach, dynamic equations of motion are formulated for linear vibration analysis, analytical formations of natural frequencies for bi-symmetric, mono-symmetric sections and the associated eigenvalue problem to more complex sections are established for *n* modes. Fundamental frequencies are given for simply supported beams, cantilever beams and double clamped beams, with I sections Channel, Te and arbitrary sections, see Figure 2.5.
In what follow, for each case of section and boundary condition motion equations are solved to obtain eigenvalues (angular velocities, natural frequencies).

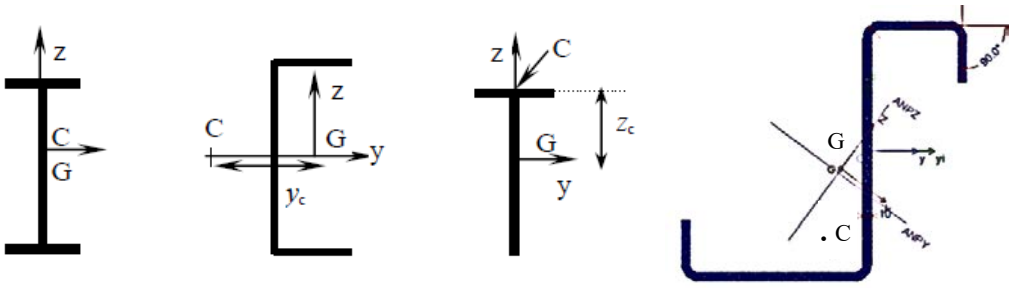

Figure 2.5: Types of thin-walled beams sections with gravity and shear centers.

2.2.3.1 Analytical solutions

Most of the analytical solutions deal with first vibration modes. In the present work, analytical solutions for higher modes of beams with any boundary conditions and arbitrary cross sections are investigated.

By inserting the analytical equations of the strain energy δU equation (2.26) and the help of material behaviour equation (2.28), the kinetic energy δT equation (2.32) and work of external loads δW equation (2.37) in the Hamilton's equation (2.22), leads to variational formulation of the governing equations in free vibration. Hereafter the development procedure of the motion equations.

$$\int_{t_1}^{t_2}\Big(\int_L \left(N\delta u' + M_z\delta v'' - M_y\delta w'' + B_\omega\delta\theta_x'' + M_{sv}\delta\theta_x'\right)dx - \int_L m\big(\dot{u}\delta\dot{u} + \dot{v}\delta\dot{v} + \dot{w}\delta\dot{w} + I_0\dot{\theta}_x\delta\dot{\theta}_x\big)dx - \int_L m\Big(z_c\big(\delta\dot{v}\dot{\theta}_x + \dot{v}\delta\dot{\theta}_x\big) - y_c\big(\delta\dot{w}\dot{\theta}_x + \dot{w}\delta\dot{\theta}_x\big)\Big)dx - \int_L \Big(m\frac{I_z}{A}(\dot{v}'\delta\dot{v}') + m\frac{I_y}{A}(\dot{w}'\delta\dot{w}') + m\frac{I_\omega}{A}(\dot{\theta}_x'\delta\dot{\theta}_x')\Big)dx - \int_L \left(q_x\delta u + q_y\delta v + q_z\delta w + m_x\delta\theta\right)dx\Big)\,\mathrm{dt} = 0 \quad (2.39)$$

By injecting the equations (2.28) in the equation below and after terms regrouping the following equation is gotten:

$$\int_{t_1}^{t_2}\int_L \Big(\big(EAu'\delta u' + EI_z v''\delta v'' + EI_y w''\delta w'' + EI_\omega \theta_x''\delta\theta_x'' + GI_t\theta_x'\delta\theta_x'\big) - m\big(\ddot{u}\delta u + \ddot{v}\delta v + \ddot{w}\delta w + I_0\ddot{\theta}_x\delta\theta_x\big) - m\Big(z_c\big(\delta\ddot{v}\theta_x + \ddot{v}\delta\theta_x\big) - y_c\big(\delta\ddot{w}\theta_x + \ddot{w}\delta\theta_x\big)\Big) - \Big(m\tfrac{I_z}{A}\big(\dot{v}'\delta\dot{v}'\big) + m\tfrac{I_y}{A}\big(\dot{w}'\delta\dot{w}'\big) + m\tfrac{I_\omega}{A}\big(\dot{\theta}_x'\delta\dot{\theta}_x'\big)\Big) - \big(q_x\delta u + q_y\delta v + q_z\delta w + m_x\delta\theta_x\big)\Big)\,dx\mathrm{d}t = 0 \qquad (2.40)$$

To solve the obtained equation (2.40), some integration, simplifications and terms regrouping are proceeded here after. First, the terms derived with respect to time in equation (2.40) are integrate by parts as follows:

$$\int_{t_1}^{t_2}\int_L (\ddot{u}\delta u)\,dx\mathrm{d}t = [\dot{u}\delta u]_{t_1}^{t_2} - \int_{t_1}^{t_2}\int_L (\dot{u}\delta\dot{u})\,dx\mathrm{d}t = \int_{t_1}^{t_2}\int_L (\dot{u}\delta\dot{u})\,dx\mathrm{d}t$$

$$\int_{t_1}^{t_2}\int_L (\ddot{v}\delta v)\,dx\mathrm{d}t = -\int_{t_1}^{t_2}\int_L (\dot{v}\delta\dot{v})\,dx\mathrm{d}t + \mathrm{BC}^*$$

$$\int_{t_1}^{t_2}\int_L (\ddot{w}\delta w)\,dx\mathrm{d}t = -\int_{t_1}^{t_2}\int_L (\dot{w}\delta\dot{w})\,dx\mathrm{d}t + \mathrm{BC}^*$$

$$\int_{t_1}^{t_2}\int_L \big(\ddot{\theta}_x\delta\theta_x\big)\,dx\mathrm{d}t = -\int_{t_1}^{t_2}\int_L \big(\dot{\theta}_x\delta\dot{\theta}_x\big)\,dx\mathrm{d}t + \mathrm{BC}^*$$

$$\int_{t_1}^{t_2}\int_L \big(\delta\ddot{v}\theta_x + \ddot{v}\delta\theta_x\big)\,dx\mathrm{d}t = -\int_{t_1}^{t_2}\int_L \big(\delta\dot{v}\dot{\theta}_x + \dot{v}\delta\dot{\theta}_x\big)\,dx\mathrm{d}t + \mathrm{BC}^*$$

$$\int_{t_1}^{t_2}\int_L \big(\delta\ddot{w}\theta_x + \ddot{w}\delta\theta_x\big)\,dx\mathrm{d}t = -\int_{t_1}^{t_2}\int_L \big(\delta\dot{w}\dot{\theta}_x + \dot{w}\delta\dot{\theta}_x\big)\,dx\mathrm{d}t + \mathrm{BC}^* \qquad (2.41a\text{-}f)$$

* BC: Boundary Conditions.

Otherwise, the simplification of the terms derived with respect to the variable *x* in the equation (2.40) leads to:

$$\int_{t_1}^{t_2}\int_L (u'\delta u')\,dx\mathrm{d}t = \int_{t_1}^{t_2}\int_L (u''\delta u)\,dx\mathrm{d}t + \mathrm{BC}^*$$

$$\int_{t_1}^{t_2}\int_L (\theta_x'\delta\theta_x')\,dx\mathrm{d}t = \int_{t_1}^{t_2}\int_L (\theta_x''\delta\theta_x)\,dx\mathrm{d}t + \mathrm{BC}^*$$

$$\int_{t_1}^{t_2}\int_L (v''_z\delta v'')\,dx\mathrm{d}t = \int_{t_1}^{t_2}\int_L \big(\delta v^{(4)}\delta v\big)\,dx\mathrm{d}t + \mathrm{BC}^*$$

$$\int_{t_1}^{t_2}\int_L (w''_z\delta w'')\,dx\mathrm{d}t = \int_{t_1}^{t_2}\int_L \big(\delta w^{(4)}\delta w\big)\,dx\mathrm{d}t + \mathrm{BC}^*$$

$$\int_{t_1}^{t_2}\int_L (\theta_x''\delta\theta_x'')\,dx\mathrm{d}t = \int_{t_1}^{t_2}\int_L \big(\theta_x^{(4)}\delta\theta_x\big)\,dx\mathrm{d}t + \mathrm{BC}^* \qquad (2.42a\text{-}e)$$

* BC: Boundary Conditions.

Moreover, the terms of equation (2.40) derived with respect to the variables x and time simplified hereafter:

$$\int_{t_1}^{t_2}\int_L (\dot{v}'_z\delta\dot{v}')\,dx\mathrm{d}t = \int_{t_1}^{t_2}\int_L (\ddot{v}''\delta v)\,dx\mathrm{d}t + \mathrm{BC}^*$$

$$\int_{t_1}^{t_2}\int_L (\dot{w}'_z\delta\dot{w}')\,dx\mathrm{d}t = \int_{t_1}^{t_2}\int_L (\delta\ddot{w}''\delta w)\,dx\mathrm{d}t + \mathrm{BC}^*$$

$$\int_{t_1}^{t_2}\int_L \left(\dot{\theta}'_x\delta\dot{\theta}'_x\right)dx\mathrm{d}t = \int_{t_1}^{t_2}\int_L \left(\ddot{\theta}''_x\delta\theta_x\right)dx\mathrm{d}t + \mathrm{BC}^* \qquad (2.43\text{a-c})$$

* BC: Boundary Conditions.

By injecting equations (2.41-2.43) in (2.40) and after terms regrouping, the following equation is obtained:

$$\int_{t_1}^{t_2}\int_L \Bigg(\left(EAu''\delta u + EI_z\delta v^{(4)}\delta v + EI_y\delta w^{(4)}\delta w + EI_\omega\theta_x^{(4)}\delta\theta_x + GI_t\theta''_x\delta\theta_x\right) - m\left(-\ddot{u}\delta u - \ddot{v}\delta v - \ddot{w}\delta w - I_0\ddot{\theta}_x\delta\theta_x\right) - m\left(-z_c\left(\frac{d^2\theta_x}{dt^2}\delta v\right) + y_c\left(\frac{d^2\theta_x}{dt^2}\delta w\right)\right) - \left(m\frac{I_z}{A}(\ddot{v}''\delta v) + m\frac{I_y}{A}(\ddot{w}''\delta w) + m\frac{I_\omega}{A}\left(\ddot{\theta}''_x\delta\theta_x\right)\right) - \left(q_x\delta u + q_y\delta v + q_z\delta w + m_x\delta\theta_x\right)\Bigg)dx\mathrm{d}t = 0 \qquad (2.44)$$

After arranging (2.44) in terms of the virtual displacement components, one gets:

$$\int_{t_1}^{t_2}\int_L \Big([EAu'' + m\ddot{u} - q_x]\delta u + \left[EI_z\delta v^{(4)} + m\ddot{v} + mz_c\frac{d^2\theta_x}{dt^2} - m\frac{I_z}{A}(\ddot{v}'') - q_y\right]\delta v + \left[EI_y\delta w^{(4)} + m\ddot{w} - my_c\frac{d^2\theta_x}{dt^2} - m\frac{I_y}{A}\ddot{w}'' - q_z\right]\delta w + \left[EI_\omega\theta_x^{(4)} + mI_0\ddot{\theta}_x - GI_t\theta''_x - m\frac{I_y}{A}(\delta\ddot{w}''\delta w) - m\frac{I_\omega}{A}\ddot{\theta}''_x - m_x\right]\delta\theta_x\Big)dx\mathrm{d}t = 0 \qquad (2.45)$$

The axial, bending and torsion motion equations are straightforward:

$$\delta u:\ m\frac{d^2u}{dt^2} + EAu'' = q_x$$

$$\delta v:\ m\left(\frac{d^2\mathrm{v}}{dt^2} - \underline{\frac{I_z}{A}\frac{d^4v}{dx^2dt^2}} + z_c\frac{d^2\theta_x}{dt^2}\right) + EI_z\left(v^{(4)}\right) = q_y$$

$$\delta w:\ m\left(\frac{d^2w}{dt^2} - \underline{\frac{I_y}{A}\frac{d^4w}{dx^2dt^2}} - y_c\frac{d^2\theta_x}{dt^2}\right) + EI_y\left(w^{(4)}\right) = q_z$$

$$\delta\theta_x:\ m\left(I_0\frac{d^2\theta_x}{dt^2} - \underline{\frac{I_\omega}{A}\frac{d^4\theta_x}{dx^2dt^2}} + z_c\frac{d^2v}{dt^2} - y_c\frac{d^2\mathrm{w}}{dt^2}\right) + EI_w{\theta_x}^{(4)} - GI_t\theta_x'' = m_x \qquad (2.46\text{a-d})$$

In these equations, the rotational terms are outlined. Let us remind when the terms are omitted, the classical motion equations are obtained [5, 33]. They are the following:

$$\delta u:\ m\frac{d^2u}{dt^2} + EAu'' = q_x$$

$$\delta v:\ m\left(\frac{d^2\mathrm{v}}{dt^2} + z_c\frac{d^2\theta_x}{dt^2}\right) + EI_z\left(v^{(4)}\right) = q_y$$

$$\delta w:\ m\left(\frac{d^2w}{dt^2} - y_c\frac{d^2\theta_x}{dt^2}\right) + EI_y\left(w^{(4)}\right) = q_z$$

$$\delta\theta_x:\ m\left(I_0\frac{d^2\theta_x}{dt^2} + z_c\frac{d^2v}{dt^2} - y_c\frac{d^2\mathrm{w}}{dt^2}\right) + EI_w{\theta_x}^{(4)} - GI_t\theta_x'' = m_x \qquad (2.47\text{a-d})$$

In the case of the free vibration all the applied loads vanish ($q_x = q_y = q_z = m_x = 0$) analytical solutions are possible according to known mode shape functions in agreement with the boundary conditions. For this aim, the displacement fields are approximated by:

$$\left(\frac{u(x,t)}{u_0}, \frac{v(x,t)}{v_0}, \frac{w(x,t)}{w_0}, \frac{\theta(x,t)}{\theta_0}\right) = f(x) \times g(t) \tag{2.48}$$

Where u_0, v_0 and θ_0 are displacement magnitudes. $f(x)$ is the space function depending on the boundary conditions of the beam. These solutions are explained hereafter for bending and torsion modes. For free vibration, the load terms vanish.

2.2.3.2 Free vibration solution attempts for simply supported beams

A simply supported beam in bending and torsion is depicted in Figure 2.6, the spatial and time functions obey to:

$$g(t) = e^{i\Omega t} \tag{2.49}$$

$$f(x) = \sin(\alpha_n x) \tag{2.50}$$

$$\text{With: } \alpha_n = \frac{n\pi}{L},\ n = 1,2\ldots N \tag{2.51}$$

In (2.49), Ω is the angular velocity. In (2.51), n is the vibration mode and N the number of modes under study.

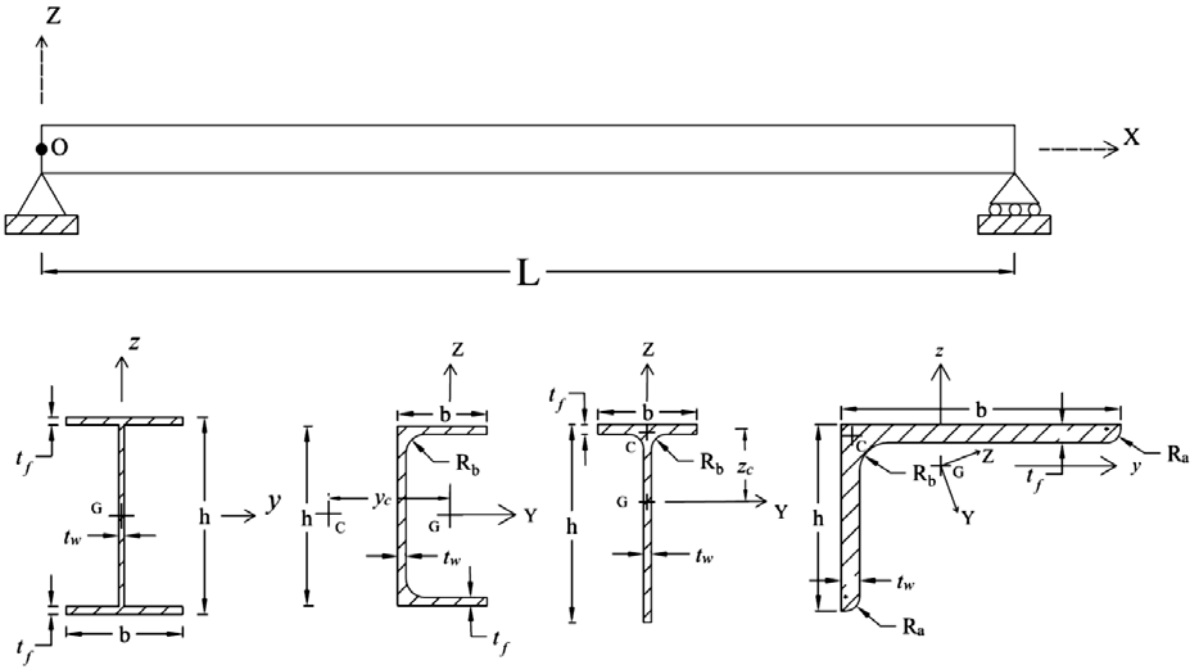

Figure 2.6: Simply supported beam with arbitrary cross-section.

Hereafter, displacements derivatives with respect to *x* and time are given by:

$$(v'(x,\mathrm{t}), w'(x,\mathrm{t}), \theta'(x,\mathrm{t})) = (v_0, w_0, \theta_0) g(t) \alpha_n \cos(\alpha_n x);$$

$$\left(v''(x,\mathrm{t}), w''(x,\mathrm{t}), \theta''(x,\mathrm{t})\right) = -(v_0, w_0, \theta_0) g(\mathrm{t}) \alpha_n^2 f(x);$$

$$(v'''(x,\mathrm{t}), w'''(x,\mathrm{t}), \theta'''(x,\mathrm{t})) = -(v_0, w_0, \theta_0) g(\mathrm{t}) \alpha_n^3 \cos(\alpha_n x);$$

$$(v^{(4)}(x,\mathrm{t}), w^{(4)}(x,\mathrm{t}), \theta^{(4)}(x,\mathrm{t})) = (v_0, w_0, \theta_0) g(\mathrm{t}) \alpha_n^4 f(x); \quad \text{(2.52a-d)}$$

$$\left(\frac{d^2 v(x,t)}{dt^2}, \frac{d^2 w(x,t)}{dt^2}, \frac{d^2 \theta(x,t)}{dt^2}\right) = -(v_0, w, \theta_0) \Omega^2 f(x) g(t) \quad (2.53)$$

Then, the angular velocities (eigenvalues) can be computed after injecting equations (2.47-50) in the equations (2.39) and making some simplifications and calculations:

$$m\left(\frac{d^2[v_0 f(x) g(t)]}{dt^2} - \frac{I_z}{A}\frac{d^2}{dx^2}\left(\frac{d^2[v_0 f(x) g(t)]}{dt^2}\right) + z_c \frac{d^2[\theta_0 f(x) g(t)]}{dt^2}\right) + EI_z\left(v^{(4)}\right) = 0$$

$$m\left(\frac{d^2[w_0 f(x) g(t)]}{dt^2} - \frac{I_y}{A}\frac{d^2}{dx^2}\left(\frac{d^2[w_0 f(x) g(t)]}{dt^2}\right) - y_c \frac{d^2[\theta_0 f(x) g(t)]}{dt^2}\right) + EI_y\left(w^{(4)}\right) = 0$$

$$m\left(I_0 \frac{d^2[\theta_0 f(x) g(t)]}{dt^2} - \frac{I_\omega}{A}\frac{d^2}{dx^2}\left(\frac{d^2[\theta_0 f(x) g(t)]}{dt^2}\right) + z_c \frac{d^2[v_0 f(x) g(t)]}{dt^2} - y_c \frac{d^2[w_0 f(x) g(t)]}{dt^2}\right) +$$
$$EI_w\left(\theta^{(4)}\right) - GI_t\theta'' = 0 \quad (2.54)$$

By applying the derivation respect to *x*, the equations become the followings:

$$m\left(-\Omega^2 v_0 f(x) g(t) - \frac{I_z}{A}[(\alpha_n)^2 \Omega^2 v_0 f(x) g(t)] + z_c[-\Omega^2 \theta_0 f(x) g(t)]\right) +$$
$$EI_z(v_0\ (\alpha_n)^4\ f(x) g(t)\ ) = 0$$

$$m\left([-\Omega^2 w_0 f(x) g(t)] - \frac{I_y}{A}[(\alpha_n)^2 \Omega^2 w_0 f(x) g(t)] - y_c[-\Omega^2 \theta_0 f(x) g(t)]\right) +$$
$$EI_y(w_0\ (\alpha_n)^4\ f(x) g(t)) = 0$$

$$m\left(I_0[-\Omega^2 \theta_0 f(x) g(t)] - \frac{I_\omega}{A}[(\alpha_n)^2 \Omega^2 \theta_0 f(x) g(t)] + z_c[-\Omega^2 v_0 f(x) g(t)] -\right.$$
$$\left. y_c[-\Omega^2 w_0 f(x) g(t)]\right) + EI_w(\theta_0 (\alpha_n)^4 f(x) g(t)) - GI_t(-\theta_0 (\alpha_n)^2 f(x) g(t)) = 0 \quad (2.55)$$

After simplification, the algebraic system of motion equations in terms of displacement amplitudes is obtained:

$$-\Omega^2 m\left(v_0 + \frac{I_z}{A}(\alpha_n)^2 v_0 + z_c \theta_0\right) + EI_z(v_0\ (\alpha_n)^4\ ) = 0$$

$$-\Omega^2 m\left(w_0 + \frac{I_y}{A}(\alpha_n)^2 \mathrm{w}_0 - y_c \theta_0\right) + EI_y(\mathrm{w}_0\ (\alpha_n)^4\ ) = 0$$

$$-\Omega^2 m\left(I_0 \theta_0 + \frac{I_\omega}{A}(\alpha_n)^2 \theta_0 + z_c v_0 - y_c w_0\right) + EI_w \theta_0\ (\alpha_n)^4 + GI_t \theta_0 (\alpha_n)^2 = 0 \quad (2.56)$$

By putting $\{U\}^t=\{v_0, w_0, \theta_0\}$ and adopting the matrix formulation, the system (2.56) is obtained as:

$$(-\Omega^2[M]+[K_e])\{U\}=\{0\} \tag{2.57}$$

The mass and the stiffness matrices $[M]$ and $[K_e]$ are the following:

$$\mathrm{M}=\begin{bmatrix} m\left(1+\frac{I_z}{A}(\alpha_n)^2\right) & 0 & mz_c \\ 0 & m\left(1+\frac{I_y}{A}(\alpha_n)^2\right) & -my_c \\ mz_c & -my_c & m\left(I_0+\frac{I_\omega}{A}(\alpha_n)^2\right) \end{bmatrix}$$

$$K_e=\begin{bmatrix} EI_z\,(\alpha_n)^4 & 0 & 0 \\ 0 & EI_y(\alpha_n)^4 & 0 \\ 0 & 0 & EI_w(\alpha_n)^4+GI_t(\alpha_n)^2 \end{bmatrix} \tag{2.58a,b}$$

This eigenvalue problem is coupled and the coupling effects depend on the shape section. The fundamental angular velocities (eigenvalues) can be obtained from the singularity condition given by:

$$det(-\Omega^2[M]+[K_e])=0 \tag{2.59}$$

Solutions are found from the vanishing conditions of the following matrix:

$$det\begin{bmatrix} -\Omega^2 m\left(1+\frac{I_z}{A}(\alpha_n)^2\right)+EI_z\,(\alpha_n)^4 & 0 & -\Omega^2 mz_c \\ 0 & -\Omega^2 m\left(1+\frac{I_y}{A}(\alpha_n)^2\right)+EI_y(\alpha_n)^4 & \Omega^2 my_c \\ -\Omega^2 mz_c & \Omega^2 my_c & -\Omega^2 m\left(I_0+\frac{I_\omega}{A}(\alpha_n)^2\right)+EI_w(\alpha_n)^4+GI_t(\alpha_n)^2 \end{bmatrix}=0 \tag{2.60}$$

Defining the uncoupled free bending and torsional angular velocities of the beam by:

$$\Omega_y^2(n)=\frac{EI_y}{m\left(1+\frac{I_y}{A}(\alpha_n)^2\right)}\,(\alpha_n)^4\;;\quad \Omega_z^2(n)=\frac{EI_z}{m\left(1+\frac{I_z}{A}(\alpha_n)^2\right)}\,(\alpha_n)^4$$
$$\Omega_\theta^2(n)=\frac{1}{m\left(I_0+\frac{I_\omega}{A}(\alpha_n)^2\right)}\left(EI_\omega(\alpha_n)^4+GI_t(\alpha_n)^2\right) \tag{2.61 a-c}$$

The system (2.60) can be simplified to:

$$det\begin{bmatrix} -\Omega^2+\Omega_z^2(n) & 0 & -\Omega^2\dfrac{z_c}{\left(1+\frac{I_z}{A}(\alpha_n)^2\right)} \\ 0 & -\Omega^2+\Omega_y^2(n) & \Omega^2\dfrac{y_c}{\left(1+\frac{I_y}{A}(\alpha_n)^2\right)} \\ -\Omega^2 z_c & \Omega^2 y_c & \left(I_0+\dfrac{I_\omega}{A}(\alpha_n)^2\right)(-\Omega^2+\Omega_\theta^2(n)) \end{bmatrix}=0 \qquad (2.62)$$

Ω_y and Ω_z are pure bending angular velocities about the strong and weak axes (*yy* and *zz*). Ω_θ is the pure torsion angular velocities, defined in (2.61a-c). This system is defined in the case of an arbitrary cross section where strong coupling is present due to shear coordinates (y_c, z_c). This matrix is full when ($y_c \neq 0$, $z_c \neq 0$). Analytical solutions are possible in presence of doubly symmetric or singly symmetric cross sections where the weak coupling is present. Some out of diagonal terms vanish. These cases are studied below.

In the case of doubly symmetric cross-section, the shear center and the centroid are coincident ($y_c=z_c=0$). Bending and torsion modes are then uncoupled. The matrix (2.62) becomes

$$det\begin{bmatrix} -\Omega^2+\Omega_z^2(n) & 0 & 0 \\ 0 & -\Omega^2+\Omega_y^2(n) & 0 \\ 0 & 0 & \left(I_0+\dfrac{I_\omega}{A}(\alpha_n)^2\right)(-\Omega^2+\Omega_\theta^2(n)) \end{bmatrix}=0 \qquad (2.63)$$

These angular velocities relationships are derived in (2.61). They include the kinematic rotational terms (the outlined parts). Let us remind that when these terms are omitted, the classical analytical solutions are straightforward:

$$\Omega_y^2(n)=\frac{EI_y}{m}(\alpha_n)^4\ ;\quad \Omega_z^2(n)=\frac{EI_z}{m}(\alpha_n)^4\ ;$$
$$\Omega_\theta^2(n)=\frac{1}{mI_0}(EI_\omega(\alpha_n)^4+GI_t(\alpha_n)^2)\ ;$$

With $\alpha_n=\frac{n\pi}{L}$ (2.64a-d)

The eigenvalue of the problem are the square roots of (2.61). They denote the angular velocity respectively (Ω_y, Ω_z and Ω_θ in (rad/s)). Moreover, they similar values can be obtained in frequency 'eigenfrequency ' f (Hertz, Hz) using the relationship.

$$f(\text{Hz})=\frac{\Omega}{2\pi} \qquad (2.65)$$

In order to remove any ambiguity present in literature, in the present study, the vibration eigenvalues are computed in rad/s or in Hz. They are mentioned in all cases under study.

In what follows, the developed analytical solutions for free vibration of 3D thin-walled beams with rotational terms illustrated in equations (2.61) are compared to classical solutions when the rotational terms are omitted equations (2.64) also to the classical pure bending solutions in 2D behavior. To this aim, a simply supported beam of 6m length and with bi-symmetric IPE 300 cross-section was taken. The geometrical and material properties of the beam are the followings: E=210 GPa, ν=0.30, G=80.07 GPa, ρ =7850kg/m^3, L=4.0m. The beam is presented in Figure 2.7.

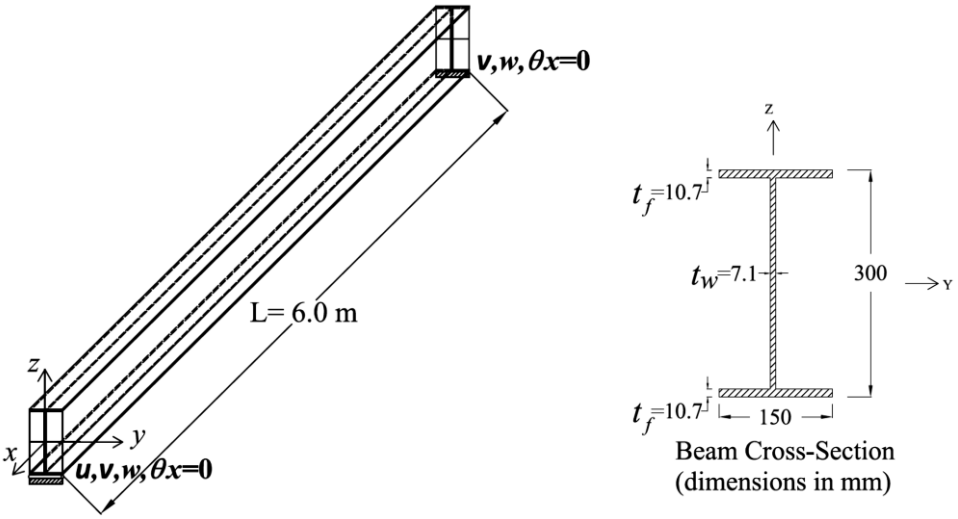

Figure 2.7: Simply supported beam with doubly-symmetric IPE300 cross-section.

Analytical solutions are carried out using the present developed model and compared to classical analytical solutions. As demonstrated before the vibration modes are uncoupled. To compare and analyze different results the seven eigenfrequencies and deformation shapes for each type of modes are depicted in Table 2.1. The classical 2D bending modes are given, followed by the lateral and the torsional vibration modes, in presence of unrestrained simply supported beam where 3D vibration behavior happens.

Table 2.1: Comparison of 3D eigenfrequencies of thin-walled beams to 2D classical beam theory, in Hz.

Mode number	**Classical Beam 2D**		Lateral bending modes		Torsional modes		Mode shape
1	**28.16**	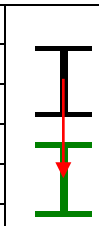	7.65	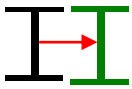	14.23	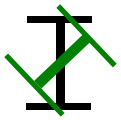	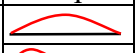
2	**112.62**		30.61		41.13		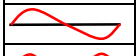
3	**253.40**		68.87		84.28		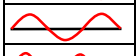
4	**450.48**		122.43		144.19		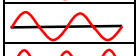
5	**703.88**		191.29		220.88		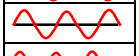
6	**1013.59**		275.46		314.19		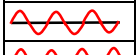
7	**1379.60**		376.05		423.10		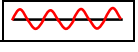

By analyzing the presented results in Table 2.1, It seems that the first lateral and torsional modes have a natural frequencies lower than the first mode obtained from classical beam theory 2D. Thus, the 2D classical beam theory is inadequate in the case of thin-walled 3D beams, this is due to the reason that lateral bending and torsional modes are always lower than the classical vertical bending modes. Moreover, one remarks that the three first natural frequencies obtained in lateral and torsional modes (underlined in the table) are less than 100 Hz. However, the modes with natural frequencies less than 100 Hz should be taken in consideration in the design procedure of 3D thin-walled beams to provide the structure stability against dynamic loads, like earthquakes, wind, machines…etc. This means that the classical beam theory happens if all the lateral and the torsional vibration modes must be removed. In practice design solutions are always adopted.

In what follows, analytical solutions are detailed for the simply supported beams with mono symmetric sections about the one bending axis such as Channels and Tee sections.

For singly symmetric cross sections with yy as symmetry axes, such as channel section depicted in Fig.2.6, one has: z_c=0 the system (2.62) becomes:

$$det\begin{bmatrix} -\Omega^2+\Omega_z^2(n) & 0 & 0 \\ 0 & -\Omega^2+\Omega_y^2(n) & \Omega^2\dfrac{y_c}{\left(1+\frac{I_y}{A}(\alpha_n)^2\right)} \\ 0 & \Omega^2 y_c & \left(I_0+\dfrac{I_\omega}{A}(\alpha_n)^2\right)(-\Omega^2+\Omega_\theta^2(n)) \end{bmatrix}=0 \qquad (2.66)$$

Thus, angular velocities are carried out the following polynomial equation:

$$\left(-\Omega^2+\Omega_z^2(n)\right)\left[\left(-\Omega^2+\Omega_y^2(n)\right)\left(I_0+\tfrac{I_\omega}{A}(\alpha_n)^2\right)\left(-\Omega^2+\Omega_\theta^2(n)\right)-\Omega^4\frac{{y_c}^2}{\left(1+\frac{I_y}{A}(\alpha_n)^2\right)}\right]=0 \qquad (2.67)$$

This relationship has three solutions. These solutions can be obtained by solving the following equations:

$$\left(-\Omega^2+\Omega_z^2(n)\right)=0 \qquad (2.68a)$$

and

$$\left[\left(-\Omega^2+\Omega_y^2(n)\right)\left(I_0+\tfrac{I_\omega}{A}(\alpha_n)^2\right)\left(-\Omega^2+\Omega_\theta^2(n)\right)-\Omega^4\frac{{y_c}^2}{\left(1+\frac{I_y}{A}(\alpha_n)^2\right)}\right]=0 \qquad (2.68b)$$

By simplifying the previous equation, one gets the following equation:

$$\left[\Omega^4\left[1-\frac{{y_c}^2}{\left(1+\frac{I_y}{A}(\alpha_n)^2\right)\left(I_0+\frac{I_\omega}{A}(\alpha_n)^2\right)}\right]-(\Omega_y^2(n)+\Omega_\theta^2(n))\Omega^2+\Omega_y^2(n)\Omega_\theta^2(n)\right]=0 \qquad (2.69)$$

Solutions of the angular eigenvalues are derived from equation (2.68a) and (2.69) as the followings: $\Omega^2 = (\Omega_1^2(n), \Omega_2^2(n), \Omega_3^2(n))$. Where the uncoupled pure bending angular velocities defined in equation (2.61b) and get to:

$$\Omega_1^2(n) = \Omega_z^2(n) \tag{2.70a}$$

The two other solutions are obtained from solutions of (2.69) and lead the coupled flexural-torsional angular eigenvalues given by:

$$\Omega_{2,3}^2(n) = \frac{(\Omega_y^2(n)+\Omega_\theta^2(n)) \pm \sqrt{(\Omega_y^2(n)-\Omega_\theta^2(n))^2+4(1-a_c)\Omega_y^2(n)\Omega_\theta^2(n)}}{2(1-a_c)} \tag{2.70b}$$

where $a_c = \frac{{y_c}^2}{\left(1+\frac{I_y}{A}(\alpha_n)^2\right)\left(I_0+\frac{I_\omega}{A}(\alpha_n)^2\right)}$ (2.70c)

Let us remind that when the rotational terms are omitted, the classical analytical solutions are obtained:

$\Omega_1^2(n) = \Omega_z^2(n) = \frac{EI_z}{m}(\alpha_n)^4$;

$$\Omega_{2,3}^2(n) = \frac{(\Omega_y^2(n)+\Omega_\theta^2(n)) \pm \sqrt{(\Omega_y^2(n)-\Omega_\theta^2(n))^2+4\frac{{y_c}^2}{I_0}\Omega_y^2(n)\Omega_\theta^2(n)}}{2(1-\frac{{y_c}^2}{I_0})} \tag{2.71}$$

In this equation, the expression of Ω_y and Ω_θ are derived according to (2.64a, c).

For singly symmetric cross sections with zz as symmetry axes, such as Tee section depicted in Fig.2.6, one has: y_c=0 the system (2.62) becomes:

$$det\begin{bmatrix} -\Omega^2+\Omega_z^2(n) & 0 & -\Omega^2\dfrac{z_c}{\left(1+\frac{I_z}{A}\left(\frac{n\pi}{L}\right)^2\right)} \\ 0 & -\Omega^2+\Omega_y^2(n) & 0 \\ -\Omega^2 z_c & 0 & \left(I_0+\dfrac{I_\omega}{A}(\alpha_n)^2\right)(-\Omega^2+\Omega_\theta^2(n)) \end{bmatrix} = 0 \tag{2.72}$$

Thus, angular velocities (eigenvalues) are carried out the following polynomial equation:

$$(-\Omega^2+\Omega_z^2(n))\left[\left(-\Omega^2+\Omega_y^2(n)\right)\left(I_0+\frac{I_\omega}{A}(\alpha_n)^2\right)(-\Omega^2+\Omega_\theta^2(n))\right] - \Omega^4\frac{{z_c}^2}{\left(1+\frac{I_z}{A}\left(\frac{n\pi}{L}\right)^2\right)}(-\Omega^2+\Omega_y^2(n)) = 0 \tag{2.73}$$

After needed simplifications and factoring operations, this equation becomes:

$$\left(-\Omega^2+\Omega_y^2(n)\right)\left[(-\Omega^2+\Omega_z^2(n))\left(I_0+\frac{I_\omega}{A}(\alpha_n)^2\right)\left(-\Omega^2+\Omega_\theta^2(n)\right) - \Omega^4\frac{{z_c}^2}{\left(1+\frac{I_z}{A}\left(\frac{n\pi}{L}\right)^2\right)}\right] = 0 \tag{2.74}$$

This relationship has three solutions. These solutions can be obtained by solving the following equations:

$$\left(-\Omega^2 + \Omega_y^2(n)\right) = 0$$

$$\left[\left(-\Omega^2 + \Omega_z^2(n)\right)\left(I_0 + \frac{I_\omega}{A}(\alpha_n)^2\right)\left(-\Omega^2 + \Omega_\theta^2(n)\right) - \Omega^4 \frac{{z_c}^2}{\left(1+\frac{I_y}{A}\left(\frac{n\pi}{L}\right)^2\right)}\right] = 0 \qquad (2.75a,b)$$

By simplifying (2.75b), one obtains:

$$\left[\Omega^4\left[1 - \frac{{z_c}^2}{\left(1+\frac{I_y}{A}\left(\frac{n\pi}{L}\right)^2\right)\left(I_0+\frac{I_\omega}{A}(\alpha_n)^2\right)}\right] - (\Omega_z^2(n) + \Omega_\theta^2(n))\Omega^2 + \Omega_z^2(n)\Omega_\theta^2(n)\right] = 0 \qquad (2.76)$$

The solutions of (2.75a) and (2.76) lead to:

$$\Omega^2 = (\Omega_1^2(n), \Omega_2^2(n), \Omega_3^2(n)) \qquad (2.77)$$

Where Ω_1 is the pure bending angular velocities (eigenvalues) and Ω_2, Ω_3 are coupled flexural-torsional angular velocities (eigenvalues). They are given by:

$$\Omega_1^2(n) = \Omega_y^2(n) \qquad (2.78a)$$

$$\Omega_{2,3}^2(n) = \frac{(\Omega_z^2(n)+\Omega_\theta^2(n)) \pm \sqrt{(\Omega_z^2(n)-\Omega_\theta^2(n))^2 + 4(1-a_t)\Omega_z^2(n)\Omega_\theta^2(n)}}{2(1-a_t)} \qquad (2.78b)$$

where $a_t = \frac{{z_c}^2}{\left(1+\frac{I_z}{A}(\alpha_n)^2\right)\left(I_0+\frac{I_\omega}{A}(\alpha_n)^2\right)}$ (2.79)

Let us remind that when the rotational terms are omitted, the classical analytical solutions are obtained:

$$\Omega_1^2(n) = \Omega_y^2(n) = \frac{EI_y}{m}(\alpha_n)^4 \qquad (2.80a)$$

$$\Omega_{2,3}^2(n) = \frac{(\Omega_z^2(n)+\Omega_\theta^2(n)) \pm \sqrt{(\Omega_z^2(n)-\Omega_\theta^2(n))^2 + 4\frac{{z_c}^2}{I_0}\Omega_z^2(n)\Omega_\theta^2(n)}}{2\left(1-\frac{{z_c}^2}{I_0}\right)} \qquad (2.80b)$$

In this equation, the expression of Ω_z and Ω_θ are derived according to (2.64b, c).

Moreover, arbitrary sections can be investigated from the system equation (2.60), by solving the 3rd degree polynomial equation carried out from the system. Putting:

$X = \Omega^2$

$$k = \left(I_0 + \frac{I_\omega}{A}(\alpha_n)^2\right) \quad K_1 = \left(1 + \frac{I_z}{A}(\alpha_n)^2\right) \quad K_2 = \left(1 + \frac{I_y}{A}(\alpha_n)^2\right) \tag{2.81}$$

One gets a cubic equation of the form:

$$aX^3 + bX^2 + cX + d = 0 \tag{2.82}$$

with: $a = -k + \frac{{y_c}^2}{K_2} + \frac{{z_c}^2}{K_1}$

$$b = k\left(\Omega_y^2(n) + \Omega_\theta^2(n) + \Omega_Z^2(n)\right) - \Omega_Z^2(n)\frac{{y_c}^2}{K_2} - \Omega_y^2(n)\frac{{z_c}^2}{K_1}$$

$$c = k\left(-\Omega_y^2(n)\Omega_\theta^2(n) - \Omega_y^2(n)\Omega_Z^2(n) - \Omega_Z^2(n)\Omega_\theta^2(n)\right)$$

$$d = k\Omega_y^2(n)\Omega_Z^2(n)\Omega_\theta^2(n) \tag{2.83}$$

The angular velocities (eigenvalues) of the beam are obtained by solving equation (2.82). This leads to 3 solutions $X_1 = \Omega_1^2(n)$, $X_2 = \Omega_2^2(n)$, $X_3 = \Omega_3^2(n)$. In this case, all the angular velocities (2.82) fully flexural-torsional. This problem is called the triply coupled free vibration problem [33].

2.2.3.3 Free vibration solution attempts for other boundary conditions

The case of cantilever beams and clamped-clamped beams is investigated below. Higher vibration modes are derived from the motion equations (2.46) by applying the appropriate boundary conditions.

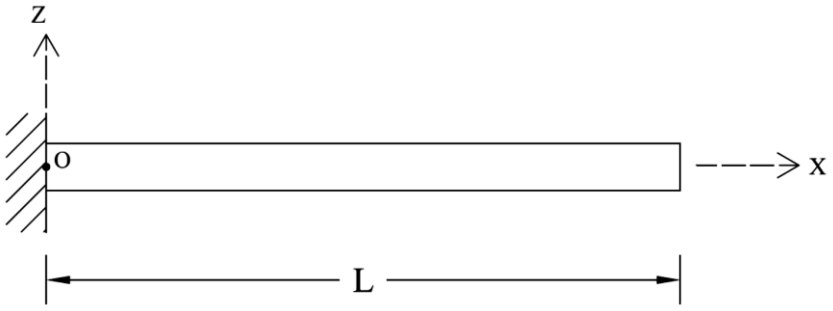

Figure 2.8: Cantilever beam with arbitrary cross-section.

In the case of a cantilever beam where the support O is fully clamped in both bending about the strong and the weak axes, and in torsion (Figure 2.8), the *n* vibration modes in cantilever beams obey to the function flexural vibration modes listed below [48]

$$F(x,\mathrm{t}) = \mathrm{F}_0(\mathrm{t})[\sin(\beta_n x) - \sinh(\beta_n x) - \alpha_n(\cos(\beta_n x) - \cosh(\beta_n x))] \tag{2.84}$$

where : $\propto_n = \frac{\sin(\beta_n l)+\sinh(\beta_n l)}{\cos(\beta_n l)+\cosh(\beta_n l)}$ (2.85)

$$for\ n = 1\ \ \beta_1 = \frac{1.87510}{l};\ for\ n = 2\ \ \beta_1 = \frac{4.69409}{l}$$

$$for\ n = 3\ \ \beta_1 = \frac{7.85473}{l}\ and\ for\ n > 3\ \ \beta_n = (2n-1)\frac{\pi}{2l} \quad (2.86)$$

The *n* torsional vibration modes obey to:

$$\theta(x,\mathrm{t}) = \theta_0(\mathrm{t})[\sin(\beta_n x)] \quad (2.87a)$$

where : $\beta_n = (2n-1)\frac{\pi}{2l}$ (2.87b)

In case of cantilever beam, angular velocities (eigenvalues) for bi-symmetric sections are given by:

$$\Omega_Z^2(n) = \frac{EI_z(\beta_n)^4}{m};\ \Omega_y^2(n) = \frac{EI_y(\beta_n)^4}{m};\ \Omega_\theta^2(n) = \frac{(\beta_n)^2}{mI_0}[EI_w(\beta_n)^2 + GJ] \quad (2.88)$$

Further, angular velocities (eigenvalues) solutions for cantilever beams with different types of cross sections are given in the appendix A.

In the case of a clamped-clamped beam where the end supports are fully clamped in both bending about the strong and the weak axes, and in torsion (Figure 2.9), the higher vibration modes are derived from the motion equations (2.46) by applying the correspondent boundary conditions.

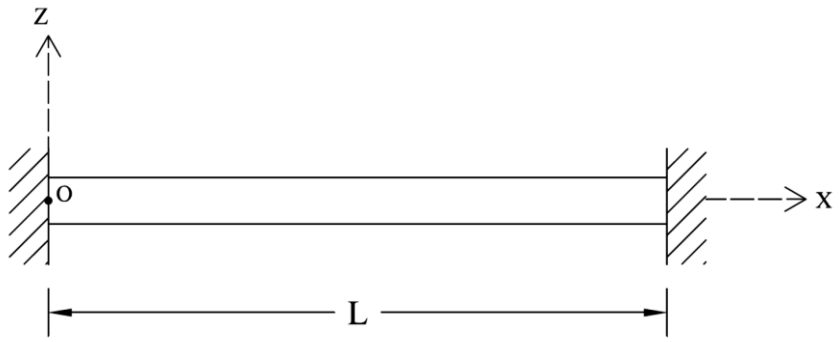

Figure 2.9: Double clamped beam with arbitrary cross-section.

In this case the *n* flexural vibration modes obey to:

$$F(x,\mathrm{t}) = \mathrm{F}_0(\mathrm{t})[\sinh(\beta_n x) - \sin(\beta_n x) + \alpha_n(\cos h(\beta_n x) - \cos(\beta_n x))] \quad (2.89)$$

where : $\propto_n = \frac{\sin h(\beta_n l)-\sin(\beta_n l)}{\cos(\beta_n l)-\cosh(\beta_n l)}$ (2.90)

$$for\ n = 1 \quad \beta_1 = \frac{4.730041}{l}$$
$$for\ n = 2 \quad \beta_1 = \frac{7.853205}{l}$$
$$for\ n > 2 \quad \beta_n = (2n+1)\frac{\pi}{2l} \tag{2.91}$$

The *n* torsional vibration modes obey to:

$$\theta(x,\mathrm{t}) = \theta_0(\mathrm{t})[\sin(\beta_n x)] \tag{2.92}$$

where : $\beta_n = (2n+1)\frac{\pi}{2l}$ (2.93)

For doubly-fixed beams, angular velocities (eigenvalues) can be obtained approximately for bi-symmetric as listed below:

$$\Omega_Z^2(n) = \frac{EI_Z(\beta_n)^4}{m}\ ;\ \Omega_y^2(n) = \frac{EI_y(\beta_n)^4}{m}\ ;\ \Omega_\theta^2(n) = \frac{1}{mI_0}[EI_w(\beta_n)^4 + (\beta_n)^2 GJ] \tag{2.94}$$

Furthermore, solutions for doubly clamped beams with different types of cross sections are given in the appendix B.

Hence, the closed form solutions are derived in this section for higher flexural-torsional vibration modes. They are then original and important in design. In what follows, the analytical solutions are compared to some benchmark solutions found in literature, as well as some commercial codes (Abaqus [64], Adina [81]), where 3D beam including warping and shell elements are customized. Overall, the free vibration is studied and the natural frequencies (eigenvalues) *f* are computed in Hertz (Hz) with (f= Ω⁄2π).

2.3 Validation and discussion

In the following, many validation examples thin-walled beams with different types of sections and boundary conditions are considered in the free vibration context. Analytical solutions are carried out for bi-symmetric sections (I cross-section), mono-symmetric sections (Chanel and Tee cross-sections) and arbitrary cross sections under different boundary conditions using the present developed model, then they are compared to classical analytical solutions without the rotational kinematic inertia terms. The aim of this comparison is to study the effect of the kinematic rotational terms in the accuracy of results when higher modes are investigated. Otherwise, different benchmarks are considered to validate our models (analytic with and without rotation terms) with literature and commercial codes. In the case of Abaqus code, shell elements (S8R) and 3D beam elements (B31OS) are used. In Adina, an efficient 3D beam element including torsion and warping has been recently implemented.

2.3.1 Simply supported beam with doubly-symmetric I cross-section

A steel beam presented in Figure 2.10 with IPE300 cross-section is considered. To study the effect of the kinematic rotational terms on the natural frequency computation, the

beam is studied in free vibration context. The natural frequencies are investigated using the analytical method that take in consideration the rotational terms developed in the section 2.2.3.2. Then, the present analytical method natural frequencies are compared to the result obtained by the analytical method without kinematic rotational terms. The geometrical and material properties of the beam are the followings:

E=210 GPa, ν=0.30, G=80.07 GPa, ρ=7850kg/m^3, L=4.0m.

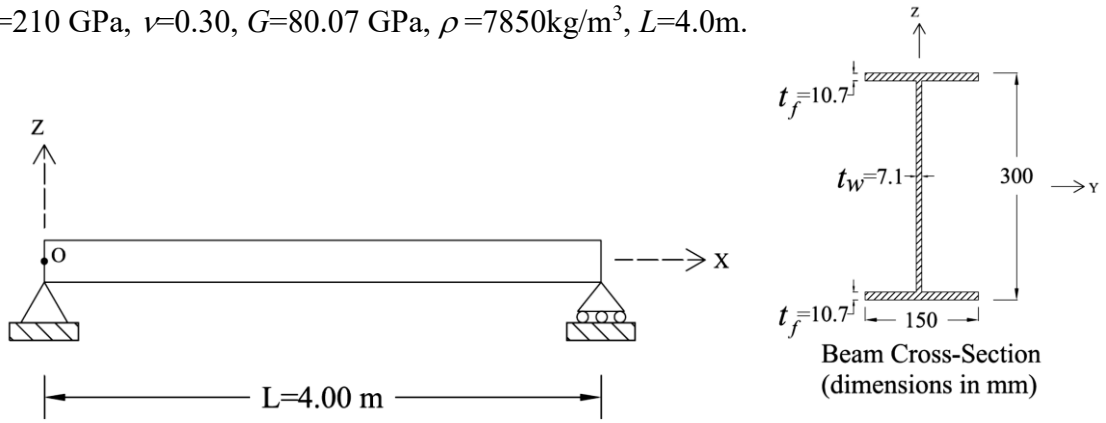

Figure 2.10: Simply supported beam with doubly-symmetric IPE300 cross-section.

The analytical natural frequencies result for this beam with/without rotational terms (detailed in the section 2.2.3.1) are listed in Table 2.2. Moreover, in the last column in this table modes types are shown.

Table 2.2: Comparison between analytical natural frequencies (Hz) with/without rotational terms for simply supported I beam.
(RTO: Rotational Terms Omitted, RTI: Rotational Terms Included, PB: Pure Bending mode, PT: Pure Torsion mode)

Mode	Analytic (RTO)	Present Analytic (RTI)	% Error relative to (RTI)	Mode type
1	17.01	17.00	0.06	PB,*zz*
2	26.89	26.88	0.04	PT
3	63.28	62.98	0.48	PB,*yy*
4	68.04	67.94	0.15	PB,*zz*
5	85.09	84.95	0.16	PT
6	153.08	152.61	0.31	PB,*zz*
7	180.54	179.84	0.39	PT
8	253.11	248.39	1.90	PB,*yy*
9	272.15	270.66	0.55	PB,*zz*
10	313.89	311.74	0.69	PT
11	425.24	421.60	0.86	PB,*zz*
12	485.25	480.08	1.08	PT
13	569.49	546.42	4.22	PB,*yy*
14	1012.42	942.75	7.39	PB,*yy*
15	1581.91	1420.90	11.33	PB,*yy*

By analyzing the presented results in Table 2.2, it seems that the natural frequencies difference between classical method without rotational terms (RTO) and the present

solutions including kinematic rotational terms becomes significant starting from the 13th vibration mode. In term of relative error between the analytical results with (RTO) and the (RTI) natural frequencies, it reaches 11%. Hence, the importance of the rotary terms presented in the mass matrix for the higher modes investigation is demonstrated.

2.3.2 Simply supported beam with singly-symmetric C cross-section

A steel beam presented in Figure 2.11 with C cross-section is considered Herein. The geometrical and material properties of the beam are the followings:

E=210 GPa, ν=0.30, G=80.07 GPa, ρ=7850kg/m^3, L=4.0m.

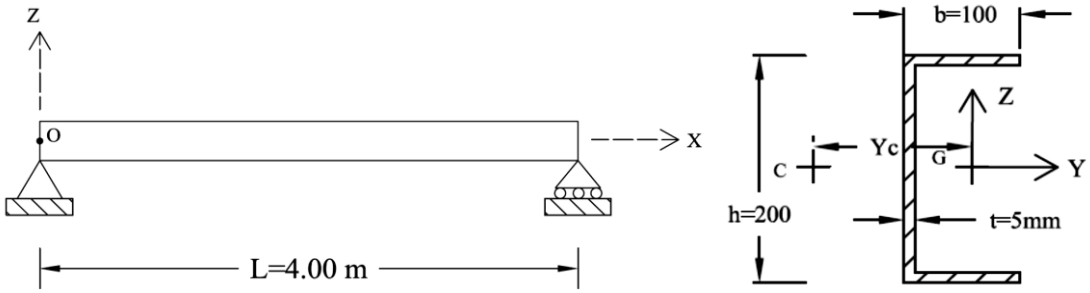

Figure 2.11: Simply supported beam with singly-symmetric channel cross-section.

The analytical natural frequencies result for this beam with/without rotational terms are listed in Table 2.3. Moreover, in the last column in this table modes types are shown.

Table 2.3: Comparison between analytical natural frequencies (Hz) with/without rotational terms for simply supported C beam.
(RTO: Rotational Terms Omitted, RTI: Rotational Terms Included, PB: Pure Bending mode, FT: Flexural-Torsional mode)

Mode	Analytic (RTO)	Present Analytic (RTI)	% Error relative to (RTI)	Mode Type
1	15.98	16.08	0.62	PB,$_{zz}$
2	16.09	15.97	0.75	FT
3	51.18	51.01	0.33	FT
4	53.23	53.17	0.11	FT
5	63.93	63.84	0.14	PB,$_{zz}$
6	114.37	114.16	0.18	FT
7	143.85	143.42	0.30	PB,$_{zz}$
8	199.84	199.22	0.31	FT
9	202.55	200.08	1.23	FT
10	255.73	254.42	0.51	PB,$_{zz}$
11	309.69	308.25	0.47	FT
12	399.57	396.46	0.78	PB,$_{zz}$
13	454.87	442.79	2.73	FT
14	808.13	771.23	4.78	FT
15	1262.31	1175.68	7.37	FT

By analyzing the presented results in Table 2.3, same as the previous example, one observes the importance of the rotary kinematic terms present in the mass matrix in dynamic analyses especially for higher modes computation. The error between the analytical solutions with/without rotational kinematic terms relative to the analytical (RTI) reaches 7% for the higher modes natural frequencies.

2.3.3 Simply supported beam with mono-symmetric T cross-section

A steel beam presented in Figure 2.12 with Tee cross-section is considered. The geometrical and material properties of the beam are the followings:

E=210 GPa, ν=0.30, G=80.07 GPa, ρ=7850kg/m^3, L=4.0m.

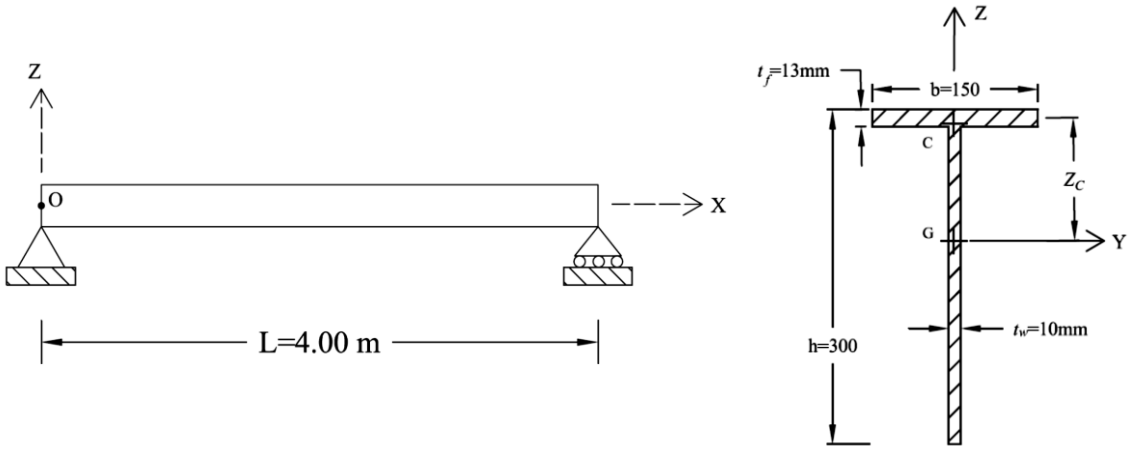

Figure 2.12: Simply supported beam with mono-symmetric Tee cross-section.

The analytical natural frequencies result for this beam with/without rotational terms are listed in Table 2.4. Moreover, in the last column in this table modes types are shown.

Table 2.4: Comparison between analytical natural frequencies (Hz) with/without rotational terms for simply supported T beam.
(RTO: Rotational Terms Omitted, RTI: Rotational Terms Included, PB: Pure Bending mode, FT: Flexural-Torsional mode)

Mode	Analytic (RTO)	Present Analytic (RTI)	% Error relative to (RTI)	Mode Type
1	7.25	7.25	0.00	FT
2	16.21	16.21	0.00	FT
3	25.18	25.18	0.00	FT
4	34.49	34.48	0.03	FT
5	44.29	44.29	0.00	FT
6	49.52	49.71	0.38	$PB_{,yy}$
7	49.82	49.38	0.89	FT
8	179.92	178.33	0.89	FT
9	198.10	195.81	1.17	$PB_{,yy}$
10	396.43	388.66	2.00	FT
11	445.72	434.40	2.61	$PB_{,yy}$
12	699.50	675.68	3.53	FT
13	792.39	757.63	4.59	$PB_{,yy}$
14	1089.15	1032.80	5.46	FT
15	1238.11	1156.21	7.08	$PB_{,yy}$

As shown in Table 2.4, the relative error percentage between the analytical solutions with/without rotational kinematic terms to the analytical (RTI) reaches 8%. Consequently, it has been proved that, for simply supported beams, the rotary terms are of high importance for the higher modes computation regardless of the section type.

2.3.4 Cantilever beam with doubly-symmetric I cross-section

A steel beam presented in Figure 2.13 with IPE300 cross-section is considered. The geometrical and material properties of the beam are the followings:

E=210 GPa, ν=0.30, G=80.07 GPa, ρ=7850kg/m^3, L=4.0m.

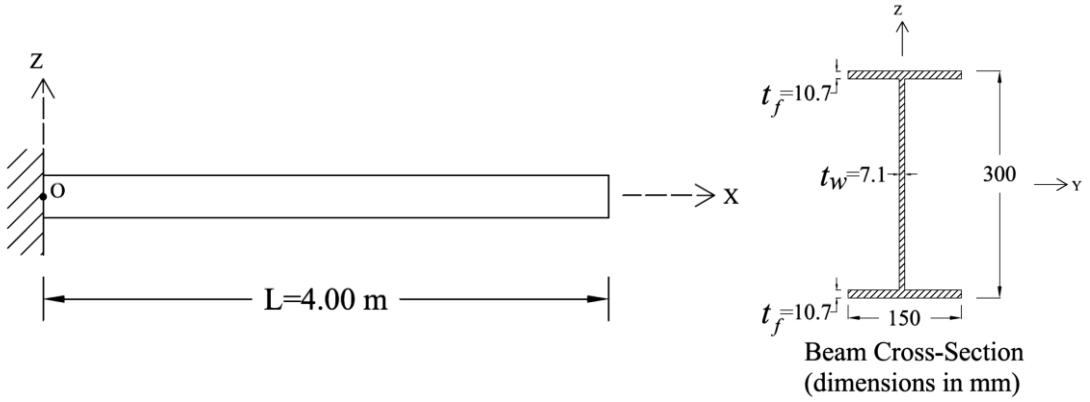

Figure 2.13: Cantilever beam with doubly-symmetric IPE300 cross-section.

The analytical natural frequencies result for this beam with/without rotational terms are listed in Table 2.5. Moreover, in the last column in this table modes types are shown.

Table 2.5: Comparison between analytical natural frequencies (Hz) with/without rotational terms for cantilever I beam.
(RTO: Rotational Terms Omitted, RTI: Rotational Terms Included, PB: Pure Bending mode, PT: Pure Torsion mode)

Mode	Analytic (RTO)	Present Analytic (RTI)	% Error relative to (RTI)	Mode Type
1	6.06	6.06	0.00	PB,*zz*
2	13.22	13.22	0.00	PT
3	22.55	22.51	0.18	PB,*yy*
4	37.99	37.96	0.08	PB,*zz*
5	51.13	51.08	0.10	PT
6	106.38	106.15	0.22	PB,*zz*
7	128.18	127.84	0.27	PT
8	141.34	139.85	1.07	PB,*yy*
9	208.47	207.59	0.42	PB,*zz*
10	242.59	241.31	0.53	PT
11	344.61	342.22	0.70	PB,*zz*
12	395.01	384.40	2.76	PT
13	395.74	391.58	1.06	PB,*yy*
14	775.51	733.66	5.70	PB,*yy*
15	1281.97	1173.22	9.27	PB,*yy*

The effect of rotary terms on the higher modes natural frequencies for a cantilever beam with bisymmetric cross-section is studied. It is shown in Table 2.5 that the relative error percentage between the analytical solutions with/without rotational kinematic terms to the analytical (RTI) reaches 9% for the higher vibration modes. Hence, these terms are of value to the higher modes natural frequencies in case of cantilever beams with a bisymmetric cross-section.

2.3.5 Cantilever beam with singly-symmetric C cross-section

A steel beam presented in Figure 2.14 with C cross-section is considered. The geometrical and material properties of the beam are the followings:

E=210 GPa, ν=0.30, G=80.07 GPa, ρ=7850kg/m^3, L=4.0m.

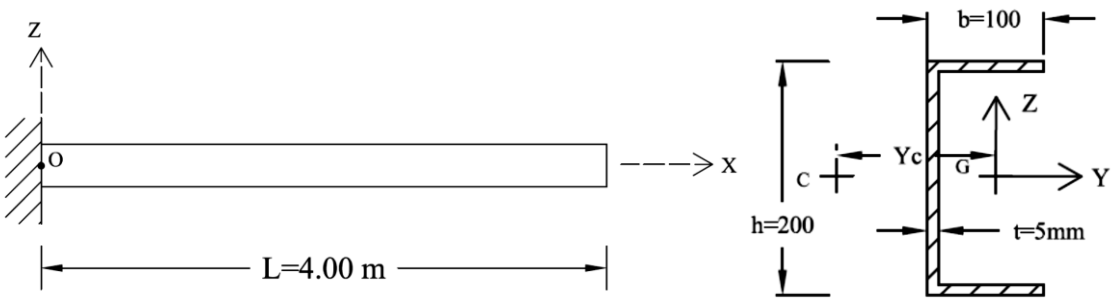

Figure 2.14: Cantilever beam with singly-symmetric channel cross-section.

The analytical natural frequencies result for this beam with/without rotational terms are listed in Table 2.6. Moreover, in the last column in this table modes types are shown.

Table 2.6: Comparison among analytical natural frequencies (Hz) with/without rotational terms for cantilever C beam.
(RTO: Rotational Terms Omitted, RTI: Rotational Terms Included, PB: Pure Bending mode, FT: Flexural-Torsional mode)

Mode	Analytic (RTO)	Present Analytic (RTI)	% Error relative to (RTI)	Mode Type
1	5.69	5.69	0.00	PB,*zz*
2	7.47	7.47	0.00	FT
3	18.75	18.72	0.16	FT
4	31.50	31.48	0.06	FT
5	35.68	35.65	0.08	PB,*zz*
6	80.78	80.67	0.14	FT
7	99.91	99.70	0.21	PB,*zz*
8	113.37	112.58	0.70	FT
9	154.06	153.68	0.25	FT
10	195.79	195.01	0.40	PB,*zz*
11	251.72	250.75	0.39	FT
12	316.16	310.23	1.91	FT
13	323.65	321.59	0.64	PB,*zz*
14	618.88	596.87	3.69	FT
15	1022.60	964.60	6.01	FT

From the depicted results in Table 2.6, it is remarkable that the relative error percentage between the analytical solutions with/without rotational kinematic terms to the analytical (RTI) reaches 6% for the higher modes. Thus, for the cantilever beams with mono-symmetric cross-sections, it was proved that the rotary terms are indispensable when the higher modes natural frequencies are investigated.

2.3.6 Cantilever beam with mono-symmetric T cross-section

A steel beam presented in Figure 2.15 with Tee cross-section is considered. The geometrical and material properties of the beam are the followings:

E=210 GPa, ν=0.30, G=80.07 GPa, ρ=7850kg/m^3, L=4.0m.

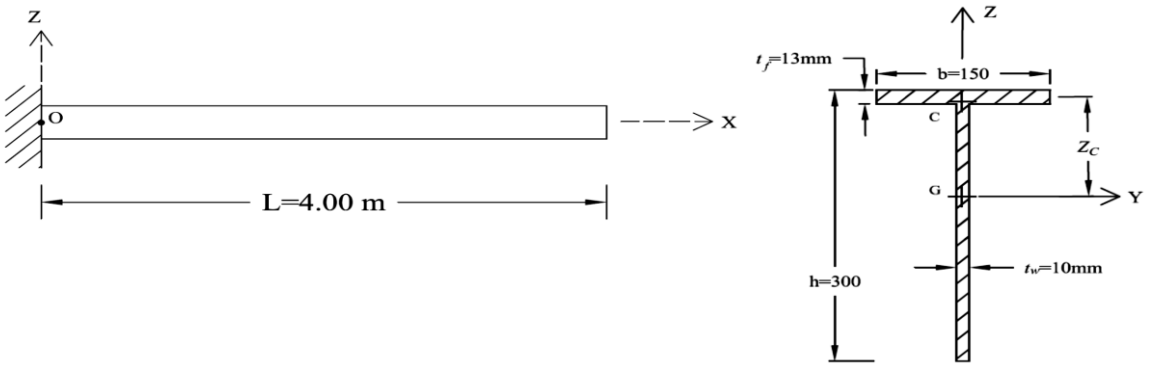

Figure 2.15: Cantilever beam with mono-symmetric Tee cross-section.

The analytical natural frequencies result for this beam with/without rotational terms are listed in Table 2.7. Moreover, in the last column in this table modes types are shown.

Table 2.7: Comparison between analytical natural frequencies (Hz) with/without rotational terms for cantilever T beam.
(RTO: Rotational Terms Omitted, RTI: Rotational Terms Included, PB: Pure Bending mode, FT: Flexural-Torsional mode)

Mode	Analytic (RTO)	Present Analytic (RTI)	% Error relative to (RTI)	Mode Type
1	3.58	3.58	0.00	FT
2	11.71	11.71	0.00	FT
3	17.64	17.62	0.11	PB,$_{yy}$
4	20.67	20.67	0.00	FT
5	21.45	21.43	0.09	FT
6	29.78	29.78	0.00	FT
7	39.32	39.32	0.00	FT
8	103.34	102.83	0.50	FT
9	110.57	109.85	0.66	PB,$_{yy}$
10	277.41	273.60	1.39	FT
11	309.59	304.06	1.82	PB,$_{yy}$
12	537.14	522.97	2.71	FT
13	606.68	585.98	3.53	PB,$_{yy}$
14	883.50	845.93	4.44	FT
15	1002.87	948.12	5.77	PB,$_{yy}$

By analyzing Table 2.7 results it can be founded that the relative error percentage between the analytical solutions with/without rotational kinematic terms to the analytical (RTI) reaches 6% for mode 15. So, it can be deduced that the rotary terms have an important

effect on the higher modes natural frequencies in case of cantilever with mono-symmetric cross-section.

2.3.7 Doubly clamped beam with doubly-symmetric I cross-section

A steel beam presented in Figure 2.16 with IPE300 cross-section is considered. The geometrical and material properties of the beam are the followings:

E=210 GPa, ν=0.30, G=80.07 GPa, ρ=7850kg/m^3, L=4.0m.

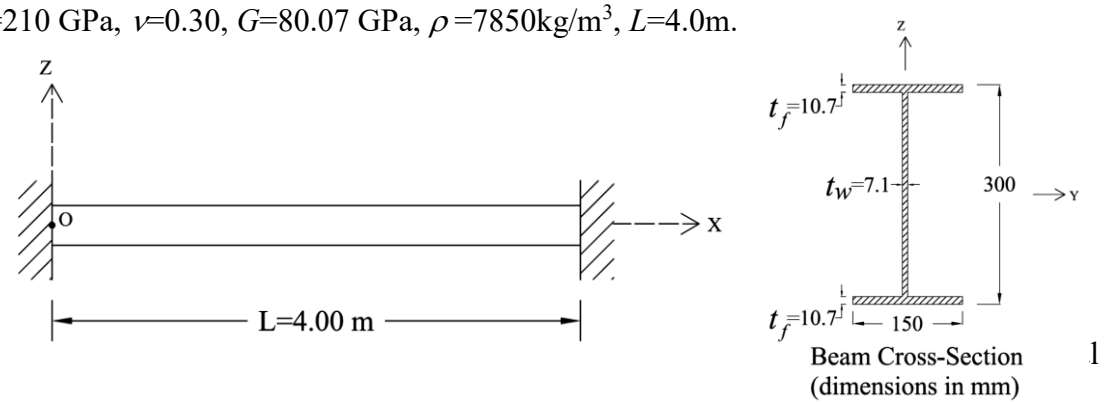

Figure 2.16: Doubly clamped beam with doubly-symmetric IPE300 cross-section.

frequencies result for this beam with/without rotational terms are listed in Table 2.8. Moreover, in the last column in this table modes types are shown.

Table 2.8: Comparison between analytical natural frequencies (Hz) with/without rotational terms for doubly clamped I beam.
(RTO: Rotational Terms Omitted, RTI: Rotational Terms Included, PB: Pure Bending mode, PT: Pure Torsion mode)

Mode	Analytic (RTO)	Present Analytic (RTI)	% Error relative to (RTI)	Mode Type
1	38.56	38.55	0.03	PB,*zz*
2	51.77	51.74	0.06	PT
3	106.29	106.11	0.17	PB,*zz*
4	128.07	127.79	0.22	PT
5	143.44	141.98	1.03	PB,*yy*
6	208.37	207.59	0.38	PB,*zz*
7	242.47	241.31	0.48	PT
8	344.44	342.22	0.65	PB,*zz*
9	395.40	384.26	2.90	PB,*yy*
10	394.81	391.58	0.82	PT
11	514.53	509.48	0.99	PB,*zz*
12	585.19	577.95	1.25	PT
13	775.14	733.66	5.65	PB,*yy*
14	1281.35	1173.22	9.22	PB,*yy*
15	1914.11	1686.25	13.51	PB,*yy*

By comparing the natural frequencies results with/without rotary terms in the case of doubly clamped beams with doubly symmetric cross sections presented in Table 2.8 a

significant relative error percentage between the analytical solutions with/without rotational kinematic terms is found. This error reach 13% for the higher modes. So, the rotary terms are essential in higher vibration mode computation in this case.

2.3.8 Doubly clamped beam with singly-symmetric C cross-section

A steel beam presented in Figure 2.17 with channel cross-section is considered. The geometrical and material properties of the beam are the followings:
E=210 GPa, ν=0.30, G=80.07 GPa, ρ=7850kg/m^3, L=4.0m.

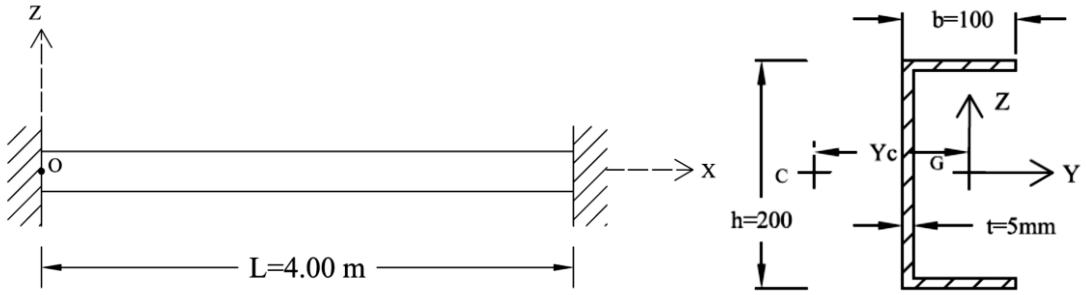

Figure 2.17: Doubly clamped beam with singly-symmetric channel cross-section.

The analytical natural frequencies result for this beam with/without rotational terms are listed in Table 2.9. Moreover, in the last column in this table modes types are shown.

Table 2.9: Comparison between analytical natural frequencies (Hz) with/without rotational terms doubly clamped C beam.
(RTO: Rotational Terms Omitted, RTI: Rotational Terms Included, PB: Pure Bending mode, FT: Flexural-Torsional mode)

Mode	Analytic (RTO)	Present Analytic (RTI)	% Error relative to (RTI)	Mode Type
1	31.92	31.90	0.06	FT
2	36.23	36.20	0.08	PB,*zz*
3	80.75	80.64	0.14	FT
4	99.87	99.66	0.21	PB,*zz*
5	115.10	114.29	0.71	FT
6	154.06	153.68	0.25	FT
7	195.79	195.01	0.40	PB,*zz*
8	251.72	250.75	0.39	FT
9	316.04	310.11	1.91	FT
10	323.65	321.59	0.64	PB,*zz*
11	373.77	371.68	0.56	FT
12	483.48	478.96	0.94	PB,*zz*
13	618.88	596.87	3.69	FT
14	1022.60	964.60	6.01	FT
15	1527.25	1403.10	8.85	FT

An important error percentage between the analytical natural frequencies without rotational kinematic terms relative to the analytical results with rotational terms (RTI) is remarked in Table 2.9. This error reaches 8% for the higher vibration frequencies. Thus, in the case of doubly clamped beams with mono-symmetric cross sections, it was validated that the rotary terms are essential for higher vibration mode computation.

2.3.9 Doubly clamped beam with mono-symmetric T cross-section

A steel beam presented in Figure 2.18 with Tee cross-section is considered. The geometrical and material properties of the beam are the followings:

E=210 GPa, ν=0.30, G=80.07 GPa, ρ=7850kg/m^3, L=4.0m.

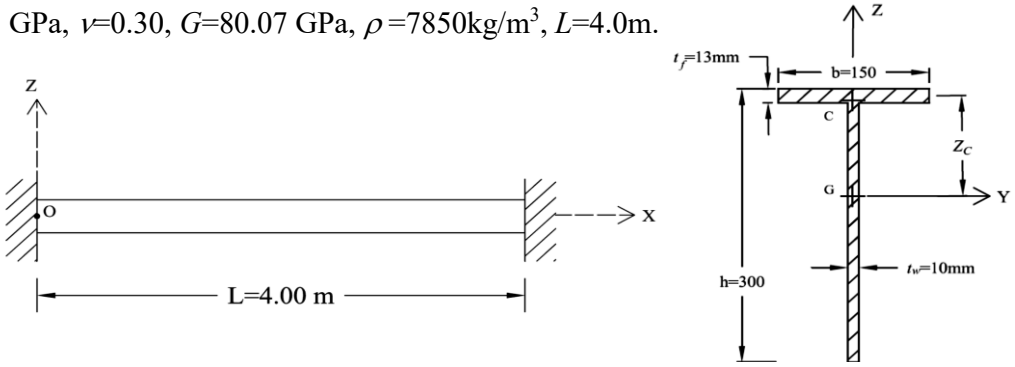

Figure 2.18: Doubly clamped beam with mono-symmetric Tee cross-section.

The analytical natural frequencies result for this beam with/without rotational terms are listed in Table 2.10. Moreover, in the last column in this table modes types are shown.

Table 2.10: Comparison between analytical natural frequencies (Hz) with/without rotational terms doubly clamped T beam.
(RTO: Rotational Terms Omitted, RTI: Rotational Terms Included, PB: Pure Bending mode, FT: Flexural-Torsional mode)

Mode	Analytic (RTO)	Present Analytic (RTI)	% Error relative to (RTI)	Mode Type
1	11.81	11.81	0.00	FT
2	20.67	20.67	0.00	FT
3	29.78	29.78	0.00	FT
4	39.32	39.32	0.00	FT
5	49.43	49.43	0.00	FT
6	104.83	104.30	0.51	FT
7	112.27	111.53	0.66	PB,*yy*
8	277.30	273.50	1.39	FT
9	309.47	303.95	1.82	PB,*yy*
10	537.14	522.97	2.71	FT
11	606.68	585.98	3.53	PB,*yy*
12	883.50	845.93	4.44	FT
13	1002.87	948.12	5.77	PB,*yy*
14	1316.44	1235.32	6.57	FT
15	1498.12	1380.59	8.51	PB,*yy*

The analysis of the results presented in Table 2.10 shows that the error percentage between the analytical natural frequencies without rotational kinematic terms and the results with rotational terms included (RTI) reach 8% when higher frequencies are investigated.

As conclusion, from all the sections types and boundary conditions the importance of rotary kinematic terms in higher vibration modes investigation is proven. In what follows, the analytical present solutions are validated by comparing to benchmark solution and a present simulations using the commercial codes (Abaqus, Adina).

2.3.10 Free vibration of a singly-symmetric cross section cantilever beam

A cantilever beam with singly symmetric channel cross section solved by Gendy [32] is concerned as the first example in the validation procedure. The geometry and the material data are given in Figure 2.19.

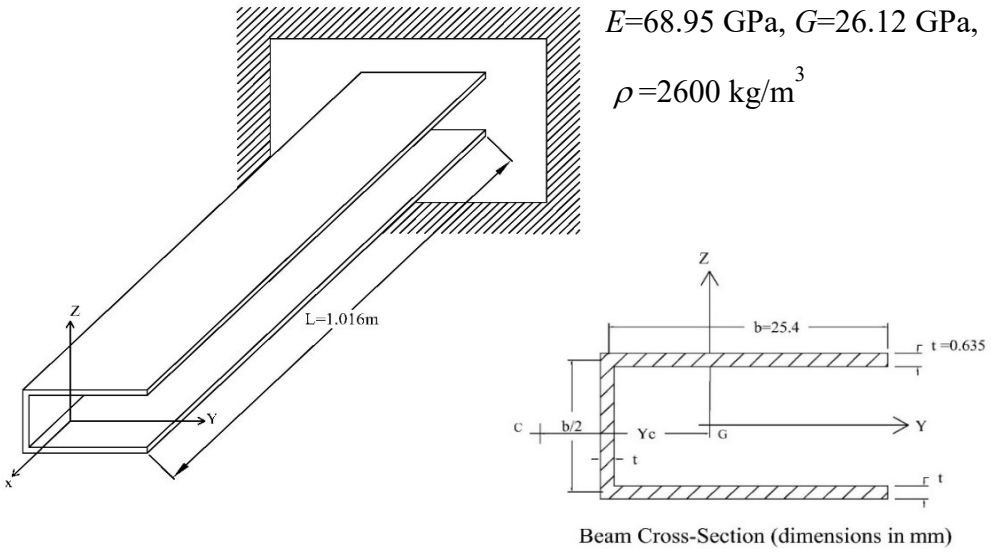

Figure 2.19: Cantilever beams with mono-symmetric channel cross-section.

For the beam represented in Figure 2.19, the first 6 vibration modes have been computed are presented in Table 2.11. Modes types are presented in (column 2), analytical solutions have been computed (column 3) and compared to the numerical solutions of the present model (column 4) and Abaqus simulations arranged in the columns 5 and 6. Benchmark solutions [32, 82] are reminded in the last columns for comparison. All the solutions are close. In comparison to [32] results, the obtained present analytical frequencies are so close to reference values. The slight difference founded is due to the interpolations done in Gendy's model element. The six first mode shapes carried out by the present analytical method match with [32, 82] references results. Second and sixth modes are pure bending. Other modes are flexural-torsional coupled. This approve that in free vibration for mono-symmetric sections about *y* axis, the beam exhibits flexural-torsional modes (*w* bending

in the strong axis *yy* and θ_x torsion about beam axis are coupled) and pure bending mode (*v* component alone leading to bending in the weak axis *zz*).

Table 2.11: Comparison between the present model and references natural frequencies (Hz) of the channel cantilever beam
(FT: flexural, torsional coupled mode; B: bending mode).

Mode	**Type**	**Present (Analytic)**	Abaqus (Shell)	Abaqus (B31OS)	Beam [82]	Shell [82]	HMC2 [32]
1	**FT**	**11.28**	11.40	11.26	11.38	11.42	11.42
2	**B**	**23.18**	23.15	23.17	23.15	23.15	23.15
3	**FT**	**43.42**	42.62	42.60	42.57	42.67	42.67
4	**FT**	**57.16**	57.79	57.40	57.67	58.17	58.05
5	**FT**	**109.01**	106.65	109.41	106.50	107.20	107.88
6	**B**	**145.17**	144.45	144.71	144.50	144.60	145.12

2.3.11 Flexural-torsional free vibration of a simply supported beam with arbitrary cross section

In this section, a simply supported beam with arbitrary non-symmetric cross section treated in Prokić [33] is considered for model validation. The geometry and the material properties of the beam are given in Figure 2.20. The position of the shear point is also viewed.

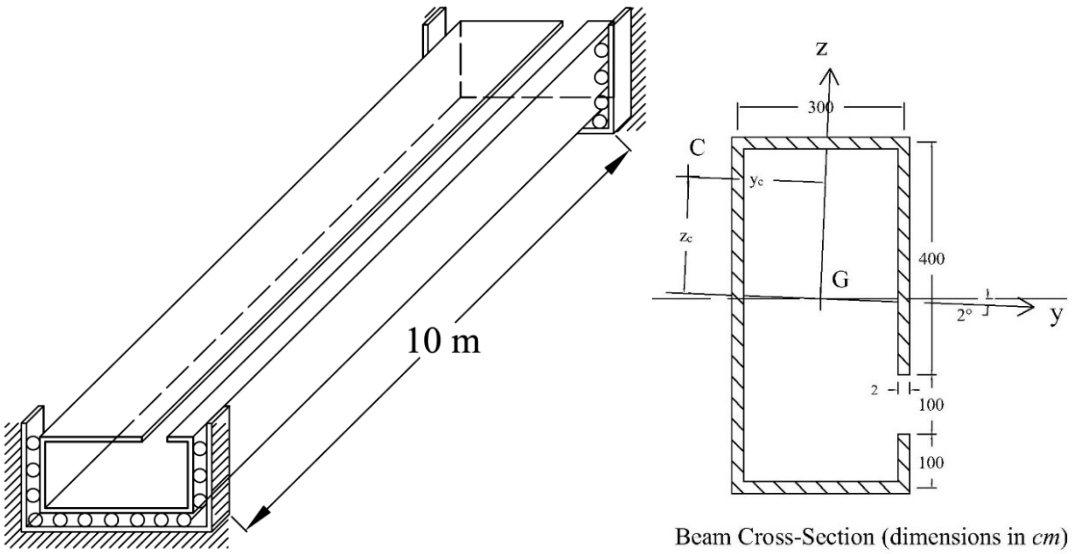

E=210 GPa, ν=0.30, G=80.07 GPa, ρ=7850kg/m^3

Figure 2.20: Simply supported beam with arbitrary cross section: geometry, sections dimensions and material properties.

The different results are summarized in Table 2.12. The natural frequency solutions given in Table 2.12a are obtained analytically and numerically by taking into account or omitting the rotational terms and warping terms. The analytical solutions are computed from three theories. The classical beam theory (CBT), omitting warping terms(WTO) are dressed in the column 2. The Vlasov's theory without rotary terms (RTO) and with rotary terms (RTI) follow in columns 3 and 4. The numerical solutions of the present model, Adina, Abaqus and Prokic benchmark values are arranged in columns 5 to 8. Taking Adina's results as reference, the errors of the different solutions are presented in Table 2.12b. Since the cross section is arbitrary, all the vibration modes are flexural-torsional and torsion governs the behavior. This is the reason why the CBT is out of order in this example. The errors of this method range between 10 and more than 90%. This fact is known and checked since long time [42, 43]. The rotary terms present in the mass matrix are important in dynamic analyses especially in presence of higher modes with frequencies higher than 100 Hz. One remarks that the error can reach 20%. The numerical solutions of the present model are in good agreement with Adina's and Prokic's solutions. Moreover, one remarks some discrepancies in Abaqus values in the case of higher modes with frequencies higher than 100 Hz.

The first nine vibration modes of the beam are pictured in Figure 2.20. Since the cross section is arbitrary, it is confirmed that all the vibration modes are flexural-torsional. One can see that the displacements v, w and θ_x are present in all the modes. The concept of triply coupled flexural-torsional adopted in literature is confirmed [33, 83]. Nevertheless, one can check that the displacements v and θ_x are predominant in modes (1, 2, 4, 5, 7 and 8). The displacements w and θ_x are important in the remaining modes.

Table 2.12: Comparison between the present models natural frequencies (Hz) and references values.
(WTO: Warping terms omitted, RTO: Rotational Terms Omitted, RTI: Rotational Terms Included)

	CBT (WTO)	Vlasov (RTO)	Present (RTI)	Adina (Beam)	Abaqus (B31OS)	Prokić [33]
n=1	3.84	8.78	8.78	8.78	8.77	8.68
	11.93	13.17	13.15	13.16	13.12	13.02
	30.07	34.30	34.11	34.12	33.36	33.83
n=2	7.84	34.41	34.22	34.23	34.07	33.86
	47.21	52.10	51.84	51.84	51.23	51.32
	116.41	135.88	131.45	131.50	121.32	130.35
n=3	11.81	76.80	76.42	76.43	75.67	75.61
	105.53	116.98	115.67	115.70	112.73	114.52
	253.43	304.99	283.91	283.90	244.30	281.51
n=4	15.77	136.29	135.12	135.10	132.78	not studied
	186.19	207.82	203.74	203.80	195.01	not studied
	432.63	541.74	480.02	480.00	386.03	not studied
n=5	19.72	212.78	209.95	210.00	204.41	not studied
	288.25	324.60	314.81	314.80	295.10	not studied
	644.80	846.15	708.16	708.20	536.93	not studied

Table 2.13: Errors values in % (Adina Results as reference)

	CBT (WTO)	Vlasov (RTO)	Present (RTI)	Abaqus	Prokić [33]
n=1	56.26	0.00	0.00	0.11	1.14
	9.37	0.08	0.08	0.30	1.06
	11.87	0.53	0.03	2.23	0.85
n=2	77.08	0.53	0.03	0.47	1,08
	8.94	0.50	0.00	1.18	1.00
	11.32	3.37	0.04	7.74	0.87
n=3	84.55	0.48	0.01	0.99	1.07
	9.01	1.12	0.03	2.57	1.02
	7.89	7.42	0.00	13.95	
n=4	88.33	0.86	0.01	1.72	
	8.64	2.00	0.03	4.31	
	6.30	12.86	0.00	19.58	
n=5	90.61	1.34	0.02	2.66	
	8.43	3.10	0.00	6.26	
	8.95	19.48	0.01	24.18	

2.4 Conclusion

In this chapter, the analytical approach of a model for the coupled vibration of beams with arbitrary thin-walled open cross-section is developed. This model treats different boundary conditions and takes into account for bending, torsion, warping and rotary kinematic terms. This leads to the assessment of the dynamic behavior of the beams more accurately compared to the solutions of classical beam theory. With the help of Hamilton's principle, the axial and flexural-torsional motion equations have been derived. Original closed form solutions are carried out for the free vibration of beams with doubly symmetric or singly symmetric and arbitrary cross sections under non-classical boundary conditions (Cantilever, doubly clamped). In the numerical applications section, the developed analytical solutions for free vibration are used to carry out the higher modes natural frequencies. In the first 9 examples, the free vibration analytical results including rotational kinematic terms are compared to the existing classical solutions in the literature. The percentage of error between the two solution methods is calculated for different sections and boundary conditions. As conclusion, the kinematic rotational terms are important to take in consideration specially for higher modes investigation, due to the relative error that reach 9% between two solution methods when we deal with high vibration modes. Moreover, the present analytical solutions have been validated also by different benchmark solutions from literature and comparisons with commercial codes present simulations results. The importance of developed solutions that take in consideration of rotational terms are proved in the list of numerical application examples by comparing obtained frequencies with the classical solutions without rotational terms and specially for the higher modes. All comparisons with numerical codes and benchmarks solutions show a good agreement with the developed solutions. The efficiency of the analytical solutions investigated seem to be accurate. Thus, analytical solutions for free vibration of thin-walled beams with arbitrary cross-sections are developed and validated using benchmark results. But, analytical method is limited for simple cases of boundary conditions. To this aim, the development of a finite element approach is needed to investigate more general cases of thin-walled beams in presence of the flexural-torsional coupled vibration. Accordingly, a finite element method is developed in the next chapter based on the present beam model and compared to the analytical present solutions. Also, the importance of the warping effect on the dynamic behavior of thin-walled beams is outlined in the chapter 3.

Chapter 3 Finite element method for vibrations of thin-walled beams

3.1 Introduction

The aim of this chapter is to develop a 3 dimensional model used to investigate the dynamic behavior of thin-walled beams with open sections using the finite element method. This model is based on two nodded beams elements.

Based on the bibliographic review for thin walled beams with open cross sections, the non-uniform torsion presented by Vlassov [5] is adopted in the developed element. In the finite element method, straight beam elements are adopted and the interpolation by polynomial functions.

In static domain, numerous finite elements models based on the Vlassov model have been developed in the literature [85-88]. In ref. [89] the stiffness matrix was developed for thin-walled beams with closed sections using cubic polynomial functions. The authors in ref. [89, 90] were introduced an independent variable ψ instead of $\theta_{x,x}$ to account shear deformation, that is important in the case of short-walled and clamped thin-walled beams (Benscoter Model). The authors of [87-92] developed a 3D element of type C° that takes into account torsion and shear deformations.

In finite element procedure, in a first step, the continuum media is discretized in the mesh process. Some elements are then defined with the connectivity nodes. In a second step, the variables are written in terms of the displacements of the degree of freedom of the basic elements. For this aim, shape function matrix and its gradient are needed. The basic element stiffness and the mass matrices are then computed by numerical integration using Gauss method. The matrices and vectors of the structure are obtained by the assembling process over the elements. In the present work, as demonstrated before, warping deformation is of primary importance for thin-walled open section. So, the warping is considered as an independent displacement with regard to classical 3D beams. Based on this assumption, each node *i* has seven Degree Of Freedom (DOF):

$\{q_e\}^t = \{u_i\ v_i\ w_i\ \theta_{xi}\ v_i'\ w_i'\ \theta_{x_i}'\}\ \ i = 1,2)$ [70].

These seven degree of freedom correspond respectively to axial about *x* axis and shear displacements about *y*, *z* axis, torsion angle about *x*, *y*, *z* axis and the derivation of θ_x about *x* correspond to the warping displacement. According to this assumption the known boundary conditions clamped, hinged and free are defined as following:

Clamped boundary: $u_i = v_i =, w_i = \theta_{x_i} = 0, v'_i = w'_i = \theta x'_i = 0,$

Hinged boundary: $u_i = v_i =, w_i = \theta_{x_i} = 0$

Free boundary: all displacements $\neq 0$

3.2 Finite element discretization

The continuous displacement vector $\{q\}$ and its gradient $\{\varphi\}$ defined previously in equation (2.23) are written as in terms of the $\{q_e\}$ as:

$$\{q\} = [N(\xi)]\{q_e\} \text{ and } \{\varphi\} = [G(\xi)]\{q_e\} \tag{3.1a,b}$$

Where $[N(\xi)]$ and $[G(\xi)]$ are respectively the shape functions and the gradient matrices (ξ is the local element coordinate). We remind that in the mesh process, linear shape functions are adopted for the displacement *u* and polynomial Hermite's functions are used in discretization of the other components (i.e: *v, w,* θ_x). According to definition equation (3.1), $\{\gamma\}$ vector defined in equation (2.23) is put as:

$$\{\gamma\} = [H]\{\varphi\} = [H][G]\{q_e\} = [B]\{q_e\} \tag{3.2a-c}$$

Where matrix [*H*] is a constant matrix defined in [70], as indicated below:

$$H = \begin{bmatrix} 1 & 0 & 0 & 0 & 0 & 0 & 0 & 0 \\ 0 & 0 & 0 & 0 & 1 & 0 & 0 & 0 \\ 0 & 0 & 0 & 0 & 0 & 1 & 0 & 0 \\ 0 & 0 & 0 & 0 & 0 & 0 & 0 & 1 \\ 0 & 0 & 0 & 0 & 0 & 0 & 1 & 0 \end{bmatrix} \tag{3.3}$$

Based on equation (3.2), one gets the following matrix formulation of the strain energy δU given by equation (2.29):

$$\begin{aligned} \delta U &= \int_L \{\delta q_e\}^t [B]^t [D][B]\{q_e\}\, dx \\ &= \bigcup_e \frac{l}{2}\int_{-1}^{1} \{\delta q_e\}^t [B]^t [D][B]\{q_e\}\, d\xi \\ &= \{\delta q_e\}^t \bigcup_e \left(\frac{l}{2}\int_{-1}^{1} [B]^t [D][B]\, d\xi\right)\{q_e\} \end{aligned} \tag{3.4}$$

$\bigcup_e$ denote the assembling process over basic elements.

From which, one can identify the stiffness matrix [*K*] of the structure from the assembly process by:

$$[K] = \bigcup_e \frac{l}{2}\int_{-1}^{1} [B]^t [D][B]\, d\xi = \bigcup_e [K]_e \tag{3.5}$$

Where $[K]_e$ is the elementary stiffness matrix. After part integration, the kinetic energy variation defined in equation (2.33) is modified to in terms of the acceleration as:

$$\delta T = -\{\delta q_e\}^t \left(\int_L \left(m[N]^t[M_1][N] + \frac{m}{A}[G]^t[M_2][G] \right) dx \right) \{\ddot{q_e}\} \tag{3.6}$$

The matrices M_1 and M_2 are defined as:

$$[M_1] = \begin{bmatrix} 1 & 0 & 0 & 0 \\ 0 & 1 & 0 & z_c \\ 0 & 0 & 1 & -y_c \\ 0 & z_c & -y_c & I_0 \end{bmatrix}$$

$$[M_2] = \begin{bmatrix} 0 & 0 & 0 & 0 & 0 & 0 & 0 & 0 \\ 0 & I_z & 0 & 0 & 0 & 0 & 0 & 0 \\ 0 & 0 & I_y & 0 & 0 & 0 & 0 & 0 \\ 0 & 0 & 0 & I_\omega & 0 & 0 & 0 & 0 \\ 0 & 0 & 0 & 0 & 0 & 0 & 0 & 0 \\ 0 & 0 & 0 & 0 & 0 & 0 & 0 & 0 \\ 0 & 0 & 0 & 0 & 0 & 0 & 0 & 0 \\ 0 & 0 & 0 & 0 & 0 & 0 & 0 & 0 \end{bmatrix}$$

(3.7a-b)

Thus, the elementary mass matrix $[M]_e$ is defined as:

$$[M]_e = \left(m[N]^t[M1][N] + \frac{m}{A}[G]^t[M2][G] \right) \tag{3.8}$$

By integration over the elements, one has:

$$\delta T = \bigcup_e \frac{l}{2} \int_{-1}^{1} \{q_e\}^t [M]_e \{\ddot{q_e}\}\, d\xi = \{\delta q_e\}^t \bigcup_e \left(\frac{l}{2} \int_{-1}^{1} [M]_e\, d\xi \right) \{\ddot{q_e}\} \tag{3.9}$$

From which one can identify the stiffness matrix [*M*] of the structure from the assembly process by:

$$[M] = \bigcup_e \frac{l}{2} \int_{-1}^{1} [M]_e\, d\xi \tag{3.10}$$

Elementary stiffness, and mass matrix definitions

To demonstrate the elementary stiffness and mass matrix, after beam discretization let us take an element between the two nodes *i*=1,2. This element is presented in Figure 3.1. Each node of this element has the seven degree of freedoms depicted in the following figure.

Figure 3.1: The two nodded element with seven degree of freedoms per node.

Displacement vector for this element is given by:

$$\{q_e\} = {}^t\{u_1\ v_1\ v'_1\ w_1\ w'_1\ \theta_{x1}\ \theta'_{x1}\ u_2\ v_2\ v'_2\ w_2\ w'_2\ \theta_{x2}\ \theta'_{x2}\} \tag{3.11}$$

By using the interpolation matrix equations (3.1) (composed of the polynomials shape functions) the displacements and torsion in (3.11) can be written as:

$$u = [N_u]\{q_e\} \quad v = [N_v]\{q_e\} \quad w = [N_w]\{q_e\} \quad \theta_x = [N_\theta]\{q_e\} \tag{3.12a-d}$$

Stiffness matrix definition:

The injection of equations (3.12) into the variation of the strain energy equation (2.29) leads to the following equation:

$$\delta U = {}^t\{q_e\}\int_L (EA\ {}^t[N_u]'[N_u]' + EI_z\ {}^t[N_v]''[N_v]'' + EI_y\ {}^t[N_w]''[N_w]'' + EI_\omega\ {}^t[N_\theta]''[N_\theta]'')\{q_e\}dx + {}^t\{q_e\}\int_L GI_t\ {}^t[N_\theta]'[N_\theta]'\{q_e\}dx \tag{3.13}$$

Furthermore, the equation (3.13) can be written in a simplified form below:

$$\delta U = {}^t\{q_e\}\int_L (EA[K_u^e] + EI_z[K_v^e] + EI_y[K_w^e] + EI_\omega[K_\theta^e]_1 + GI_t[K_\theta^e]_2)\{q_e\}dx \tag{3.14}$$

With: $[K_u^e] = \int_L {}^t[N_u]'[N_u]'$

$$[K_v^e] = \int_L {}^t[N_v]''[N_v]''$$

$$[K_w^e] = \int_L {}^t[N_w]''[N_w]''$$

$$[K_\theta^e]_1 = \int_L {}^t[N_\theta]''[N_\theta]''$$

$$[K_\theta^e]_2 = \int_L {}^t[N_\theta]'[N_\theta]' \tag{3.15a-e}$$

So, the elementary stiffness matric is given by:

$$[K^e] = EA[K_u^e] + EI_z[K_v^e] + EI_y[K_w^e] + EI_\omega[K_\theta^e]_1 + GI_t[K_\theta^e]_2 \tag{3.16}$$

The shape functions [73, 93] used in the present finite element model are C^0 for the two first and C^1 functions type for the others. C^1 functions and their first order derivative exist and are continuous. Otherwise, the first order derivatives of these functions in weak form can be integrated. Adding to this, C^1 functions have an acceptable with smoothness no jumps and no kinks, so there are continuously differentiable.

The adopted shape functions are defined by:

$$N_1(\xi) = \frac{(1-\xi)}{2}$$

$$N_2(\xi) = \frac{(1+\xi)}{2}$$

$$N_3(\xi) = \frac{(1-\xi)^2(2+\xi)}{4}$$

$$N_4(\xi) = \frac{l^e}{8}(1-\xi)^2(1+\xi)$$

$$N_5(\xi) = \frac{(1+\xi)^2(2-\xi)}{4}$$

$$N_6(\xi) = \frac{l^e}{8}(1+\xi)^2(\xi-1) \qquad (3.17a\text{-}f)$$

It should be noted that these equations are obtained by supposing that:

$\xi = \frac{2x}{l^e} - 1$ with l^e is the element length, $x \in [-1\ 1]$ and $\xi \in [-1\ 1]$.

Consequently, the elementary stiffness matric can be written as below:

$$[K^e] = \begin{bmatrix} K_{11} & 0 & 0 & 0 & 0 & 0 & 0 & K_{1\,8} & K_{1\,9} & K_{1\,10} & 0 & 0 & 0 & 0 \\ & K_{22} & K_{2\,3} & 0 & 0 & 0 & 0 & 0 & K_{2\,9} & K_{210} & 0 & 0 & 0 & 0 \\ & & K_{33} & 0 & 0 & 0 & 0 & 0 & 0 & 0 & K_{3\,11} & K_{3\,12} & 0 & 0 \\ & & & K_{44} & K_{45} & 0 & 0 & 0 & 0 & 0 & K_{4\,11} & K_{4\,12} & 0 & 0 \\ & & & & K_{55} & 0 & 0 & 0 & 0 & 0 & 0 & 0 & K_{6\,13} & K_{6\,14} \\ & & & & & K_{66} & K_{67} & 0 & 0 & 0 & 0 & 0 & K_{7\,13} & K_{7\,14} \\ & & & & & & K_{77} & 0 & 0 & 0 & 0 & 0 & 0 & 0 \\ & & & & & & & K_{88} & 0 & 0 & 0 & 0 & 0 & 0 \\ & & & & & & & & K_{99} & K_{9\,10} & 0 & 0 & 0 & 0 \\ & & & & & & & & & K_{10\,10} & 0 & 0 & 0 & 0 \\ & & & & & & & & & & K_{11\,11} & K_{10\,11} & 0 & 0 \\ & & & & & & & & & & & K_{11\,11} & 0 & 0 \\ & & & & & & & & & & & & K_{13\,13} & K_{13\,14} \\ & & & & & & & & & & & & & K_{14\,14} \end{bmatrix} \qquad (3.18)$$

With:

$K_{11} = EA\int_L N_1'^2 dx;\ K_{18} = EA\int_L N_1'N_2' dx;\ K_{19} = EI_z\int_L N_3''N_5'' dx;\ K_{1\,10} = EI_z\int_L N_3''N_6'' dx$

$K_{22} = EI_z\int_L N_3''^2 dx;\ K_{23} = EI_z\int_L N_3''^2 N_4''^2 dx;\ K_{29} = EI_z\int_L N_4''N_5'' dx;$

$K_{2\,10} = EI_z\int_L N_4''N_6'' dx;\ K_{3\,3} = EI_z\int_L N_4''^2 dx;\ K_{3\,11} = EI_y\int_L N_3''N_5'' dx$

$K_{3\,12} = EI_y\int_L N_3''N_6'' dx;;\ K_{44} = EI_y\int_L N_3''^2 dx\ ;\ K_{45} = EI_y\int_L N_3''^2 N_4''^2 dx$

$K_{4\,11} = EI_y\int_L N_4''N_5'' dx;\ K_{4\,12} = EI_y\int_L N_4''N_6'' dx;\ K_{55} = EI_y\int_L N_4''^2 dx$

$K_{66} = EI_\omega\int_L N_3''^2 dx;\ K_{67} = EI_\omega\int_L N_3^{"}N_4^{"}dx + GI_t\int_L N_3'N_4' dx$

$K_{6\,13} = EI_\omega\int_L N_3^{"}N_5^{"}dx + GI_t\int_L N_3'N_5' dx;\ K_{6\,14} = EI_\omega\int_L N_3^{"}N_6^{"}dx + GI_t\int_L N_3'N_6' dx$

$K_{77} = EI_\omega\int_L N_4''^2 dx;\ K_{7\,13} = EI_\omega\int_L N_4^{"}N_5^{"}dx + GI_t\int_L N_4'N_5' dx$

$K_{7\,14} = EI_\omega\int_L N_4^{"}N_6^{"}dx + GI_t\int_L N_4'N_6' dx;\ K_{88} = EA\int_L N_2'^2 dx$

$K_{99} = EI_z\int_L N_5''^2 dx;\ K_{9\,10} = EI_z\int_L N_5''^2 N_6''^2 dx;\ K_{10\,10} = EI_z\int_L N_6''^2 dx$

$K_{11\,11} = EI_y\int_L N_5''^2 dx;\ K_{11\,12} = EI_y\int_L N_5''^2 N_6''^2 dx;\ K_{12\,12} = EI_y\int_L N_6''^2 dx$

$K_{13\,13} = EI_\omega\int_L N_5^{"2}dx + GI_t\int_L N_5'^2 dx;\ K_{13\,14} = EI_\omega\int_L N_5^{"}N_6^{"}dx + GI_t\int_L N_5'N_6' dx$

$K_{14\,14} = EI_\omega\int_L N_6^{"2}dx + GI_t\int_L N_6'^2 dx$ (3.19)

Mass matrix definition:

The kinetic energy variation has been derived in equation (2.33).in terms of the displacement and rotation velocities. It is reminded below.

$$\delta T = \int_L -m\left(\ddot{u}\delta u + \ddot{v}\delta v + \ddot{w}\delta w + I_0\ddot{\theta}_x\delta\theta_x + z_c\left(\delta v\ddot{\theta}_x + \ddot{v}\delta\theta_x\right) - y_c\left(\delta w\ddot{\theta}_x + \ddot{w}\delta\theta_x\right)\right)dx - \int_L \left(m\frac{I_z}{A}\ddot{v}'\delta v' + \mathrm{m}\frac{\mathrm{I_y}}{\mathrm{A}}\ddot{\mathrm{w}}'\delta w' + m\frac{I_\omega}{A}\ddot{\theta}_x'\delta\theta_x'\right)dx \quad (3.20a)$$

In matrix formulation, the kinetic variation becomes:

$$\delta T = -\int_L {}^t\{\delta q\}[M_1]\{\ddot{q}\}dx - \int_L {}^t\{\delta\varphi\}[M_2]\{\ddot{\varphi}\}dx \quad (3.20b)$$

Mass matrices $[M_1]$ and $[M_2]$ are elementary mass matrices. Using the relationships between the vectors $\{q\}$, $\{\varphi\}$ and the DOF vector $\{q_e\}$. Comparison of the present natural frequencies to benchmark values

$$\delta T = -{}^t\{\delta q_e\}\left(\int_L \left(m\ {}^t[N][M_1][N] + \frac{m}{A}\ {}^t[G][M_2][G]\right)dx\right)\{\ddot{q_e}\} \quad (3.20c)$$

For harmonic motion with angular velocity Ω the displacement vector and his second derivative with respect to time are given as follows:

$$\{q_e(t)\} = \{q_e\}e^{i\Omega t} \text{ and } \{\ddot{q_e}(t)\} = -\Omega^2\{q_e(t)\} \tag{3.20d}$$

By injecting the equations (3.12) into the variation of the kinetic energy equation (2.33) the following equation is gotten:

$$\delta T = {}^t\{\delta q_e\}(-\Omega^2)\int_L -m\Big({}^t[N_u][N_u] + {}^t[N_v][N_v] + {}^t[N_w][N_w] + I_0\,{}^t[N_\theta][N_\theta] + z_c\big({}^t[N_\theta][N_v] + {}^t[N_v][N_\theta]\big) - y_c\big({}^t[N_\theta][N_w] + {}^t[N_w][N_\theta]\big)\Big)dx\{q_e\} + {}^t\{\delta q_e\}(-\Omega^2)\int_L \Big(m\tfrac{I_z}{A}\,{}^t[N_v]'[N_v]' + \mathrm{m}\tfrac{\mathrm{I_y}}{\mathrm{A}}\,{}^t[N_w]'[N_w]' + m\tfrac{I_\omega}{A}\,{}^t[N_\theta]'[N_\theta]'\Big)dx\{q_e\} \tag{3.21}$$

With: $[M_u^e]_1 = \int_L {}^t[N_u][N_u]$, $[M_u^e]_2 = \int_L {}^t[N_u]'[N_u]'$

$[M_v^e]_1 = \int_L {}^t[N_v][N_v]$, $[M_v^e]_2 = \int_L {}^t[N_v]'[N_v]'$

$[M_w^e]_1 = \int_L {}^t[N_w][N_w]$, $[M_w^e]_2 = \int_L {}^t[N_w]'[N_w]'$

$[M_\theta^e]_1 = \int_L {}^t[N_\theta][N_\theta]$, $[M_\theta^e]_2 = \int_L {}^t[N_\theta]'[N_\theta]'$

$[M_{\theta v}^e] = \int_L {}^t[N_\theta][N_v] + {}^t[N_v][N_\theta]$, $[M_{\theta w}^e] = \int_L {}^t[N_\theta][N_w] + {}^t[N_w][N_\theta]$

(3.22)

The force vector can be deduced by injecting equation (3.1) in the external load work equation (2.38), one gets:

$$\delta W = \int_L {}^t\{\delta q_e\}\,{}^t[N(\xi)]\{f\}dx \tag{3.23}$$

The integration over the elements of equation (3.23) gives the following relationship:

$$\delta W = {}^t\{\delta q_e\}\bigcup_e\left(\frac{l}{2}\int_{-1}^{1} {}^t[N]\{f\}\,d\xi\right) \tag{3.24}$$

From which one can identify the force vector $\{F\}$ of the structure from the assembly process by:

$$\{F\} = \bigcup_e \frac{l}{2}\int_{-1}^{1} {}^t[N]\{f\}_e\,d\xi \tag{3.25}$$

3.3 Generic resolution of thin-walled structures

Returning to the dynamic motion equation (2.22) and using the matrix form of δU, δT, δW defined in equations (3.4, 3.21 and 3.24), the following expression is gotten:

$$[K]\{d\} + [M]\{\ddot{d}\} = \{F\} \tag{3.26}$$

When damping is present, similar system can be obtained. In the case of viscous damping, the equation (3.26) becomes:

$$[K]\{d(t)\} + [C]\{\dot{d}(t)\} + [M]\{\ddot{d}(t)\} = \{F(t)\} \tag{3.27}$$

Where $[C]$ is the damping matrix. The solution of the system (3.27) is admitted as periodic in the form:

$$\{d(t)\} = \{\Phi\}e^{i\Omega t} \tag{3.28}$$

3.3.1 Finite element formulation of thin-walled structures free vibrations

Thus, natural frequencies are carried out by means of the free vibration analysis by putting equation (3.28) and ($\{F\} = \{0\}, [C] = [0]$) in motions equations (3.27). In such cases, the solution of the system (3.27) is periodic in the form:

$$\{d(t)\} = \{\Phi\}e^{i\Omega t} \tag{3.28}$$

This leads to the classical eigenvalue problem:

$$(-\Omega^2[M] + [K])\{\emptyset\} = \{0\} \tag{3.29}$$

Vibration modes (angular velocities Ω_j and the eigenvectors $\{\emptyset_j\}$) are obtained by solving the eigenvalue problem. The system in equation (3.29) admits as many solutions as the number of DOF. In the presence of high number of DOF, research of all the solutions should be cumbersome and difficult to obtain. In practice, only the lower modes are of interest. An efficient solver for lower modes is then highly recommended.

3.3.2 Forced vibration of thin-walled structures in frequency domain (Steady-state dynamic analysis)

Steady-state dynamic analysis provides the amplitude and phase of the response of a system due to harmonic excitation at a given frequency. Usually such analysis is done as a frequency sweep by applying the loading at a series of different frequencies and recording the response. Otherwise, the steady-state modal dynamic analysis is a linear perturbation procedure, used to calculate the steady-state dynamic linearized response of a system to harmonic excitation. This method is detailed and used in the developed finite element approach to study the forced vibration of thin-walled beams.

3.3.2.1 Steady state modal analysis

In a mode-based steady-state dynamic analysis the response is based on modal superposition techniques; the modes of the system must first be extracted using the eigenfrequency extraction procedure. The number of modes extracted must be sufficient to model the dynamic response of the system adequately.

When defining a mode-based steady-state dynamic step, you specify the frequency ranges of interest and the number of frequencies at which results are required in each range (including the bounding frequencies of the range). In addition, the type of frequency spacing can be used linear or logarithmic or nonlinear with more points around the naturals frequencies.

In case of forced vibration with an imposed pulsation ϖ, the steady state modal method is applied in the solution [11, 44]. According to this method, solution is gotten by following two steps: the first begins by the free vibration analysis in order to get n_m specific vibration modes. In the second step, motion equations (3.27) are projected on the mode basis as:

$$\{d\} = [\emptyset]\{X\}e^{i\varpi t} \tag{3.30}$$

Where $[\emptyset]$ is the free vibration mode matrix. One gets the following system:

$$(-\varpi^2[\emptyset]^T[M][\emptyset] + i\varpi[\emptyset]^T[C][\emptyset] + [\emptyset]^T[K][\emptyset])\{X\} = [\emptyset]^T\{F_0\} \tag{3.31}$$

In the present study, structure damping is defined as Rayleigh type and it is given by:

$$[C] = \alpha[M] + \beta[K] \tag{3.32}$$

Where α and β are the mass stiffness proportional coefficients.

Defining the following modal matrix terms:

Generalized mass: $m_j = \{\emptyset_j\}^t[M]\{\emptyset_j\}$; (3.33a)

Generalized stiffness: $k_j = \{\emptyset_j\}^t [K] \{\emptyset_j\}$; (3.33b)

Generalized force: $f_j = \{\emptyset_j\}^t \{F_0\}$; (3.33c)

Generalized damping: $c_j = \{\emptyset_j\}^t [C] \{\emptyset_j\}$; (3.33d)

The solution of the problem sought in a real and imaginary parts $\{X\} = \{A\} + i\{B\}$, where the components are given by:

$$A_j(\varpi) = \frac{f_j(k_j - \varpi^2 m_j)}{(k_j - \varpi^2 m_j)^2 + \varpi^2 c_j^2} \quad (3.34)$$

$$B_j(\varpi) = \frac{-f_j \varpi c_j}{(k_j - \varpi^2 m_j)^2 + \varpi^2 c_j^2} \quad (3.35)$$

The real and the imaginary parts of the displacement vector are given by

$$\{X_{Re}(\varpi)\} = \sum_{j=0}^{n_m} A_j \{\emptyset_j\} \quad (3.36)$$

$$\{X_{Im}(\varpi)\} = \sum_{j=0}^{n_m} B_j \{\emptyset_j\} \quad (3.37)$$

The displacement magnitude results from:

$$\{X\} = \sqrt{\{X_{Re}\}^2 + \{X_{Im}\}^2} \quad (3.38)$$

By this way, the finite element approach of the model in free and forced vibrations has been described. 3D beams with 2 nodes and 7 DOF per node has been adopted in the mesh process. The present finite element (referred here B3Dw) is implanted in Maltab [80]. Warping, rotational kinematic terms as well as flexural-torsional couplings are taken into consideration. The present model is validated below on the basis of some benchmark solutions, commercial codes Abaqus [64], Adina [81] and original test results found in literature. It is noticeable that, the eigenfrequencies *f* are computed in Hz with ($f = \Omega/2\pi$).

3.3.2.2 Study base motion effect (earthquakes)

Sometimes the support of the structure undergoes motion, this phenomenon is called base motion. The commons example of base motion is when the structure is subjected to earthquakes. Let $\{y(t)\}$ denote the base displacement signal in time domain. The acceleration $\{\ddot{y}(t)\}$ can be carried out as second derivative of the displacement signal $\{y(t)\}$. Moreover, by applying Fourier Transformation the acceleration signal in time domain can be transformed to frequency domain $\{\ddot{Y}(\omega)\}$. The motion equation (3.27) in this case becomes as follows:

$$(-\omega^2 [\emptyset]^T [M][\emptyset] + i\omega [\emptyset]^T [C][\emptyset] + [\emptyset]^T [K][\emptyset])\{X\} = [\emptyset]^T \{F_0\} \quad (3.39)$$

When $\{F_0\} = [M]\{\ddot{Y}(\omega)\}$ (3.40)

Therefore, the steady state solution is carried out from this equation as demonstrated in section 3.3.2.1.

3.3.2.3 Vibration excitation with random signal

In this paragraph, the response of a structure subjected to a random response defined as a nondeterministic continuous excitation that is expressed in a statistical intellect by a cross-spectral density (CSD) matrix. The same steps used in the steady-state modal method detailed previously in section 3.3.2.1 and to investigate response spectrum of harmonic signal are used for the investigation of a random signal response. The procedure consists to compute the eigenvalues (angular velocities, eigenfrequencies) by free vibration study of the un-damped structure, then to calculate the corresponding power spectral densities (PSD) of response variables (acceleration, displacements, etc.) by the same steady state modal analysis.

The response of random excitation signals is treated in frequency domain. Therefore, random response is carried out from integration of a series of sinusoidal vibrations. signals. Hence, the response of a random signal is obtained by the same steady-state solution method presented before.

When the structure is excited by a random load defined as a single time record or a cross-correlation of time records. A Fourier transformation (described in chapter 1) of this signal is proceeded to provide the matrix of cross-spectral density functions [R (f)] in the frequency domain. A range of frequencies is chosen in which the structure response will be carried out. This range depend to some considered structure modes.

The theory of random response analysis is detailed in the following references, Clough and Penzien [94], Hurty and Rubinstein [95], and Thompson [96].

It I important to note that the excitation should be ergodic. This means, the time average is the same for several samples of the excitation.

3.4 Numerical application and analysis

In this part, different benchmarks are considered to validate the developed finite element model B3Dw with literature and commercial codes. Otherwise, some present examples are studied and compared to commercial codes to prove the accuracy of the present model in both free and forced vibration domain. In the case of Abaqus code, shell elements (S8R) and 3D beam elements (B31OS) are used. In Adina, an efficient 3D beam element including torsion and warping has been recently implemented. It should be noted that in the validation examples the elements size have chosen in B3Dw models with respect to beams sections and lengths. For the considered examples, the size of elements was about 0.1 m, thus, a model with only 10 to 60 elements (for beams of length 1m - 6m) was sufficient to converge the calculation in order to obtain accurate results. Otherwise, for shell elements thousands of elements was needed, that cost a long calculation time.

3.4.1 Free vibration of a singly-symmetric cross section cantilever beam

The cantilever beam with singly symmetric channel cross section solved by Gendy [32] studied in chapter 2 is re-concerned here as the first example in the validation procedure. The geometry and the material data are given in Figure 3.2.

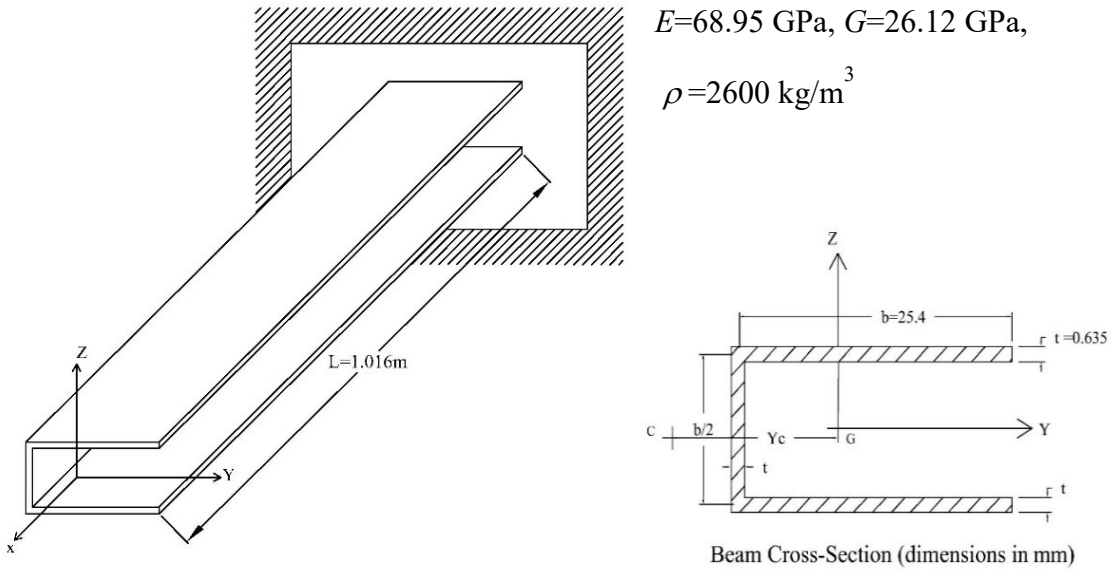

Figure 3.2: Cantilever beams with mono-symmetric channel cross-section.

For the beam represented in Figure 3.2, the first 6 vibration modes have been computed are presented in Table 3.1. Modes types are presented in (column 2), analytical solutions have been computed (column 3) and compared to the numerical solutions of the present model (column 4) and Abaqus simulations arranged in the columns 5 and 6. Benchmark solutions [32, 82] are reminded in the last columns for comparison. All the solutions are close. In comparison to [32] results, the obtained B3Dw frequencies are so close to reference values. The slight difference founded is due to the interpolations done in Gendy's model element. The six first mode shapes carried out by B3Dw element match with [32, 82] references results. Second and sixth modes are pure bending. Other modes are flexural-torsional coupled. This approve that in free vibration for mono-symmetric sections about *y* axis, the beam exhibits flexural-torsional modes (*w* bending in the strong axis *yy* and θ_x torsion about beam axis are coupled) and pure bending mode (*v* component alone leading to bending in the weak axis *zz*).

Table 3.1: Comparison of the present natural frequencies to benchmark values (values in Hz, **FT**: flexural, torsional coupled mode; **B**: bending mode).

Mode	**Type**	**Present (Analytic)**	Present (B3Dw)	Abaqus (Shell)	Abaqus (B31OS)	Beam [82]	Shell [82]	HMC2 [32]
1	**FT**	**11.28**	11.34	11.40	11.26	11.38	11.42	11.42
2	**B**	**23.18**	23.16	23.15	23.17	23.15	23.15	23.15
3	**FT**	**43.42**	43.36	42.62	42.60	42.57	42.67	42.67
4	**FT**	**57.16**	57.50	57.79	57.40	57.67	58.17	58.05
5	**FT**	**109.01**	109.36	106.65	109.41	106.50	107.20	107.88
6	**B**	**145.17**	145.01	144.45	144.71	144.50	144.60	145.12

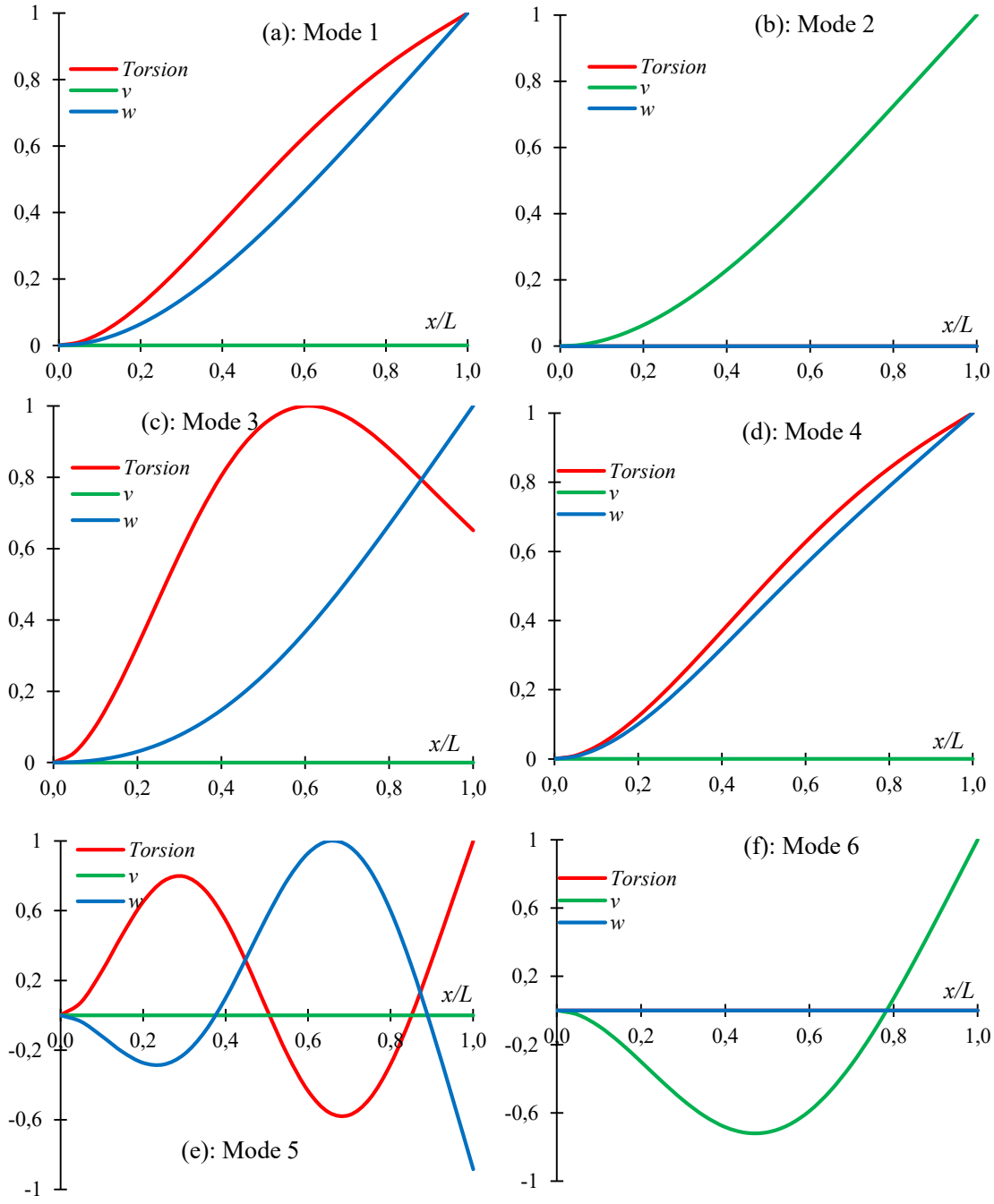

Figure 3.3: The first 6 free vibration mode shapes of the channel beam (a-f: mode 1-6)

Otherwise, Figure 3.3 illustrates the six first mode shapes carried out by B3Dw element. One observes that the second and sixth mode (Figure 3.3b, f) are pure bending uncoupled modes. All other modes are flexural-torsional coupled modes (Figure 3.3a, c, d and e) These results are mentioned in references [32, 70]. It is then confirmed that in free vibration for mono-symmetric sections, the beam exhibits flexural-torsional modes (w and θ_x coupled) and pure bending mode (v component alone leading to bending in the weak axis zz).

3.4.2 Flexural-torsional free vibration of a simply supported beam with arbitrary cross section

In this section, the simply supported beam with arbitrary non-symmetric cross section treated in Prokić [33] is also re-considered for B3Dw model validation. The geometry and the material properties of the beam are given in Figure 3.4. The position of the shear point is also viewed.

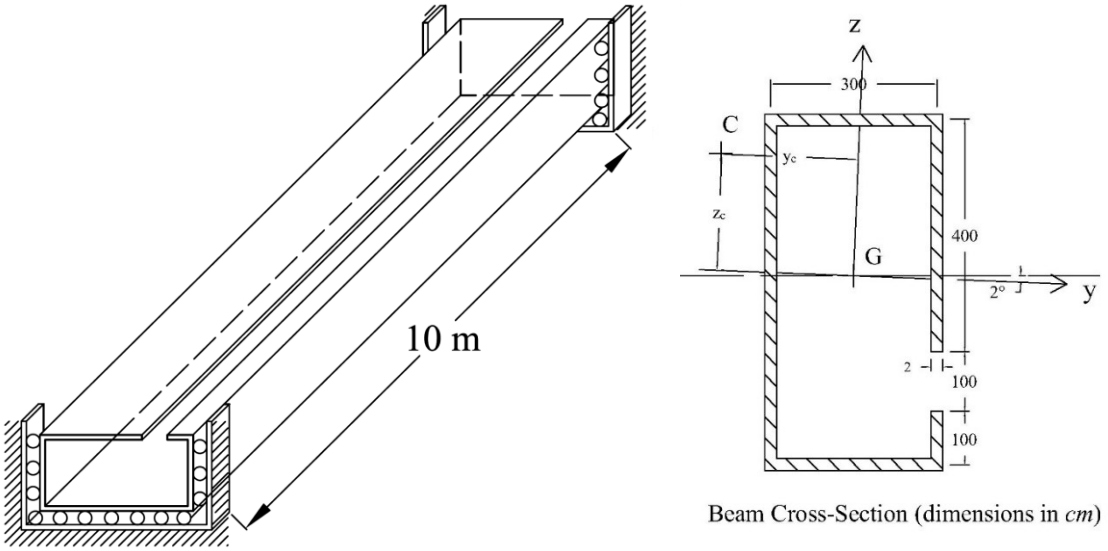

E=210 GPa, ν=0.30, G=80.07 GPa, ρ=7850kg/m^3

Figure 3.4 : Simply supported beam with arbitrary cross section: geometry, sections dimensions and material properties.

The different results are summarized in Table 3.2. The natural frequency solutions given in Table 3.2a are obtained analytically and numerically by taking into account or omitting the rotational terms and warping terms. The analytical solutions are computed from three theories. The classical beam theory (CBT), omitting warping terms(WTO) are dressed in the column 2. The Vlasov's theory without rotary terms (RTO) and with rotary terms (RTI) follow in columns 3 and 4. The numerical solutions of the present model, Adina, Abaqus and Prokic benchmark values are arranged in columns 5 to 8. Taking Adina's results as reference, the errors of the different solutions are presented in Table 3.2b. Since the cross section is arbitrary, all the vibration modes are flexural-torsional and torsion governs the behavior. This is the reason why the CBT is out of order in this example. The errors of this method range between 10 and more than 90%. This fact is known and checked since long time [42, 43]. The rotary terms present in the mass matrix are important in dynamic analyses especially in presence of higher modes with frequencies higher than 100 Hz. One remarks that the error can reach 20%. The numerical solutions of the present model are in good agreement with Adina's and Prokic's solutions. Moreover, one remarks some discrepancies in Abaqus values in the case of higher modes with frequencies higher than 100 Hz.

The first nine vibration modes of the beam are pictured in Figure 3.5. Since the cross section is arbitrary, it is confirmed that all the vibration modes are flexural-torsional. One can see that the displacements v, w and θ_x are present in all the modes. The concept of triply coupled flexural-torsional adopted in literature is confirmed [33, 83]. Nevertheless, one can check that the displacements v and θ_x are predominant in modes (1, 2, 4, 5, 7 and 8). The displacements w and θ_x are important in the remaining modes.

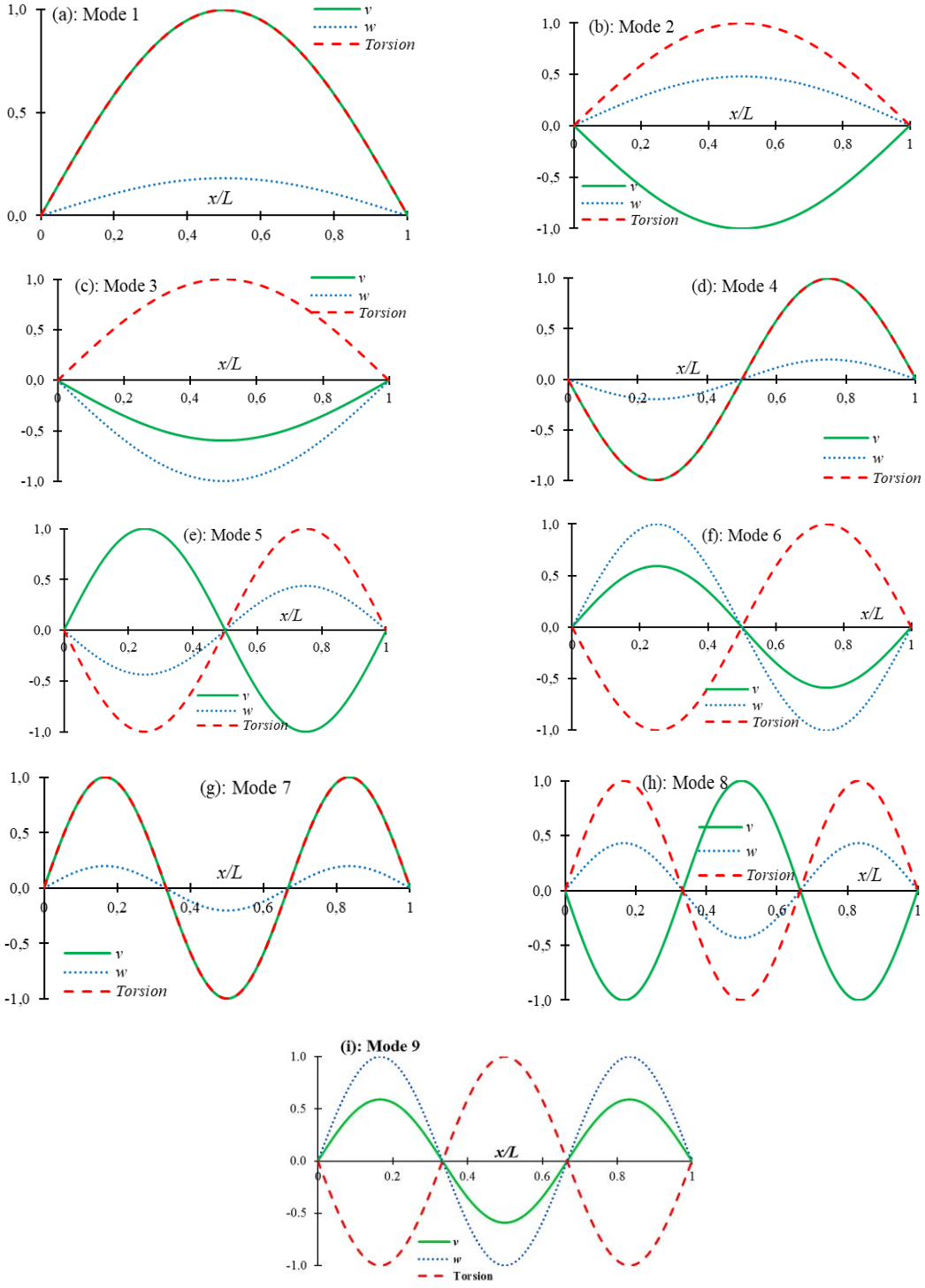

Figure 3.5 : The first nine free vibration mode shapes of the beam.

Table 3.2: Comparison between the present models natural frequencies (Hz) and references values.
(WTO: Warping terms omitted, RTO: Rotational Terms Omitted, RTI: Rotational Terms Included)

	CBT (WTO)	Vlasov (RTO)	Present (RTI)	Present (B3Dw)	Adina (Beam)	Abaqus (B31OS)	Prokić [33]
n=1	3.84	8.78	8.78	8.78	8.78	8.77	8.68
	11.93	13.17	13.15	13.16	13.16	13.12	13.02
	30.07	34.30	34.19	34.12	34.12	33.36	33.83
n=2	7.84	34.41	34.28	34.23	34.23	34.07	33.86
	47.21	52.10	51.81	51.84	51.84	51.23	51.32
	116.62	135.88	133.79	131.45	131.50	121.32	130.35
n=3	11.81	76.80	76.27	76.43	76.43	75.67	75.61
	105.27	116.98	115.53	115.68	115.70	112.73	114.52
	261.49	304.99	283.70	283.92	283.90	244.30	281.51
n=4	15.77	136.29	134.64	135.13	135.10	132.78	not studied
	186.19	207.82	203.30	203.75	203.80	195.01	not studied
	449.75	541.74	510.25	480.03	480.00	386.03	not studied
n=5	19.72	212.78	208.81	209.96	210.00	204.41	not studied
	288.25	324.60	313.81	314.84	314.80	295.10	not studied
	644.80	846.15	712.28	708.17	708.20	536.93	not studied

Table 3.2 (continue) : Errors values in % (Adina Results as reference)

	CBT (WTO)	Vlasov (RTO)	Present (RTI)	Present (B3Dw)	Abaqus	Prokić [33]
n=1	56.26	0.00	0.00	less than 0.5%	0.11	1.14
	9.37	0.08	0.08		0.30	1.06
	11.87	0.53	0.21		2.23	0.85
n=2	77.08	0.53	0.15		0.47	1,08
	8.94	0.50	0.06		1.18	1.00
	11.32	3.37	1.74		7.74	0.87
n=3	84.55	0.48	0.21		0.99	1.07
	9.01	1.12	0.15		2.57	1.02
	7.89	7.42	0.07		13.95	
n=4	88.33	0.86	0.34		1.72	
	8.64	2.00	0.25		4.31	
	6.30	12.86	6.30		19.58	
n=5	90.61	1.34	0.57		2.66	
	8.43	3.10	0.31		6.26	
	8.95	19.48	0.58		24.18	

3.4.3 Hong Hu Chen benchmark numerical study

Chen [22] introduced a finite element method for the coupled vibration analysis of thin-walled beams with a generic open section. The developed element has two nodes with seven degrees of freedom per node. in the model he used the kinematics of the Euler beam, the d'Alembert principle, and the virtual work principle. Stiffness mass matrix are obtained by differentiating the element deformation nodal force vector and element inertial nodal force vector with respect to the element nodal parameters and their second time derivatives, respectively.

To validate his model Chen took five numerical examples from literature [33, 41, 47], then he studied the free vibration problem of these beams under five different boundary conditions presented in Figure 3.6.

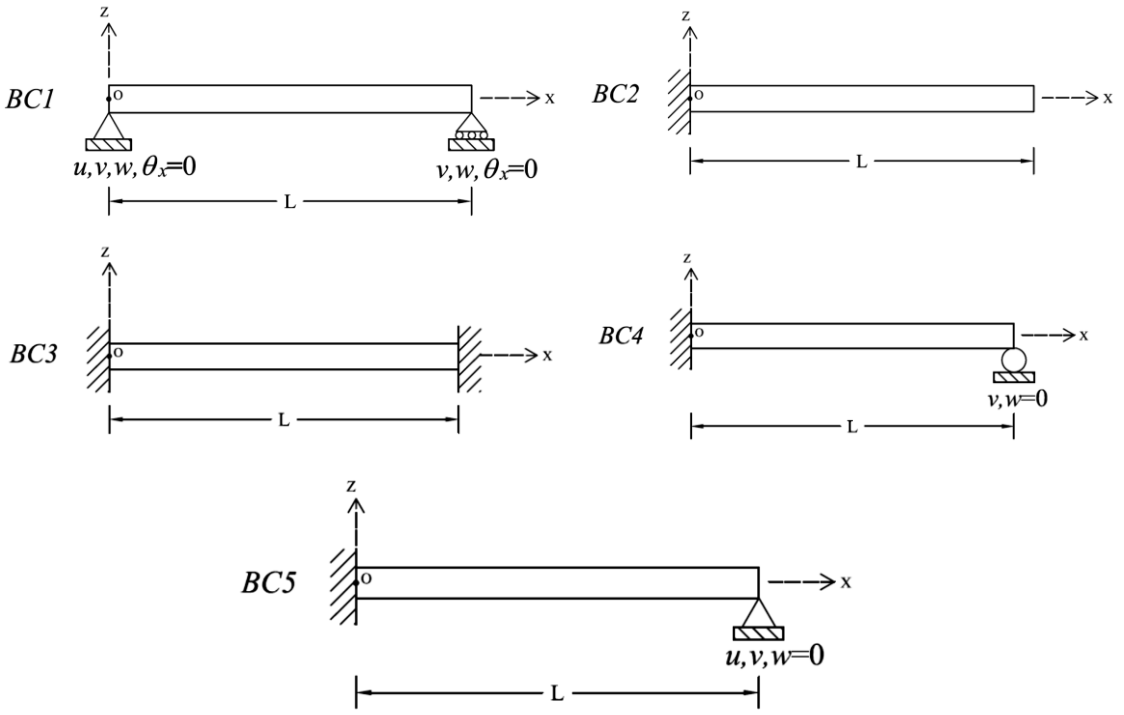

Figure 3.6: Five boundaries conditions studied by Chen. (BC1-BC5)

For the studied beams the sections, geometry and materials properties are depicted in the following Figures (3.7-3.11):

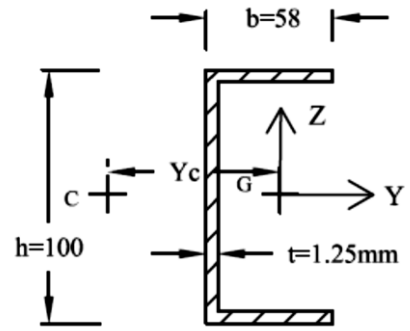

Beam geometry and material properties:
L= 1.28 m
A= 2.669 cm^2
I_y= 0.450 cm^4
I_z= 9.396 cm^4
I_t= 0.014 cm^4
I_ω= 163.6 cm^6
y_c= -37.71 mm
z_c= 0 mm
E= 216.4 GPa
G= 80.1 GPa
m= 2.095 kg/m

Figure 3.7: Beam 1 with channel cross section.

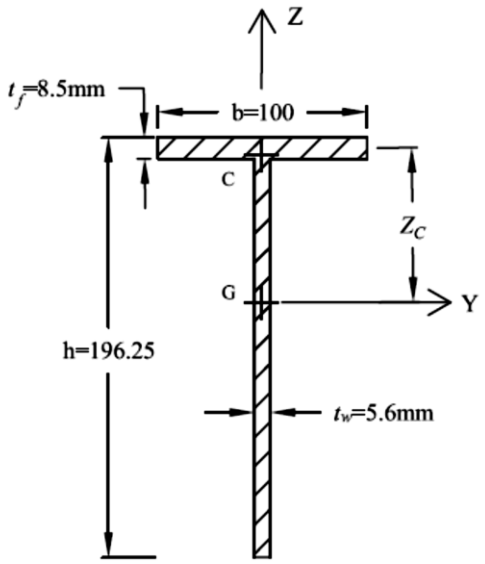

Beam geometry and material properties:
L= 2.00 m
A= 19.252 cm^2
I_y= 768.39 cm^4
I_z= 71.1143 cm^4
I_t= 3.17103 cm^4
I_ω= 38.6899 cm^6
y_c= 0 mm
z_c= 53.88 mm
E= 210 GPa
G= 80.77 GPa
ρ= 7800 kg/m^3

Figure 3.8: Beam 2 with Tee cross section.

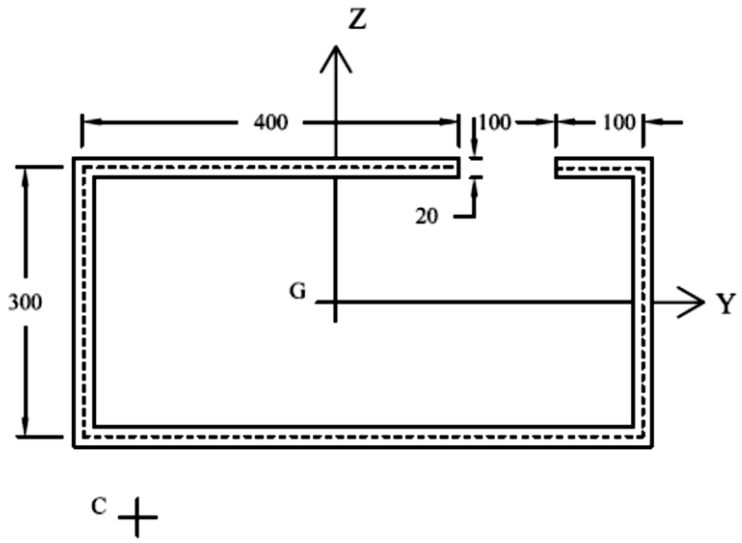

Beam geometry and material properties:
L= 10.00 m
A= 340 cm^2
I_y= 58114.6 cm^4
I_z= 175303 cm^4
I_t= 453.333 cm^4
I_ω= 128016000 cm^6
y_c= -0.23526 m
z_c= -0.31147 m
E= 210 GPa
G= 80.7 GPa
ρ= 8.002 kN.s^2/m^4

Figure 3.9: Beam 3 with arbitrary cross section.

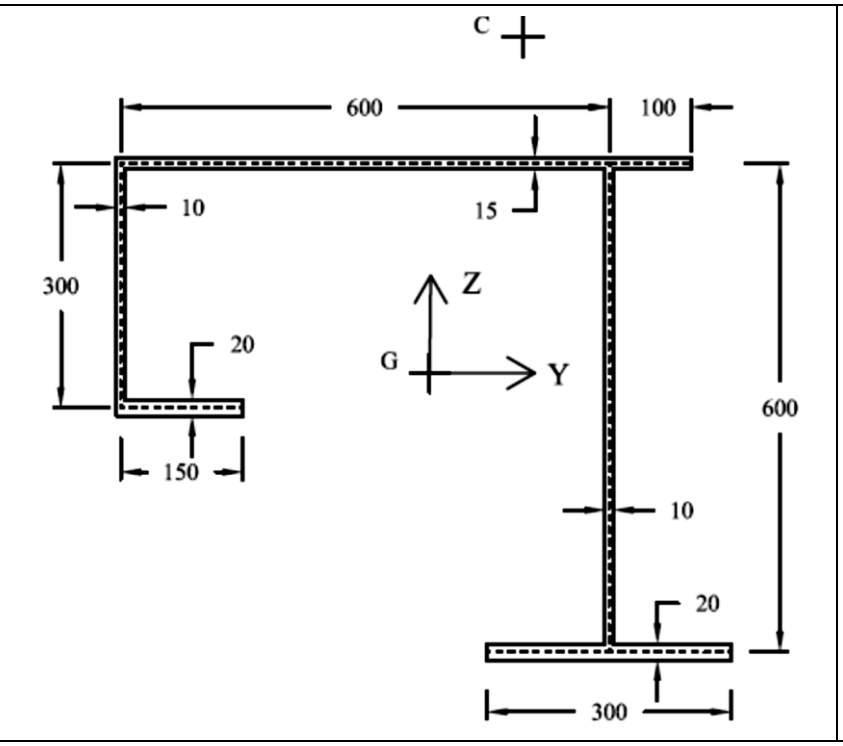

Beam geometry and material properties:
L= 10.00 m
A= 285 cm^2
I_y= 102858 cm^4
I_z= 239265 cm^4
I_t= 228.750 cm^4
I_ω= 92633300 cm^6
y_c= -0.19755 m
z_c= 0.39183 m
E= 210 GPa
G= 80.7 GPa
ρ= 8.002 kN.s^2/m^4

Figure 3.10: Beam 4 with arbitrary cross section.

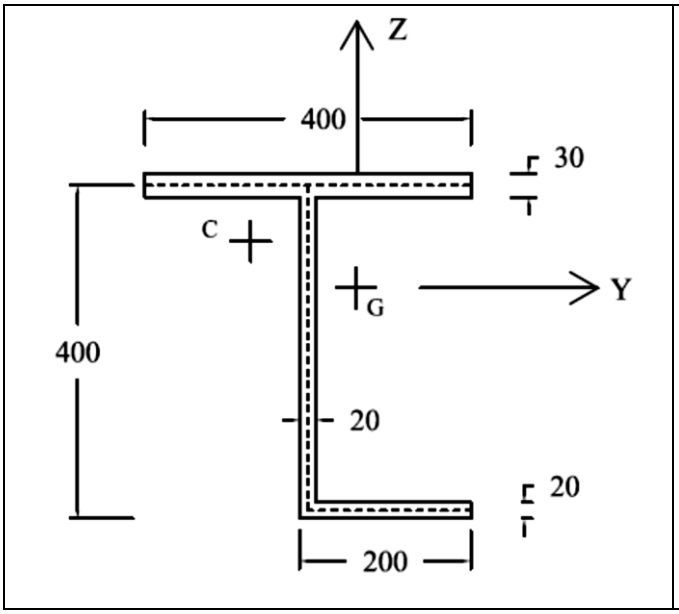

Beam geometry and material properties:
L= 10.00 m
A= 240 cm^2
I_y= 66582.7 cm^4
I_z= 18213.9 cm^4
I_t= 520.000 cm^4
I_ω= 3942550 cm^6
y_c= -0.054809 m
z_c= 0.086555 m
E= 210 GPa
G= 80.7 GPa
ρ= 8.002 kN.s^2/m^4

Figure 3.11: Beam 5 with arbitrary cross section.

Hereafter, in Tables 3.3-3.7 a comparison among the given results of free vibration natural frequencies and the developed FEM (B3Dw) in order to validate the present model with different sections types and boundary condition.

Table 3.3: Comparison between the present models and references values of angular velocities Ω (rad/s) and vibration modes.
(*W*: flexural mode, *T*: torsional mode, *V*: lateral bending mode)

Mode	Beam 1, BC1				Beam 1, BC2			
	Present	References		Mode type	**Present**	References		Mode type
	B3Dw	BC1M[47]	BC1CM[22]		**B3Dw**	BC2CM[47]	BC2x[22]	
1	**421.65**	421.73	421.59	*W,T*	**159.40**	159.40	159.38	*w,t*
2	**591.98**	x	592.83	*V*	**211.01**	x	211.31	*v*
3	**1653.70**	1656.69	1653.48	*W,T*	**616.75**	619.21	616.68	*w,t*
4	**1717.53**	1732.59	1717.33	*W,T*	**932.63**	934.00	932.51	*w,t*
5	**2360.46**	x	2363.83	*V*	**1318.45**	x	1320.33	*v*
6	**3698.70**	3714.81	3698.25	*W,T*	**2576.24**	2585.97	2575.91	*w,t*
7	**5283.50**	x	5291.02	*V*	**3674.23**	x	3679.45	*v*
8	**6445.14**	x	6445.14	*A*	**3757.42**	3866.61	3757.01	*w,t*
9	**6544.69**	6596.09	6544.06	*W,T*	**5018.68**	x	5018.13	*w,t*
10	**6688.36**	x	6687.65	*W,T*	**6445.14**	x	6445.14	*Axial*

Table 3.3 (continue)

Mode	Beam 1, BC3				Beam 1, BC4		
	Present	References		Mode type	**Present**	Reference	Mode type
	B3Dw	BC3CM[47]	BC3x[22]		**B3Dw**	BC4CM[22]	
1	**938.33**	938.71	938.20	W,T	**163.63**	163.61	w,t
2	**1341.60**	x	1343.52	V	**924.62**	925.95	v
3	**2574.19**	2579.75	2573.86	W,T	**932.13**	932.01	w,t
4	**3684.93**	x	3690.20	V	**2554.90**	2554.59	w,t
5	**3881.34**	3924.04	3880.90	W,T	**2701.09**	2700.77	w,t
6	**5026.30**	5050.68	5025.75	W,T	**2986.38**	2990.64	v
7	**7184.00**	x	7194.27	*V*	**5016.28**	5015.73	*w,t*
8	**8273.54**	8344.01	8272.94	*W,T*	**6197.44**	6206.27	*v*
9	**10388.32**	x	10387.20	*W,T*	**6445.14**	6445.14	*Axial*
10	**11786.89**	x	11803.90	*V*	**8218.80**	8218.19	*w,t*

Table 3.3: (continue)

Mode	Beam 1, BC5		
	Present	Reference	Mode type
	B3Dw	BC5CM [22]	
1	**163.63**	163.61	*w,t*
2	**924.62**	925.95	*v*
3	**932.13**	932.01	*w,t*
4	**2554.90**	2554.59	*w,t*
5	**2701.09**	2700.77	*w,t*
6	**2986.38**	2990.64	*v*
7	**5016.28**	5015.73	*w,t*
8	**6197.44**	6206.27	*v*
9	**8218.80**	8218.19	*w,t*
10	**8476.46**	8475.59	*w,t*

Table 3.4: Comparison between the present models and references values of angular velocities Ω (rad/s) and vibration modes.
(*W*: flexural mode, *T*: torsional mode, *V*: lateral bending mode)

Mode	Beam 2, BC1			Beam 2, BC2		
	Present	Reference	Mode	**Present**	Reference	Mode
	B3Dw	BC1x [22]		**B3Dw**	BC2CM [22]	
1	**190.81**	190.81	*V,T*	**78.42**	78.42	*v,t*
2	**401.87**	401.87	*V,T*	**173.53**	173.56	*v,t*
3	**463.22**	463.22	*V,T*	**287.48**	287.48	*w*
4	**729.53**	729.54	*V,T*	**351.21**	351.24	*v,t*
5	**804.87**	804.87	*W*	**582.23**	582.34	*v,t*
6	**1007.25**	1007.27	*V,T*	**809.51**	809.52	*v,t*
7	**1303.69**	1303.76	*V,T*	**890.98**	891.15	*v,t*
8	**1336.59**	133.60	*V,T*	**1182.91**	1183.18	*v,t*
9	**1623.63**	1623.85	*V,T*	**1488.28**	1488.77	*v,t*
10	**1970.74**	1971.33	*V,T*	**1777.21**	1777.21	*w*

Table 3.4: (continue)

Mode	Beam 2, BC3			Beam 2, BC4		
	Present	Reference	Mode	**Present**	Reference	Mode
	B3Dw	BC3x [22]		**B3Dw**	BC4CM [22]	
1	**244.82**	244.89	*V,T*	**121.82**	121.84	*v,t*
2	**506.17**	506.32	*V,T*	**350.95**	350.98	*v,t*
3	**727.78**	727.93	*V,T*	**502.62**	502.69	*v,t*
4	**807.07**	807.18	*V,T*	**655.44**	655.50	*v,t*
5	**1070.07**	1070.44	*V,T*	**887.31**	887.49	*v,t*
6	**1384.15**	1384.71	*V,T*	**1182.02**	1182.30	*v,t*
7	**1720.17**	1721.10	*V,T*	**1256.34**	1256.35	*w*
8	**1822.36**	1822.37	*W*	**1484.04**	1484.51	*v,t*
9	**2029.91**	2029.95	*V,T*	**1667.78**	1667.83	*v,t*
10	**2087.43**	2089.05	*V,T*	**1832.32**	1833.24	*v,t*

Table 3.4: (continue)

Mode	Beam 2, BC5		
	Present	Reference	Mode
	B3Dw	BC5CM [22]	
1	**121.82**	121.84	*v,t*
2	**350.95**	350.98	*v,t*
3	**502.62**	502.69	*v,t*
4	**655.44**	655.50	*v,t*
5	**887.31**	887.49	*v,t*
6	**1182.02**	1182.30	*v,t*
7	**1256.34**	1256.35	*w*
8	**1484.04**	1484.51	*v,t*
9	**1667.78**	1667.83	*v,t*
10	**1832.32**	1833.24	*v,t*

Table 3.5: Comparison between the present models and references values of of angular velocities Ω (rad/s) and vibration modes.

Mode	Beam 3, BC1			Beam 3, BC2	
	Present	References		Present	Reference
	B3Dw	BC1CM [22]	BC1CM [33]	**B3Dw**	BC2CM [22]
1	**54.54**	54.41	54.41	**20.56**	20.56
2	**81.83**	81.83	81.83	**30.27**	30.27
3	**212.57**	212.57	212.57	**79.36**	79.36
4	**212.73**	212.74	212.73	**120.46**	120.46
5	**322.45**	322.45	322.45	**181.25**	181.25
6	**475.06**	475.07	475.05	**331.19**	331.2
7	**719.54**	719.56	719.57	**462.95**	462.95
8	**804.70**	804.90 (A)	x	**501.21**	501.21
9	**818.99**	819.00	819.01	**644.38**	644.42
10	**839.94**	840.03	x	**804.70**	804.9(A)
11	**1267.38**	1267.51	x	**972.61**	972.67
12	**1305.14**	1305.48	x	**1058.84**	1059.01
13	**1768.75**	1768.81	1768.75	**1241.28**	1241.3
14	**1867.82**			**1571.83**	

Table 3.5: (continue)

Mode	Beam 3, BC3		Beam 3, BC4		Beam 3, BC5	
	Present	Reference	**Present**	Reference	**Present**	Reference
	B3Dw	BC3x [22]	**B3Dw**	BC4CM [22]	**B3Dw**	BC5CM [22]
1	**120.71**	120.71	**28.47**	28.47	**28.47**	28.47
2	**183.35**	183.35	**105.74**	105.74	**105.74**	105.74
3	**330.70**	330.70	**143.98**	143.98	**143.98**	143.98
4	**474.68**	474.68	**306.10**	306.10	**306.10**	306.10
5	**502.33**	502.33	**341.72**	341.73	**341.72**	341.73
6	**645.23**	645.27	**425.37**	425.38	**425.37**	425.38
7	**977.49**	977.56	**628.97**	629.00	**628.97**	629.00
8	**1061.50**	1061.68	**804.70**	804.9(A)	**856.98**	857.03
9	**1269.73**	1296.75	**856.98**	857.03	**1013.03**	1013.10
10	**1577.15**	1577.75	**1013.03**	1013.10	**1072.74**	1072.85
11	**1600.86**	1601.13	**1072.74**	1072.85	**1430.95**	1431.19
12	**1609.43**	1611.04(A)	**1430.95**	1431.19	**1569.97**	1570.48
13	**2189.18**	2190.78	**1569.97**	1570.48	**1609.43**	1611.04(A)
14	**2364.40**		**2061.07**		**2061.07**	

Table 3.6: Comparison between the present models and references values of angular velocities Ω (rad/s) and vibration modes.
(*W*: flexural mode, *T*: torsional mode, *V*: lateral bending mode)

Mode	Beam 4, BC1			Beam 4, BC2	
	Present	References		**Present**	Reference
	B3Dw	BC1CM [22]	BC1CM [33]	**B3Dw**	BC2CM [22]
1	**51.05**	51.05	51.05	**19.90**	19.9
2	**101.41**	101.41	101.41	**36.28**	36.28
3	**197.83**	197.83	197.83	**84.57**	84.57
4	**233.71**	233.71	233.71	**112.35**	112.35
5	**402.91**	402.91	402.91	**225.30**	225.3
6	**441.49**	441.50	441.48	**307.97**	307.98
7	**780.73**	780.81	x	**509.02**	509.03
8	**804.70**	804.9(A)	x	**599.02**	599.06
9	**897.67**	897.70	897.74	**624.97**	624.98
10	**904.15**	904.15	904.15	**804.70**	804.9(A)
11	**1213.73**	1214.04	x	**984.65**	984.82
12	**1574.75**	1574.92	x	**1209.15**	1209.22
13	**1738.21**	1739.13	x	**1362.36**	1362.38
14	**1939.98**	1940.05	1939.99	**1462.62**	1463.16

Table 3.6: (continue)

Mode	Beam 4, BC3		Beam 4, BC4		Beam 4, BC5	
	Present	Reference	**Present**	Reference	**Present**	Reference
	B3Dw	BC3x [22]	**B3Dw**	BC4CM [22]	**B3Dw**	BC5CM [22]
1	**112.22**	112.22	**21.28**	21.28	**21.28**	21.28
2	**229.58**	229.58	**111.88**	111.88	**111.88**	111.88
3	**307.25**	307.25	**158.91**	158.91	**158.91**	158.91
4	**526.86**	526.86	**306.30**	306.30	**306.30**	306.30
5	**599.50**	599.54	**365.52**	365.52	**365.52**	365.52
6	**628.51**	628.53	**509.62**	509.63	**509.62**	509.63
7	**986.63**	986.80	**599.00**	599.04	**599.00**	599.04
8	**1219.38**	1219.46	**804.70**	804.9(A)	**981.04**	981.20
9	**1402.46**	1402.48	**981.04**	981.20	**1054.68**	1054.73
10	**1466.77**	1467.33	**1054.68**	1054.73	**1142.00**	1142.01
11	**1609.43**	1611.04(A)	**1142.00**	1142.01	**1461.38**	1461.92
12	**1987.84**	1988.18	**1461.38**	1461.92	**1609.43**	1611.04(A)
13	**2037.48**	2038.97	**1776.20**	1776.45	**1776.20**	1776.45
14	**2616.05**	2616.21	**2028.09**	2029.51	**2028.09**	2029.51

Table 3.7: Comparison between the present models and references values of of angular velocities Ω (rad/s) and vibration modes.
(*W*: flexural mode, *T*: torsional mode, *V*: lateral bending mode)

Mode	Beam 5, BC1			Beam 5, BC2	
	Present	References		**Present**	Reference
	B3Dw	BC1CM [22]	BC1CM [33]	**B3Dw**	BC2CM [22]
1	**42.41**	42.41	42.41	**15.48**	15.48
2	**74.91**	74.91	74.91	**29.18**	29.18
3	**99.48**	99.48	99.48	**47.64**	47.64
4	**150.87**	150.87	150.87	**92.68**	92.68
5	**227.12**	227.12	227.12	**148.38**	148.38
6	**304.82**	304.82	304.81	**203.39**	203.39
7	**357.85**	357.86	357.85	**232.30**	232.31
8	**474.64**	474.66	474.64	**342.03**	342.04
9	**508.80**	508.85	x	**409.04**	409.06
10	**766.41**	766.58	x	**553.94**	553.95
11	**792.09**	792.11	792.13	**627.86**	627.93
12	**804.70**	804.90(A)	x	**649.09**	649.16
13	**822.66**			**804.70**	
14	**1078.57**			**920.50**	

Table 3.7: (continue)

Mode	Beam 5, BC3		Beam 5, BC4		Beam 5, BC5	
	Present	Reference	**Present**	Reference	**Present**	Reference
	B3Dw	BC3x [22]	**B3Dw**	BC4CM [22]	**B3Dw**	BC5CM [22]
1	**84.94**	84.94	**39.24**	39.24	**39.24**	39.24
2	**127.94**	127.94	**74.36**	74.36	**74.36**	74.36
3	**203.43**	203.43	**126.16**	126.16	**126.16**	126.16
4	**213.46**	213.46	**148.00**	148.00	**148.00**	148.00
5	**331.35**	331.36	**222.27**	222.28	**222.27**	222.28
6	**392.33**	392.35	**290.06**	290.06	**290.06**	290.06
7	**553.66**	553.67	**405.20**	405.22	**405.20**	405.22
8	**624.11**	624.20	**453.38**	453.38	**453.38**	453.38
9	**632.75**	632.79	**550.74**	550.77	**550.74**	550.77
10	**909.99**	910.30	**644.05**	644.14	**644.05**	644.14
11	**1031.69**	1031.86	**804.70**	804.9(A)	**891.64**	891.86
12	**1073.88**	1073.95	**891.64**	891.86	**926.87**	926.92
13	**1250.55**		**926.87**		**959.35**	
14	**1526.18**		**959.35**		**1249.77**	

From these numerical examples, by analyzing Tables 3.3-3.7 it is remarkable that the angular velocities Ω (rad/s) and the vibration modes for thin-walled beams with different boundary conditions and arbitrary cross sections types match well with the benchmarks

results. Thus, the accuracy of the developed FEM (B3Dw) is demonstrated in free vibration context.

3.4.4 Double clamped cruciform cross-section beam

More recently, the free vibration of doubly clamped thin-walled beam with cruciform cross section was studied theoretically and experimentally by Piana *et al.* [58]. The beam length, the material properties and the cross section dimensions are shown in Figure 3.12. Based on experimental setup, the eigenfrequencies of the beam were extracted by mean of impulses provided by a hammer and measurement of displacements using sensors.

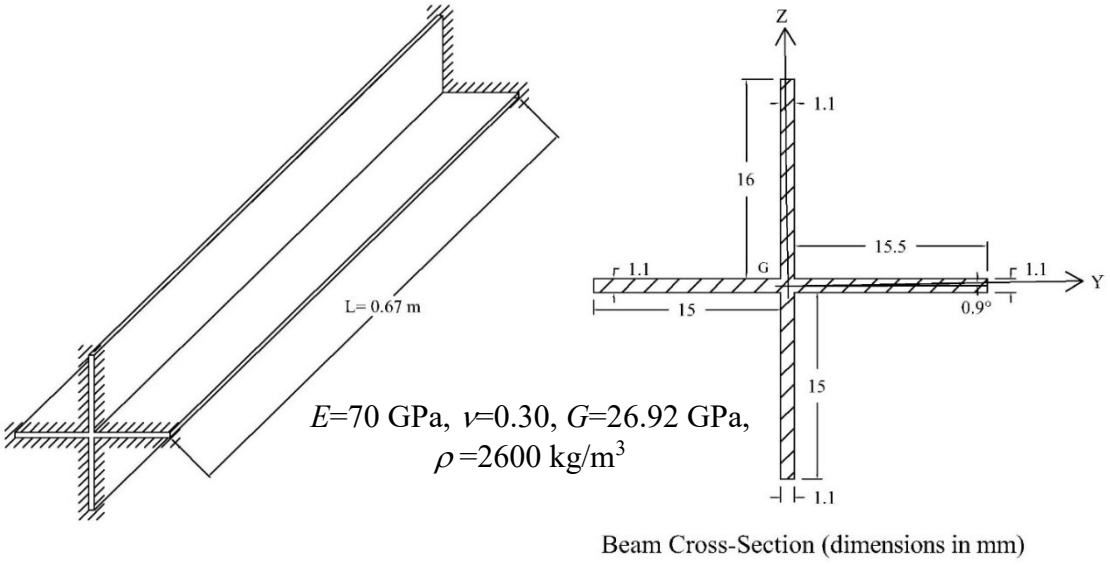

Figure 3.12: Double clamped beam with cruciform cross section.

Piana *et al.* [58] adopted a numerical model in order to compute the beam vibration modes. It is important to note that, the authors have compared results for simulation of beam with perfect cruciform symmetrical cross section and other one who takes into consideration of manufacturing imperfections. They founded that the effect of imperfection in section is important in studying of the dynamic behavior. The resonance frequencies have been computed by the present finite element model, Abaqus simulation and compared to Piana's results in case of imperfect section. These results are presented in Table 3.8 In addition, Abaqus simulations are also reported. It is important to note that in present model only 30 elements are used in the mesh process.

Table 3.8: Numerical and experimental natural frequencies comparison (values in Hz).

Mode	Test Results [58]	Imperfect cruciform cross-section			Mode Type
		Numerical Results [58]	Present B3Dw	Abaqus B31OS	
1	161.87	165.66	165.56	166.05	Mode 1:Torsion
2	275.47	263.75	266.97	265.38	Mode 1:*v*, bending
3	284.18	269.90	273.34	271.63	Mode 1:*w*, bending
4	325.43	331.69	331.17	332.16	Mode 2:Torsion
5	486.13	499.17	496.79	498.28	Mode 3:Torsion
6	667.84	667.49	662.34	664.31	Mode 4:Torsion
7	741.30	716.75	734.71	725.23	Mode 2:*v*, bending
8	767.30	733.04	752.20	742.02	Mode 2:*w*, bending
9	813.39	838.93	827.96	830.47	Mode 5:Torsion

One remarks that all the numerical solutions are close to test results of the imperfect cruciform cross-section. The accuracy of the present finite element is then justified. The free vibration of beams with arbitrary cross sections and boundary conditions have been tested successfully by the present finite element model (B3Dw) in the previous examples. The ability of the element to obtain higher vibration modes with good accuracy has been proved. In the next section, the performance of the model in the case of braced structures is studied.

3.4.5 A simply supported beam under base motion load (Earthquake, El Centro records, acc_NS)

In order to study the forced vibration behavior of beams subjected to base motion excitation, a simply supported beam subjected to an earthquake (El Centro records, acc_NS) signal is considered. The earthquake load is considered as base motion applied to the beam supports in *y* direction and in torsion respectively. For this aim, a steel beam with IPE300 cross section presented in Figure 2.10 is taken. Beam geometry and material properties are the followings: cross section dimensions, h=300mm, b=150mm, t_f =10.7mm, t_w=7.1mm, beam total slenderness L=6m, the used materials elasticity, Poisson coefficient, shear modulus and material density are respectively $E = 210\ GPa$, $\nu = 0.3$, G= 80.77 GPa, $\rho = 7800\ kg/m^3$. The beam supports are subjected to two different types of base motions respectively. The seismic record (El Centro records, acc_NS) is adopted as excitation signal in *y* direction v=v_{EQ} subjected to the supports see Figure 3.13a, then used as torsional base motion θ_x= $\theta_{x\ EQ}$ subjected to the beam boundary conditions as depicted in Figure 3.13.b. The beam material is steel, so a small value of damping is taken into consideration based on the reference loss factor for steel material mentioned in Table 1.2. So, the calculated damping values in the [C] matric are c_v=$c_{\theta x}$=106 N.s/m for the node corresponding to the beam mind point. (otherwise damping values for all other nodes are taken c =0).

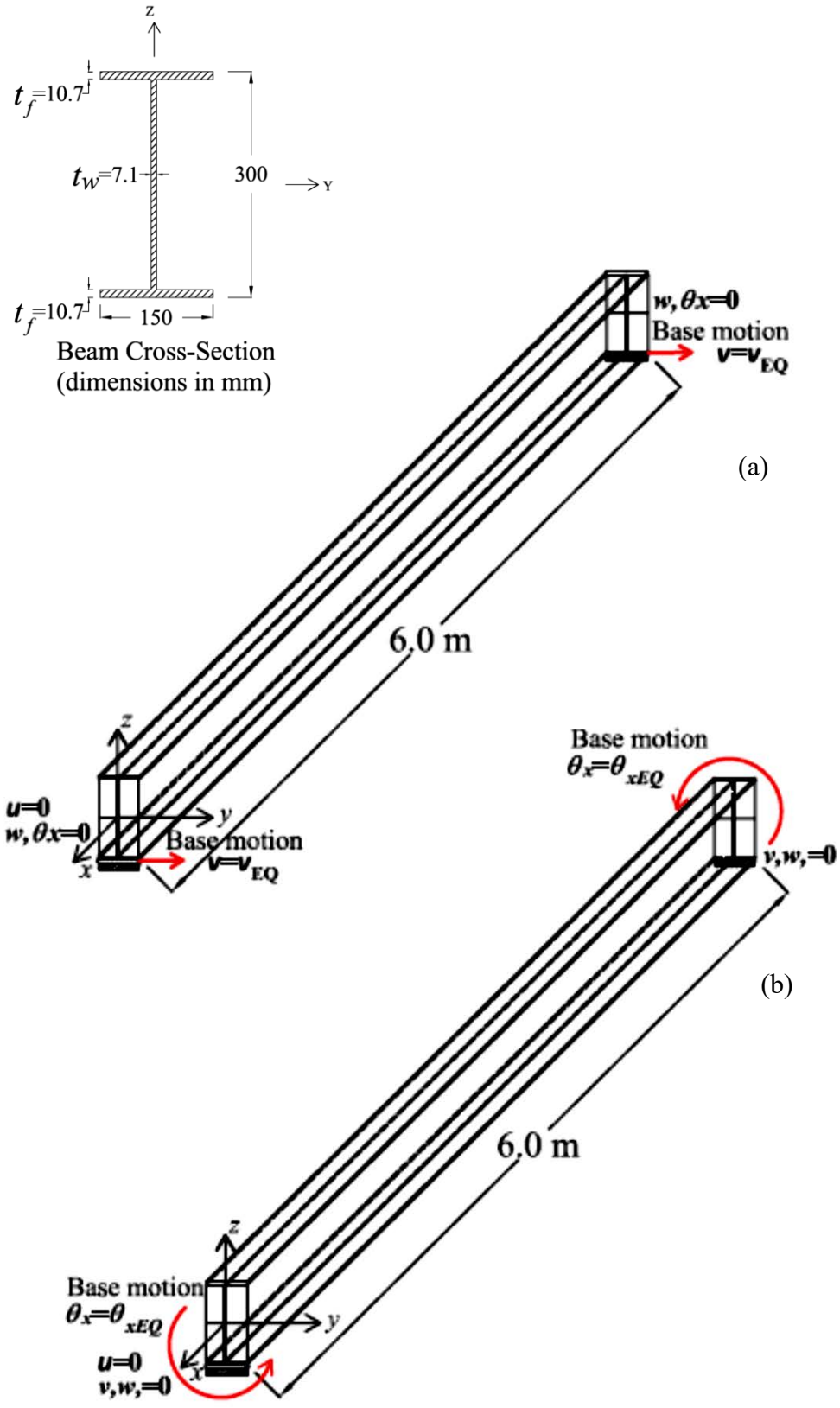

Figure 3.13: Simply supported beam with IPE300 cross section subjected to (a) lateral and (b) torsional base motions

The earthquake recorded by (El Centro records, acc_NS) is subjected to the beam to carry out the dynamic response spectrum of a structure under base motion condition. El Centro records are tabulated, series of accelerations and the corresponding times are depicted in the table given by El Centro. In this table each 0.02 second the acceleration is registered, the earthquake total duration is 53 seconds. This data is transformed to frequency domain by applying Fourier Transformation, using the FFT algorithm implemented in Matlab. The original signal in time domain and the transformed signal in frequency domain are plotted and presented in Figure 3.14 given below.

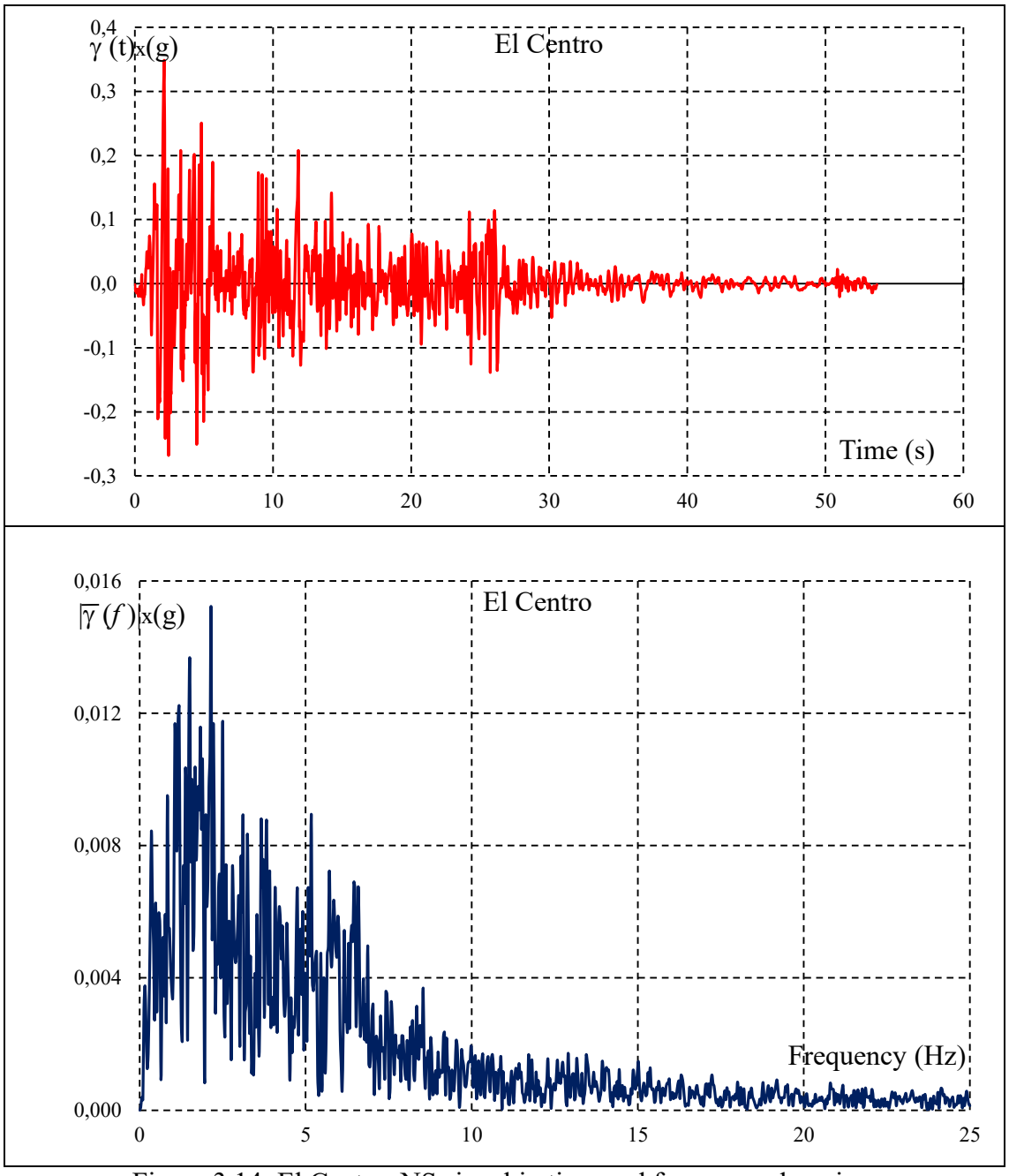

Figure 3.14: El Centro_NS signal in time and frequency domains.

By applying earthquake recorded signal (El Centro_NS) presented in Figure 3.14 as base motion (v_{EQ} in y direction) of the simply supported beam depicted in Figure 3.13. In this example the beam is low damped. The displacement response spectrum of the beam midpoint is carried out using B3Dw element. Otherwise, to validate the present element the same model is studied using Abaqus commercial code and results are depicted in the same graph in Figure 3.15.

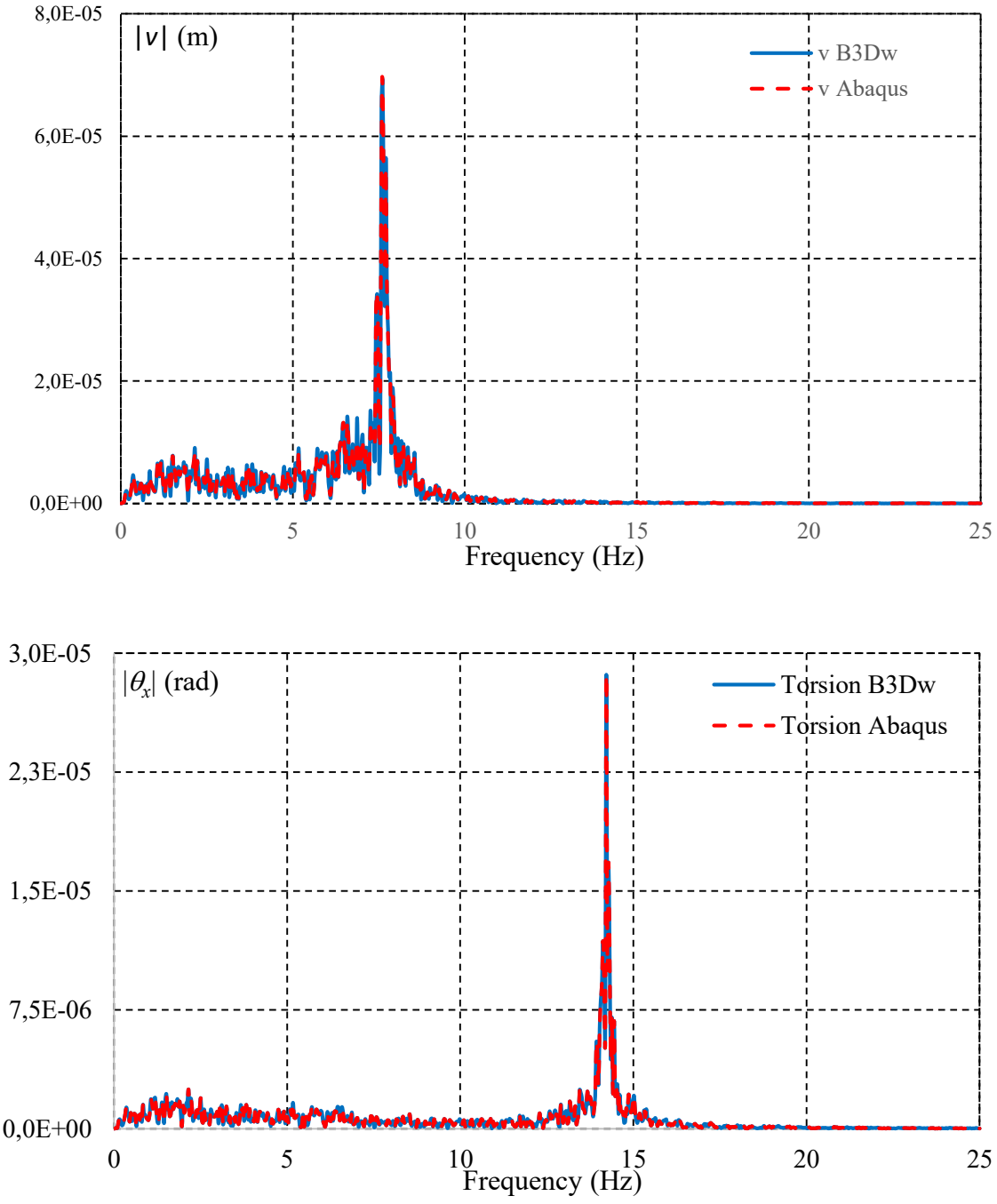

Figure 3.15: Lateral displacement and torsional response spectra of the I beam midpoint, subjected to El Centro_NS earthquake signal.

By analyzing the response spectra results shown in Figure 3.15, it is remarkable that the response spectrum of the beam midpoint obtained by B3Dw match well with Abaqus ones. Thus, the efficiency of the present method can be significantly proved compared with Abaqus commercial code results.

3.4.6 Forced vibration analysis of thin-walled beams doubly-symmetrical section

The dynamic behavior of a doubly-symmetric cross section under harmonic 3D forces is considered in this paragraph. To this aim, an IPE300 beam with two different boundary conditions (cantilever, simply supported) are studied in forced vibration analysis. The geometry and the martial data are available in Figure 3.16.

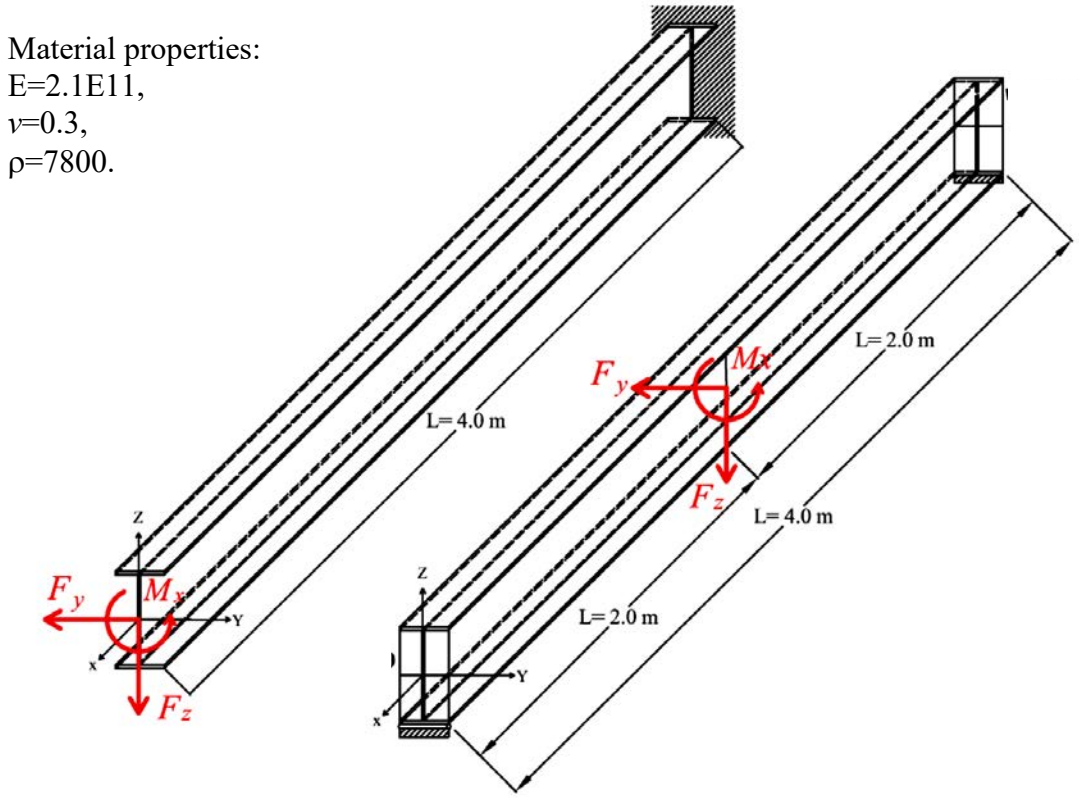

Figure 3.16: Cantilever and simply supported beam with IPE300 cross section and applied loads F_y, F_z, M_x.

To study the forced vibration behavior of these beams the following harmonic forces and moments are applied at the free end of the beam in the case of cantilever beam and at mid-point of the simply supported beam. The amplitude of the concentrated forces are F_y =1kN, F_z =1kN and torsional moment amplitude is given by M_x =1kNm. The Rayleigh damping coefficients are taken from literature for steel beams materials, as follows $\alpha = \beta$ =1*10^{-3}. The beam response spectrum displacements and torsion angle magnitudes at the free end for the cantilever beam and at the mid-point of the simply supported beam are

obtained and plotted in frequency domain, the range of frequencies in this study is taken between 1-200 Hz. As well as in the free vibration investigation, for the doubly-symmetric section the vibration modes are uncoupled in forced vibration.

Thus, frequencies are pure bending or torsion. The dynamic behavior of the cantilever beam at the tip end in presence of the bending force F_y is depicted in Figure 3.17, bending force F_z is depicted in Figure 3.18 and torsional momentum M_x is depicted in Figure 3.19. So, in Figure 3.17 only the lateral displacement v is present when force F_y is applied, in Figure 3.18 only the flexural displacement w is present when force F_z is applied and in Figure 3.19 only the torsion angle θ_x is present when M_x is applied. Otherwise, peaks values are present at the frequencies (6.15 - 38.41 Hz) in Figure 3.17, (22.52 Hz) in Figure 3.18 and (12.72 Hz) in Figure 3.19, which are respectively eigenfrequencies in y, z and torsion. This value is exactly the same to the frequency of the free vibration analysis.

For the simply supported beam the point is taken in the middle of the beam. The (amplitude of displacements and rotation) dynamic response spectra obtained in presence of the bending force F_y is depicted in Figure 3.20, bending force F_z is depicted in Figure 3.21 and torsional momentum M_x is depicted in Figure 3.22. So, in Figure 3.20 only the lateral displacement v is present when force F_y is applied, in Figure 3.21 only the flexural displacement w is present when force F_z is applied and in Figure 3.22 only the torsion angle θ_x is present when M_x is applied. Otherwise, peaks values are present at the frequencies (17.24Hz) in Figure 3.20, (61.48 Hz) in Figure 3.21 and (26.18 Hz) in Figure 3.22, which are respectively eigenfrequencies in y, z and torsion. This value is exactly the same to the frequency of the free vibration analysis.

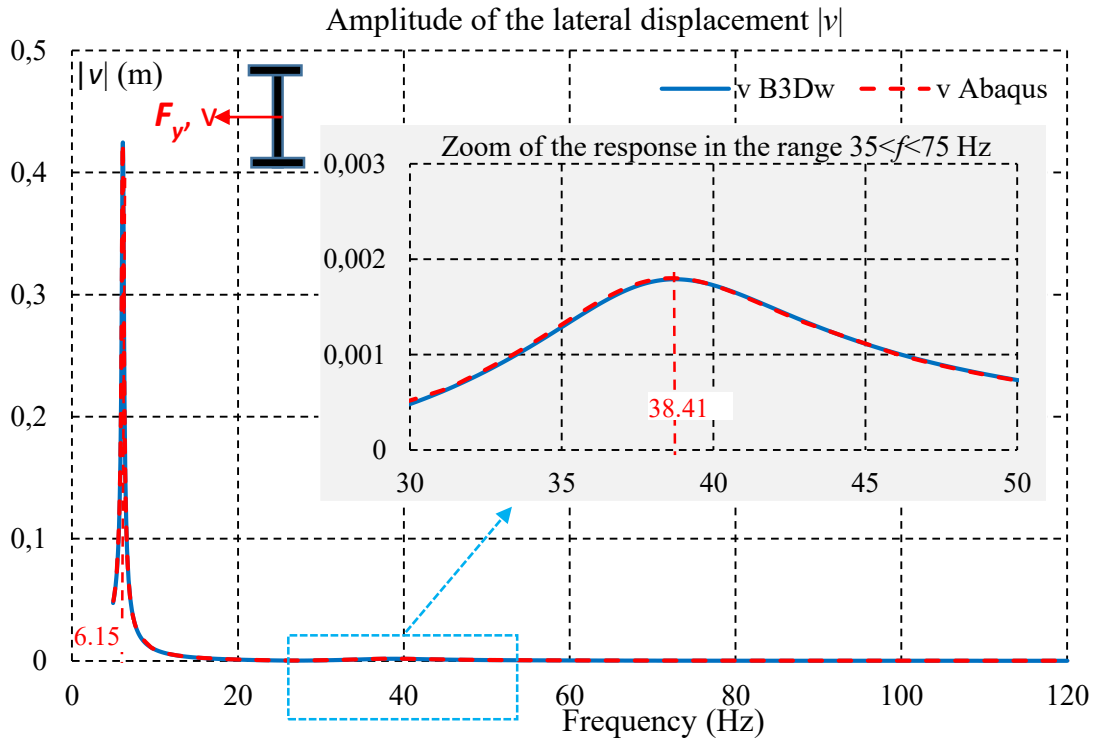

Figure 3.17: Lateral response at the tip of the IPE300 cantilever beam under harmonic force F_y in frequency range $2<f<120$ Hz.

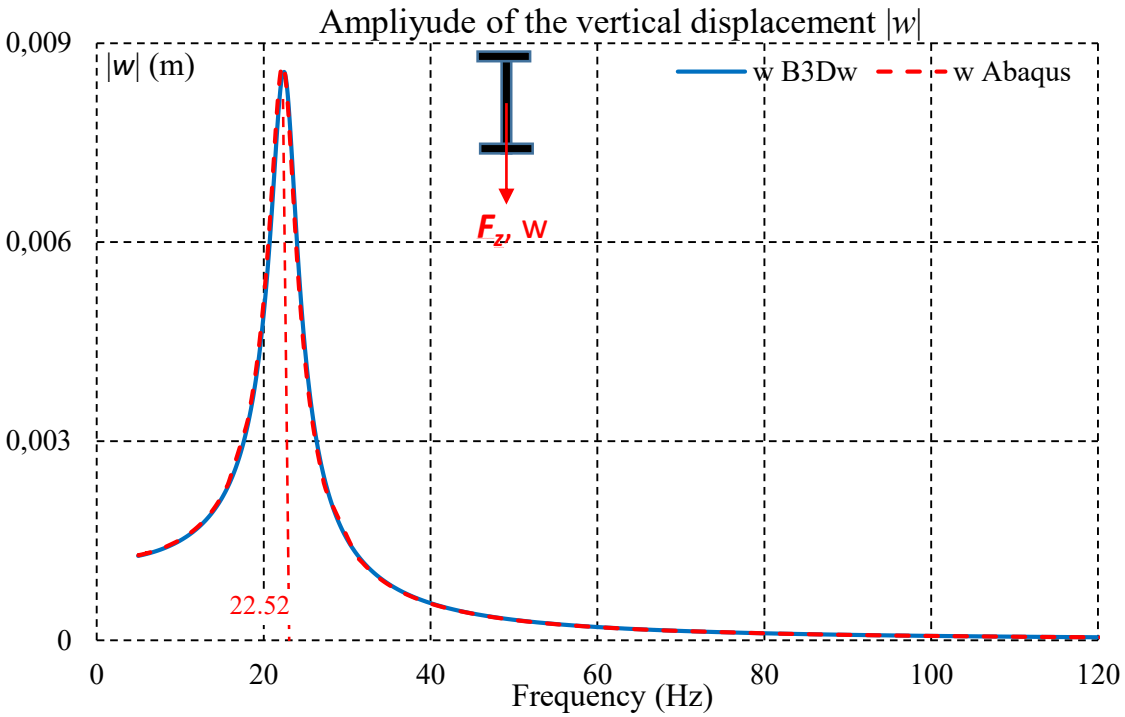

Figure 3.18: Vertical response at the tip of the IPE300 cantilever beam under harmonic force F_z in frequency range 2<f<120 Hz.

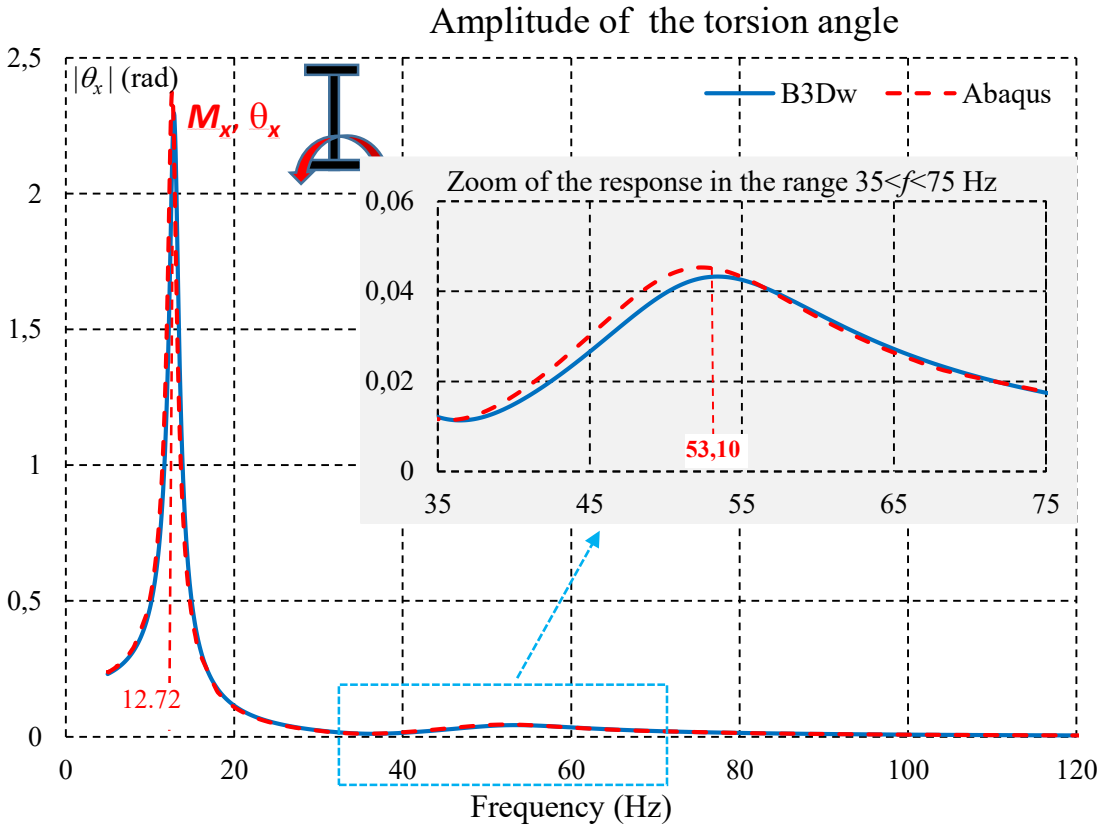

Figure 3.19: Torsion response at the tip of the IPE300 cantilever beam under harmonic momentum M_x in frequency range 2<f<120 Hz.

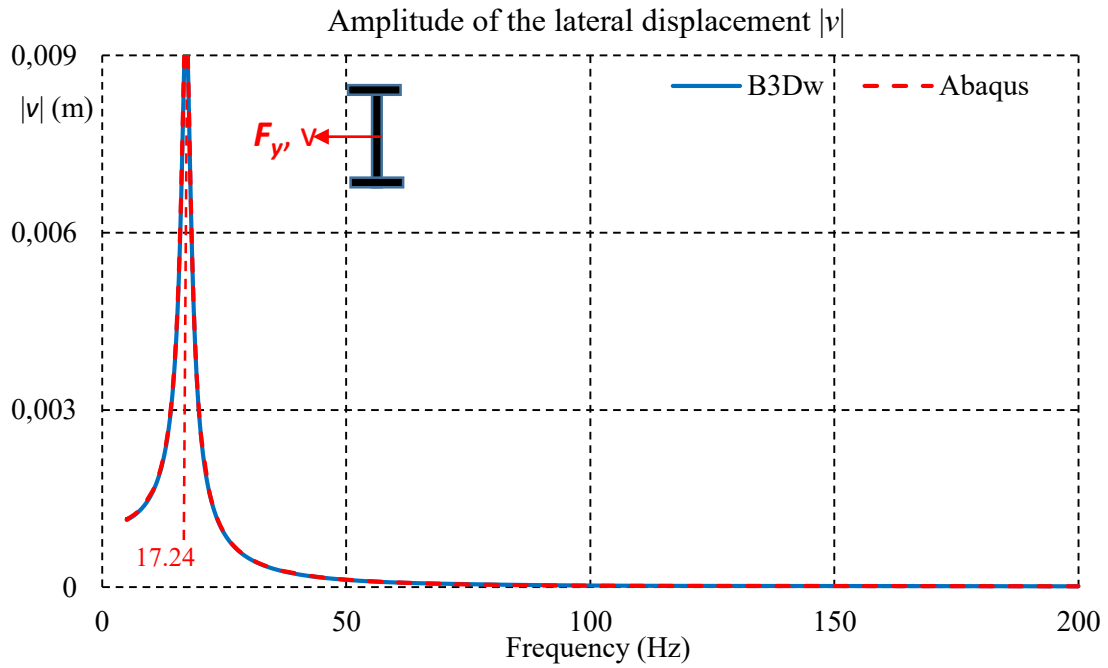

Figure 3.20: Lateral response at the mid-point of the IPE300 simply supported beam under harmonic force F_y in frequency range $2<f<200$ Hz.

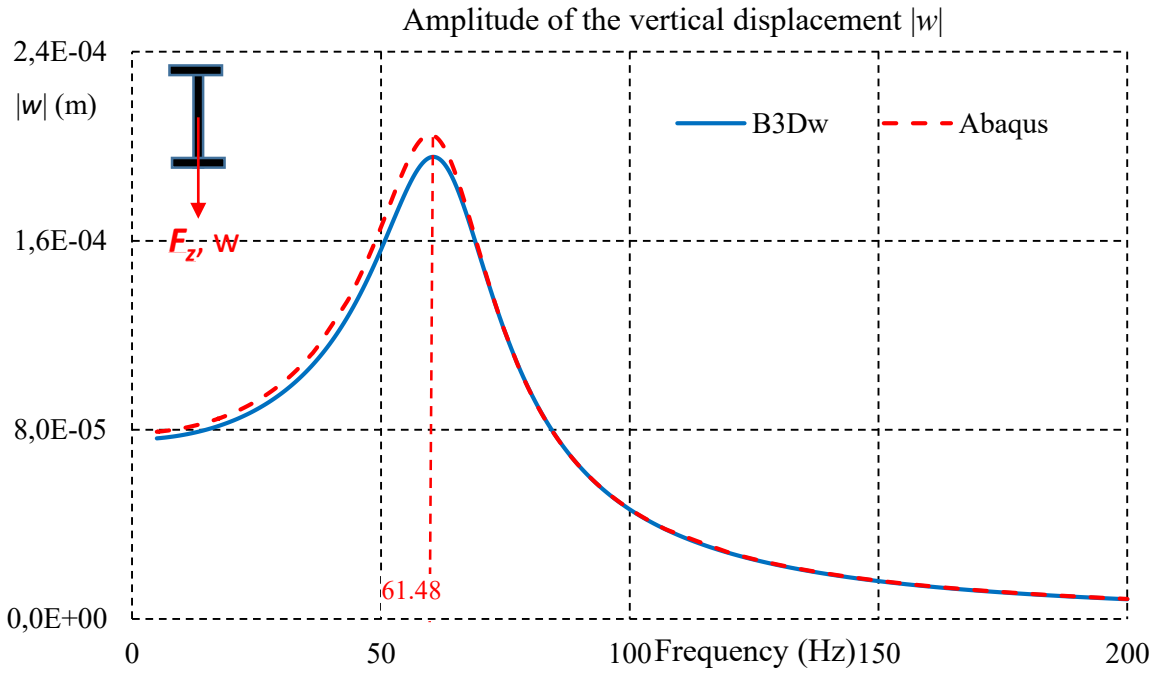

Figure 3.21: Vertical response at the mid-point of the IPE300 simply supported beam under harmonic force F_z in frequency range $2<f<200$ Hz.

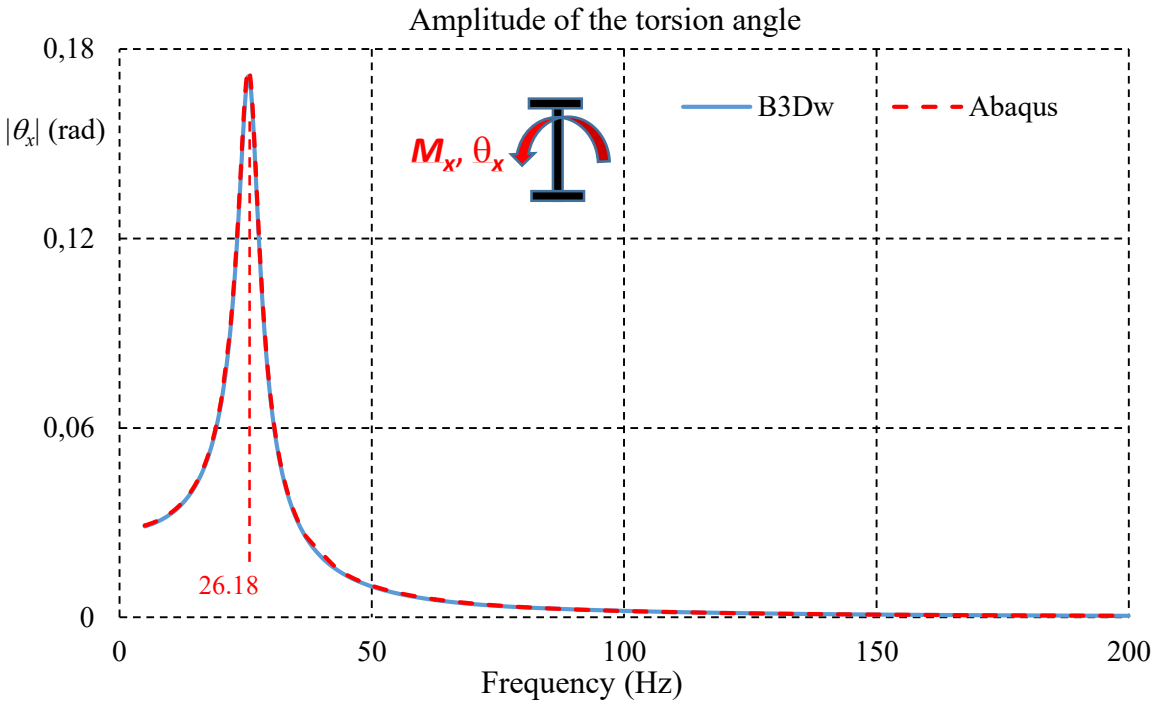

Figure 3.22: Torsional response at the mid-point of the IPE300 simply supported beam under harmonic momentum M_x in frequency range $2<f<200$ Hz.

As conclusion, the agreement of the present finite element model (B3Dw) and Abaqus simulations are very good for doubly-symmetrical sections whatever the boundary conditions are chosen.

3.4.7 Forced vibration analysis of thin-walled beams mono-symmetrical Tee section

The dynamic behavior of a mono-symmetric cross section under harmonic 3D forces is considered in this paragraph. To this aim, a Tee beam with two different boundary conditions (cantilever, simply supported) are studied in forced vibration analysis. Beam geometry are the followings: A=5.92E-03 m^2; I_y=7.89E-06 m^4; I_z=3.377E-05 m^4; I_t=4.09E-07 m^4; I_ω=1.44E-9 m^6; Y_c=0m; Z_c=0.0172m. The material properties, applied loads with their locations and beams perspectives are depicted in Figure 3.23.

Material properties:
E=210 GPa, ν=0.3,
ρ=7800 kg/m^3.

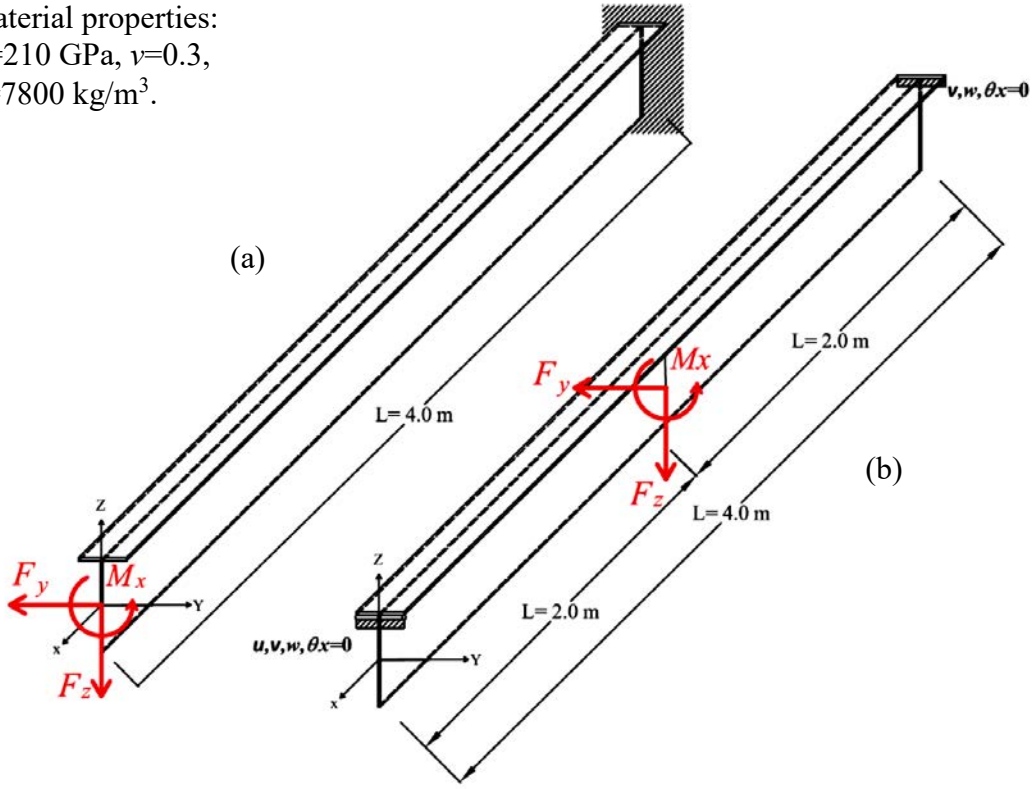

Figure 3.23: Cantilever and simply supported beam with Tee cross section and applied loads F_y, F_z, M_x. (a: cantilever, b: simply supported beam)

To study beam forced vibration behavior of the following harmonic forces and moments are applied at the free end of the beam in the case of cantilever beam and at mid-point of the simply supported beam: concentrated forces F_y =1 kN, F_z =1kN and torsional moment M_x =1 kNm. The Rayleigh damping coefficients are taken from literature for steel beams materials, as follows $\alpha = \beta = 1*10^{-3}$. The beam response spectrum displacements and torsion angle magnitudes at the free end for the cantilever beam and at the mid-point of the simply supported beam are obtained and plotted in frequency domain, the range of frequencies in this study is taken between 1-200 Hz. As well as in the free vibration investigation, for the mono-symmetric section the vibration modes are flexural-torsional v and θ_x coupled and only the lateral displacement w is present in forced vibration.

Thus, frequencies are pure bending about the strong axis y (component w) or flexural-torsional coupling (presence of weak bending displacement component v and torsion θ_x). The dynamic response spectra obtained in presence of the bending force F_y or/and torsional momentum M_x are depicted in Figures. 3.24, 3.26 and bending force F_z is depicted in Figure 3.25. So, in Figure 3.24 the lateral displacement v is present when force F_y or/and torsional momentum M_x is applied due to coupling effect, in Figure 3.25 only the flexural displacement w is present when force F_z is applied and in Figure 3.26 the torsion angle θ_x is present at the same time v displacement is remarked due to the coupling effect when force F_y or/and M_x is applied. Otherwise, peaks values are present at the frequencies (17.24 Hz) in Figure 3.24, (7.01 Hz) in Figure 3.25 and (17.24 Hz) in Figure 3.26, which are respectively the coupled eigenfrequencies in y lateral bending and torsion (same natural frequencies) or only z eigenfrequencies. These values and the natural frequencies obtained by the free vibration analysis are exactly the same.

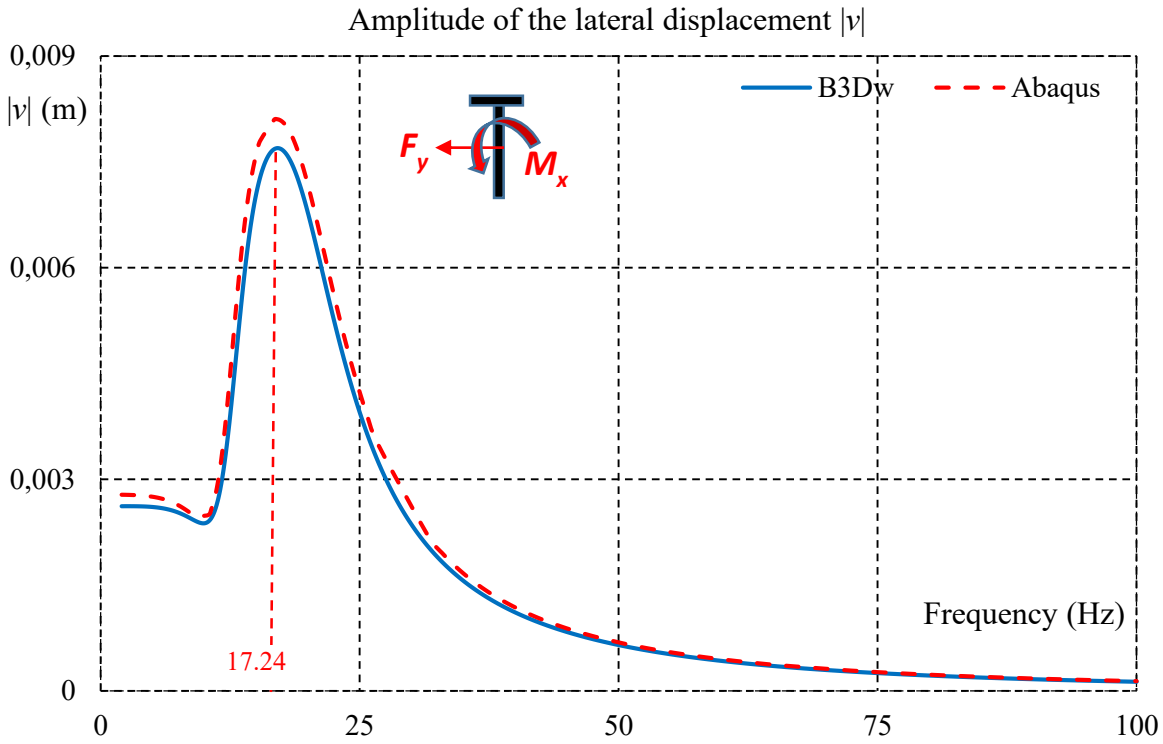

Figure 3.24: Lateral response at the tip of the Tee cantilever beam under harmonic force F_y and momentum M_x in frequency range $2<f<100$ Hz.

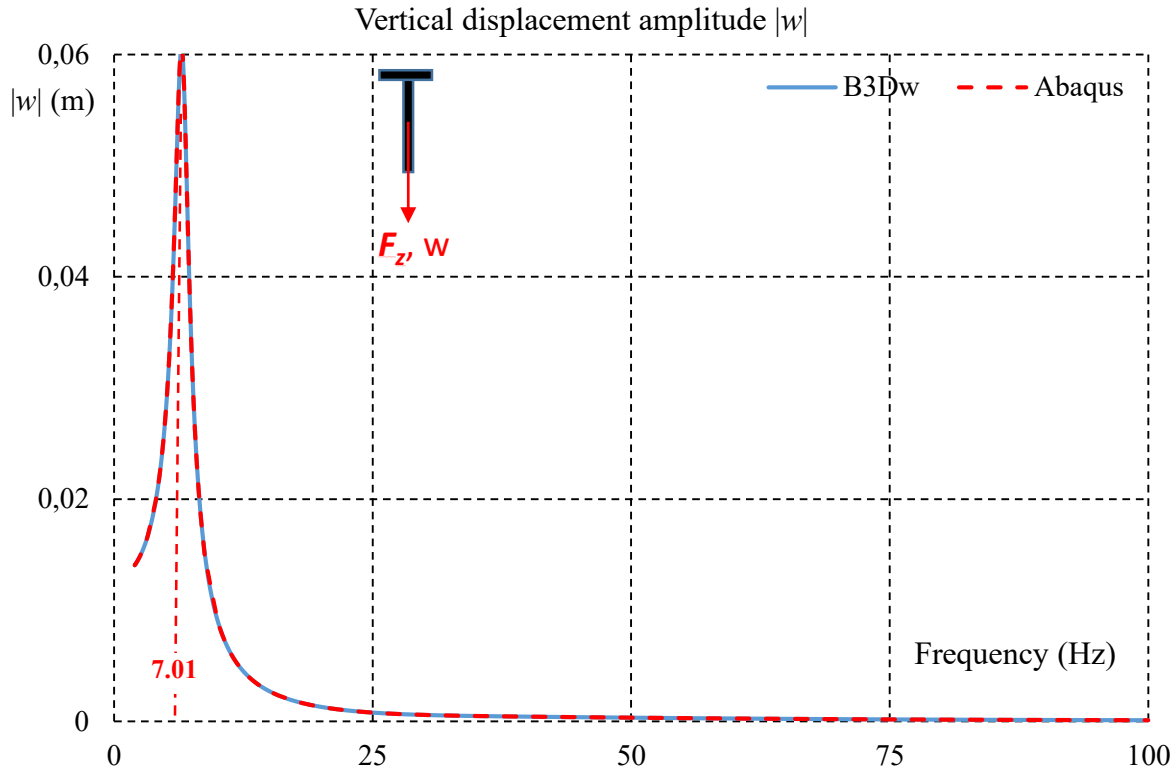

Figure 3.25: Vertical response at the tip of the Tee cantilever beam under harmonic force F_z in frequency range $2<f<100$ Hz.

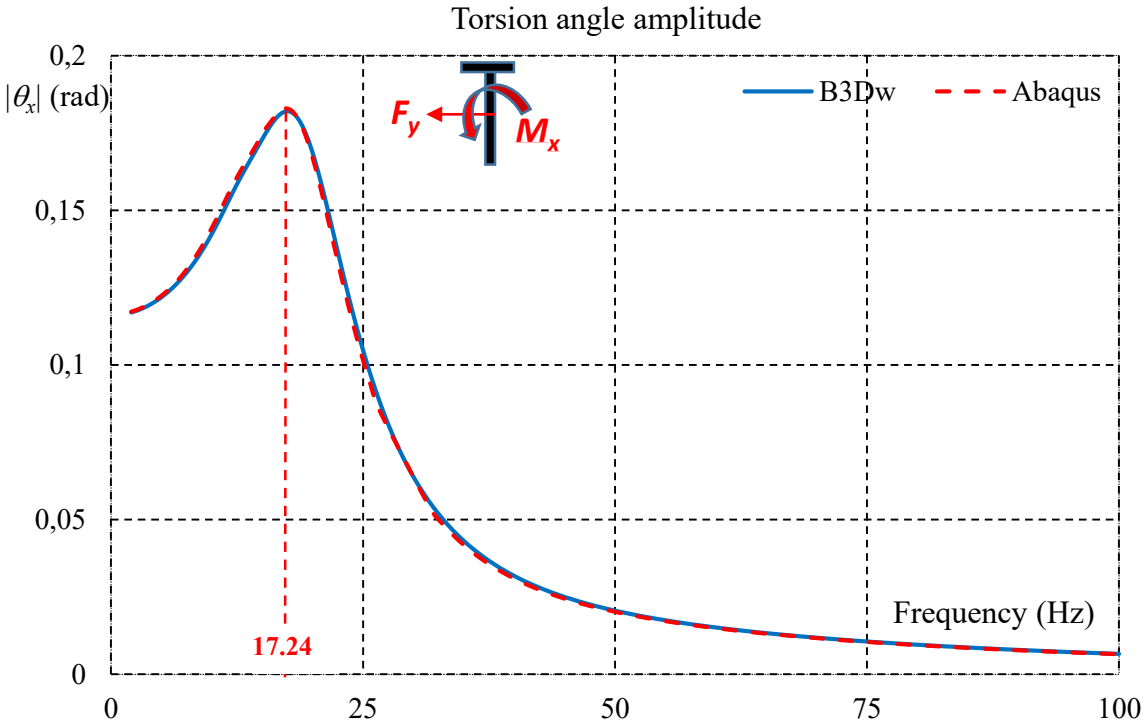

Figure 3.26: Torsion response at the tip of the Tee cantilever beam under harmonic force F_y and momentum M_x in frequency range $2<f<100$ Hz.

For the simply supported beam the point is taken in the middle of the beam.

For the simply supported beam the point is taken in the middle of the beam. The dynamic response spectra obtained in presence of the bending force F_y or/and torsional momentum M_x are depicted in Figures. 3.27, 3.29 and bending force F_z is depicted in Figure 3.28. Moreover, due to coupling effect for mono-symmetric sections in Figure 3.27 the lateral displacement v is present when force F_y or/and torsional momentum M_x is applied. Otherwise, in Figure 3.28 only the flexural displacement w is present only when force F_z is applied. Thus, In Figure 3.29 the torsion angle θ_x is present at the same time v displacement due to the coupling effect when force F_y or/and M_x is applied. Furthermore, peaks values are respectively present at the frequencies (35.27, 42.76 Hz) in Figure 3.27, (18.79 Hz) in Figure 3.28 and (35.27, 42.76 Hz) in Figure 3.29, which are coupled eigenfrequencies in y and torsion when F_y or/and M_x is applied or uncoupled z modes only when force F_z is applied. These values are exactly the same to the frequency of the free vibration analysis.

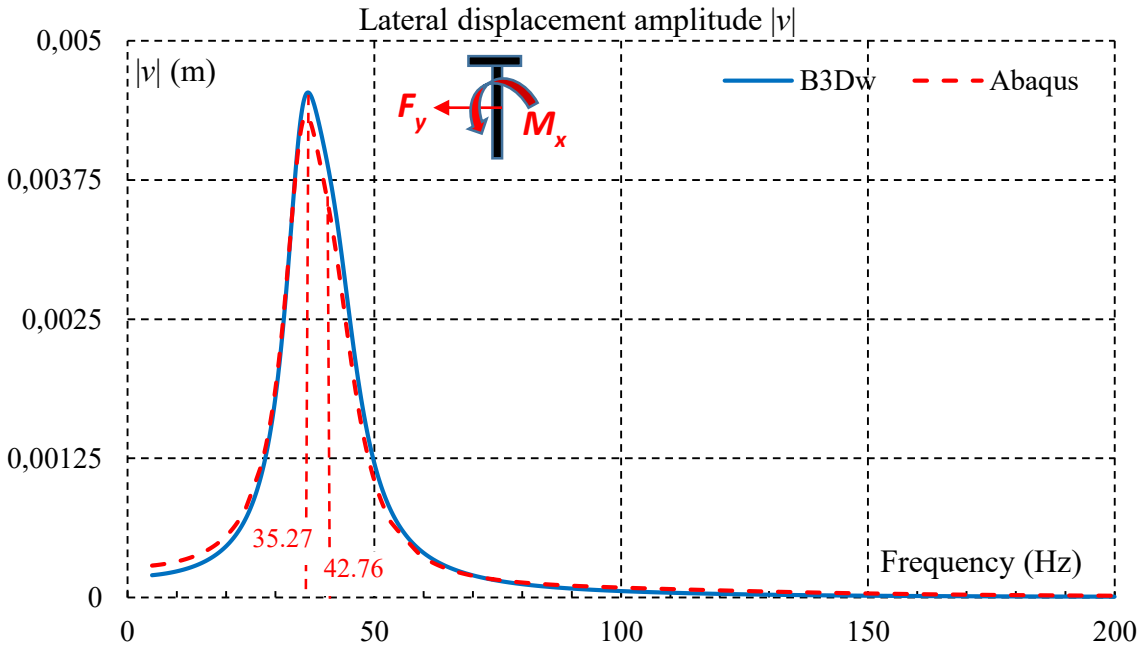

Figure 3.27: Lateral response at the mid-point of the Tee simply supported beam under harmonic force F_y and momentum M_x in frequency range $2<f<200$ Hz.

By zooming over the frequencies 30-45 Hz, it is remarkable that the curve of displacement v is slightly affected by the flexural-torsional coupled mode of eigenfrequency 42.76 Hz. Thus, this mode is dominated by torsion.

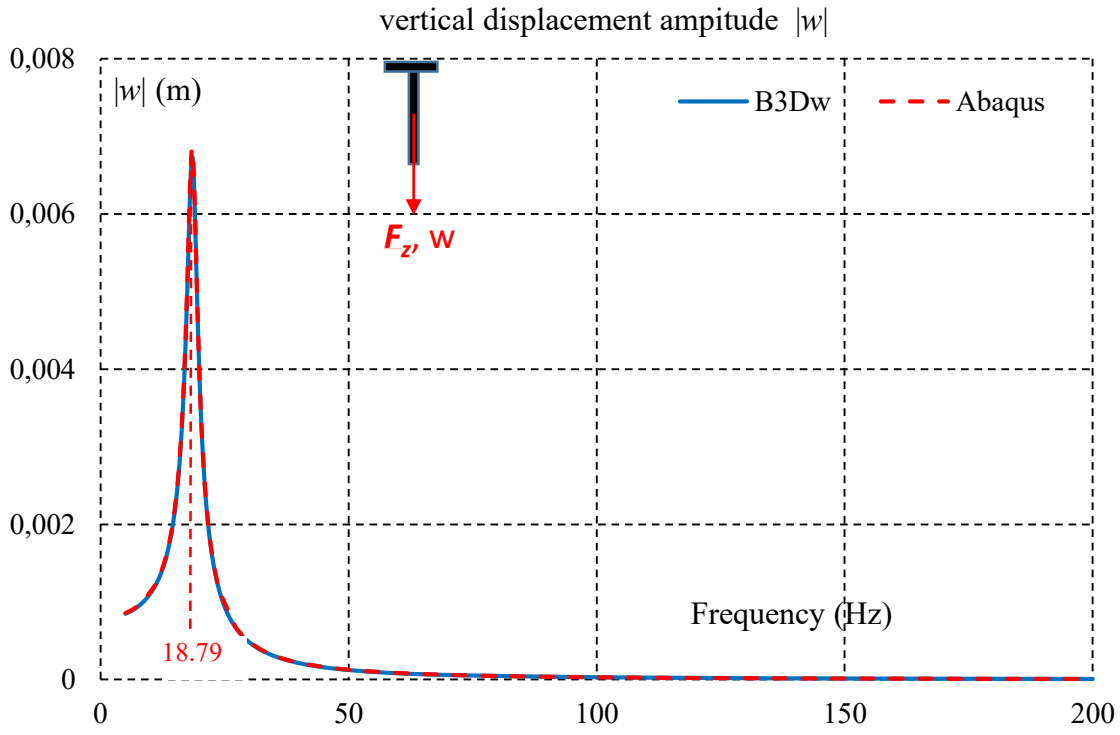

Figure 3.28: Vertical response at the mid-point of the Tee simply supported beam under harmonic force F_y in frequency range 2<f<200 Hz.

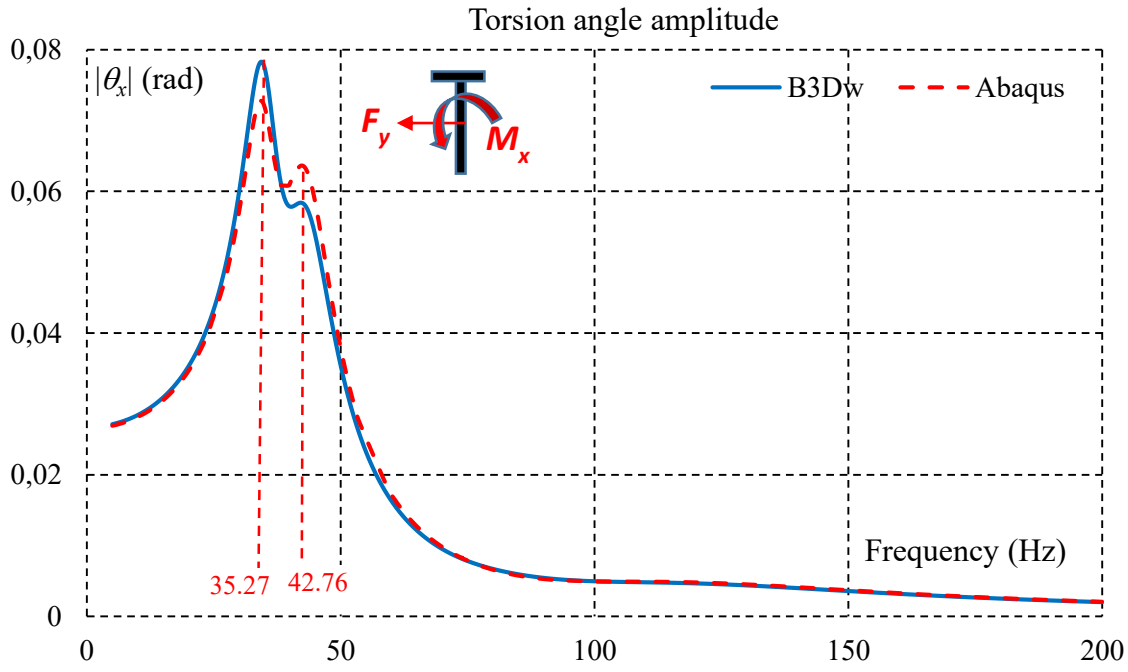

Figure 3.29: Amplitude response at the mid-point of the Tee simply supported beam under harmonic force F_y and momentum M_x in frequency range 2<f<200 Hz.

As conclusion, the agreement of the present finite element model (B3Dw) and Abaqus simulations are very good for mono-symmetrical sections whatever the boundary conditions are chosen.

3.4.8 Forced vibration analysis of thin-walled beams with mono-symmetrical channel section

The dynamic behavior of a singly symmetric cross section under harmonic 3D forces is considered in this paragraph. To this aim, the singly symmetric channel cantilever beam studied in free vibration in Example 3.1 is re-concerned in the forced vibration analysis. The geometry and the martial data are available in Figure 3.30. To study beam forced vibration behavior of the following harmonic forces and moments are applied at the free end of the beam: concentrated force F_y =1N and torsional moment M_x =0.01Nm. The Rayleigh damping coefficients are taken from literature for steel beams materials, as follows $\alpha = \beta = 10^{-3}$. The beam response spectrum displacements and torsion angle magnitudes at the free end are obtained and plotted in frequency domain, the range of frequencies in this study is taken between 1-150 Hz. With the help of the free vibration analysis studied in the example 3.1, 6 vibration modes are present. The frequency values have been depicted in Table 3.1. In this range 4 frequencies are Flexural-torsional present at frequencies (11.38, 43.36, 57.50, 109.36 Hz). Two frequencies are pure bending present at the frequencies 23.16 and 145.01 Hz). The dynamic behavior of the beam at the tip end in presence of the bending force F_y is depicted in Figure 3.31. Only the lateral displacement v is present. A peak value is present at the frequency (23.16 Hz). This value is exactly the same to the first bending frequency of the free vibration analysis. The agreement of the present finite element model (B3Dw) and Abaqus simulations are very good.

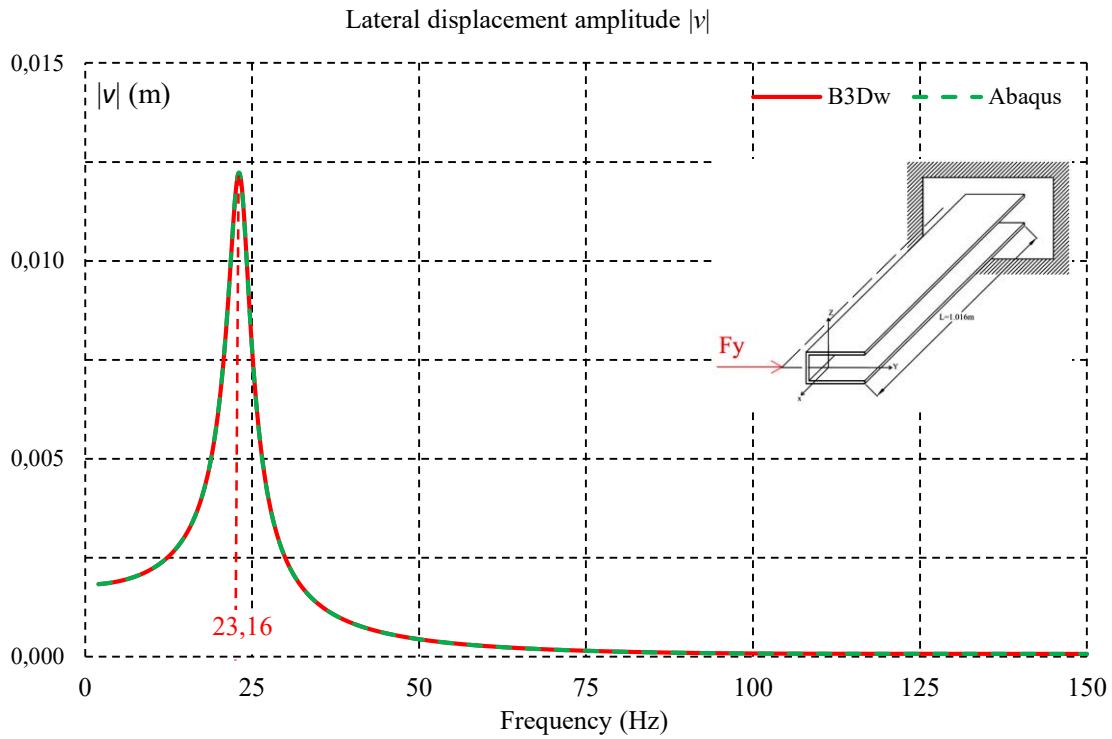

Figure 3.30: Lateral response at the tip of the C cantilever beam under harmonic force F_y in frequency range $2<f<150$ Hz.

The dynamic behavior of the beam at the tip end in presence of the torsion moment M_x is pictured in Figure 3.31. In this load case, the beam exhibits a flexural-torsional behavior. Both the displacement w and the torsion θ_x are present. They are depicted in Figure 3.31a, b. In both the two curves, peaks are present at the frequencies (11.38, 43.02 and 57.40 Hz). These values are very close the flexural-torsional frequencies obtained in the free vibration analysis. Again a good agreement between the present model and Abaqus simulations is remarked. Under the two load cases, the displacements of the beam around the first bending frequency (23.16 Hz) and the first flexural-torsional frequency (11.38 Hz) are very important compared the other beam response over the rest eigenfrequencies. The amplitudes of the higher eigenfrequencies are very limited compared to the first one. A zoom of the beam behavior is depicted on Figure 3.31a, b, in the area $25<f<75$ Hz. This is the reason that the other higher eigenfrequencies (109.36 and 145.01 Hz) are not observed in the forced vibration analysis, since they are over damped. This phenomenon is always observed in dynamic behavior.

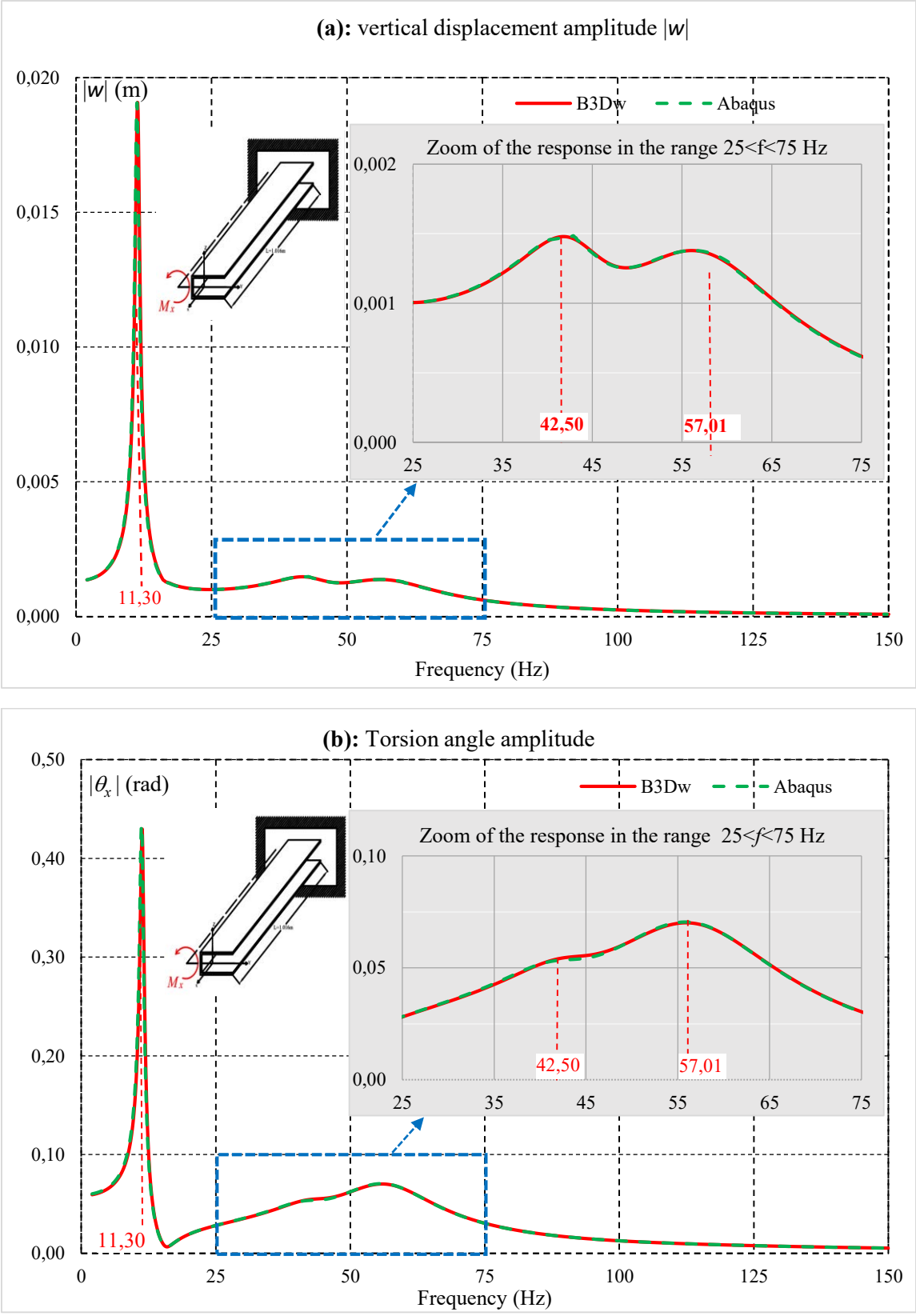

Figure 3.31: Flexural-torsional dynamic response amplitude at the tip of the C cantilever beam under harmonic torsion moment M_x in the range $2<f<150$ Hz.
(a): vertical displacement w; (b): torsion angle θ_x.

In brief, the developed FEM (B3Dw) is validated in this section by means of benchmark results and a present numerical simulations using commercial codes. On the other hand, the developed element accuracy is proven in both free and forced vibrations in this section, the effect of bi-coupling for mono-symmetrical sections and three-coupling of modes for arbitrary cross sections were also demonstrated in several examples. Response spectra are carried out for different loads types. The FFT was applied to transform earthquake signal from time to frequency domain. For all possible cases B3Dw was compared and validated in a series of validation numerical examples.

Furthermore, the validation of B3Dw in case of arbitrary cross sections is treated in chapter 5. In this chapter some arbitrary sections are considered and studied in both free and forced vibration domain, original experimental tests are proceeded. In order to validate the developed model, test results are compared to numerical methods B3Dw and Abaqus simulations.

3.5 Conclusion

It is known that for thin-walled beams under arbitrary boundary conditions and arbitrary cross section shape the analytical solutions for dynamic behavior becomes cumbersome, so the finite element approach is followed. To this aim, a finite element approach of a model for the triply coupled vibration of beams with arbitrary thin-walled open cross-section is developed. This model treats different boundary conditions and takes into account for bending, torsion, warping and rotary kinematic terms. This leads to the assessment of the dynamic behavior of the beams more accurately compared to the solutions of classical beam theory. With the help of Hamilton's principle, the axial and flexural-torsional motion equations have been derived. In the finite element approach, 3D beams with 2 nodes and 7 degrees of freedom per node have been adopted in the mesh process. The warping is considered as an independent degree of freedom. This beam element (B3Dw) is implanted in Matlab. The model has been already used successfully in statics, buckling, lateral buckling and nonlinear analysis. In the present work, the free and forced vibration have been investigated. In free vibration, higher vibration modes are possible by the help of an efficient solver available in Matlab. In forced vibration, a solution method based on the present model has been detailed. The beam behavior is studied in the frequency domain under any dynamic forces. To carry out the dynamic response spectra of the thin-walled beams the steady state modal analysis is adopted. Rayleigh damping is taken into account in this model. In the chapter 2 and 3, the analytical and the finite element model have been validated by the help of benchmark solutions of the literature and to author's simulations on commercial codes. Good agreement is remarked. The efficiency of the analytical solutions and the finite element approach investigated seem to be accurate. The importance of warping and kinematic rotational terms are well studied in the numerical applications. In the following chapter the presented analytical model and the finite element method are developed to take in account the effect of intermediate viscoelastic springs. Then, these methods are used to studies the vibration control (in terms of frequencies and displacements) of thin-walled structures by means of adding intermediate dashpots and elastic springs on parallel.

Chapter 4 Experimental analysis on free and forced vibrations of thin-walled beams

4.1 Introduction

In order to improve the structure strength against vibration effects and to save materials by getting optimum sections, a developed finite element method was used to study the 3D vibration behavior of thin walled beams. This numerical method presented by the author was compared to the benchmarks and the commercial code results. However, in literature the experimental studies on dynamic behavior on thin-walled beams exist but are limited.

In this context, the most important experimental studies founded in the literature are listed and analyzed in what follows. Klausbruckner [54] investigated the free vibration behavior of Channel beams using Electro-Optic Holography and Heterodyne Hologram Interferometry technics. The results are compared to FEM simulations and other closed form solutions. Ambrosini [55, 56], presented an experimental free vibration study for doubly unsymmetrical open sections thin walled beams. The test results are used to validate the theoretical and numerical models. Ribeiro [57], using experimental test explored the non-linear vibration of a hinged-hinged beam excited by sinusoidal forces. In the study, higher modes were analyzed and proved the existence of internal mode resonance. More recently, Piana *et al.* [57] based on experimental tests, extracted the natural frequencies of aluminum thin-walled beam with non-symmetric crucify cross section. In the study, authors confirm the effects of geometric imperfections on the dynamic behavior. These imperfections are included in the numerical analysis. By this way, the test and the numerical results were close. Zhou *et al.* [59] adopted the hammer test technique in the free vibration of uniform and non-uniform thin walled beams. The results are compared to numerical results of the transfer differential transform method. Frequency response curves were presented and compared to experimental test. In this study, the damping effect has not been taken into account.

These experimental tests are necessary to prove the accuracy and reality of developed theoretical and numerical methods. The literature review of the previous quoted works contributes certainly to the assessment of the dynamic behavior of thin-walled beams. Moreover, more of them are limited to free vibration context. The dynamic behavior under dynamic loadings are limited to numerical approaches. To this aim, in the present study, experimental tests studies on free and forced vibrations of thin walled beams with arbitrary sections are considered and presented in this chapter. The flexural-torsional dynamic behavior of thin-walled beams is investigated by experimental Beams natural frequencies and dynamic response spectra were investigated. By means of an instrumental hammer test, specimens natural frequencies are extracted. On the other hand, the shaker machine is used to compute the specimen's response spectra. In test studies, more than

10 modes were carried out and high frequencies in the range 1-600 Hz, were used in forced vibration. Experimental tests results are used to validate the presented finite element method. Finally, comparison among test data and numerical methods results given by home code B3Dw and commercial code Abaqus, proves the efficiency of numerical method to predict experimental results with high accuracy.

The numerical and experimental results of the present work are compared to other numerical simulations made on a commercial code. Test results match well the numerical simulations of the present model. Compared to classical models where rotational terms are neglected, more accurate results are then obtained especially in presence of higher vibration and coupled modes. The experimental results and the finite element simulations of the present model are in good agreement.

In the section 4.2, the experimental setup for the free and forces vibration of arbitrary cross section beams is described. Then, the hammer test and shaker machine equipment are detailed. Test results are presented in the section 4.3. Loss factor are determined experimentally for each mode then modal damping are calculated in section 4.4. The numerical and test comparisons are discussed in section 4.5. In section 4.6, a test study about dynamic behavior of braced beams is presented. The concluding remarks close the work at section 4.7.

4.2 Experimental setup

In this experimental study, investigations on non-symmetric cross-sections with various boundary conditions are proceeded. The experimental setups are exposed which the aim is to show the difference solicitations (free and forced vibration).

In what follows, five sets of tests are performed to carry out beams natural frequencies and response spectra under harmonic excitation. Before tests proceeding, some basic measurements were taken to verify specimen's masses, sections geometries and beams lengths. It's important to note that cross-sections dimensions vary slightly along the beam length due to manufacturing imperfection. However, in this study the section was considered as uniform along beam length. On the other hand, mechanical characteristics was taken from manufacturer stated values. Beam material considered as elastic linear isotropic and homogenous. In general, three boundary conditions are adopted in all tests, these boundary conditions are: clamped –free, clamped – clamped and simply supported. Mainly, two types of experiments are proceeded in this study that are free and forced vibrations tests. In what follows, the procedure for each test type is detailed.

4.2.1 Free vibration test procedure

Free vibration tests are performed by means an impact hammer. The impact position and force are carefully chosen to keep the hypothesis of the small perturbation. Otherwise, some mono-axial acceleration sensors, were installed on the specimens to detect beam motion continually during testing period.

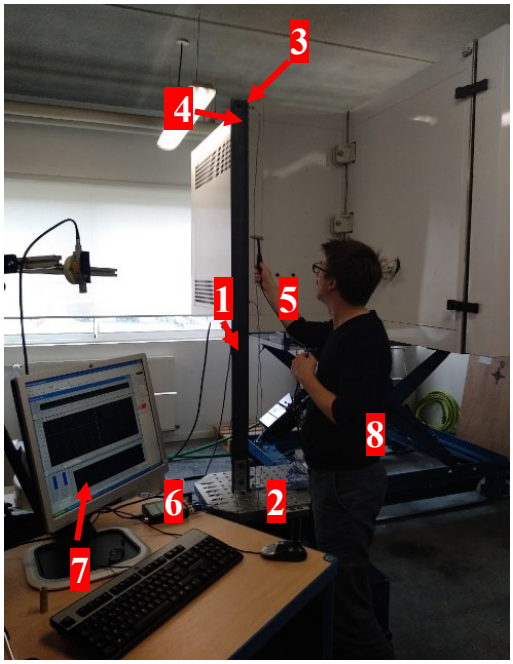

1-Tested beam.

2-Clamped end.

3-Free end.

4-Acceleration sensors.

5-Instrumented Hammer

6- Acquisition system (Photon +, Brüel & Kjaer)

7-Computer & signal treatment software.

8-Test operator.

Figure 4.1: Free vibration test procedure using an instrumental hammer.

In Figure 4.1 a detailed example of free vibration test experiment setup. It includes, a cantilever beams clamped by means of some manufactured steel parts to control displacements, rotations and warping of the clamped end. Otherwise, one acceleration sensors are installed at the middle of the beam and two at the free end. The operator uses an instrumented hammer to excite the beam by several impulses to record the responses spectra used to carry out natural frequencies. The Hammer test setup process includes the following steps. After applying the boundary condition, several acceleration sensors are installed in different location on the beam. The transducers are fixed to the beam with different orientations attached with wax, which allow us to measure bending and torsion vibrations modes.

The impact hammer and the mono-axial accelerometers are connected to the acquisition system (Photon +, Brüel and Kjaer). Temporal signals are acquired and treated with the software RT.pro (Dynamic Signal Analysis). A Fourier Transform is processed to obtain the frequencies responses of the structure and the results are visualized on the computer. The frequency range of the dynamic acquisition is focused between 1 to 500Hz. The experimental setup flow chart for the free vibration test is shown in Figure 4.2.

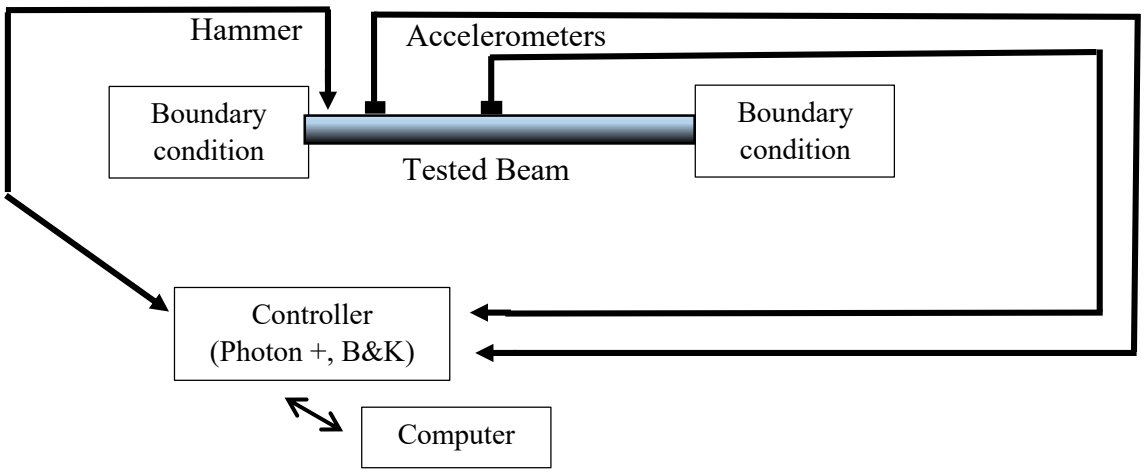

Figure 4.2: Flowchart of experimental setup for the free vibration with hammer.

Otherwise, it is important to note that both transducers have light weight features so the dynamic identification tests can be performed without perturbing the mass of the specimen. The acceleration sensor are PCB Piezotronics - sensor type (4508) sensing element PZ23had a high precision. It has sensitivity -2 up to 3% for dynamic acquisitions at 5-1000Hz, maximum frequency 8 KHz. The cut-off frequency is 10 kHz, sampling frequency is 0.312Hz and the averaging can be employed using Hanning or Hamming codes.
After assembling the test setup, as mentioned before the sensors located at different locations on the beam record the response spectra. Then, the first *n* natural frequencies were extracted using peak picking method from the obtained responses spectra once the specimen was subjected to given impulses using an instrumental hammer shown in Figure 4.1.

4.2.2 Forced vibration test procedure

For forced vibration test, the open section beams are clamping with one of this extremity to the table of the shaker. Then, accelerometers are attached to the beam in some chosen locations. The shaker does the vibration solicitation with a harmonic excitation in frequency domain. The vibrations are controlled and measured by a controller device (UCON system). The vibration amplitude of the shaker is controlled thanks to an accelerometer (PCB Piezotronics - sensor type 4508). The range of frequency excitation is between 1 and 400 Hz. The cut-off frequency is 4 kHz, sampling frequency is 0.01Hz and no averaging employed.
In what follows, Figure 4.3 shows a flowchart of the experimental setup, which measure beam displacement magnitude response spectra curves at sensors locations. Moreover, a picture of the test setup is depicted in Figure 4.4.

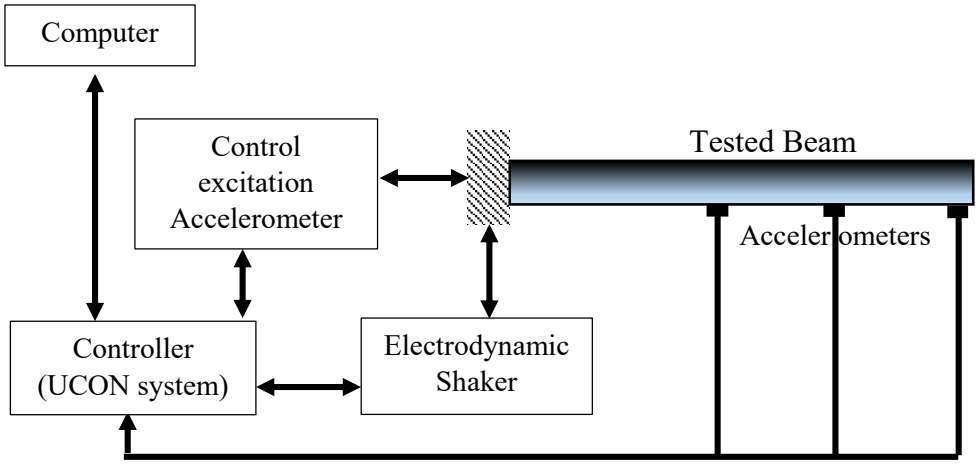

Figure 4.3: Flowchart of experimental setup for the forced vibration.

The amplitude of the shaker is chosen to minimize nonlinear vibrations typically 1g acceleration. The acceleration of the beam's vibration is measured by four uniaxial accelerometers, fixed on different points of the beam. The amplitude of the shaker is chosen to minimize nonlinear vibrations typically 1g acceleration. The boundary condition of the beam is clamped-free. Two beams with different materials, sections and lengths were tested.

1-Tested beam.

2-Clamped end.

3-Acceleration sensors.

4-Shaker engine

Figure 4.4: Experimental setup of the Forced vibration test with shaker machine.

It is important to note that for each specimen the test should be repeated several times to ensure the repeatability condition and to verify that the results are with high accuracy. According to this, the same test was repeated minimum three times.

4.2.3 Acquisition device and Sensors characteristics

The acquisition device Type: Brüel and Kjaer (PHOTON+), this controller is featured with 4 channels 32-bit processing; device can measure signals with frequency up to 84 kHz. Signals are treated by the software RT.pro (Dynamic Signal Analysis).

In testing procedure RT.pro software was used to save and treat signals detected by acceleration sensors. Signals are instantly recorded, then post processed by performing a Fourier Transform to obtain finally frequencies accelerations data.

In the test procedure, Accelerations are recorded by means of uniaxial accelerometers of type PTZ (Brüel and Kjaer DeltaTron 4508), fixed on the beam. The PZT sensor transforms acceleration to electric signal, it does not need power supply. The weight of the accelerometer is 4.8g. Hence, the sensors when are attached to the beam in some different locations can affect slightly the natural frequencies due to additional masses located in the attached points. So on, the natural frequencies measured can be shifted when the accelerometers locations changed.

After explaining the experimental procedures for free and forced tests and giving a brief about the used instruments. In what follows, let us present the used specimens and gives the geometrical and mechanical properties for each one. After that, the sensors locations, boundary conditions and experimental model details are shown.

4.3 Specimens properties

A set of specimens with L cross-sections (non-symmetrical section called arbitrary) having different dimensions, materials properties and lengths were chosen. The typical cross-section of the beam is depicted in Figure 4.5. Moreover, geometrical and material properties of the cross-sections and beams lengths are listed in Table 4.1. It should be noted that, beams with different dimensions, materials and under different boundary conditions was chosen intentionally to show the impact of all these factors on vibrations modes. Also, to study the coupling effect of the arbitrary cross-sections.

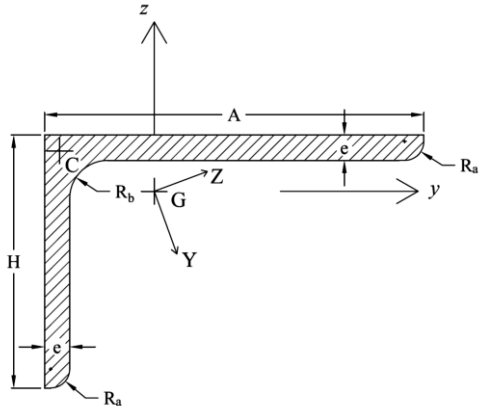

Figure 4.5: Cross-section of the Beam including dimensions, centroid, shear center position and principle axis locations.

Table 4.1: Specimens properties
(SS: Simply supported, CC: clamped -clamped, CF: clamped –free).

Beam	Test code	Useful length L(cm)	Width A (mm)	Height H (mm)	Th. (mm)	Curvature radius $R_a - R_b$	ν	Young's modulus (GPa)	Mass density kg/m^3	Boundary condition
Beam1	T1	160	50	30	3	2 – 4.5	0.33	69	2700	CC
Beam2	T2	170	60	40	4	3 – 6	0.33	69	2700	SS
Beam2	T3	180	60	40	4	3 – 6	0.33	69	2700	CF
Beam3	T4	185	80	60	7	4 – 8	0.3	210	7850	CF
Beam2	T5	160	60	40	4	3 – 6	0.33	69	2700	CC

In the following section, the beams boundary conditions and sensors locations are detailed. Adding to this, perspective views of beams is presented showing the boundary conditions, sensors locations over the beam length and cross-sections.

4.4 Boundary conditions

Three boundary conditions were adopted in this study. They are given by clamped - free, clamped - clamped and simply supported. Different tests boundary conditions and sensors locations are presented in the following lists of figures. In Figure 4.6, it can be seen the forced vibration test setup configuration that involve: axis orientations, sensors locations and beams boundary conditions of a cantilever beam. Furthermore, for free vibration tests the setups configurations including axis orientations, sensors locations and beams boundary conditions for the clamped - free beam is presented in Figure 4.7, for the clamped - clamped beam shown in Figure 4.8 and for the simply supported beams depicted in Figure 4.9. These various conditions are chosen to validate the developed model in free and forced vibrations with different cases of supports.

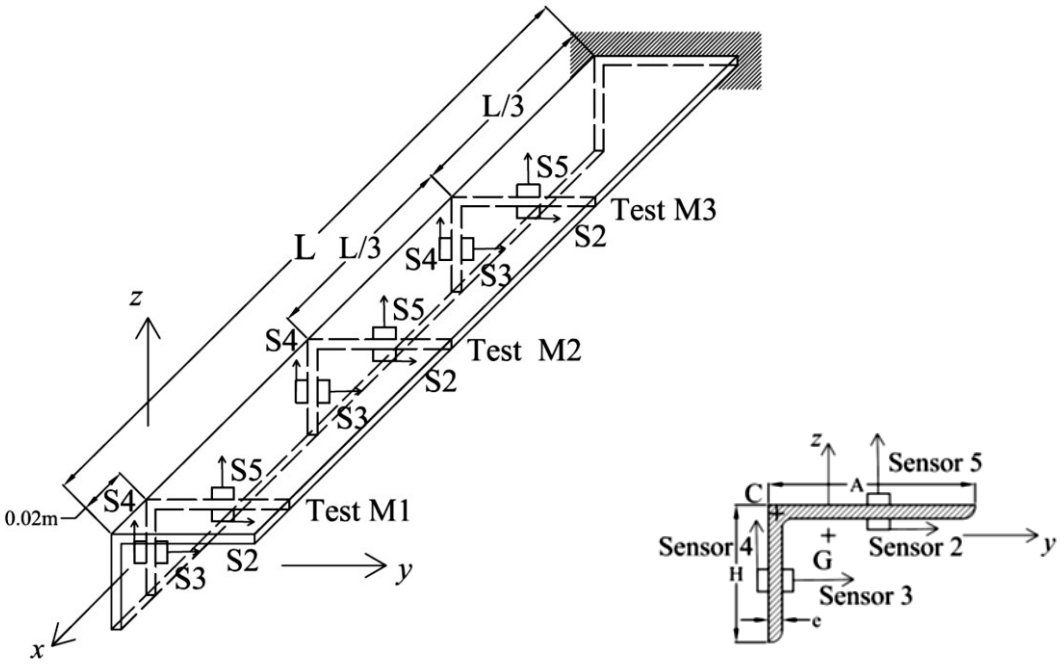

Figure 4.6: Forced vibration tests setup for a cantilever beam, configuration involves axis orientations and sensors locations.

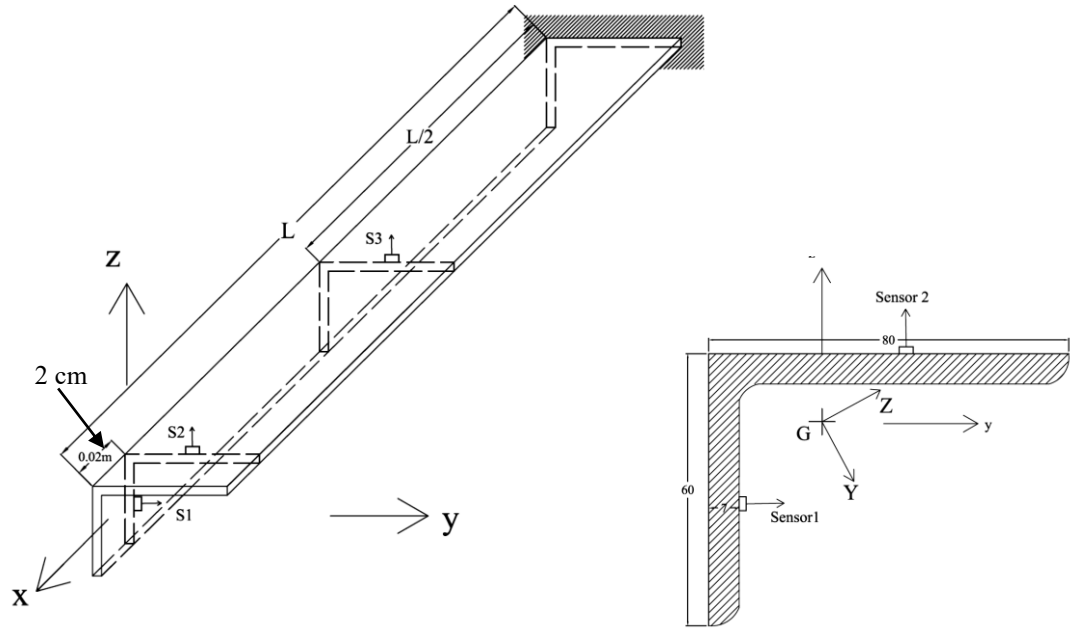

Cross section dimensions with centroid position, main bending axes and sensor positions.

Figure 4.7: Free vibration tests setup configuration including: axis orientations, sensors locations for the cantilever beam.

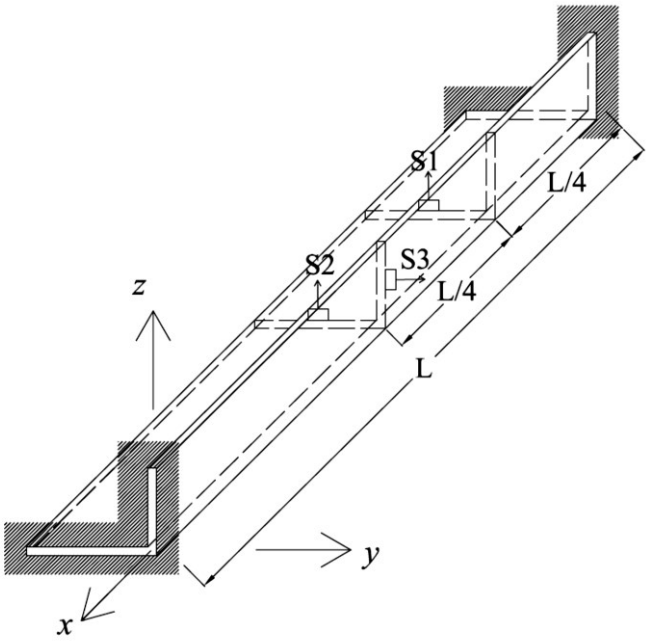

Figure 4.8: Free vibration tests setup configuration including: axis orientations, sensors locations and beams boundary conditions for the clamped - clamped beams.

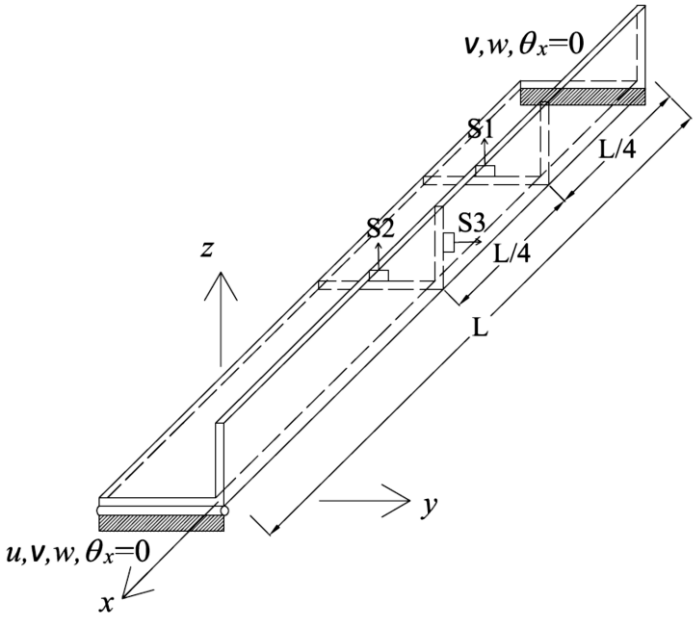

Figure 4.9: Free vibration tests setup configuration including: axis orientations, sensors locations and beams boundary conditions for the simply supported beams.

4.5 Experimental tests results

Many results can be carried out from the experimental tests, such as the displacement amplitude spectrum measured by the sensors installed on the beam. As examples the dynamic response spectra provided from the forced vibration test of a cantilever beam is shown in Figure 4.10.

In these tests, excitation is generated using a shaker. Acceleration response spectra are recorded by accelerometers fixed at different points on the beam free end. Then, these response spectra are compared to the forced vibration numerical simulations.

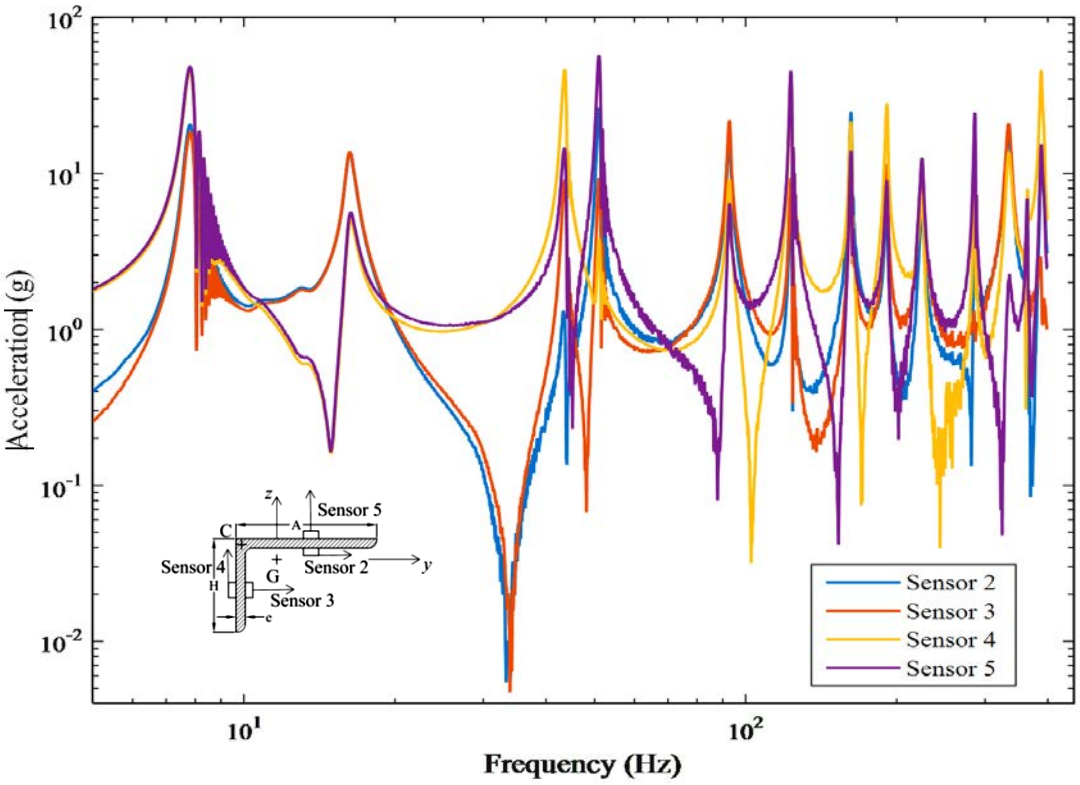

Figure 4.10: Acceleration response spectra from sensors S2-S5 attached on the beam 2 free end (forced vibration test –T3).

Moreover, the natural frequencies can be carried out from the response spectrum by using the peak-picking method [97]. Then, the experimental natural frequencies are compared to the numerical results in the validation process.

Otherwise, from the acceleration spectra recorded by different sensors, it seems that for each natural frequency the amplitudes of the relative peaks are different depending of the sensor locations. However, the frequency values are the same independent of the sensor locations. This means that the vibration modes of the beam can be detected with all sensors. Thus, the vibration modes are coupled on the y and z directions. As conclusion, the vibration modes for beams with non-symmetric thin-walled open cross sections are

flexural-torsional coupled. Let us note that, each test was repeated several times to verify the repeatability condition inherent precision of the measurement equipment subsequently to insure results accuracy. According to this, the same test was repeated minimum three times. In the following sections the free and forced vibration response spectra recorded by all sensors carried out from tests are presented respectively.

4.5.1 Impact hammer tests results

In this section, the acceleration response spectra obtained from different tests presented in Table 4.1 are depicted respectively. Later on, these response spectra are used to carry out the natural frequencies for each test and sensor separately. The obtained eigenvalues (natural frequencies) are used to validate the repeatability condition, also by analyzing these results vibration modes can be identified. After that, the collected natural frequencies are compared to numerical simulation results in the following section.

4.5.1.1 Impact hammer test on a double clamped beam 1

Proceeding with impact hammer test to carry-out the natural frequencies of Beam 1 with L (50x30x3mm) cross-section under clamped-clamped boundary conditions. The beam material is aluminum. The test was repeated 5 times in order to verify that the obtained response spectra are with high accuracy. The beam geometry, cross-section dimensions and material properties are given in Figure 4.5 and Table 4.1. Furthermore, the sensors locations are shown in Figure 4.8. Test procedure details are presented in the section 4.2. The measured response spectra are depicted in the following Figure 4.11.

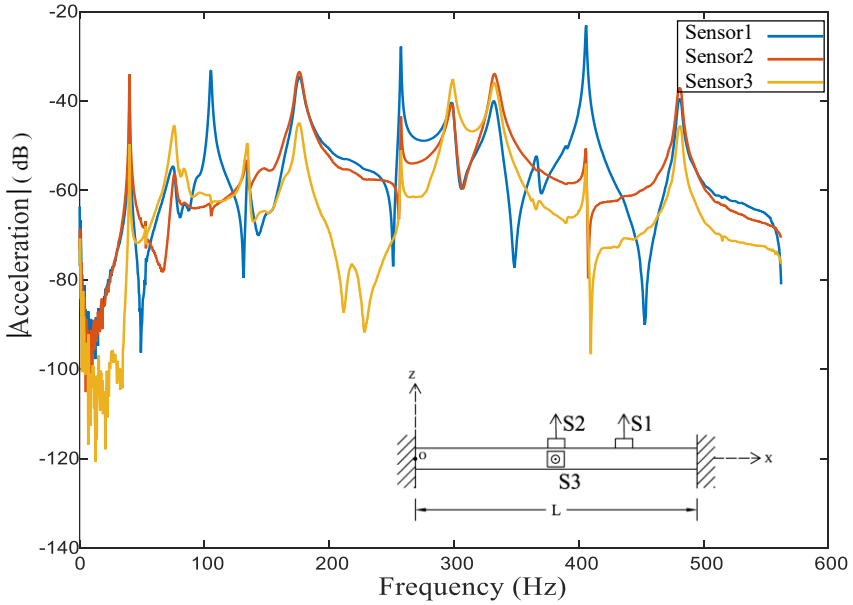

Figure 4.11: Acceleration response spectra for beam 1, (free vibration test -T1).

According to Figure 4.11, one remarks that the acceleration spectra recorded by the three sensors 2 and 3 located at the middle of the beam have peaks at the same frequencies regardless the measurement direction (y, z). This results match well with the concept of flexural-torsional coupled modes for beams with arbitrary cross-sections. But, it is noticeable that the peaks recorded by the sensor 1 differs from the other sensors. Mainly, near to the frequencies 100 Hz and 400 Hz the sensor 1 record some peaks however, the amplitudes recorded by the sensors 2 and 3 are almost null. This is due to the locations of the sensors on the beam, see Figure 4.8. As conclusion, depending to the mode shapes and sensors locations some frequencies can be recorded by sensor 1 and others by sensors 2 and 3. So, it is necessary to install sensors in different locations of the beam to record all natural frequencies.

4.5.1.2 Impact hammer test on a simply supported beam

In order to carry out the experimental natural frequencies data for a simply supported beam, a set of impact hammer tests are performed on the Beam 2 with 60x40x4mm L cross-section. The beam material is aluminum and the used boundaries conditions are simply supported. The geometry of the cross-section and material properties are given in Figure 4.5 and Table 4.1. Moreover, the sensors locations are shown in Figure 4.9. Test procedure details are presented in the section 4.2. The obtained response spectra are depicted in the following Figure 4.12.

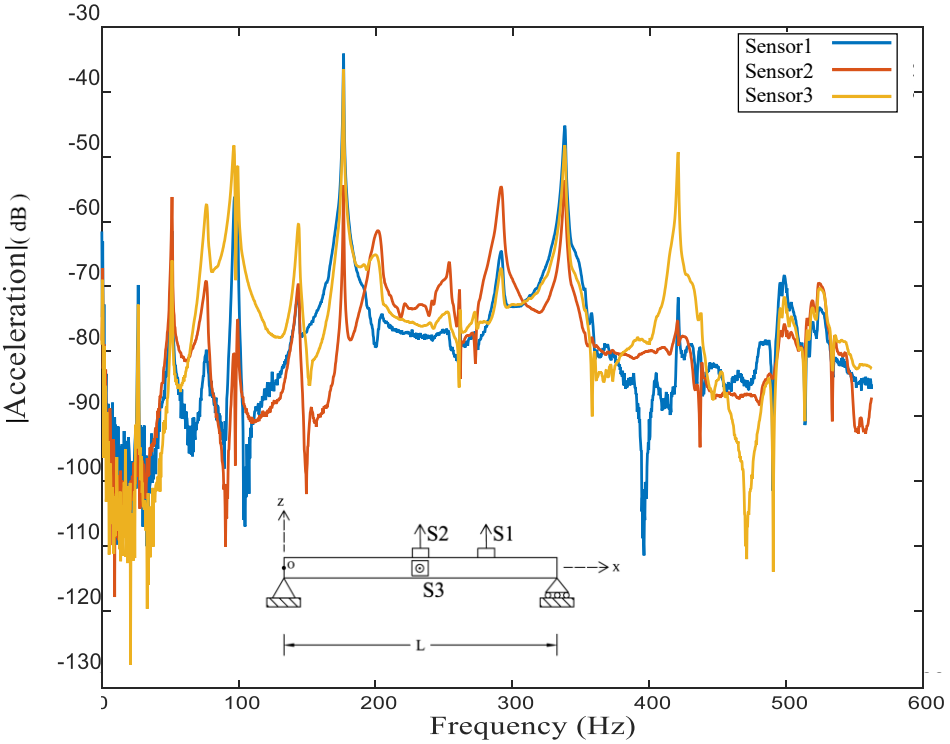

Figure 4.12: Acceleration response spectra for beam 2, (free vibration test –T2).

By analyzing Figure 4.12, one remarks that the acceleration spectra recorded by the three sensors 2 and 3 have peaks at the same frequencies, even though they measure the accelerations in different directions. The reason is that modes are flexural-torsional coupled for asymmetric cross-sections. Otherwise, peaks frequencies and amplitudes of the response spectrum recorded by the sensor 1 differs from the other sensors. This is due to the locations of the sensors on the beam. There is difficulty to carry out the natural frequencies in the range of frequencies 200 to 300 Hz and 450 to 600 Hz for these sensors locations. This due to mode shapes of the beam when the natural frequencies are reached in these frequencies ranges.

4.5.1.3 Impact hammer test on a double clamped beam 2

The impact hammer test was performed in order to investigate the natural frequencies of Beam 2 with L (60x40x4mm) cross-section under clamped-clamped boundary conditions. The beam material is aluminum. The test was repeated 5 times in order to verify that the obtained response spectra are with high accuracy. The beam geometry, cross-section dimensions and material properties are given in Figure 4.5 and Table 4.1. Furthermore, the sensors locations are shown in Figure 4.8. Test procedure details are presented in the section 4.2. The measured response spectra are depicted in the following Figure 4.13.

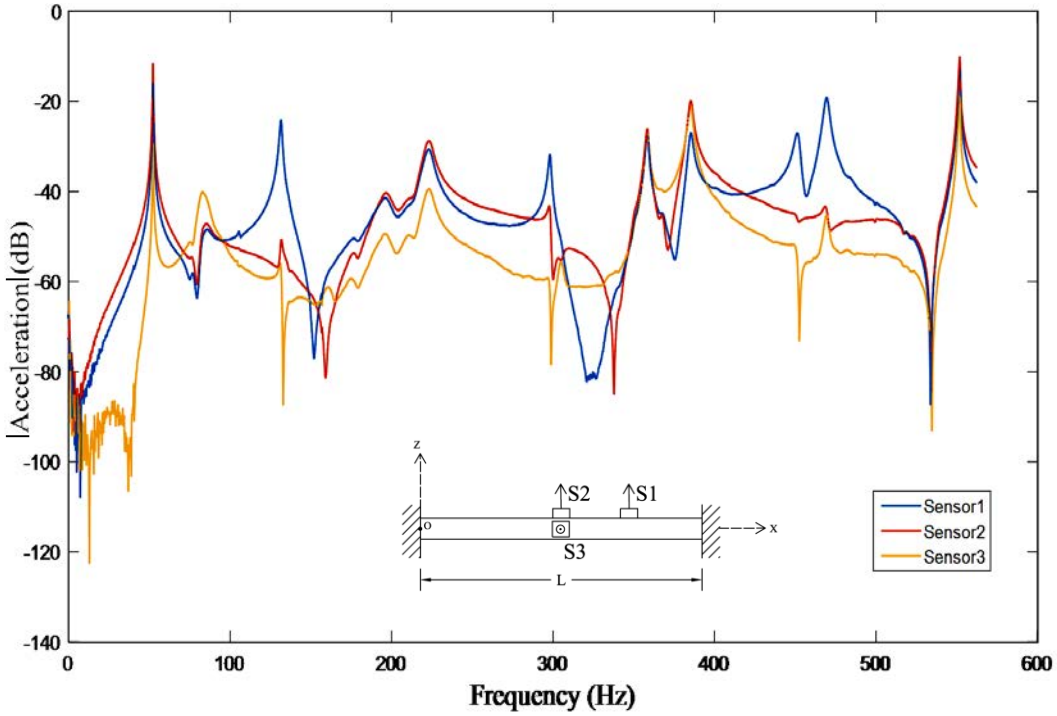

Figure 4.13: Acceleration response spectra for beam 2, (free vibration test –T5).

By analyzing Figure 4.13, one remarks that the acceleration spectra recorded by the three sensors 2 and 3 located at the middle of the beam have peaks at the same frequencies regardless the measurement direction (y, z). This results match well with the concept of

flexural-torsional coupled modes for beams with arbitrary cross-sections. But, it is noticeable that the peaks recorded by the sensor 1 differs from the other sensors. Mainly, near to the frequencies 130 Hz and between 400 and 500 Hz the sensor 1 record some peaks however, the amplitudes recorded by the sensors 2 and 3 are almost null. This is due to the locations of the sensors on the beam, see Figure 4.8. As conclusion, concerning mode shapes and sensors locations some frequencies can be recorded by sensor 1 and others by sensors 2 and 3.

4.5.1.4 Impact hammer test on a cantilever beam

In order to get the natural frequencies of the cantilever beam 3 with L (80x60x6mm) cross-section, the hammer test was performed. The beam material is steel and the boundary conditions are clamped-free. The test was repeated 5 times to verify the repeatability condition. The beam geometry, cross-section dimensions and material properties are given in Figure 4.5 and Table 4.1. Furthermore, the sensors locations are shown in Figure 4.7. Test procedure details are presented in the section 4.2. The measured response spectra are depicted in the following Figure 4.14.

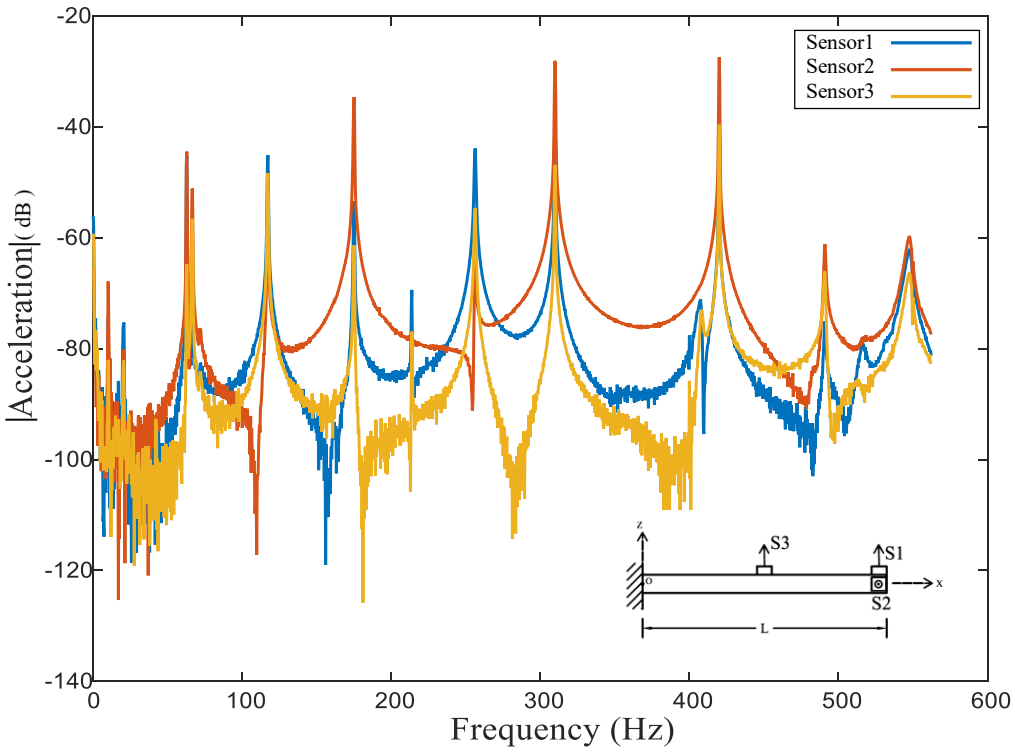

Figure 4.14: Acceleration response spectra for beam 3, (free vibration test –T4).

From Figure 4.14, one observes that all the natural frequencies are recorded by the sensors 2 and 3 located at the beam free end. Because in the case of cantilever beams the free end moves for all vibration modes. Also the beam cross-section is arbitrary so flexural-

torsional coupled modes are predictable. The peaks recorded by the sensor 1 differs from the other sensors. This is due to the sensors locations. Moreover, Sensors 1and3 shows a peak around the frequency to 220 Hz this is due to excitation direction and dominant modes that are in z direction around this resonance frequency.

4.5.2 Forced vibration test results for cantilever beam

Shaker machine is used to carry-out the response spectra and natural frequencies of the beam 2 that have a L cross-section with dimensions 60x40x4mm. The beam material is aluminum and the boundary conditions are clamped-free. Test procedure details are presented in the section 4.2. The beam geometry, cross-section dimensions and material properties are given in Figure 4.5 and Table 4.1. Furthermore, the sensors locations are shown in Figure 4.6. The test was repeated 5 times at 3 different beam locations and the obtained response spectra carried out by the installed sensors are depicted in Figures 4.15-4.17.

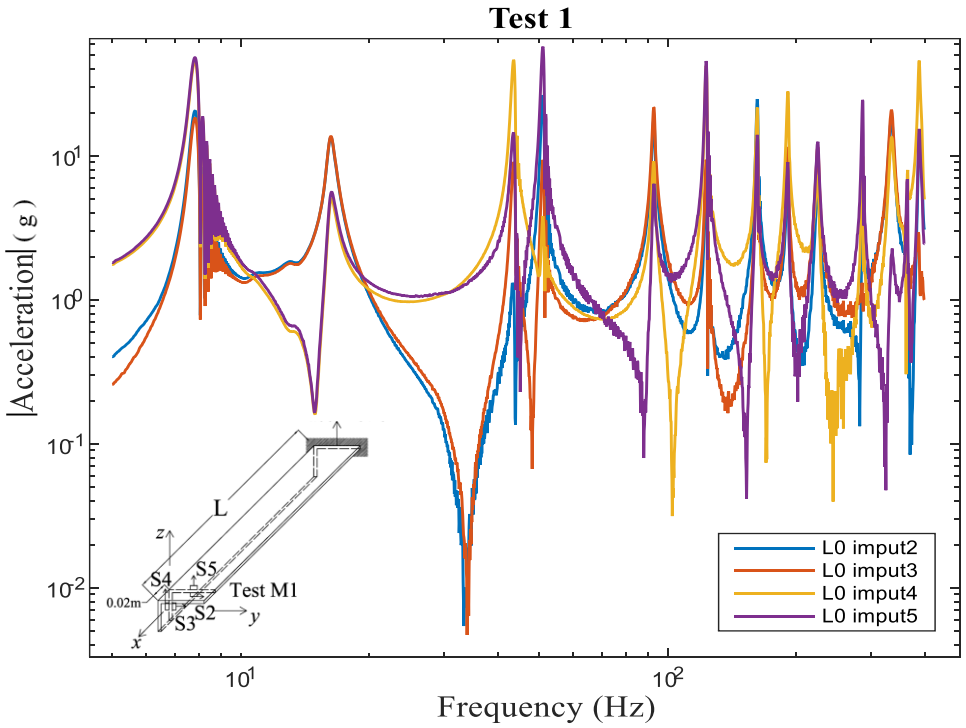

Figure 4.15: Test 1 acceleration response spectra for beam 2, (forced vibration test –T3).

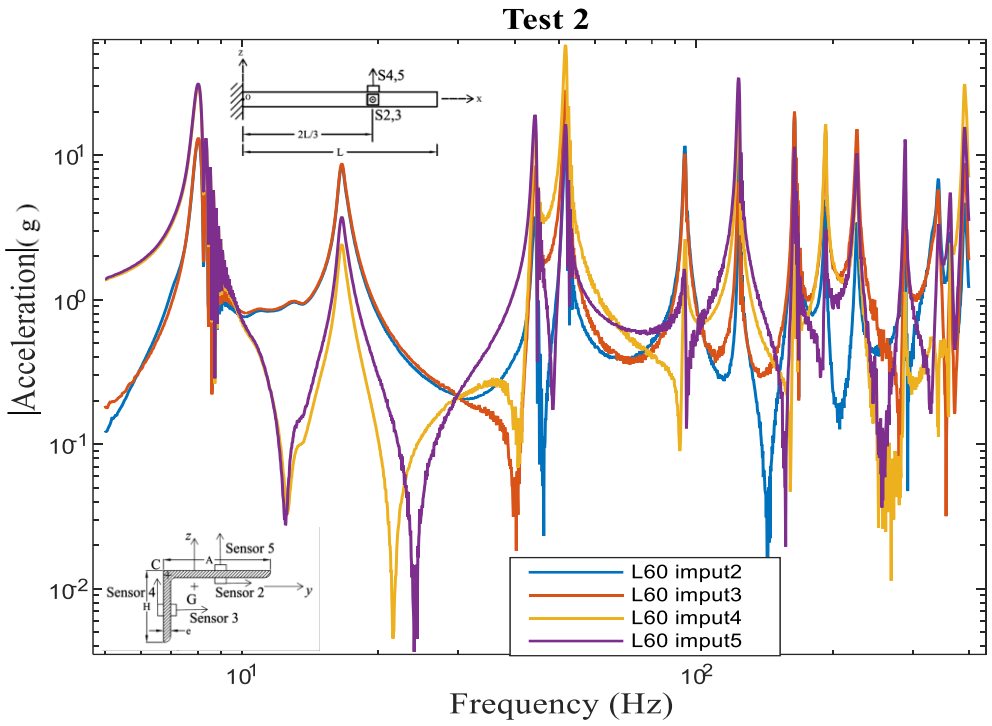

Figure 4.16: Test 2 acceleration response spectra for beam 2, (forced vibration test –T3).

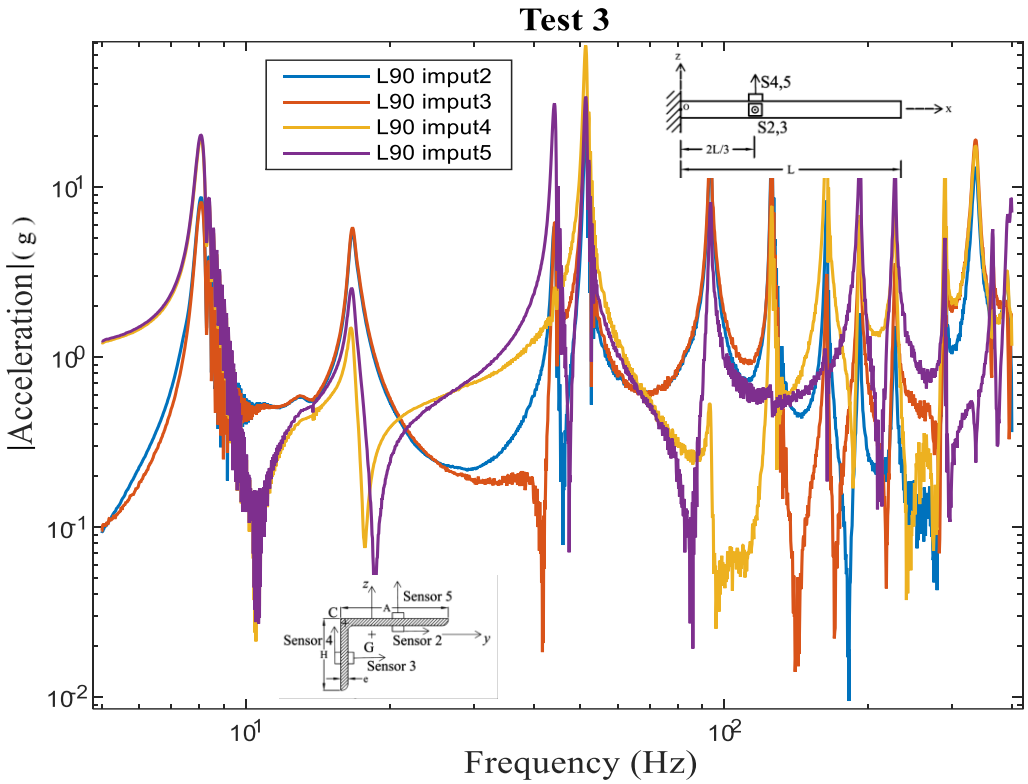

Figure 4.17: Test 3 acceleration response spectra for beam 2, (forced vibration test –T3).

By analyzing Figures 4.15-4.17, one observe that almost the same response spectra are recorded by all sensors in each test. This is can be explained by the sensors locations. In each test all sensors are located at the same cross-section in different directions. Moreover, from the response spectra it seems that all vibration modes are recorded by the 4 sensors. So, from tests results it concluded that for 3D thin-walled beams with arbitrary cross-sections all vibration modes are triply coupled. It is remarkable that the tests 2 and 3 are in accord with test one results, so the repeatability condition is achieved.

4.6 Repeatability condition for the test results

The repeatability condition for the test results is defined as the closeness of the agreement between the results of successive measurements of the same measure made under the same measurement conditions.

It should be noted that, these conditions called repeatability conditions and include: same procedure, same observer, same measuring instrument used under the same conditions, same place, repetition during a short period of time. Otherwise, repeatability can be expressed quantitatively using the dispersion characteristics of the results.

Other condition is applied that is called Fidelity condition and it is defined as the close agreement between independent results obtained under stipulated conditions. Fidelity depends only on the distribution of random errors and has no relation to the true or specified value. The fidelity measure is expressed in terms of infidelity and is calculated from the standard deviation of the test results. Less fidelity is reflected by a larger standard deviation. The term "independent test results" means results obtained in a manner not influenced by a previous result on the same test material or the like. Quantitative measures of fidelity critically depend on stipulated conditions. The repeatability and reproducibility conditions are particular sets of extreme conditions.

In all performed tests, the repeatability condition was applied to ensure that the experimental results are achieved with high accuracy. This condition was effected by repeating of each test more than three times and using several accelerometers in the same test distributed over the specimen. Then, different recorded response spectra for each beam are compared and relative errors are carried out. Therefore, the mean error between all results are less than 1 %, which accord to the repeatability condition.

4.7 Validation of the numerical model by comparison to experimental results

In this section comparison studies between the tests and numerical simulations results is presented. The objective of this study is to check the accuracy of the developed FEM (B3Dw) in free and forced vibrations.

4.7.1 Free vibration

The experimental studies performed with the hammer test on beams with non-symmetric cross sections under different boundary condition gives the natural frequencies data that can be used for the validation of B3Dw results. On the other hand, numerical models for the tested beams have been developed using B3Dw. These models are reproduced on the present experimental tests. Hereafter, three beams with clamped - free, clamped - clamped and simply supported boundary conditions are studied. The experimental results for these beams were compared with the numerical simulations and with commercial code Abaqus (B31OS).

In the following tables, the free vibration natural frequencies carried out from the numerical calculations and the experimental tests are presented and compared. In Tables 4.2 and 4.6, there are depicted the results of the Beam 1 (test T1) and Beam 2 (test T5) where the beams are clamped on these both extremities. Considering Table 4.3, in this table the results of Beam 2 (test T2) with the boundary conditions simply supported are presented. Tables 4.4 and 4.5, comprise the results for Beam 2 (Test 3) and Beam 3 (Test 4) under cantilever boundary conditions.

Table 4.2: Numerical and experimental comparison of natural frequencies for Beam1, Test T1 (values in Hz).

Mode	**Test**	B3Dw	Error %	Abaqus (B31OS)	Error %
1	**40.01**	42.00	5.00	43.01	7.54
2	**75.30**	78.36	4.06	79.53	5.62
3	**105.02**	106.71	1.63	107.97	2.83
4	**133.01**	143.81	8.13	144.99	9.02
5	**175.03**	177.58	1.47	180.31	3.03
6	**257.12**	254.32	1.04	257.60	0.23
7	**287.31**	301.93	5.20	307.74	7.23
8	**332.24**	340.04	2.42	342.18	3.06
9	**365.37**	380.00	4.11	382.32	4.75
10	**405.64**	400.00	1.23	401.81	0.79

Table 4.3: Numerical and experimental comparison of natural frequencies for Beam2, Test T2 (values in Hz).

Mode	**Test**	B3Dw	Error %	Abaqus (B31OS)	Error %
1	**26.56**	25.66	3.4	26.79	0.9
2	**51.10**	50.56	1.0	57.70	12.9
3	**76.09**	71.83	5.6	100.83	32.5
4	**96.98**	102.12	5.3	110.73	14.2
5	**142.68**	138.69	2.8	165.31	15.9
6	**176.53**	181.06	2.6	194.27	10.1
7	**252.83**	233.61	7.6	280.72	11.0
8	**289.70**	295.73	2.1	302.49	4.4
9	**338.53**	337.36	0.3	361.54	6.8
10	**421.03**	402.06	4.5	439.99	4.5
11	**498.05**	476.15	4.4	500.98	0.6
12	**521.03**	506.39	2.8	517.31	0.7
13	**554.70**	557.73	0.5	593.97	7.1

Table 4.4: Numerical and experimental comparison of natural frequencies for Beam2, Test T2 (values in Hz).

Mode	**Test**	B3Dw	Error%	Abaqus (B31OS)	Error%
1	**8.03**	7.61	5.23	7.53	6.2
2	**16.74**	17.49	4.73	17.47	4.6
3	**43.01**	42.57	1.01	42.28	1.7
4	**50.03**	49.88	0.24	49.87	0.3
5	**93.54**	94.61	1.74	94.72	1.8
6	**123.04**	119.53	2.82	118.75	3.5
7	**161.21**	160.67	0.20	160.52	0.3
8	**190.04**	189.00	0.53	189.37	0.3
9	**221.10**	219.83	0.53	219.53	0.7
10	**289.01**	278.31	3.70	273.43	5.4

Table 4.5: Numerical and experimental comparison of natural frequencies for Beam3, Test T4 (values in Hz).

Mode	**Test**	B3Dw	Error%	Abaqus (B31OS)	Error%
1	**10.00**	10.50	5.00	10.71	7.13
2	**20.60**	22.03	6.94	22.66	9.98
3	**62.80**	59.36	5.48	56.89	9.42
4	**66.60**	68.99	3.59	68.19	2.39
5	**117.18**	123.95	5.78	120.37	2.72
6	**175.01**	172.78	1.27	166.88	4.64
7	**213.18**	213.96	0.36	210.17	1.41
8	**256.03**	261.18	2.02	249.51	2.54
9	**310.02**	308.43	0.51	289.79	6.52
10	**408.10**	395.82	3.01	369.10	9.56

Table 4.6: Numerical and experimental comparison of natural frequencies for Beam2, Test T5 (values in Hz).

Mode	**Test**	B3Dw	Error %	Abaqus (B31OS)	Error %
1	**52.19**	54.12	3.57	55.70	6.7
2	**84.53**	86.92	2.8	87.38	3.4
3	**131.68**	132.40	0.6	132.91	0.9
4	**196.08**	202.16	3.1	206.47	5.3
5	**222.73**	217.92	2.2	218.21	2.0
6	**358.25**	357.28	0.3	360.69	0.7
7	**385.08**	395.03	2.6	393.16	2.1
8	**451.53**	447.02	1.0	444.96	1.5
9	**469.80**	490.08	4.3	474.96	1.1
10	**552.18**	527.55	4.5	525.57	4.8

A minimum number of ten natural frequencies are compared experimentally and numerically to reach high frequencies. The results present a good agreement. In general, our model has closer values than the commercial code whatever the boundary conditions, sections, materials, and length.

A small discrepancy in term of frequencies between experimental and numerical does not exceed 4% in case of B3Dw code, and 7% for Abaqus results. Thus, the presented code B3Dw is more accurate than Abaqus because the flexural and torsional coupling rotational kinematic terms as well as cross section warping are taken into account. The relative error does not exceed 4% in mean value. The acceptable error can be explained by: manufacturing imperfections of specimens, precision of the boundary condition, noise…

In order to enhance the vibration analysis, for each frequency mode shape type should be studied. Since the cross sections are arbitrary it is confirmed that all modes are flexural-torsional coupled. To verify the concept of triply coupled flexural-torsional modes, nodal displacements are studied. The first three modes of (Beam2, Test T3, Cantilever) carried out from B3Dw are depicted in Figure 4.18 and compared to experimental displacements shown in the response spectra of different sensors distributed on different locations and directions on specimens. Numerical results depicted in Figure 4.18 show that displacements v, w and θ_x are presented in all modes. On the other hand, experimentally, for each natural frequency all sensors record accelerations, so for all modes beam motions are flexural-torsional coupled. Thus, numerical and experimental results agree with the concept of flexural-torsional coupling for arbitrary cross sections. Finally, it should be noted that in this experimental study mode shapes and dominate modes are not exanimated. Because, with only 4 sensors it is not easy to reconstitute mode shapes. But later one, it will be possible by the help of the new installed equipment vibrometer laser. Using this equipment dynamic response spectra can be obtained for a series of points without contact. Consequently, more accurate results can be carried out experimentally and mode shapes can be well investigated.

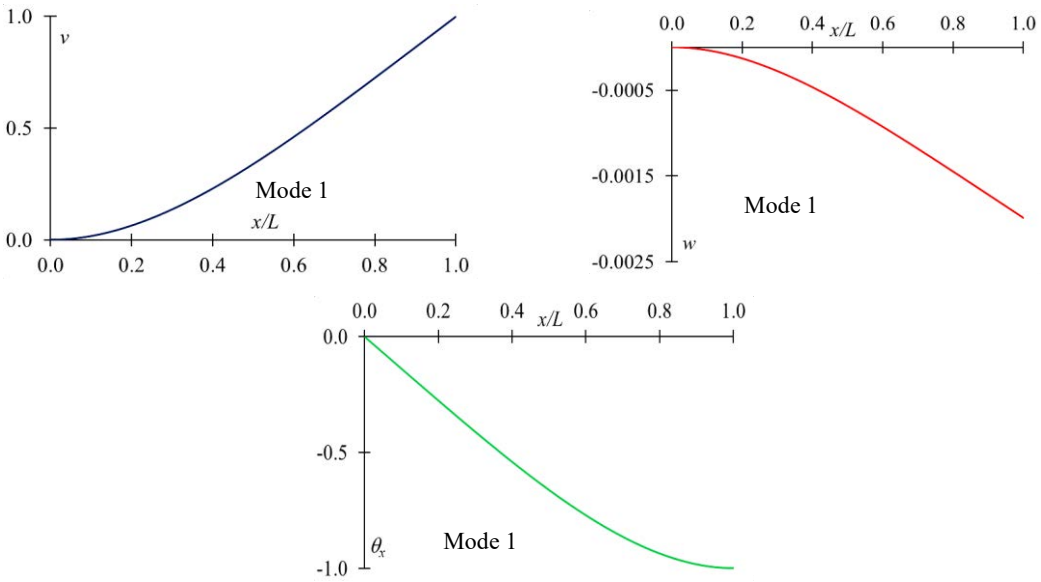

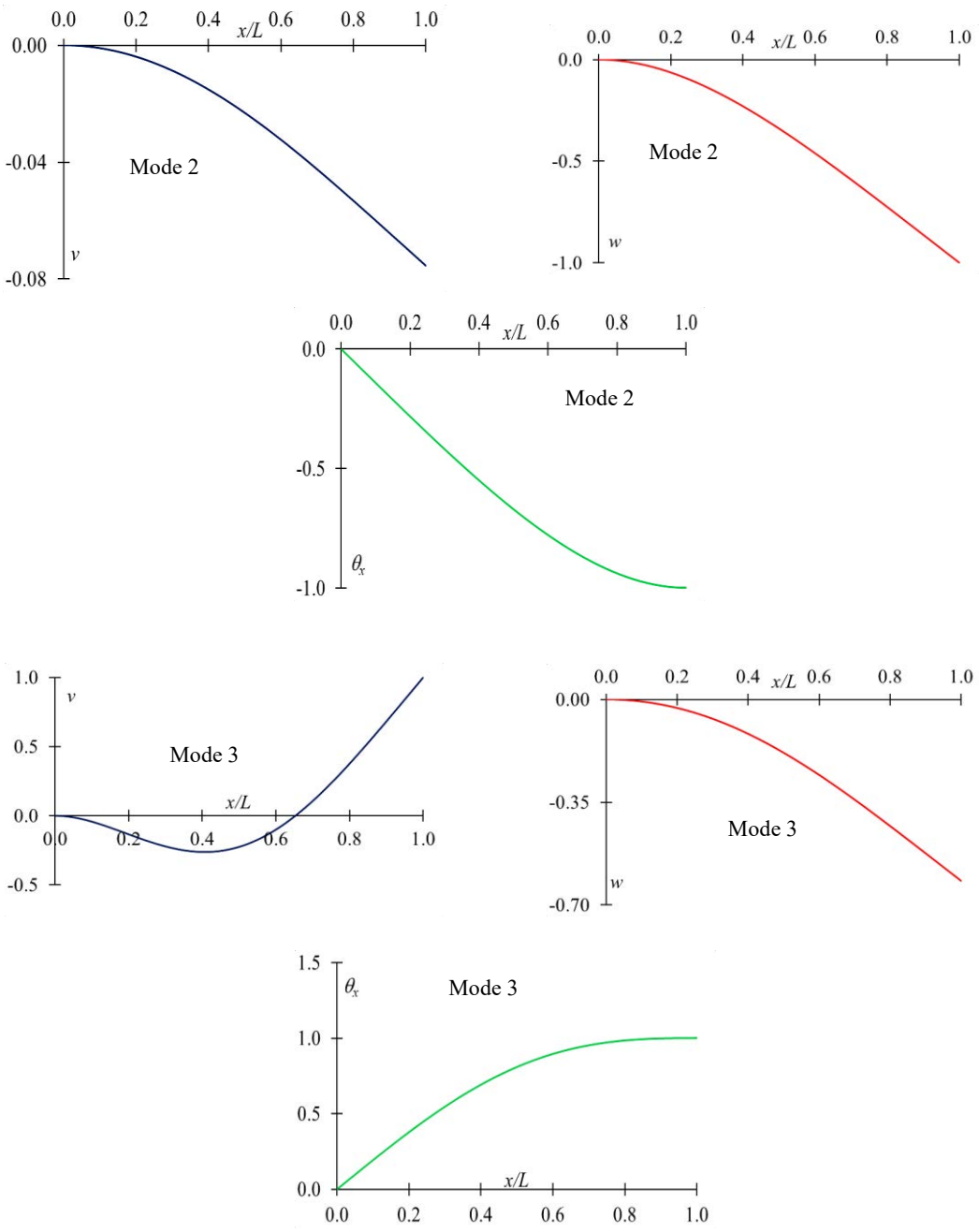

Figure 4.18: First three vibration modes of the beam2 under clamped free boundary conditions obtained by B3Dw.

4.7.2 Forced vibration

For the forced vibration analyses, the cantilever beam B2 (L-section 60x40x4mm) is chosen to be tested. The length of the beam is divided in 3 regions (M1 to M3), which located at the 20 mm of the free extremity, at 2L/3 and at L/3, respectively. Vibration responses measure thanks to four accelerometers fixed on the specimen (Figure 4.6). To compare the experimental results given by measurement and the numerical models (B3Dw and commercial code), there are integrated to obtain the vibration displacement.

In Figure 4.19, the sensors 2 and 3 are placed on the region located at the 20mm of the free extremity (M1). The sensors are noticeable on the *y*-direction. So, the displacements response spectra recorded by the sensors 2 and 3 are compared to the numerical simulations results obtained by B3Dw and commercial code Abaqus in *v* direction.

In Figure 4.20, the sensors 4 and 5 are placed on the region located at the 20mm of the free extremity (M1). The sensors are noticeable on the *z*-direction. So, the displacements response spectra recorded by the sensors 4 and 5 are compared to the numerical simulations results obtained by B3Dw and commercial code Abaqus in *w* direction.

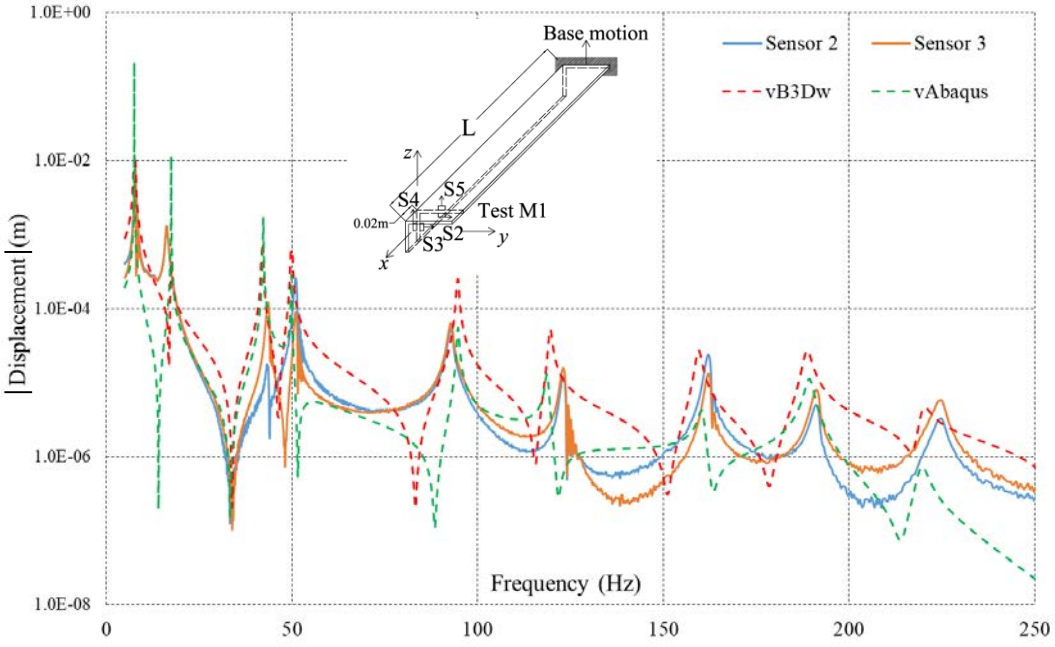

Figure 4.19: Displacement as a function of the frequency measured by the sensors (2 and 3) at location M1, for beam 2, compared to the numerical simulations.

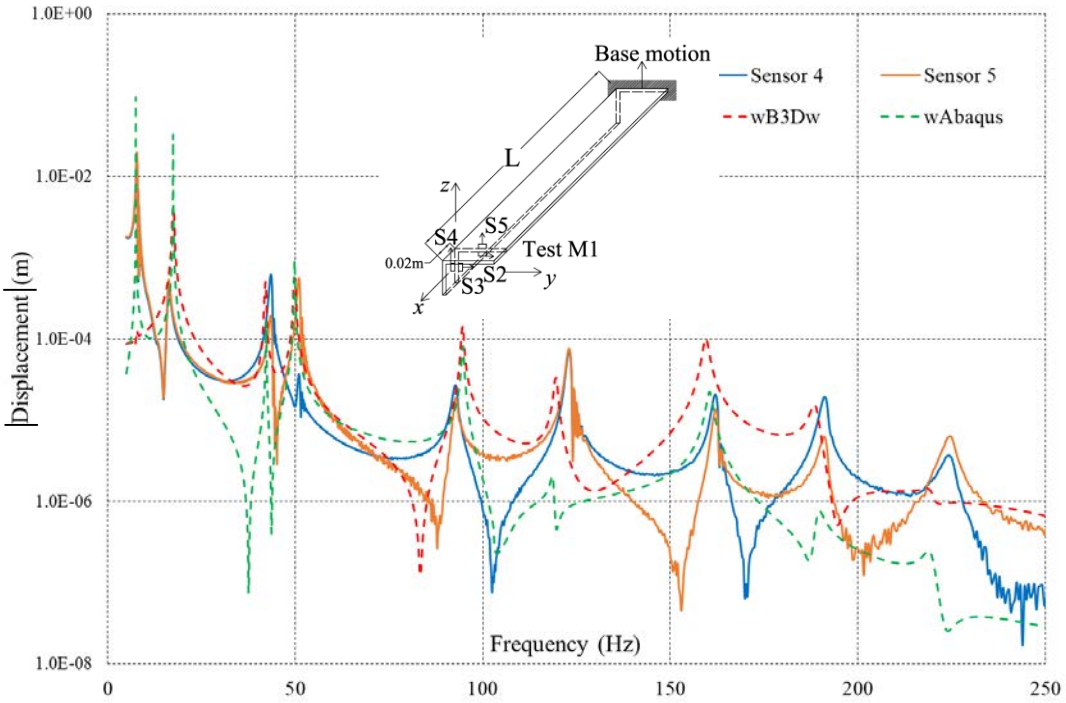

Figure 4.20: Displacement as a function of the frequency measured by the sensors (4 and 5) at location M1, for beam 2, compared to the numerical simulations.

Considering displacements form Figures 4.19 and 4.20, the vibration modes are coupled. The curves show that the resonance spectra are accurate form our simulation and the Abaqus results on the *y* and *z* direction. The resonance frequencies are a good agreement as the same on free vibration study. The amplitudes of the displacement are closer for our model whatever the direction.

Figures 4.21 and 4.22 present the response spectra recorded by the sensors located on region (M2), at distance equal to 2L/3 from the clamped end of the beam. In the same graphs similar results obtained by the numerical simulations are depicted. Figure 4.21 shows the sensors on the *y* direction when Figure 4.22 is on the *z* direction.

In Figure 4.21, the displacements response spectra recorded by the sensors 2 and 3 are compared to numerical simulations results obtained by B3Dw and commercial code Abaqus in *v* direction.

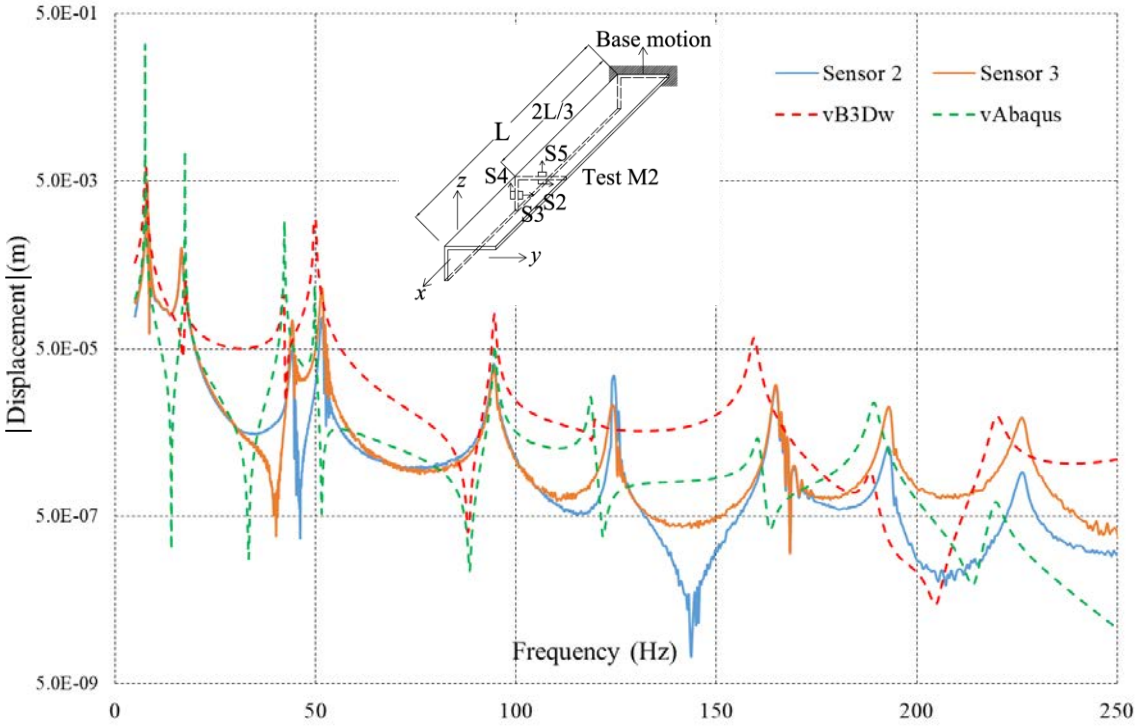

Figure 4.21: Displacement as a function of the frequency measured by the sensors (2 and 3) at location M2, for beam 2, compared to the numerical simulations.

In Figure 4.22, the sensors 4 and 5 are placed on the region located at L/3 from the free extremity (M2). The sensors are noticeable on the *z*-direction. Displacements response spectra carried out from test are compared to numerical simulations results obtained by B3Dw and commercial code Abaqus in *w* direction.

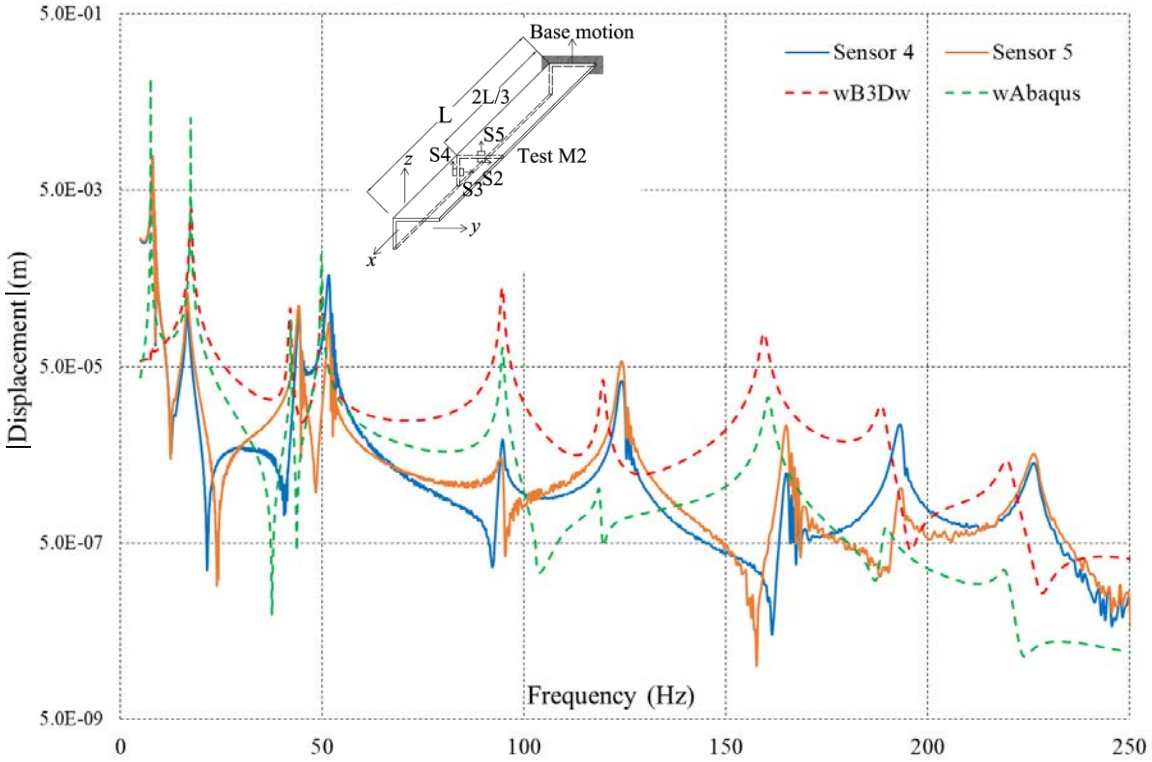

Figure 4.22: Displacement as a function of the frequency measured by the sensors (4 and 5) at location M2, for beam 2, compared to the numerical simulations.

By analyzing M2 test response spectra depicted in Figures 4.21 and 4.22, the same remarks can be taken as M1 that are the followings, all modes are coupled modes are coupled. Otherwise, the accuracy of B3Dw results comparing to experimental results whatever the location of measuring point on the beam. Other observation is that when the location of measuring point become closer to the clamped end of the beam displacements amplitudes decreases as shown previously in mode shapes presented in Figure 4.18. It seems that, for some modes corresponding to the natural frequencies higher than 150Hz the natural frequencies obtained by numerical methods are slightly shifted from the experimental results. This shift does not exceed 4% in term of error it is acceptable and can be explained by different reasons: (The 4 sensors weight located in the same point, section manufacturing imperfection, noise, sensors accuracy…. etc.). To improve this work and get more accurate results the new equipment vibrometer laser will be used later.

Figures 4.23 and 4.24 present results from the sensors on region (M3), which its located at the length equal to L/3 from the clamped end of the beam. In the same graphs similar results obtained by the numerical simulations are depicted. Figure 4.23 shows the sensors on the *y*- direction when Figure 4.24 shows on the *z*-direction.

In Figure 4.23, the sensors 2 and 3 are placed on the region located at 2L/3 from the free extremity (M3). The sensors are noticeable on the *y*-direction. So, test results collected from these sensors are compared to numerical displacements results obtained by B3Dw and commercial code Abaqus in *v* direction.

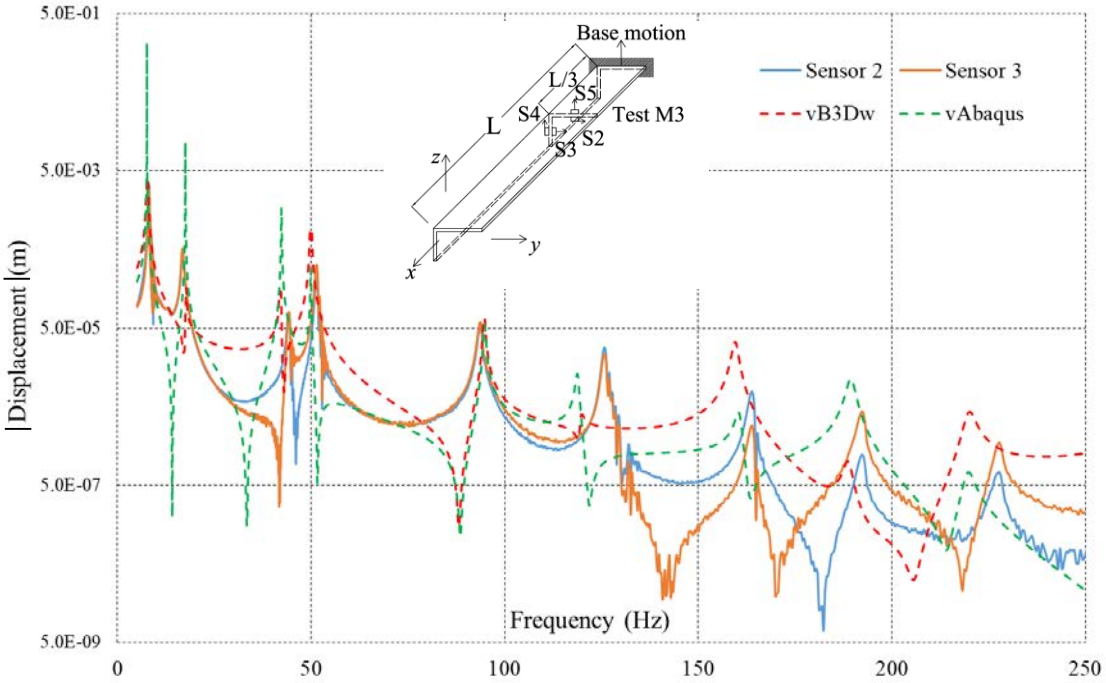

Figure 4.23: Displacement as a function of the frequency measured by the sensors (2 and 3) at location M3, for beam 2, compared to the numerical simulations.

In Figure 4.24, the sensors 4 and 5 are placed on the region located at 2*L*/3 from the free extremity (M3). The sensors are noticeable on the *z*-direction. Dynamic response spectra carried out from test are compared to numerical displacements results obtained by B3Dw and commercial code Abaqus in *w* direction.

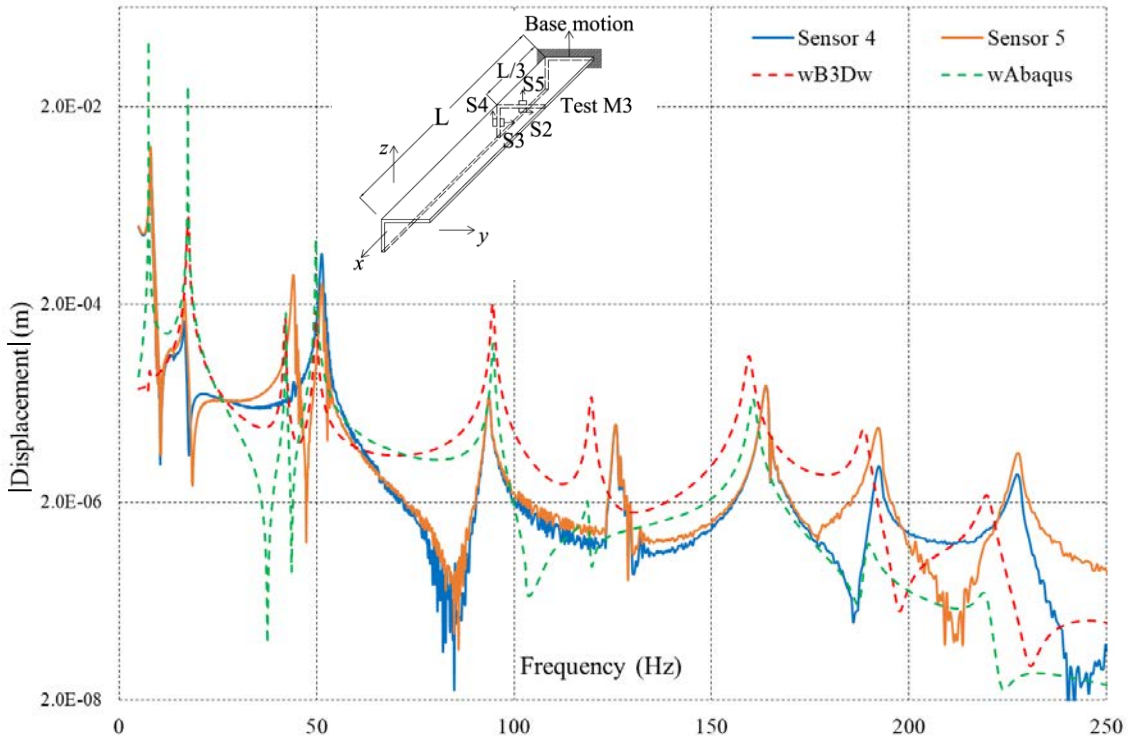

Figure 4.24: Displacement as a function of the frequency measured by the sensors (4 and 5) at location M3, for beam 2, compared to the numerical simulations.

Considering displacements shown in Figures 4.23 and 4.24, as M1 and M2 it is noticeable that all modes are coupled modes are coupled. Also, B3Dw match well with experimental tests results. Otherwise, it is remarkable that displacements amplitudes are lower than the displacements recorded in M1 and M2, because of the point is the nearest to clamped side of the beam.

Figures 4.19 to 4.24 presented above, displacement response curves in directions *v* and *w* obtained by B3Dw match well with experimental curves. Some little shifts of curves peaks are noted and can be explained as acceptable error between natural frequencies measured experimentally and numerically. This error doesn't exceed 3% comparing B3Dw to experimental results which is so reasonable when doesn't exceed 6%. This error can be explained as sensors sensibility, noise, manufacturing imperfection of specimens, the influence of 4 sensors masses on the structure near to resonance…etc. Another remarkable point is that the curves amplitude of experimental and numerical methods is also comparable. The small difference shown in graphs are due to sensors weight effect and section imperfection and transducers sensibilities. These difference do not exceed 4.5% by comparing B3Dw to experimental results and 6.7% in case of Abaqus results. Further, B3Dw curves are closer to test ones more than Abaqus ones. Adding to this, experimental and numerical results show that, all modes are presented in different points of measurement over the beam and in different directions of measurement this prove the coupling effect of modes for non-symmetrical sections types. Thus, the presented B3Dw

method is validated furthermore in forced vibration investigation by comparing it to experimental test results.

Finally, for each mode the dominant displacement can be determined by comparing different sensors amplitudes for the same natural frequency (peak). For each peak a comparison of amplitudes of all sensors in different location give the followings: Mode 1 *w* dominated, Mode 2 *v* dominated, Mode 3 *w* dominated, Mode 4 *w* dominated, Mode 4 *v* dominated, Mode 6 *w* dominated, Mode 7 *v* dominated, Mode 8 *w* dominated, Mode 9 *w* dominated, Mode 10 *v* dominated. These results match well with numerical results obtained by B3Dw.

4.8 Effect of intermediate bracings

In order to improve the vibration behavior of 3D structures against vibration, recourse to braces in design are commonly adopted in engineering practices as in bridges frames buildings and many other mechanical structures. In the present example, one considers the effects of lateral bracing on the vibration behavior of beams with arbitrary cross-sections. For this aim, one considers a doubly-clamped beam with/without bracing tested in free vibration by means of an instrumental hammer. Beam geometry, material properties and experimental setup are depicted in Figure 4.25. In the figure, it is shown that the three accelerometers were installed at different locations and directions on the beam to record the response spectra. A full brace is added at the mid-span to restrict the displacement in *w* direction. The dynamic response spectra recorded by sensor 3 from 1 tests with/without brace are depicted in Figure 4.26.

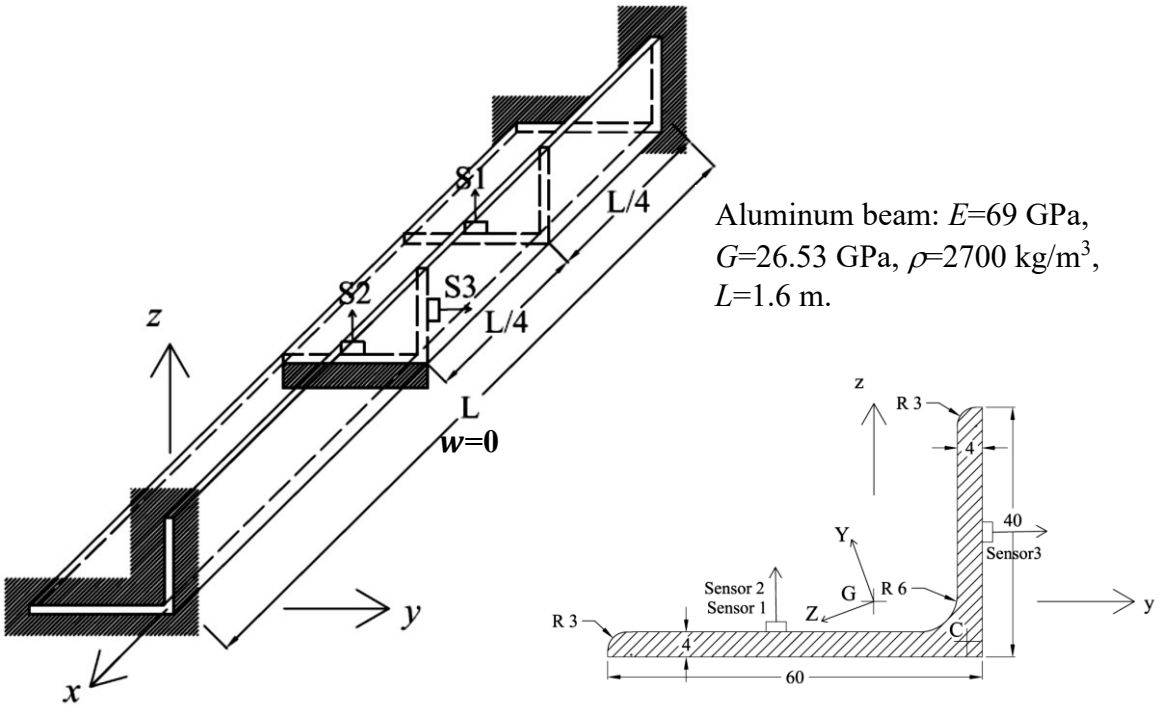

Figure 4.25: Beam geometry, material properties and sensors locations for beam with intermediate brace.

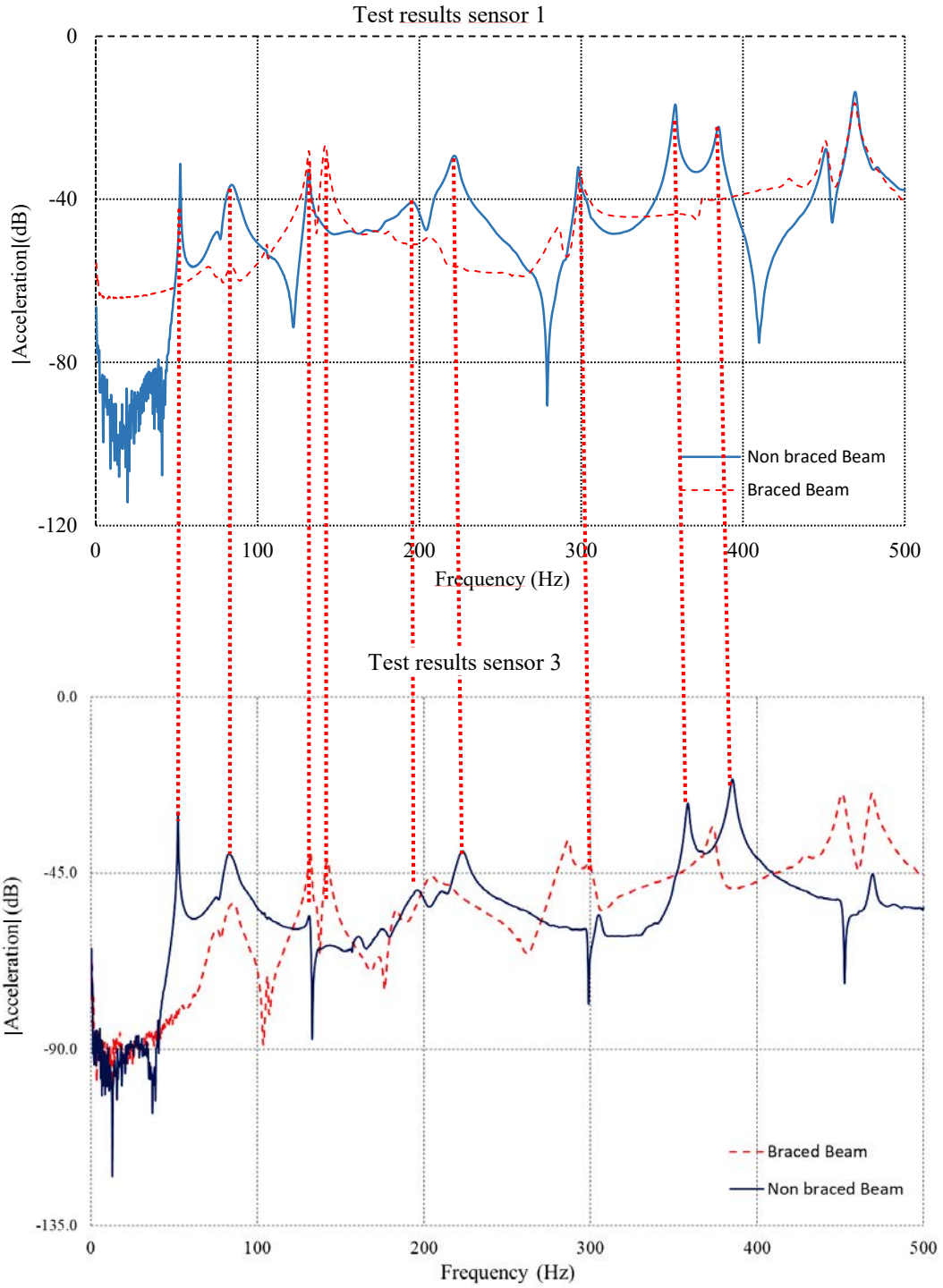

Figure 4.26: Response spectra recorded by sensors 1and 3
from vibration tests of beam with/without brace.

By analyzing the response spectra depicted in Figure 4.26 for beams without/with brace, it seems that the same natural frequencies are obtained by the different sensors. Otherwise, by adding one lateral brace at mid-span the first resonance frequency (52.19 Hz) disappeared and other peaks are shifted. In order to compare test data to numerical results, the natural frequencies are carried out from the response spectra. In what follows, the first 8 natural frequencies for beams with/without brace carried out from tests and numerical simulations are arranged in Table 4.7.

Table 4.7: Numerical-experimental comparison of natural frequencies (Hz) for doubly-clamped beam with/without brace at mid-span.

Mode	**Test without brace**	B3Dw without brace	|Error| % B3Dw/Test	**Test with brace**	B3Dw with brace	|Error| % B3Dw/Test
1	**52.19**	54.12	3.57	**-**	-	-
2	**84.53**	86.92	2.8	**84.96**	82.00	3.5
3	**131.68**	132.40	0.6	**141.90**	141.34	0.4
4	**196.08**	202.16	3.1	**208.00**	210.00	1.0
5	**222.73**	217.92	2.2	**299.70**	299.73	0.0
6	**358.25**	357.28	0.3	**373.80**	372.38	0.4
7	**385.08**	395.03	2.6	**440.60**	424.64	3.6
8	**451.53**	447.02	1.0	**469.10**	476.54	1.6

A comparison among the B3Dw and the experimental results in Table 4.7 show that the mean value of the relative errors between tests and the present FEM natural frequencies is smaller than 3 % for both unrestrained and braced beams. Thus, it shows a very good agreement between the results obtained with the FEM simulations and those obtained in the tests. Therefore, the developed method B3Dw is validated in case of braced beams. Moreover, by analyzing the results depicted in Table 4.7, it is remarkable that in presence of one brace the first mode is vanished and all others frequencies were increased. Consequently, in case of arbitrary section, due to the flexural-torsional coupling effect all natural frequencies are considerably increased by introducing lateral braces along the beam. By this way, it is proven the importance of adding braces for bending and torsion vibration control of thin-walled beams with arbitrary cross-sections. This procedure can be followed and the beam can be strengthened efficiently by lateral supports.

4.9 Conclusion

In this chapter, experimental tests for free and forced vibrations on thin-walled beams with arbitrary open cross sections have been investigated. Tests on beams with three different boundary conditions are performed (Simply supported, cantilever and clamped-clamped). Hammer tests were realized in free vibration procedure to obtain the natural frequencies. In forced vibration tests, a shaker machine is used to carry out the beam response spectra in frequency domain. Test setup procedures were well demonstrated in this work. Tests are investigated in the range1 to 600 Hz. More than 10 modes are present. The behavior exhibits coupled flexural-torsional vibration modes. Dominant modes were also investigated in this work.

Test results were used to compared among numerical simulations made possible by a finite element formulation investigated in the present work, where 3D beams elements allowing warping are adopted in mesh process (B3Dw element). Abaqus commercial software is also used in the validation of the free vibration and forced vibration results. This comparison shows a very good agreement between numerical solutions given by B3Dw and the experimental results. The dynamic behavior exhibits flexural-torsional couplings present in both numerical analyses and tests, also the predominant modes gotten by B3Dw agree with experimental results. The present model matches well with the free and forced vibration experiments. The efficiency of the numerical and experimental setup constitutes then a good background for future coming works.

The effect of introducing intermediate bracings to control bending and torsional vibration was treated also numerically and experimentally. It is observed that in presence of intermediate supports, the vibration behavior of the beam against the lower natural frequencies is improved. Otherwise, in case of arbitrary section, all natural frequencies are considerably increased by introducing lateral braces along the beam. This concept can be used in vibration control for structures to improve the stability of slender beams against torsion and other undesirable modes. A new concept was deducted from the last example that by adding n intermediate viscoelastic braces to an unrestrained beam the first n modes can be removed and beam displacements are reduced near to resonance. Thus, the importance of adding viscoelastic braces in vibration controlled is proven.

Chapter 5 Vibration of braced beams

5.1 Introduction

This study is important in design of buildings and bridges structures. In fact, the vibration behavior is predominated by the presence of the torsion modes and lateral bending modes. In the case of slender unrestrained beams, these modes are always lower than the classical vertical bending modes (2D plane modes). Let us remind that in design, plane modes are more appropriate than the lateral and torsion modes. Nowadays, in order to improve the vibration behavior of 3D structures against torsion modes, recourse to braces in design are commonly adopted in engineering practices as in bridges frames buildings and many other mechanical structures (Figure 5.1) [98].

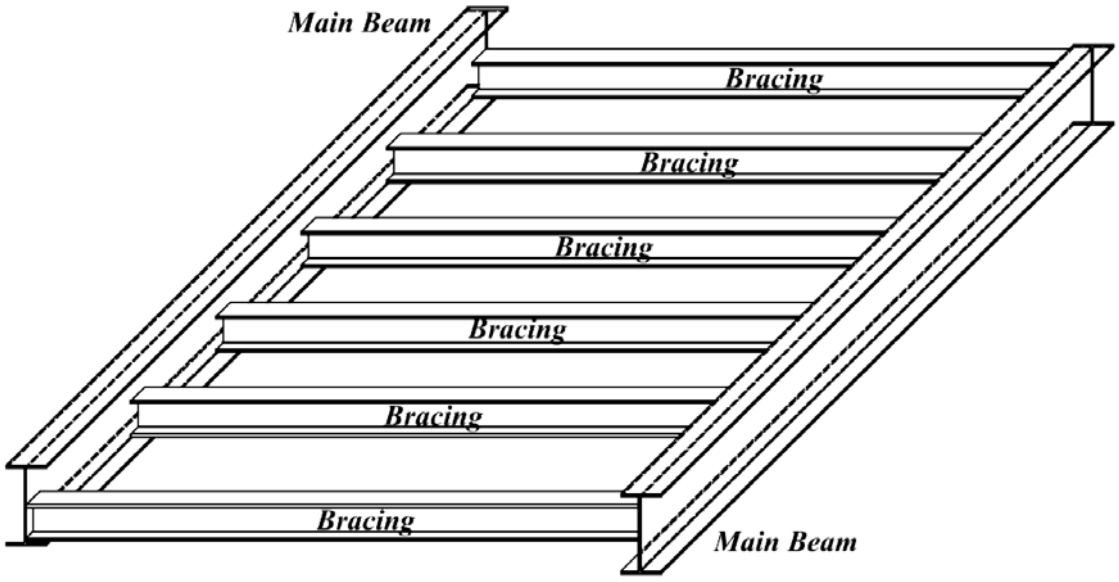

Figure 5.1: Braced beams: an example of two main beams with some lateral bracings.

The challenge consists of finding the optimum number and the spacing positions of the braces in order to reduce the lateral bending and torsion mode effects.

In the literature, braces are adopted as solution to improve the stability of thin-walled beams in both static and dynamic contexts. In static, to improve the strength of slender beams and columns against buckling and lateral buckling intermediate bracings are adopted. The effects of bracings have considered by several works in static. The Influence of restraints on the Stability of slender beams to lateral instability was studied in [99]. Winter [100] developed an elementary method to compute the strength and rigidity of lateral elastic supports in order to provide full bracing to columns and beams. Taylor and Ojalvo [101] presented elastic solutions to lateral-torsional buckling of I-beams with torsional restraints. Moreover, many authors study the elastic lateral and torsional braces in lateral buckling control in refs. [8, 102, 103]. Recently, Nguyen [104] proposed an

approximate method to predict the critical buckling moment and stiffness requirements of I-section beams with discrete torsional bracing. The model is limited to simply supported beams under uniform bending moments. Finite element simulations have been carried out and shell elements have been customized. McCann [105] investigated the lateral torsional buckling capacity of beams with elastic restraints present along the beam. In this work, simply supported beams under uniform moments have been investigated and an optimization procedure for the bracing height effect is suggested. The equivalent initial imperfection method of structures sensitive to flexural and torsional buckling have been investigated in Aguero [106]. More recently, Zhang [107] studied the lateral-torsional buckling of cantilever beams in presence of lateral elastic braces. Pezeshky [108] investigated the influence of bracing position on LTB capacity of cantilever and simply supported beams and highlighted the effect of braces position on beam buckling capacity.

In the dynamic context, the vibration behavior, of braced beams has been investigated in several works. Numerous papers have been devoted to this problem, Akesson [109] obtained the required stiffness in order to enhance the free vibration behavior of beams. Rao [110] developed the frequency equation of a beam with an intermediate support by the continuity conditions at the supported point. Abromovich and Hamburger [111] studied the variation of the free vibration frequencies of a cantilever beam with uniform cross section with Timoshenko shear theory. The effects of translational and rotational springs and an additional tip mass have been considered. In the study, a semi analytical procedure has been followed in investigation of the vibration analysis [112]. Wang [113] evaluated numerically the minimum stiffness of an elastic support for beams with different end conditions to affect the fundamental natural frequency. Wang *et al.* [114] investigated the frequency of a beam with regard to the position of a simple intermediate support by the discrete method. Moreover, they determine the optimum positions of elastic supports based on the frequency sensitivity. Albarracın *et al.* [115] calculated the effect of an intermediate support when the ends of the beam have elastic constraints. Maurizi *et al.* [116] gave a concise thematic recension about free vibrations of Bernoulli–Euler beams with intermediate elastic support. Gokdag H. and Kopmaz O. [53] studied the coupled flexural-torsional free and forced vibrations of a beam with mono-symmetric open cross section with tip and/or in-span attachments using a developed analytical method. The lateral vibration behavior of a beam with intermediate supports was investigated by Wang *et al.* [117]. They reported that the natural frequency is significantly affected by the stiffness of the intermediate spring. Gokdag and Kopmaz [118] proposed an analysis model for the coupled bending and torsion vibration of a beam with intermediate bracings. However, they consider intermediate supports as linear springs that prevent lateral displacement.

More recently, Nguyen [84] studied effects of bracing on torsion modes only. He derived an analytical method to determine the required stiffness for the intermediate torsional braces to control torsional vibration modes. The natural frequency of torsional vibration is considerably increased with increasing the number of bracing points along the beam. Then, he verified the developed method by numerical simulations using Abaqus commercial code. Moreover, in [51, 52] analytical expressions for the exact frequency response of coupled bending–torsional beams carrying an arbitrary number of viscoelastic

dampers and attached masses, subjected to harmonically varying, arbitrarily placed polynomial loads were derived. In the model warping effects included. Generalized functions were used to model response discontinuities at the application points of dampers/masses. In this context, the exact dynamic Green's functions of the beam were used.

In this study, one considers the effects of bracing on both the free vibration bending and torsion modes. Then, the effect of elastic springs used in parallel with viscous springs is also investigated to control vibration modes and displacement in the same time which is more efficient. Otherwise, the optimal distribution method of bracings is also studied.

In what follows, a kinematic model for free and forced vibrations of thin-walled beams with intermediate viscoelastic braces is detailed in section 5.2. Then, particular analytical solutions for free vibration of beams with bisymmetric open cross sections and intermediate lateral elastic springs is developed in section 5.3. The analytical solutions are limited in a simple cases of beams with bisymmetric cross sections, for more complicated cases these solutions become cumbersome. To this aim the requirement of the finite element method that can be used for any complicated cases of boundary conditions and section. Hence, a finite element method for free and forced vibration investigation with the effect of intermediate discrete or distributed viscous and/or elastic springs is developed and detailed in section 5.4. This developed element is used to study vibration control of beams by adding of intermediate elastic and viscous braces. Furthermore, presented element can be used to simulate the response of beams subjected to random signals, like earthquakes. This element is called B3Dw and it is implemented on Matlab software. These solutions take in consideration of kinematic rotational terms. So it can be used to compute higher vibration modes with accuracy. These solutions can be found in [120]. In part 5.5 the model is validated by comparing to some benchmark results in free and forced vibration. Also the model is validated by experimental test in the chapter 5. By conclusion, the effect of intermediate braces in vibration control is studied in the numerical examples. Finally, in section 5.6 the conclusion comprises a summary about the effect of the number and distribution of intermediate braces as well as the required stiffness for elastic springs. In the same section the importance of dashpots installed in parallel with the elastic spring is also outlined.

5.2 Brace design

Bracing are divided into two main categories: lateral and torsional bracing. These braces connected the main beams with specific positions as illustrated in Figure 5.1 below. Moreover, the effect of braces varies depending on their types (beams, bars…etc.) and the way of their connection to the main beams, as demonstrated in Figure 5.2.

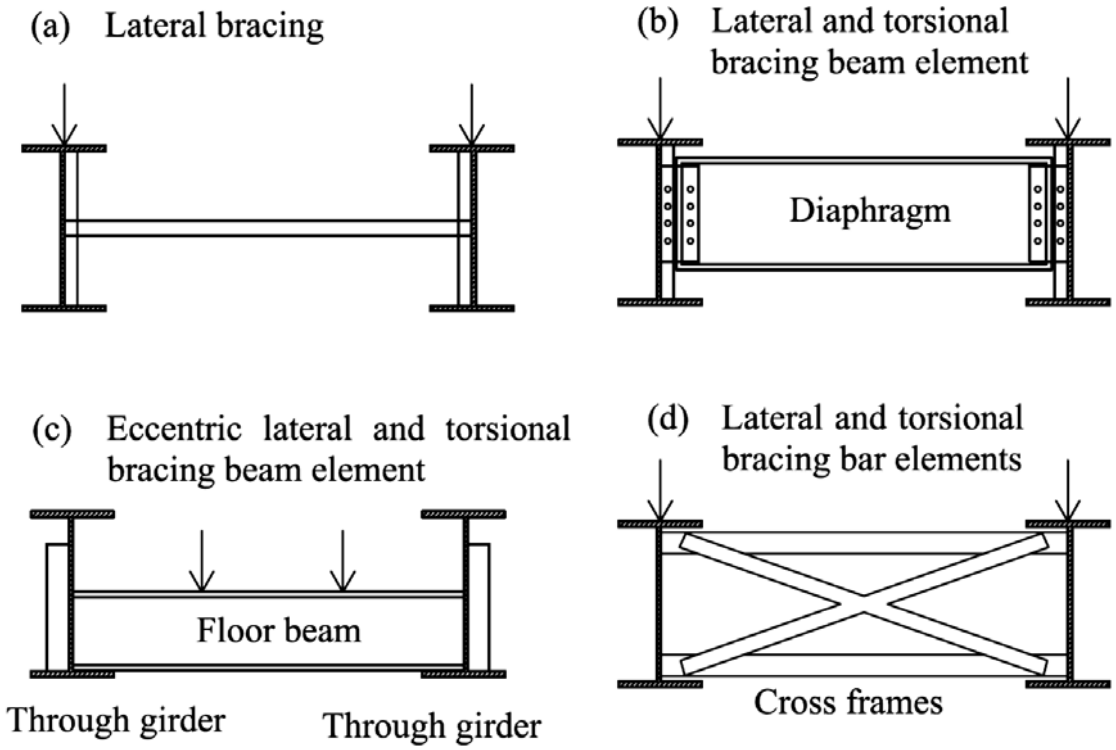

Figure 5.2: Types of intermediate lateral and torsional elastic bracings.

Lateral bracing restrains lateral displacement as its name implies. The effectiveness of a lateral brace is related to the degree that twist of the cross section is restrained. Otherwise, torsional braces can be used to restrain the torsional degree of freedom of structural elements. Also, sections warping is controlled by using this type of braces.

For a simply supported I-beam the shear center is located at the web center point. Moreover, when it is subjected to dynamic loads, the top flange can move laterally much more than the bottom flange (warping effect). Therefore, a lateral brace restricts twist best when it is located at the middle of web as shown in Figure 5.2a. A torsional brace can be differentiated from a lateral brace in that twist of the cross section is restrained directly, as in the case of twin beams with a cross frame or diaphragm between the members shown in Figure 5.2b, d. Some systems such as concrete slabs can act both as lateral and torsional braces. Further, Figure 5.2c shows an eccentric lateral and torsional bracing system. By comparing to the others systems depicted in Figure 5.2 it is less effective due to the

eccentricity of braces elements. In the present study this type of bracing systems is not taken in consideration.

It is known to be considered that 3D thin-walled beams are subjected to lateral and torsional vibration modes. For this reason, bracing that controls both lateral movement and twist is more effective than lateral or torsional braces acting alone. Bracing can be divided into several categories as: relative, discrete (nodal) and continuous (decking). A relative brace system controls the relative lateral movement between two points along the span of the girder. The diagonal brace prevents 2 points in two different main beams from moving different amounts. Discrete systems can be represented by individual lateral springs along the span length. All these bracings are considered in structural design as elastic springs.

Viscous springs or nodal dampers known as dashpots are used to control vibration of the structure when they are present together with the elastic springs. These are used to control the displacements of certain points of structures when they are subjected to dynamic loads. The dampers lateral and torsional types are presented in Figure 5.3.

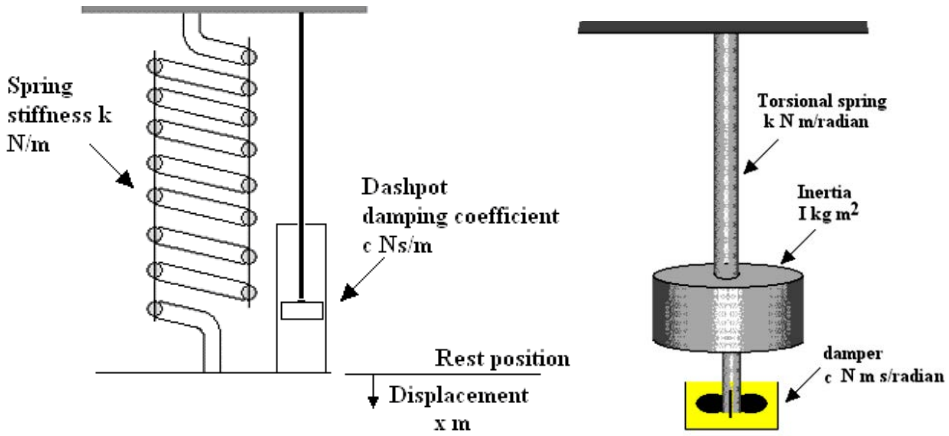

Figure 5.3: Lateral and torsional viscous springs installed in parallel with elastic springs.

In what follows, elastic and viscous braces are added to thin-walled beams to improve the beams stability against vibration behavior, in other word, vibration control. For this reason, the developed analytical and finite element model are extended to take in consideration the effect of intermediate discrete or continues additional intermediate braces.

5.2.1 Vibration control by means of elastic bracings

In this section, efficient methods for removing or reducing undesirable vibration in slender beams are presented. The acceptable levels of vibration can easily be investigated, then the levels to be eliminated or reduced can be quantified. Vibrations can be in different forms of disturbance displacement, velocity, acceleration, and transmitted forces. To reduce transmission of vibration from the source to the structure, the most effective solutions are the followings:

- Enhance the vibration behavior and reduce the effect of undesirable vibration modes, by adding some lateral and torsional elastic braces to the beam. These braces must be located in the optimal location to improve the structure.

- Reduce the displacement amplitudes at resonance, by using viscous springs (dashpots). These dashpots can be implemented in the same location of the springs or in another position justified by design conditions.

Solutions of vibration problems of structures in presence of elastic springs and dashpots by analytical procedure should be cumbersome. Recourse to semi analytical and the FEM is then more powerful. For this aim, the finite element beam element developed in chapter 2 for unbraced beams is extended here to the case of braced beams in presence of elastic springs and viscous dashpots.

5.2.2 Dynamic behavior of braced beams

The straight element with thin-walled open section previously studied in chapter 2 is reconsidered in this section with additional intermediate discrete or continues elastic springs and dashpots distributed over the beam length. The thin-walled element with intermediate viscoelastic braces becomes as depicted in Figure 5.4. Same as detailed in the previous section 2.2, the rectangular system of coordination (G,x,y,z) is used, with G is the cross section center, the x-axis is parallel to the length of the beam. The shear center was noted C, its co-ordinates in Gyz are (y_c, z_c). Vlasov's model for non-uniform torsion is used in this model. The displacements components of M can be derived from those of the shear center and centroid points. Then the motion equations are derived using Hamilton's principle. Numerical Solutions for free and forced vibration of thin-walled beams are detailed using finite element approach in presence in presence of elastic springs and viscous dashpots.

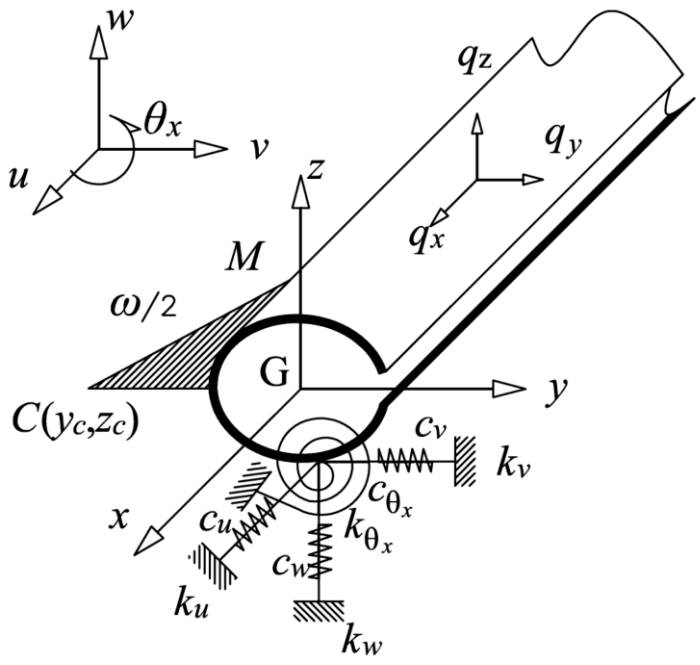

Figure 5.4: Thin-walled open section element with additional viscoelastic braces.

The beam strain energy variation δU is based on the classical beam part δU_b and the contribution of the additional elastic 3D springs δU_s. They are given by:

$$\delta U_b = \int_L (EAu'\delta u' + EI_z v''\delta v'' - EI_z w''\delta w'' + EI_\omega \theta_x''\delta\theta_x'' + GI_t\theta_x'\delta\theta_x')\,dx = \int_L \{\delta\gamma\}^t[D]\{\gamma\}\,dx \quad (5.1)$$

$$\delta U_s = \int_L k_u u\delta u + k_v v\delta v + k_w w\delta w + k_{\theta_x}\theta_x\delta\theta_x = \int_L \{q\}^t[k_s]\{q\}dx \quad (5.2)$$

$$\delta U = \delta U_b + \delta U_s \quad (5.3)$$

Where $[K_s]$ is the spring stiffness matrix and his components are $(k_u, k_v, k_w, k_{\theta_x})$.

The variation expression of kinetic energy δT of a straight thin-walled element demonstrated in 2.2 is given by:

$$\delta T = \int_L m\left(\dot{u}\delta\dot{u} + \dot{v}\delta\dot{v} + \dot{w}\delta\dot{w} + I_0\dot{\theta}_x\delta\dot{\theta}_x\right)dx + \int_L m\left(z_c(\dot{\theta}_x\delta\dot{v} + \dot{v}\delta\dot{\theta}_x) - y_c(\dot{\theta}_x\delta\dot{w} + \dot{w}\delta\dot{\theta}_x)\right)dx + \int_L \left(m\frac{I_z}{A}(\dot{v}'\delta\dot{v}') + m\frac{I_y}{A}(\dot{w}'\delta\dot{w}') + m\frac{I_\omega}{A}(\dot{\theta}_x'\delta\dot{\theta}_x')\right)dx$$

$$\delta T = \int_L m\{\delta\dot{q}\}^t[M_1]\{\dot{q}\}dx + \int_L \frac{m}{A}\{\delta\dot{\varphi}\}^t[M_2]\{\dot{\varphi}\}dx \quad (5.4)$$

In forced vibration, the variation expression of external load work δW is the following:

$$\delta W = \int_L \left(q_x \delta u + q_y \delta v + q_z \delta w + m_x \delta \theta_x\right) dx = \int_L \{\delta q\}^t \{f\} dx \quad (5.5)$$

Taking account for the presence of the classical viscous damping $\delta \Gamma_b$ in the beam and the additional damping $\delta \Gamma_d$ due to the presence of dashpots, the damping variation parts are given by:

$$\delta \Gamma_b = \int_L \left(C_u \dot{u} \delta u + C_v \dot{v} \delta v + C_w \dot{w} \delta w + C_{\theta_x} \dot{\theta}_x \delta \theta_x\right) dx = \int_L \{\delta q\}^t [C_b] \{\dot{q}\} dx \quad (5.6)$$

$$\delta \Gamma_d = \int_L \left(c_u \dot{u} \delta u + c_v \dot{v} \delta v + c_w \dot{w} \delta w + c_{\theta_x} \dot{\theta}_x \delta \theta_x\right) dx = \int_L \{\delta q\}^t [C_d] \{\dot{q}\} dx \quad (5.7)$$

$$\delta \Gamma = \delta \Gamma_b + \delta \Gamma_d \quad (5.8)$$

Where: $[C_b]$ is the beam damping matrix and his components are $(C_u, C_v, C_w, C_{\theta_x})$.

$[C_d]$ is the dashpot damping matrix and his components are $(c_u, c_v, c_w, c_{\theta_x})$.

5.2.3 Motion equations

Based on the strain energy defined in equation (5.3), the kinetic energy equation (5.4), the load contribution equation (5.5) and the damping equation (5.8), the motion equations of the beam fulfil the extended Hamilton's principle given by [11]:

$$\begin{cases} \int_{t_1}^{t_2} \delta(U + \Gamma - T - W) \mathrm{d}t = 0 \\ \delta q(t_1) = \delta q(t_2) \end{cases} \quad (5.9)$$

In the case of free vibration all the forces vanish, after integrations and term collections the motion equations become:

$$\delta u : \; m \frac{d^2 u}{dt^2} + EAu'' + k_u u = 0$$

$$\delta v : \; m \left(\frac{d^2 v}{dt^2} - \frac{I_z}{A} \frac{d^4 v}{dx^2 dt^2} + z_c \frac{d^2 \theta_x}{dt^2}\right) + EI_z \left(v^{(4)}\right) + k_v v = 0$$

$$\delta w : \; m \left(\frac{d^2 w}{dt^2} - \frac{I_y}{A} \frac{d^4 w}{dx^2 dt^2} - y_c \frac{d^2 \theta_x}{dt^2}\right) + EI_y \left(w^{(4)}\right) + k_w w = 0$$

$$\delta \theta_x : \; m \left(I_0 \frac{d^2 \theta_x}{dt^2} - \frac{I_\omega}{A} \frac{d^4 \theta_x}{dx^2 dt^2} + z_c \frac{d^2 v}{dt^2} - y_c \frac{d^2 w}{dt^2}\right) + EI_w \theta_x{}^{(4)} - GJ\theta_x'' + k_{\theta_x} \theta_x = 0 \quad (5.10a\text{-}d)$$

From these equations, analytical solutions have been derived for the free vibration behavior of a beam in presence of discrete springs. These solutions are possible for any direction and in torsion for a beam with doubly symmetric cross section. These are compared to finite element simulations and to benchmark solutions hereafter.

5.3 Finite element formulation for braced thin-walled beams

According to the strain, kinetic energies of braced beams derived in the equations (5.3-5.4), the damping in presence of dashpots and the external load work given in the equations (5.5-5.8), the motion equations of the beam are carried out from the Hamilton's principle (5.9). By following the same procedure detailed in the section 3.2 the motion equation presented in equations (3.27) is gotten with the stiffness, damping and mass matrices [K], [C] and [M] are respectively given as follows:

$$[K_b] = \sum_e \frac{l}{2}\int_{-1}^{1}[B]^t[D][B]\,d\xi \tag{5.11}$$

$$[K_s] = \sum_e \frac{l}{2}\int_{-1}^{1}[N]^t[K_s][N]\,d\xi \tag{5.12}$$

$$[K] = [K_b] + [K_s] \tag{5.13}$$

$$[M] = \sum_e \frac{l}{2}\int_{-1}^{1} m[N]^t[M_1][N] + \frac{m}{A}[G]^t[M_2][G]\,d\xi \tag{5.14}$$

And the force vector $\{F\}$ is defined as:

$$\{F(t)\} = \sum_e \frac{l}{2}\int_{-1}^{1}[N]^t\{f(t)\}_e\,d\xi \tag{5.15}$$

The structural damping is defined as $[C] = [C_b] + [C_d]$. (5.16)

The beam damping used here is Rayleigh type and it is given by: $[C_b] = \alpha[M] + \beta[K_b]$ where α and β are the mass stiffness proportional coefficients. In presence of viscous damping, the dashpot damping matrix is given by:

$$[C_d] = \sum_e \frac{l}{2}\int_{-1}^{1}[N]^t[c_d][N]\,d\xi \tag{5.17}$$

The free and forced vibration problems of beams is investigated in the present work numerically by solving the motion equation after computing the stiffness, damping and mass matrices [K], [C] and [M] defined in equations (5.13),(5.14) and (5.16) and the force vector $\{F\}$ equation (5.15). The solution procedure has been detailed in chapter 3.

5.4 Numerical applications

In the literature Nguyen [84] had solved the free vibration problem for simply supported beams with bi-symmetric sections and intermediate discrete rotational elastic braces. In the coming section, Nguyen results are first taken as reference in the validation procedure. Effect of lateral bending springs are studied after in both free and forced vibration. The elastic spring combined with dashpots effects are considered in forced vibration.

5.4.1 Torsion free vibration of braced thin-walled beams

Nguyen [84] investigated the torsion free vibration behavior of braced beams on presence of elastic torsion springs. An analytical and finite element approaches using shell elements have been performed in this study. In the numerical study, S4R shell element has been adopted. Nguyen's simulations are considered here as comparison to the present model. The geometric and material properties of IG1 are the followings: b=230, h=900, t_f=16, t_w=12 *mm.* L_b=5.5*m,* E=200GPa, G=76.9 GPa. ρ=7800kg/m^3.

In the study, Nguyen has investigated the free vibration of the three IG1 beams depicted in Figure 5.5(a-c), where beams with 1, 2 and 3 torsional springs have been taken. These beams are considered here.

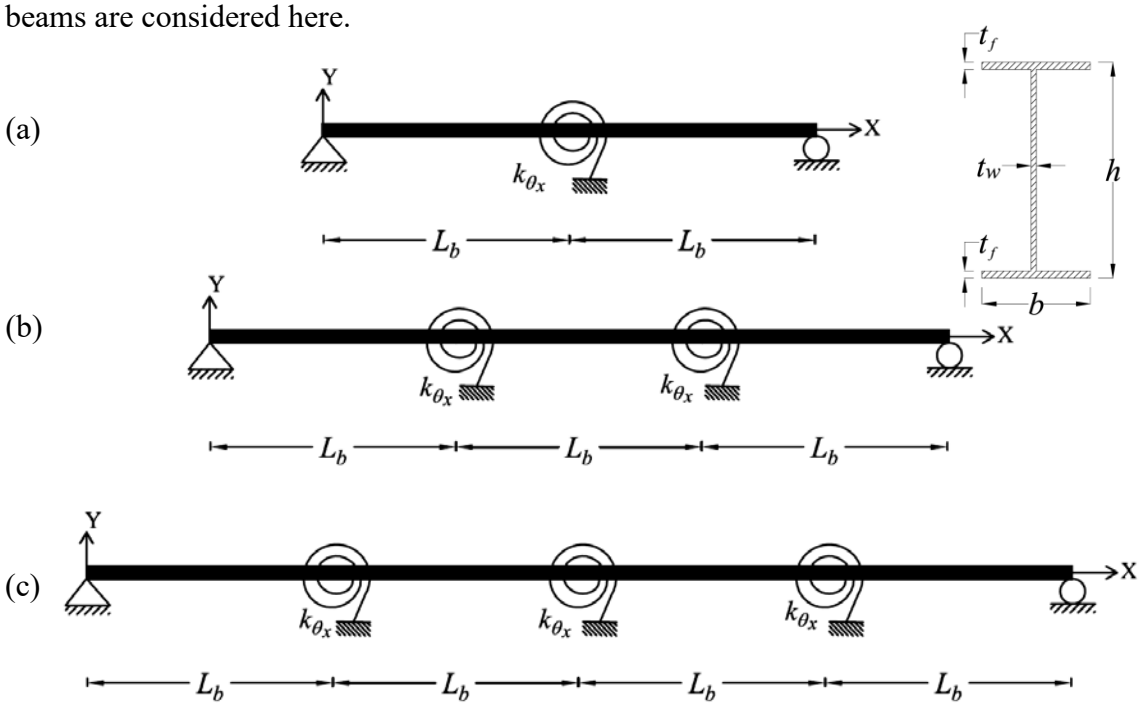

Figure 5.5: IG1 beam with 1-3 torsional braces.

Figures 5.6 to 5.8 show the comparison studies of the present model and the analytical results of Nguyen [84].

In Figure 5.6, the variation of dimensionless torsion frequency in terms of the torsion spring stiffness is reported in presence of 1 spring. The numerical solutions of the present model and Abaqus beam element are depicted. One remarks, that the frequency varies non linearly from frequency of the 1st mode (f_1=9.11 Hz) to the 2nd mode frequency (f_2=29.58 Hz). The ratio is 3.25. To reach the 2nd mode the required stiffness is k_{max}=12.10^5 Nm/rad. In this example, the present model and Abaqus simulations are in good agreement with Nguyen results.

The variation of the frequency in presence of 2 springs is depicted in Figure 5.7. Here, the vibration behavior passes from the 1st mode frequency (f_1=5.072 Hz) to the 3rd mode (f_3= 29.579 Hz) when the spring stiffness is increased. The frequencies ratio between the braced and unrestrained beam frequencies is 5.83. To reach the 3rd mode the required stiffness is k_{max}=12.10^5 Nm/rad. Here, one remarks that the present model and Abaqus simulations are in good agreement, but it seems that Nguyen's results are different.

Figure 5.8 shows the variation of the frequency in presence of 3 springs is. It is found that the vibration frequency varies from the 1st mode frequency to the 4th mode springs is depicted in Figure 5.8. Here, the vibration behavior passes from the 1st mode frequency (f_1=3.503 Hz) to the 4th mode frequency (f_4= 29.579 Hz) by increasing the spring stiffness. The ratio is 8.45. To reach the 4th mode the required stiffness is k_{max}=12.10^5 Nm/rad. One remarks here that the present model and Abaqus simulations are in good agreement. Some disagreement Nguyen's analytical results are observed.

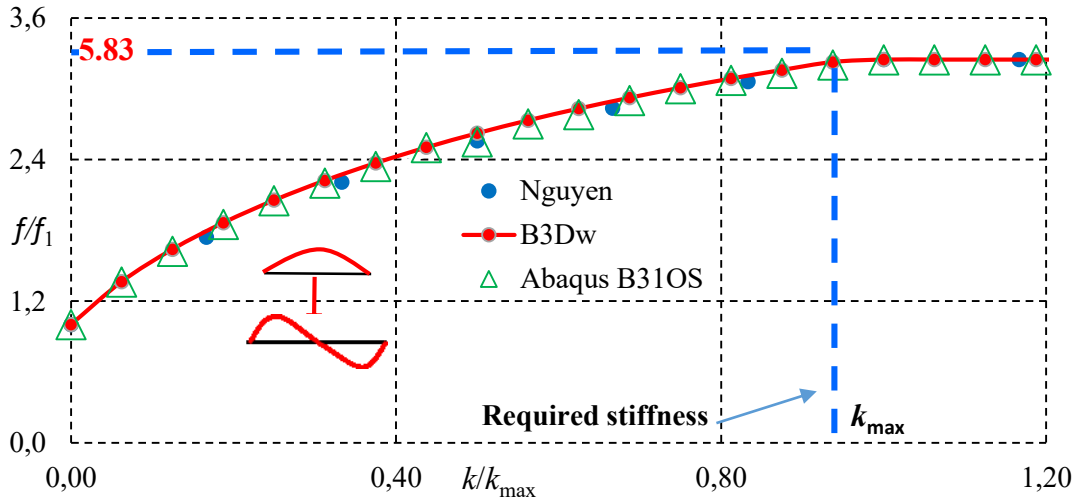

Figure 5.6: Numerical simulations and comparisons of the dimensionless torsion frequency in terms of the spring stiffness (for IG1 beam with single torsion spring).

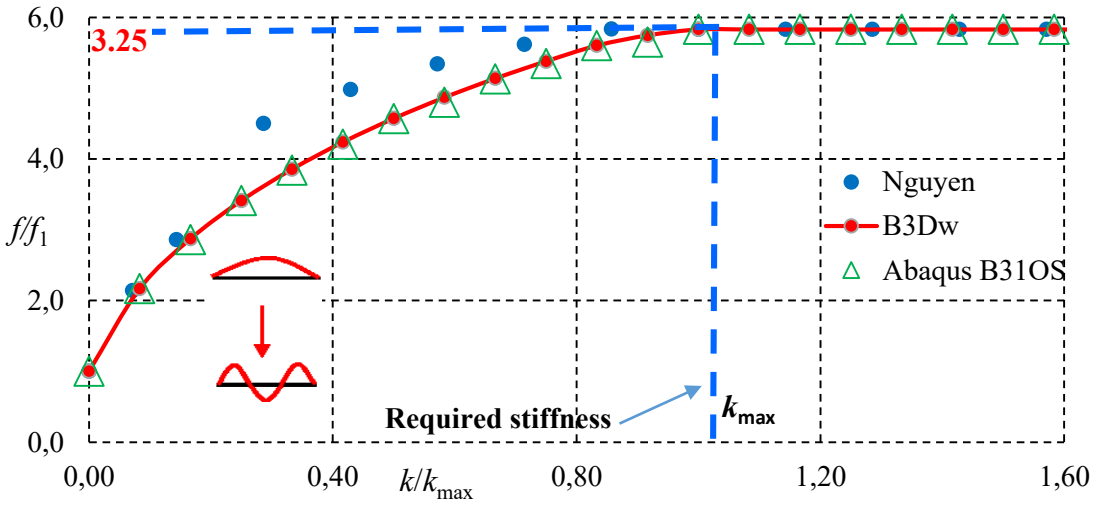

Figure 5.7: Numerical simulations and comparisons of the dimensionless torsion frequency in terms of the spring stiffness (for IG1 beam with 2 torsion springs).

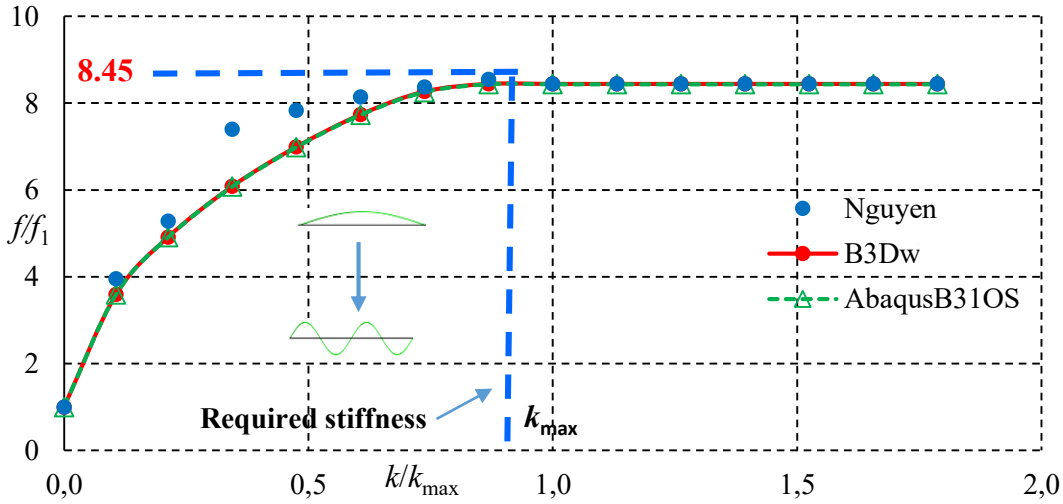

Figure 5.8: Numerical simulations and comparisons of the dimensionless torsion frequency in terms of the spring stiffness (for IG1 beam with 3 torsion springs).

From these examples, one observes that after the required stiffness k_{max} is reached the frequency becomes independent to spring stiffness even though the springs stiffness is increasing. Thus, when the required stiffness is attended the springs become full braces. Otherwise, natural frequencies of the first 4 torsion modes and the required stiffness's obtained by the present model seems to be more accurate than Nguyen's estimations when higher torsion modes are researched.

In what follows, the study is extended to braced beams in presence of some lateral elastic springs are added to beams IG1. The free vibration of the braced beam is investigated

using B3Dw element and compared to Abaqus beam element. Let us remind that Nguyen's study has been limited only to torsion springs.

5.4.2 Lateral free vibration of braced thin-walled beams

The aim of this study is to prove that the lateral braces are extremely important to improve the vibration behavior of thin-walled beams as well as torsion braces. So, the lateral free vibration behavior of braced beams with lateral elastic springs is investigated in this example. In the study beams with IG1 cross-sections shown in Figure 5.9(a-c) are considered with 1,2 and 3 lateral elastic braces to investigate the effect of these braces on free vibration lateral modes. To this aim, B3Dw and Abaqus commercial code simulations are compared to the present analytical method results.

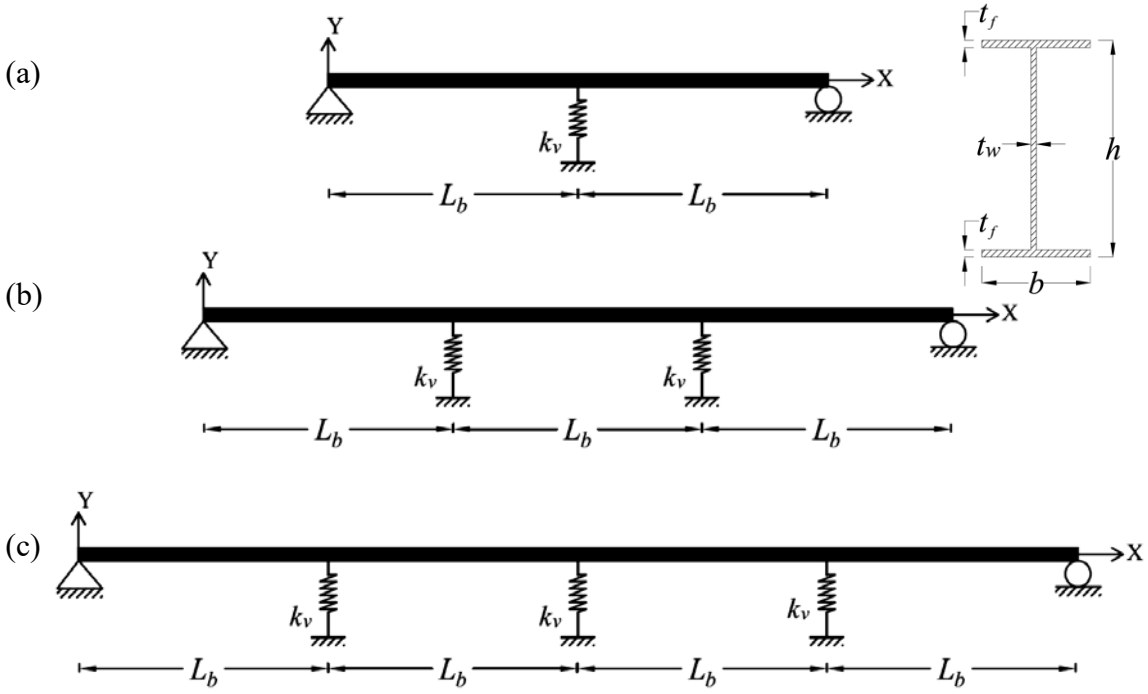

Figure 5.9: IG1 beam with 1-3 lateral braces.

Figures 5.10-5.12 depicts the comparison studies of the present model and Abaqus simulations.

In Figure 5.10, the variation of dimensionless lateral bending mode frequency in terms of the lateral spring stiffness is reported in presence of 1 spring. The analytical and numerical solutions of the present model besides Abaqus simulations are depicted. One remarks, that the frequency varies non linearly from frequency of the 1st mode (f_1=5.27 Hz) to the 2nd mode frequency (f_2=21.09 Hz). The ratio is 4. To reach the 2nd mode the required stiffness is k_{max}=52.5.10^5 N/m. One remarks that the present model and Abaqus simulations are in good agreement with analytical developed method results.

The variation of the frequency in presence of 2 springs is depicted in Figure 5.11. Here, the vibration behavior passes from the 1st mode frequency (f_1=2.344 Hz) to the 3rd mode (f_3= 21.090 Hz) by increasing the spring stiffness. The frequencies ratio between the braced and unrestrained beam frequencies is 9. To reach the 3rd mode the required stiffness is k_{max}=52.5.10^5 N/m. Good agreement is observed between the present model and Abaqus simulations.

Figure 5.12 shows the variation of the frequency in presence of 3 springs is. It is found that the vibration frequency varies from the 1st mode frequency to the 4th mode springs is depicted in Figure 5.12. Here, the vibration behavior passes from the 1st mode frequency (f_1=1.318 Hz) to the 4th mode frequency (f_4= 29.579 Hz) by increasing the spring stiffness. The ratio is 16. To reach the 4th mode the required stiffness is k_{max}=52.5.10^5 N/m. Furthermore, one remarks that the present model and Abaqus simulations are in good agreement, with the developed analytical results.

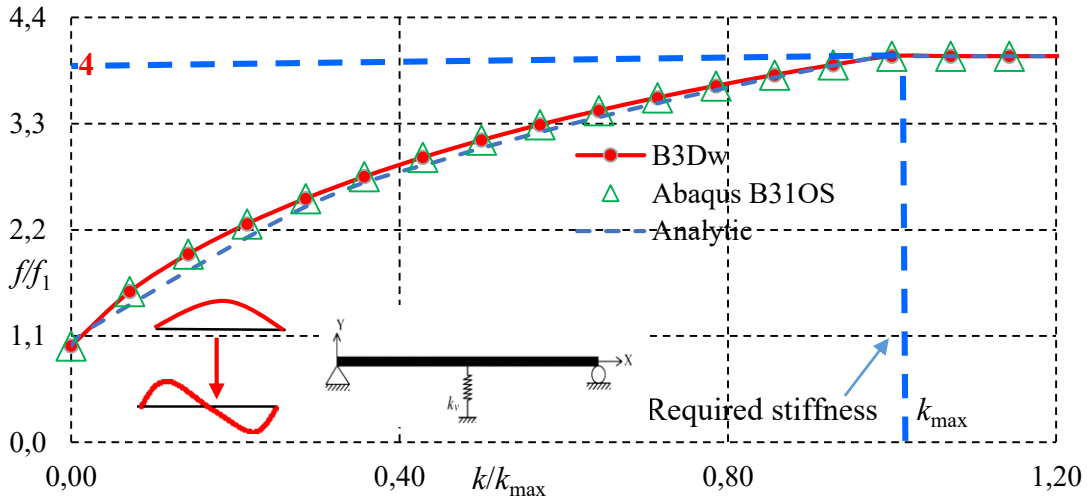

Figure 5.10: Comparison of analytical and numerical dimensionless lateral bending frequency in terms of the spring stiffness for IG1 beam with a single lateral spring.

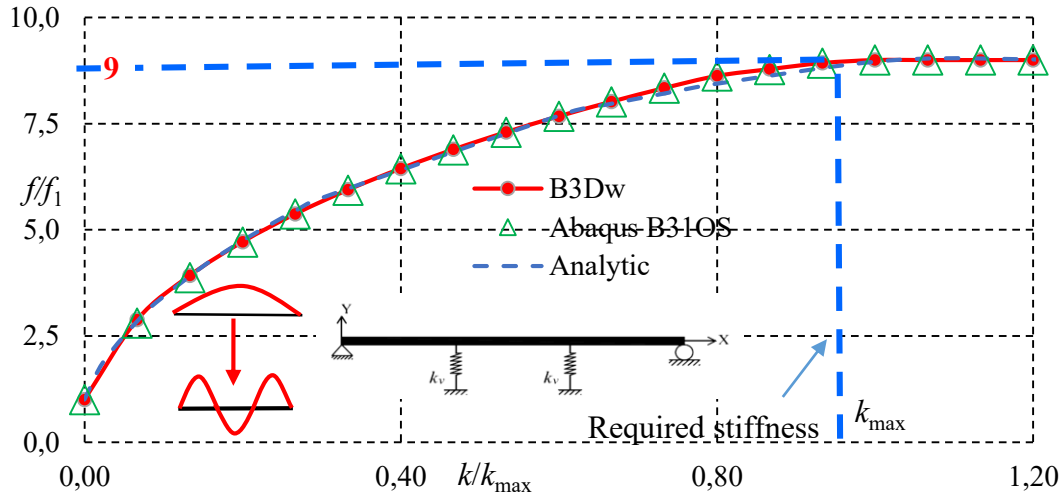

Figure 5.11: Comparison of analytical and numerical dimensionless lateral bending frequency in terms of the spring stiffness for IG1 beam with 2 lateral springs.

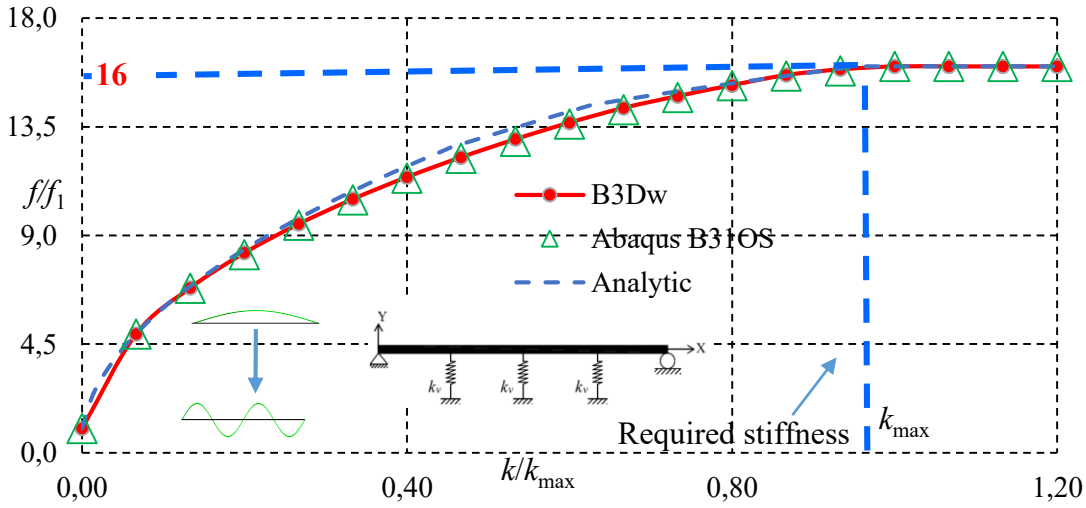

Figure 5.12: Comparison of analytical and numerical dimensionless lateral bending frequency in terms of the spring stiffness for IG1 beam with 3 lateral springs.

From the aforementioned results, it is noticeable that, the eigenvalue (natural frequencies) of beams increases with the increases of the stiffness k of the intermediate braces until this stiffness reaches the required stiffness value k_{max}. After that, the frequency remains constant even though the stiffness k is increasing.

The present is validated in case of torsional and lateral braces. The FEM model investigated here is more efficient that the analytical solutions which are limited to simply supported beams with doubly symmetric cross sections.

In 3D behavior, the vibration of slender and unrestrained beams is predominated by lateral bending and torsion modes (modes v, θ_x). In order to improve the vibration behavior of 3D structures against vibration, recourse to braces in design is an efficient tool commonly adopted. As mentioned before, many references like [84] was treated the effect of the elastic braces only in free vibration behavior. In the present work, beams with viscous and elastic braces are studied in free and forced vibration. Some braced beams with IPE300 cross-section are considered. These braced beams are depicted in Figures 5.13a-c where 1,2 and 3 viscoelastic braces are added respectively to the unrestrained IPE300 beam case. The geometry and material properties of the beam are: (h=300, b=150, t_f=10.7, t_w=7.1mm, E=210, G=80.77 GPa, ρ=7800 kg/m3).

5.5 Conclusion

In this chapter, the dynamic behavior of beams with intermediate viscous and elastic braces have been investigated. The finite element approach developed for vibration of unrestrained thin-walled 3D beams in the chapter 3 has been extended to the braced beams cases by taking in account the effect of additional elastic springs and dashpots. Analytical solutions for free vibration analysis of simply supported beams with bisymmetric sections and lateral elastic braces were carried out. The required stiffness for the full brace condition is possible either in bending or in torsion. The finite element model can be applied to more general cases. It has been validated by comparison to benchmark solutions and Abaqus simulations. The obtained results seem to be more accurate and can be applied in the behavior of the unrestrained and brace thin-walled beams in both statics and dynamics. In the dynamic behavior investigated in the present work, free and forced vibration in presence of elastic springs and viscous dashpots are possible for any type of cross-sections. The boundary conditions should be arbitrary.

The effisciency of the model in presence of elastic and dashpot has been studied in forces vibration. The results are in good agreement with Abaqus simulations.

Conclusion and Perspectives

The dynamic behavior of 3D thin-walled beams with arbitrary open cross-sections shape and boundary conditions was investigated. Moreover, the vibration control of these elements by adding elastic and viscoelastic springs (called braces) was studied. This work is divided to three axes: the first axis was developing a model for thin-walled 3D beams that takes in consideration all characteristics of this structural elements especially the warping effect that is indispensable and critical for this type of sections. Thereafter, this model was used to carry out analytical solutions in static and dynamic. Original exact analytical solutions for free vibration of beams with arbitrary cross-section were detailed and used to compute the higher modes. However, it was proven that the analytical solutions are limited to simple cases so the necessity of development a finite element method. Due to this, based on the developed model a finite element method for thin-walled beams with open cross-sections (called B3Dw) was created and used to solve vibration problems of such beams. Then B3Dw was implemented in Matlab. The validation of developed analytical and finite element methods was by comparing to benchmark solutions and experimental tests. Thus, the second axis of this work was to execute a list of experimental tests on thin-walled beams with arbitrary open cross section in free and forced vibration. Hence, experimental tests were achieved in LEM3 laboratory on more than one specimens and compared to the developed element results. Based on tests the developed solutions were validated. The third axis was to study the effect of additional intermediate braces in vibration control by the help of the developed element. This study was about the type of braces (elastic-viscous), characteristics (required stiffness and damping coefficient), necessary number of braces and distribution method to obtain the optimum vibration control.

The followed steps used to reach the research objectives was firstly, based on a beam element a model was developed. This model takes into account the warping effect and kinematic rotational terms. After that, based on the developed model the motion equations were derived to carry out the analytical solutions for free vibration of thin-walled beams under different boundary conditions. As result, analytical solutions for higher free vibration modes in bending, torsion and flexural-torsional coupled modes was established. It should be noted that the effects of rotational inertial kinematic terms for bending, torsion, warping and rotary kinematic terms were considered in the model, for these reasons the developed solutions were more accurate when the higher modes are computed. Moreover, new analytical solutions for different boundary conditions were presented. so it gives exact solutions for the higher modes. Otherwise, many examples were solved using the developed solutions and results was compared to the classical beam theory to prove the importance of these terms. On the other hand, it was proven that, when the rotary inertia terms are neglected the natural frequencies are obtained with a relative error more than 10% comparing to the present solutions for the higher modes. Furthermore, it was proven that the analytical solutions are limited to the simple cases of sections and boundary condition. Due to this, a finite element based on the presented

model is developed. The developed numerical method consists on a seven degrees of freedom beam element. The finite element formulation was detailed for thin-walled beam, where the warping was considered as an additional degree of freedom with the six classical degree of freedoms. In the numerical integration of the discreet elements, the Hermite's polynomials were used. In this regard, a modal analysis along with a numerical integration was performed. The natural frequencies and the corresponding mode shapes were determined by solving the related eigenvalue problem.

By applying the steady state modal analysis method, the forced vibrations response spectra were carried out in the frequency domain. In forced vibration Rayleigh damping type was adopted. The developed element can also be used to solve forced vibration excited random signals (like earthquakes).

The vibration behavior for thin-walled beams can be improved by increase of the lower natural frequencies of the structure. Recourse to braces is an efficient solution in order to remove the undesirable bending and torsion vibration modes. The developed analytical and the finite element models were extended to braced beams by taking in account the effect of intermediate viscoelastic springs. These methods were used to study the vibration control of thin-walled structures in presence of intermediate elastic springs and or viscous dashpots. The efficient methods for removing or reducing undesirable vibration were detailed in this work.

The accuracy of the models is proven by comparison with benchmark solutions, numerical simulations using commercial codes.

Experimental studies on the flexural-torsional dynamic behavior of thin-walled beams are scant. For this aim, experimental tests for free and forced vibrations on thin-walled beams with arbitrary open cross sections had been investigated in this work. Tests on beams with three different boundary conditions were performed. Hammer tests were realized in free vibration procedure to obtain the natural frequencies. In forced vibration tests, a shaker machine was used to carry out the beam response spectra in frequency domain. The behavior of the studied beams exhibits coupled flexural-torsional vibration modes.

Test results were compared among numerical simulations made possible by a finite element formulation investigated in the present work, and other numerical simulations made possible with other commercial codes. This comparison was shown a very good agreement between numerical solutions given by B3Dw and the experimental results. The dynamic behavior exhibits flexural-torsional couplings present in both numerical analyses and tests. The efficiency of the numerical and experimental setup constitutes then a good background for future coming works.

The effect of introducing intermediate bracings to control bending and torsional vibration was treated also experimentally and numerically. It was observed that in presence of intermediate supports, the vibration behavior of the beam against the lower natural frequencies is improved. Otherwise, in case of arbitrary section, all natural frequencies are considerably increased by introducing lateral braces along the beam. This concept can

be used in vibration control for structures to improve the stability of slender beams against torsion and other undesirable modes.

To go further in the study, the non-prismatic sections, the composite materials and the effect of additional mass at braces locations can be taken into account. Using thin-walled tapered beams are also important for more of weight saving. In design these structures are used in the aim to obtain the maximum possible of weight saving by changing the beam inertia and stiffness when it is needed along the beam length. For these beams, the 3D vibration behavior becomes a promising research topic.

Composite beams are nowadays widely used in many types of structures in the fields of engineering because of their quality and their high performances making it possible to resist the various stresses. In recent decades, these structures have been evolving towards composite materials with a gradient of properties (Functionally Graded Materials, FGM). The properties of these materials vary gradually and continuously one or two directions of the structure. Their use is growing with the use of composites and recent developments in 3D printing techniques. These structures are very sensitive to the shear effect both static and dynamic both linear and non-linear under static and dynamic loads.

Another point that can be reconsidered to improve the model used to study vibration behavior of beams with intermediate braces is to introduce the mass effect of braces on the bracing points. This contribution can give more realistic results for design.

Moreover, in the model the effect of shear deformation in the sections is not taken into consideration, this has an influence on the natural frequencies and mode shapes important with some types of closed sections. In order to take into account. Improved models using shear deformation should be considered

The presented analytical and FEM models could serve as a starting point for further profound study of the subject and may be considered as a first step tending to more complete formulations accounting for other aspect that have not been considered here, such as, shear and distortions deformations, tapered beam; and other non-isotropic material as composites and FGM materials.

Résumé

Le secteur de la construction nécessite l'utilisation d'une quantité importante de matériaux de nature différente, comme l'acier, le bois, le béton, le verre…. Cette utilisation abondante et sans contrôle a un impact négatif sur l'environnement, en raison de l'extraction de matières premières qui conduit à la raréfaction de la matière première et une consommation importante d'énergie pour arriver au produit fini. Les législateurs travaillent à la création de réglementations rigoureuses concernant la construction, afin de faire respecter les normes visant à limiter les impacts environnementaux des projets de construction. En conséquence, les concepteurs tentent de trouver de nouvelles méthodes durables réduisant les coûts et limitant l'impact des projets de construction sur l'environnement.

À cette fin, la recherche de meilleures méthodes, impose de trouver de nouvelles solutions dans les projets de construction comprenant des utilisations intelligente et optimale des matériaux de construction. Cela passe par l'amélioration de la résistance des matériaux qui induit une réduction de leur poids. Les éléments à parois minces et élancés constituent un bon compromis. Afin de ne pas pénaliser la résistance de ces éléments vis-à-vis des forces axiales et de flexion, des sections transversales en I, C, L ou tubulaires sont très adoptées.

La plupart des poutres à parois minces ont une bonne résistance à la flexion par rapport l'axe fort, mais une faible résistance à la flexion par rapport l'axe faible et en torsion. De plus, les éléments élancés sont très sensibles aux instabilités comme le flambement, le déversement ou le voilement en présence des parois très minces. C'est la raison pour laquelle le comportement d'un élément sollicité initialement en compression est contrôlé par le flambement où les modes en flexion et torsion peuvent être présents. De même, une poutre en flexion par rapport à l'axe fort peut être instable en présence des instabilités de flexion torsion qui peuvent apparaître dans le cas des poutres non retenues latéralement (phénomène de déversement). Ainsi, le comportement plan de ces structures peut être une exception plutôt qu'une règle. De même, en dynamique, les modes de vibration 3D type flexion torsion sont souvent présents avec des fréquences très basses par rapport aux modes de vibration classique en flexion pure plane.

Le comportement des poutres à section transversale ouverte à parois minces est prédominant par torsion où le gauchissement peut être important. Des modèles de calcul adaptés doivent être utilisés dans ce cas. Le comportement 2D des poutres est très bien maîtrisé aussi bien théorique que numérique. Dans le cas d'un comportement 3D en flexion torsion, les solutions analytiques sont limitées à des cas élémentaires et des formes de sections les plus simples comme les sections en I symétriques. En présence, des conditions d'appui quelconques et des sections à formes non symétriques, les solutions analytiques sont rares et les modèles numériques implémentés dans les codes de calcul peuvent être défaillants.

Motivations et objectifs

Après avoir évalué les phénomènes d'instabilité, la contribution originale de notre travail réside dans le développement de modèles théorique et numérique pour le comportement dynamique et vibratoire des poutres à parois minces et à sections ouvertes en présence des modes de type flexion torsion. Des solutions analytiques sont dérivées pour les modes de vibrations des poutres à section ouvertes arbitraires. Un modèle élément fini de poutre 3D avec gauchissement est décrit et implémenté. Il permet de traiter le comportement statique, et dynamique dans le cas des vibrations libres et forcées. Des poutres à conditions d'appuis quelconques et sections à formes quelconques sont possibles. Par ailleurs, une campagne d'essais expérimentaux est réalisée dans le but d'étudier et de comprendre le comportement dynamique et vibratoires des poutres à parois minces. Les modèles théorique, numérique et expérimental sont comparés.

Le travail réalisé au cours de cette thèse est présenté dans ce rapport et est intitulé en cinq chapitres, les travaux présentés dans chaque chapitre et les résultats trouvés sont résumés dans ce qui suit :

Au chapitre 1, étude bibliographique de la littérature pour comprendre le comportement mécanique des poutres à parois minces. Tout d'abord, le comportement 3D en flexion-torsion des poutres à sections ouvertes à parois minces est examiné. On montre que la torsion présente un effet de gauchissement, le théorème de Saint-Venant ne convient donc pas pour résoudre le problème de torsion dans le cas d'une section à parois minces. Ainsi, l'exigence d'une théorie de la torsion non uniforme pour ce type de poutres s'impose. D'ailleurs, la théorie de torsion non uniforme est détaillée en présentant le modèle de torsion avec gauchissement utilisé pour les poutres à parois minces. Sinon, les travaux précédents sur la dynamique des poutres à parois minces sont passés en revue. Les références traitant des vibrations linéaires libres et forcées sont bien étudiées et résumées dans ce chapitre. Dans la littérature la contribution sur ce domaine sont fréquentes, de nombreuses études théoriques, numériques et expérimentales ont été réalisées pour étudier le comportement vibratoire des poutres à parois minces et à sections ouvertes. Parmi ces études, les références les plus importantes qui ont un impact et ajoutent à ce sujet sont, en présence de torsion, certains modèles sont formulés conformément à la théorie de Saint-Venant, à la fois en statique et en dynamique [2, 3]. Dans Gere et Lin [4], la méthode de Rayleigh-Ritz a été utilisée pour étudier la vibration libre couplée en flexion-torsion de poutres uniformes présentant diverses conditions aux limites. De plus, dans le cas de structures à parois minces avec des sections transversales ouvertes, la torsion est prédominante par le gauchissement et le couplage torsionnel en flexion, en particulier dans le cas de sections transversales arbitraires. À notre connaissance, le modèle de Vlasov [5] est l'un des premiers modèles à inclure les phénomènes de gauchissement dans le comportement des poutres à parois minces dans les années 1930. On trouvera d'autres références dans ce domaine dans [6, 8-11]. Le recours à des modèles numériques est important car il permet d'étendre l'étude à des cas plus généraux où les solutions analytiques deviennent lourdes. De nombreux modèles ont été développés pour l'analyse vibratoire d'éléments à parois minces. Les premières tentatives d'application de

la méthode des éléments finis (FEM) aux vibrations couplées de poutres à parois minces ont été étudiées dans [14, 15]. Ohga *et al.* [17] ont étudié la vibration libre des éléments à parois minces à sections ouvertes et fermées par la méthode de la matrice de transfert. [18, 19] ont présenté une analyse analytique des vibrations linéaires des sections ouvertes du composite I et des sections en C. La vibration libre de poutres de sections transversales arbitraires a été étudiée dans [24, 25]. Par la suite [26, 27] ont appliqué la quadrature différentielle au modèle de Vlasov pour la vibration d'éléments à parois minces. Ambrosini *et al.* [28] a utilisé un modèle modifié de Vlasov pour l'analyse dynamique linéaire. Le comportement dynamique non linéaire de la section I à double symétrie en torsion a été étudié par Rozmarynowski et Szymczak [29] en utilisant l'approche des éléments finis. Plus récemment, un modèle de dynamique non linéaire a été formulé dans Egidio *et al.* [30]. La méthode des échelles multiples a été appliquée pour les mouvements en régime permanent et la stabilité des poutres à sections mono-symétriques.

Dans la littérature, de nombreux autres travaux approfondis ont étudié la vibration libre des poutres à parois minces. Yaman [31] a résolu la vibration libre des poutres a parois minces en présences des modes couplés par une approche de propagation d'ondes. Certaines références ont validé les méthodes numériques par des essais expérimentaux. Comme Piana *et al.* [62] qui ont comparé les résultats expérimentaux de vibration libre des poutres aux fréquences propres numériques. Dans l'étude des poutres en aluminium à parois minces et section crois légèrement non symétrique soumises à des forces axiales sont étudiés. Gendy et Saleeb [32] ont développé une méthode des éléments finis pour l'analyse du comportement en vibrations libres. Sur la base de la méthode de l'énergie, Prokić [33] a déduit les équations de mouvement différentiel des poutres à parois minces en torsion à la flexion avec croisement arbitraire et a étudié les vibrations couplées triplement libres. Une méthode semi-analytique est étudiée pour les poutres en appui simple. Mohri *et al.* [41] ont étudié le comportement vibratoire des poutres à parois minces pré-déformées et post-déformées à sections ouvertes selon un modèle non linéaire tenant compte des effets de couplage en torsion en flexion et de gauchissement. La plupart des travaux précédents traitaient le problème des vibrations d'un point de vue analytique ou numérique. L'effet des termes de rotation en flexion et en torsion est toujours omis. Lorsqu'elles sont comptabilisées, des procédures semi-analytiques ou des simulations de codes commerciaux sont suivies [28, 46, 62]. Des vibrations forcées sous des charges périodiques ou aléatoires sont disponibles dans [11, 48].

De plus, dans ce chapitre les types d'amortissement sont indiqués et utilisés dans le modèle de vibrations forcées. D'autre part, la méthode de transformation de Fourier (FT) est détaillée et utilisée ultérieurement pour convertir les signaux du domaine temporel au domaine fréquentiel. Ensuite, de cette analyse bibliographique, nous pourrons bien définir la problématique, le cadre et les moyens à utiliser dans la présente étude. Enfin, les objectifs du sujet de recherche sont clairement illustrés à la fin de ce chapitre. En ce qui suive le développement de modèle pour analyser le comportement dynamique des poutres a parois minces et sections ouvertes dans lequel les termes rotationnels sont pris en compte qui fournit des solutions plus avancées avec haut précision. Ainsi, des solutions

analytiques originaux pour résoudre le problème de vibration libre des poutres à sections arbitraires en se basant sur ce modèle sont détaillé dans ce qui suive. Ces solutions permettent d'apporter les hautes fréquences propres de telles types des poutres sous différentes conditions aux limites avec une haute précision.

Le chapitre 2 est consacré à la présentation de la méthode d'analyse des vibrations des poutres à parois minces. Sur la base du modèle de poutres à parois minces et de l'approche de Galerkin, des équations dynamiques du mouvement sont formulées. En utilisant le principe de Hamilton, des équations dynamiques de mouvements sont dérivées. Dans un premier temps, un modèle de vibrations libres et forcées est introduit. La cinématique du modèle est détaillée, puis la formulation variationnelle des équations de mouvement est développée. Après cela, des solutions analytiques originales pour les modes supérieurs sont dérivées dans un contexte de vibration libre. Ces solutions concernent les sections non symétriques et les différentes conditions aux limites. Dans le cadre de vibrations forcées, les solutions dans le domaine fréquentiel (analyse modal) sont adoptées. Dans le modèle, l'amortissement passif est pris en compte (le type de Rayleigh a été adopté). Enfin, certains exemples numériques de référence sont pris en compte pour la validation du modèle, puis la conclusion est tirée. Dans les neuf premiers exemples, les résultats analytiques des vibrations libres, y compris les termes d'inertie de rotation, sont comparés aux solutions classiques existantes dans la littérature. Le pourcentage d'erreur entre les deux méthodes de solution est calculé pour différentes sections et conditions aux limites. En conclusion, il est important de prendre en considération les termes de rotation cinématiques, en particulier pour l'investigation des modes supérieurs, l'erreur relative atteignant 9% entre deux méthodes de résolution lorsque nous traitons des modes supérieures de vibrations. De plus, les solutions analytiques actuelles ont également été validées par différentes solutions de référence tirées de la littérature et des comparaisons avec les codes commerciaux présentent les résultats de simulations. L'importance des solutions développées qui prennent en compte les termes de rotation est démontrée dans la liste des exemples d'application numériques en comparant les fréquences obtenues aux solutions classiques sans termes de rotation et spécialement pour les modes supérieurs. Toutes les comparaisons avec des solutions de codes numériques et de références montrent un bon accord avec les solutions développées. L'efficacité des solutions analytiques étudiées semble être exacte. Comme les solutions analytiques sont limitées à des cas simples des sections et des conditions au limites, alors l'utilisation des méthodes des éléments finis devient alors nécessaire pour l'analyse du comportement dynamique des poutres à parois minces. Pour cette raison notre modèle, présenté précédemment, est utilisée pour le développement d'une méthode numérique pour l'étude de vibrations des poutres à parois minces dans le chapitre suivant.

Au chapitre 3, une méthode par éléments finis pour les vibrations des poutres à parois minces, basée sur le modèle présenté au chapitre 2, est détaillée. Tout d'abord, une introduction à la méthode des éléments finis est présentée, puis la formulation en éléments finis de structures à parois minces est démontrée. Ensuite, la discrétisation par éléments

finis est illustrée. Ensuite, les matrices d'éléments sont dérivées, suivies de la procédure d'assemblage pour obtenir les matrices globales de la structure entière. Ci-après, des solutions génériques de structures à parois minces sont détaillées. Dans les vibrations libres, les valeurs propres et les vecteurs propres sont étudiés. Sinon, en méthode de vibration forcée, une méthode d'analyse modale en régime permanent a été adoptée pour obtenir un spectre de réponse dynamique dans le domaine fréquentiel. Dans cette méthode, l'amortissement est pris en compte, par (type Rayleigh). En outre, la Méthode des Eléments Finis peut être utilisé pour étudier l'effet de mouvement de base (séisme), l'excitation vibratoire avec signal aléatoire (harmonique). Il est connu que pour les poutres à parois minces soumises à des conditions limites arbitraires et à des sections transversales arbitraires, les solutions analytiques du comportement dynamique deviennent compliquées et par suite l'approche par éléments finis est obligatoirement suivie. À cette fin, une approche par éléments finis d'un modèle pour la vibration des poutres en 3D avec des sections ouvertes à parois minces arbitraires est développée dans ce chapitre. Notons que, dans ce cas les modes de vibrations sont couplés (flexion-flexion-torsion). Ce modèle traite différentes conditions aux limites et prend en compte les termes cinématique de flexion, de torsion, de gauchissement et de rotation. Cela conduit à une évaluation plus précise du comportement dynamique des poutres à parois minces par rapport aux solutions de la théorie des poutres classique. À l'aide du principe de Hamilton, les équations de mouvement de torsion axiale et en flexion ont été dérivées. Dans l'approche par éléments finis, des poutres 3D à 2 nœuds et à 7 degrés de liberté par nœud ont été adoptés dans le processus de maillage. Le gauchissement est considéré comme un degré de liberté indépendant. Cet élément de poutre (B3Dw) est implanté dans Matlab. Le modèle a déjà été utilisé avec succès en statique, flambement, flambement latéral et analyse non linéaire. Dans le présent travail, les vibrations libres et forcées ont été étudiées. En vibration libre, des modes de vibration plus élevés sont possibles à l'aide d'un solveur efficace disponible dans Matlab. En vibration forcée, la méthode modale à l'état d'équilibre est adoptée. Le comportement de la poutre est étudié dans le domaine fréquentiel sous toutes les forces dynamiques. L'amortissement de Rayleigh est pris en compte dans ce modèle. Dans les chapitres 2 et 3, les modèles analytiques et par éléments finis ont été validés à l'aide de solutions de référence de la littérature et de simulations faites sur des codes de calcule commerciaux (Abaqus, Adina). Bon accord est remarqué. L'efficacité des solutions analytiques et l'approche par éléments finis étudiée semblent être précises.

Au chapitre 4, des tests expérimentaux sur les vibrations libres et forcées sont effectués pour valider la méthode théorique analytique et les modèles numériques développée. Tout d'abord, dans l'introduction, certaines références de littérature relative au essais expérimentaux concernant la vibration des poutres à parois minces sont analysées. Deuxièmement, la configuration et les procédures expérimentales sont détaillées. Troisièmement, les propriétés des échantillons sont données. Les résultats des tests sont ensuite présentés et discutés. Ces résultats sont les fréquences propres, le type de mode, les spectres de réponse dynamique, les facteurs de perte et les valeurs d'amortissement pour chaque mode. Après la collecte des données des tests, ils sont utilisés pour valider

le modèle numérique dans un contexte de vibration libre et forcée. Sinon, certains tests sont effectués après l'introduction de renforts intermédiaires. Par la suite, les méthodes théoriques et numériques présentées sont validées en comparant les résultats de la vibration 3D de poutres à sections ouvertes et à parois minces arbitraires avec les valeurs de référence, les codes commerciaux et les résultats expérimentaux. Dans ce chapitre, des essais expérimentaux de vibrations libres et forcées sur des poutres à parois minces avec des sections transversales ouvertes arbitraires ont été étudiés. Des essais sur des poutres avec trois conditions aux limites différentes sont effectués (en appui simple, encastré libre et bi-encastré). Des essais en utilisant le marteau de choc ont été réalisés dans une procédure de vibration libre pour obtenir les fréquences propres. Pour les tests de vibrations forcées, le pot vibrant a été utilisé pour obtenir les spectres de réponse des poutres dans le domaine fréquentiel. Les procédures de configuration des tests ont étés bien démontrées dans ce travail. Les tests sont étudiés dans la plage allant de 1 à 400 Hz. Plus de 10 modes sont présentés. Le comportement présente des modes de vibration en torsion flexion couplés. Les modes dominants ont également été étudiés dans ce travail.

Les résultats des tests ont été utilisés pour comparer des simulations numériques rendues possibles par une formulation d'éléments finis étudiée dans le présent travail, où des éléments de poutres 3D permettant le gauchissement sont adoptés dans le processus de maillage (élément B3Dw). Le logiciel commercial Abaqus est également utilisé dans la validation des résultats de vibrations libres et de vibrations forcées. Cette comparaison montre un très bon accord entre les solutions numériques données par B3Dw et les résultats expérimentaux. Le comportement dynamique présente des couplages flexion-torsion présents à la fois dans les analyses et les tests numériques, les modes prédominants obtenus par B3Dw étant également en accord avec les résultats expérimentaux. Le modèle actuel correspond bien aux expériences de vibrations libres et forcées. L'efficacité de la configuration numérique et expérimentale constitue donc un bon fond pour les travaux à venir.

Cependant, pour améliorer la résistance de la structure aux effets de vibrations et économiser les matériaux en obtenant des sections optimales, une solution possible consiste à augmenter la rigidité en ajoutant des ressorts élastiques discrets ou répartis (supports élastiques). Le ressort élastique contribue à la matrice de rigidité élastique de la structure. En augmentant la constante de rigidité du support élastique, le comportement vibratoire (fréquences et modes) varie en conséquence.

Il est important de rappeler qu'en génie civil, le recours à cette solution est fréquent. C'est le cas des poutres et des poteaux contreventés dans les bâtiments ou des contreventements latéraux dans les ponts. Ces solutions sont adoptées dans la pratique, mais seule une procédure empirique est utilisée. Il est connu que sans ces éléments secondaires, la résistance totale du bâtiment n'est pas garantie et le risque de défaillance dû à des déformations hors du plan est présent.
Une autre solution consiste à utiliser des ressorts visqueux discrets (dashpots) en parallèle avec des ressorts élastiques pour contrôler les déplacements de la structure lorsque celle-

ci est soumise à des efforts dynamiques. Dans ce cas, les déplacements de modes de fréquences et de structure sont contrôlés.
Les points importants à étudier sont le nombre, la distribution et la rigidité et le facteur d'amortissement nécessaires pour atteindre la conception optimale. Pour le contrôle des vibrations, l'ingénieur est invité à proposer des solutions améliorées pour le comportement des vibrations. Les fréquences propres inférieures peuvent être éliminées par des supports élastiques adéquats. Les solutions suivantes peuvent être adoptées si nous sommes intéressés par un mode particulier. Lorsque la raideur du ressort est suffisante, on peut supprimer le premier mode et passer directement au mode 2 où la fréquence propre est 4 fois plus élevée que le premier. En présence de 3 supports élastiques, on accède directement au troisième mode avec une valeur propre 9 fois supérieure au premier.
Cette procédure peut être suivie dans le cas de présence de parois minces en présence de modes de vibration 3D en présence de modes de flexion et de torsion et peut être renforcée par des supports élastiques adéquats. De plus, sous des vibrations forcées, des ressorts visqueux peuvent être adoptés afin de réduire les déplacements de structures proches de la fréquence de résonance.

Le travail est suivi de simulations analytiques et numériques en utilisant le modèle élément fini que nous avons développé par nous et des codes commerciaux : Abaqus, Adina…. etc.

Dans ce qui suit, le modèle analytique présenté et la méthode des éléments finis sont expansés pour prendre en compte l'effet des ressorts viscoélastiques intermédiaires. Ensuite, ces méthodes sont utilisées pour étudier le contrôle des vibrations (en termes de fréquences et de déplacements) de structures à parois minces en ajoutant des ressorts visqueux intermédiaires et des ressorts élastiques parallèles.

Dans le chapitre 5 l'effet des entretoises sur le contrôle des vibrations des poutres à parois minces est étudié. Premièrement, dans l'introduction, différents types d'entretoises (ressorts) sont présentés et un résumé des travaux existants est fourni. De plus, des types des ressorts élastiques et visqueux sont introduits dans le modèle. La cinématique du modèle avec des entretoises intermédiaires est alors détaillée. Après cela, les équations de mouvement sont dérivées en présence des ressorts intermédiaires. Analytiquement, certaines solutions particulières sont possibles dans le cas de sections à double symétrie avec des ressorts élastiques latéraux et en torsion. La formulation en éléments finis pour les poutres à parois minces avec des entretoises intermédiaires en vibrations libres et forcées avec des entretoises intermédiaires viscoélastiques est détaillée et est utilisée pour étudier le contrôle de la vibration des poutres à parois minces. Les applications numériques des poutres avec des ressorts élastiques intermédiaires en vibration libre et des ressorts viscoélastiques en vibration forcée sont bien étudiées. Enfin, un nouveau concept est conclu dans le contrôle des vibrations peut être utilisé pour optimiser les sections. Ce chapitre décrit en détail les méthodes efficaces pour éliminer ou réduire les

vibrations indésirables. Quelques solutions efficaces ont été données qui sont les suivantes :

- Modification de la fréquence propre du système lorsque la fréquence de forçage ne peut pas être modifiée. Dans ce but, un nombre d'entretoises latérales et de torsion est ajouté à la poutre. Ces entretoises doivent être ajoutées en fonction de l'étude de localisation optimale.

- Introduire un mécanisme de dissipation de puissance en ajoutant des ressorts visqueux (dashpots), distribués de la même manière que les ressorts. Ces ressorts visqueux peuvent être implémentés au même endroit et parallèlement aux ressorts. (Ou matériaux viscoélastiques).

De plus, diverses solutions développées pour le contrôle des vibrations ont été testées avec un élément B3Dw implanté sur Matlab. Certains exemples numériques sont considérés pour étudier l'effet des ressorts élastiques, visqueux et viscoélastiques dans le contrôle du comportement en vibration. Le développement de solutions de contrôle des vibrations peut être utilisé dans des systèmes à base fixe ou vibrante (séisme). Dans tous les exemples, le MEF B3Dw implémenté sur MATLAB a été utilisé pour résoudre des problèmes de contrôle des vibrations.

En contrôlant les vibrations des poutres à parois minces en modifiant les fréquences propres, on a ajouté au support des entretoises de torsion et / ou latérales. La solution de ce problème à l'aide de la méthode analytique se limite aux cas simples de de poutres à sections bi-symétriques et conditions aux limites articulées. Pour les poutres avec des sections non symétriques et pour les conditions aux limites compliqués, les solutions analytiques deviennent lourdes, d'où l'importance du MEF B3Dw développé et utilisé pour étudier le comportement vibratoire des poutres à sections arbitraires et des conditions d'appui quelconques en présence des entretoises de flexion ou en torsion.

On observe qu'en présence de supports élastiques intermédiaires, le comportement dynamique des poutres vis-à-vis des fréquences propres plus basses (qui sont les plus dangereux sur la stabilité des structures) en torsion ou en flexion faible est amélioré. Le nombre et la distribution des ressorts ont été étudiés pour obtenir le nombre optimal des appuis pour le contrôle des vibrations. En présence des poutres à sections non symétriques, toutes les fréquences propres sont considérablement augmentées en introduisant des entretoises latérales le long de poutre. Ce concept peut être utilisé dans le contrôle des vibrations des structures afin d'améliorer la stabilité des poutres minces contre la torsion et d'autres modes indésirables.

Synthèse et perspectives

Le modèle de poutre présenté ne permet pas résoudre les sections non prismatiques, ne peux pas être utiliser dans les cas des matériaux composites et ne prend pas en compte l'effet de masse supplémentaire aux emplacements des entretoises.

Il est évident que, l'utilisation de poutres ayant des sections non-uniformes à parois minces est également importante pour gagner du poids. En principe, le concepteur utilise ces types de poutres pour obtenir le maximum de gain de poids en modifiant l'inertie et la rigidité de la poutre lorsque cela est nécessaire sur la longueur de la poutre. Pour ces poutres, le comportement vibratoire 3D devient plus complexe, du fait de la rigidité et de la masse non constante le long de la structure.

Les poutres en matériaux composites sont aujourd'hui largement utilisées dans de nombreux types de structures dans les domaines de l'ingénierie en raison de leur qualité et de leurs performances élevées permettant de résister aux diverses sollicitations exigences. Depuis quelques décennies, ces structures évoluent vers des matériaux composites à gradient de propriétés (Functionnaly Graded Materials, FGM). Les propriétés de ces matériaux varient progressivement et continuellement une ou deux directions de la structure. Leur utilisation est accroissant avec l'utilisation de composites et les développements récents des techniques d'impression 3D. Ces structures sont très sensibles à l'effet de cisaillement à la fois statique et dynamique aussi bien linéaire et en non linéaire sous charges statiques et dynamiques.

References

[1] Heyliger P. R., and Reddy J. N. (1988). A higher order beams finite element for bending and vibration problems. *Journal of sound and vibration, 126*(2), 309-326.

[2] Friberg P. O. (1983). Coupled vibrations of beams-an exact dynamic element stiffness matrix. *International Journal for numerical methods in engineering, 19*(4), 479-493.

[3] Dokumaci E. (1987). An exact solution for coupled bending and torsion vibrations of uniform beams having single cross-sectional symmetry. *Journal of Sound and Vibration,* 119(3), 443-449.

[4] Gere J. M., and Lin Y. K. (1958). Coupled vibrations of thin-walled beams of open cross section. *Journal of Applied Mechanics, 25*(3), 373-378.

[5] Vlasov V.Z. (1961). Thin-walled Elastic Beams. *Moscow, 2nd edition, translated from Russian and published for the national Science foundation, Washington, DC*.

[6] Timoshenko S. P., Young D. H., and Weaver Jr W. (1974). Vibration problems in engineering. *John Wiley and Sons.*

[7] Bishop R. E. D., Cannon S. M., and Miao S. (1989). On coupled bending and torsional vibration of uniform beams. *Journal of sound and vibration,* **131**(3), 457-464.

[8] Trahair N. S. (1993). Flexural-torsional buckling of structures. *E and FN Spon, London.*

[9] Bleich F. (1952). Buckling strength of metal structures. *New York, McGraw-Hills.*

[10] Chajes A., (1974). Principles of structural stability theory. *Prentice-Hall. Inc, Englewood Cliffs, New Jersey.*

[11] Petyt M. (2010). Introduction to finite element vibration analysis. *Cambridge university Press.*

[12] Banerjee J. R. (1989). Coupled bending–torsional dynamic stiffness matrix for beam elements. *International journal for numerical methods in engineering, 28*(6), 1283-1298.

[13] Banerjee J. R. (1999). Explicit frequency equation and mode shapes of a cantilever beam coupled in bending and torsion. *Journal of Sound and Vibration, 224*(2), 267-281.

[14] Mei C. (1970). Coupled vibrations of thin-walled beams of open section using the finite element method. *International Journal of Mechanical Sciences, 12*(10), 883-891.

[15] Barsoum R. S. (1971). Finite element method applied to the problem of stability of a non-conservative system. *International Journal for Numerical Methods in Engineering, 3*(1), 63-87.

[16] Friberg P. O. (1985). Beam element matrices derived from Vlasov's theory of open thin-walled elastic beams. *International Journal for Numerical Methods in Engineering, 21*(7), 1205-1228.

[17] Ohga, M. Takao H., and Hara T. (1995). Natural frequencies and mode shapes of thin-walled members. *Computers and structures, 55*(6), 971-978.

[18] Lee J., and Kim S. E. (2002). Flexural-torsional coupled vibration of thin-walled composite beams with channel sections. *Computers and structures, 80*(2), 133-144.

[19] Lee J., and Kim S. E. (2002). Free vibration of thin-walled composite beams with I-shaped cross-sections. *Composite Structures, 55*(2), 205-215.

[20] Pestel E. C., and Leckie F. A. (1963). Matrix methods in Elastomechanics. *McGraw-Hi11*.

[21] Ebner A. M., and Billington D. P. (1968). Steady state vibration of damped Timoshenko beams. *Journal of the Structural Division, 94*(3), 737-760.

[22] Chen H. H., and Hsiao K. M. (2008). Quadruply coupled linear free vibrations of thin-walled beams with a generic open section. *Engineering Structures, 30*(5), 1319-1334.

[23] De Borbon F., Mirasso A., and Ambrosini D. (2011). A beam element for coupled torsional-flexural vibration of doubly unsymmetrical thin walled beams axially loaded. *Computers and Structures, 89*(13-14), 1406-1416.

[24] Tanaka M., and Bercin A. N. (1999). Free vibration solution for uniform beams of nonsymmetrical cross section using Mathematica. *Computers and structures, 71*(1), 1-8.

[25] Arpaci A., and Bozdag E. (2002). On free vibration analysis of thin-walled beams with nonsymmetrical open cross-sections. *Computers and structures, 80*(7-8), 691-695.

[26] Chen C. N. (2000). Dynamic equilibrium equations of non-prismatic beams defined on an arbitrarily selected co-ordinate system. *Journal of sound and vibration*, *230*(2), 241-260.

[27] Cortínez V. H., Piovan M. T., and Machado S. P. (2001). DQM for vibration analysis of composite thin-walled curved beams.

[28] Ambrosini R. D., Riera J. D., and Danesi R. F. (2000). A modified Vlasov theory for dynamic analysis of thin-walled and variable open section beams. *Engineering Structures*, *22*(8), 890-900.

[29] Rozmarynowski B. and Szymczak C. (1984). Non-linear free torsional vibrations of thin-walled beams with bisymmetric cross-section. *Journal of Sound and Vibration*, *97*(1), 145-152.

[30] Di Egidio A., Luongo A. and Vestroni F. (2003). A non-linear model for the dynamics of open cross-section thin-walled beams Part I: formulation. *International Journal of non-linear Mechanics*, *38*(7), 1067-1081.

[31] Yaman Y. (1997). Vibrations of open-section channels: a coupled flexural and torsional wave analysis. *Journal of Sound and Vibration*, *204*(1), 131-158.

[32] Gendy A. S. and Saleeb A. F. (1994). Vibration analysis of coupled extensional/flexural/torsional modes of curved beams with arbitrary thin-walled sections. *Journal of Sound and Vibration*, *174*(2), 261-274.

[33] Prokić A. (2005). On triply coupled vibrations of thin-walled beams with arbitrary cross-section. *Journal of Sound and Vibration*, *279*(3-5), 723-737.

[34] Prokić A. (2006). On fivefold coupled vibrations of Timoshenko thin-walled beams. *Engineering Structures*, *28*(1), 54-62.

[35] Carrera E., Giunta G., and Petrolo M. (2011). Beam structures: classical and advanced theories. *John Wiley and Sons.*

[36] Carrera E., Cinefra M., Petrolo M., and Zappino E. (2014). Finite element analysis of structures through unified formulation. *John Wiley and Sons.*

[37] Carrera E., and Varello A. (2012). Dynamic response of thin-walled structures by variable kinematic one-dimensional models. *Journal of Sound and Vibration*, *331*(24), 5268-5282.

[38] Carrera E., and Pagani A. (2014). Free vibration analysis of civil engineering structures by component-wise models. *Journal of Sound and Vibration*, *333*(19), 4597-4620.

[39] Pagani A., Augello R., and Carrera E. (2018). Frequency and mode change in the large deflection and post-buckling of compact and thin-walled beams. *Journal of Sound and Vibration*, *432*, 88-104.

[40] Carrera E., and Filippi M. (2016). A refined one-dimensional rotordynamics model with three-dimensional capabilities. *Journal of Sound and Vibration*, *366*, 343-356.

[41] Mohri F., Azrar L. and Potier-Ferry M. (2004). Vibration analysis of buckled thin-walled beams with open sections. *Journal of Sound Vibration*, *275*, 434-446.

[42] Arpaci A., Bozdag S. E. and Sunbuloglu E. (2003). Triply coupled vibrations of thin-walled open cross-section beams including rotary inertia effects. *Journal of Sound and Vibration*, *260*(5), 889-900.

[43] Banerjee J. R., Guo S. and Howson W. P. (1996). Exact dynamic stiffness matrix of a bending-torsion coupled beam including warping. *Computers and structures*, *59*(4), 613-621.

[44] Rao S. S. (2004). Mechanical vibrations. Prentice Hall, 5th Edition.

[45] Eslimy S. H. R., Banerjee J. R. and Sobey A. J. (1996). Response of a bending–torsion coupled beam to deterministic and random loads. *Journal of Sound and Vibration*, *195*(2), 267-283.

[46] Hashemi S. M. and Richard M. J. (2000). A Dynamic Finite Element (DFE) method for free vibrations of bending-torsion coupled beams. *Aerospace Science and Technology*, *4*(1), 41-55.

[47] Jun L., Rongying S., Hongxing H. and Xianding J. (2004). Coupled bending and torsional vibration of axially loaded Bernoulli–Euler beams including warping effects. *Applied Acoustics*, *65*(2), 153-170.

[48] Jun L., Wanyou L., Rongying S. and Hongxing H. (2004). Coupled bending and torsional vibration of nonsymmetrical axially loaded thin-walled Bernoulli–Euler beams. *Mechanics Research Communications*, *31*(6), 697-711.

[49] Gökdağ H. and Kopmaz O. (2005). Coupled bending and torsional vibration of a beam with in-span and tip attachments. *Journal of Sound and Vibration*, *287*(3), 591-610.

[50] Prokić A. and Lukić D. (2007). Dynamic analysis of thin-walled closed-section beams. *Journal of Sound and Vibration*, *302*(4-5), 962-980.

[51] Burlon A., Failla G. and Arena F. (2017). Coupled bending and torsional free vibrations of beams with in-span supports and attached masses. *European Journal of Mechanics-A/Solids*, *66*, 387-411.

[52] Burlon A., Failla G. and Arena F. (2018). Coupled bending–torsional frequency response of beams with attachments: exact solutions including warping effects. *Acta Mechanica*, *229*(6), 2445-2475.

[53] Librescu L. and Song O. (2005). Thin-walled composite beams: theory and application (Vol. 131). *Springer Science and Business Media.*

[54] Klausbruckner M. J. and Pryputniewicz R. J. (1995). Theoretical and experimental study of coupled vibrations of channel beams. *Journal of Sound and Vibration*, *183*(2), 239-252.

[55] Ambrosini D. (2009). On free vibration of nonsymmetrical thin-walled beams. *Thin-Walled Structures*, *47*(6-7), 629-636.

[56] Ambrosini D. (2010). Experimental validation of free vibrations from nonsymmetrical thin walled beams. *Engineering Structures*, *32*(5), 1324-1332.

[57] Ribeiro P., Carneiro R. (2004). Experimental detection of modal interaction in the non-linear vibration of a hinged–hinged beam. *Journal of sound and vibration*, *277*(4-5), 943-954.

[58] Piana G., Lofrano E., Manuello A. and Ruta G. (2017). Natural frequencies and buckling of compressed non-symmetric thin-walled beams. *Thin-Walled Structures*, *111*, 189-196.

[59] Zhou J., Wen S., Li F. and Zhu Y. (2018). Coupled bending and torsional vibrations of non-uniform thin-walled beams by the transfer differential transform method and experiments. *Thin-Walled Structures*, *127*, 373-388.

[60] Bazant Z. P. and El Nimeiri M. (1973). Large-deflection spatial buckling of thin-walled beams and frames. *ASCE J Eng Mech Div*, *99*(EM6), 1259-1281.

[61] Yang Y. B. and McGuire W. (1984). A procedure for analysing space frames with partial warping restraint. *International Journal for Numerical Methods in Engineering*, *20*(8), 1377-1398.

[62] Morrell P. J. B., Riddington J. R., Ali F. A. and Hamid H. A. (1996). Influence of joint detail on the flexural/torsional interaction of thin-walled structures. *Thin-walled structures*, *24*(2), 97-111.

[63] Basaglia C., Camotim D. and Silvestre N. (2012). Torsion warping transmission at thin-walled frame joints: kinematics, modelling and structural response. *Journal of Constructional Steel Research*, *69*(1), 39-53.

[64] Hibbitt, H. D., Karlsson, B. I., and Sorensen, P. (2006). ABAQUS theory manual, version 6.3. *Pawtucket, Rhode Island, USA*.

[65] Mikell P. Groover (2019). Fundamentals of Modern Manufacturing. *John Wiley and Sons, Inc.,Fourth Edition, 2010.*

[66] Zhang J., Perez R. J., and Lavernia E. J. (1993). Documentation of damping capacity of metallic, ceramic and metal-matrix composite materials. *Journal of Materials Science*, *28*(9), 2395-2404.

[67] Sun C.T., and Lu Y.P. (1995). Vibration damping of structural elements. *Prentice Hall PTR.*

[68] Cremer L., and Heckl M. (2013). Structure-borne sound: structural vibrations and sound radiation at audio frequencies. *Springer Science and Business Media*.

[69] Mohri F., Brouki A. and Roth J. C. (2003). Theoretical and numerical stability analyses of unrestrained, mono-symmetric thin-walled beams. *Journal of Constructional Steel Research*, *59*(1), 63-90.

[70] Mohri F., Damil N. and Ferry M. P. (2008). Large torsion finite element model for thin-walled beams. *Computers and Structures*, *86*(7-8), 671-683.

[71] Mohri F., Bouzerira C. and Potier-Ferry M. (2008). Lateral buckling of thin-walled beam-column elements under combined axial and bending loads. *Thin-Walled Structures*, *46*(3), 290-302.

[72] Mohri F., Damil, N. and Potier-Ferry M. (2012). Pre-buckling deflection effects on stability of thin-walled beams with open sections. *Steel and Composite Structures*, *13*(1), 71-89.

[73] Jacob F. and Ted B. (2007). *A first course in finite elements*. Wiley.

[74] Liu G. R. and Quek S. S. (2003). The finite element method: a practical course.

[75] Bathe K. J. (2006). Finite element procedures. *Klaus-Jurgen Bathe.*

[76] Dong S. B., and Wolf Jr J. A. (1973). Effect of transverse shear deformation on vibrations of planar structures composed of beam-type elements. *The Journal of the Acoustical Society of America*, *53*(1), 120-127.

[77] Mohri F., Azrar L. and Potier-Ferry M. (2001). Flexural–torsional post-buckling analysis of thin-walled elements with open sections. *Thin-walled structures*, *39*(11), 907-938.

[78] Mohri F., Eddinari A., Damil N. and Ferry M. P. (2008). A beam finite element for non-linear analyses of thin-walled elements. *Thin-Walled Structures*, *46*(7-9), 981-990.

[79] Mohri F., Damil N. and Potier-Ferry M. (2010). Linear and non-linear stability analyses of thin-walled beams with monosymmetric I sections. *Thin-Walled Structures*, *48*(4-5), 299-315.

[80] MATLAB, R. (2015). The MathWorks Inc. *Natick, MA*.

[81] ADINA, R. Inc. 71 Elton Avenue, Watertown, MA 02472, USA.

[82] Noor A. K., Peters J. M. and Min B. J. (1989). Mixed finite element models for free vibrations of thin-walled beams. *Finite Elements in Analysis and Design*, *5*(4), 291-305.

[83] Vo T. P., Lee J. and Lee K. (2010). On triply coupled vibrations of axially loaded thin-walled composite beams. *Computers and structures*, *88*(3-4), 144-153.

[84] Nguyen C. T., Moon J. and Lee H. E. (2011). Natural frequency for torsional vibration of simply supported steel I-girders with intermediate bracings. *Thin-Walled Structures*, *49*(4), 534-542.

[85] Barsoum R. S. and Gallagher R. H. (1970). Finite element analysis of torsional and torsional–flexural stability problems. *International Journal for Numerical Methods in Engineering*, *2*(3), 335-352.

[86] Dvorkin E. N., Celentano D., Cuitino A. and Gioia G. (1989). A Vlasov beam element. *Computers and structures*, *33*(1), 187-196.

[87] Dhatt G. and Batoz J. L. (1990). Modélisation des structures par éléments finis : poutres et plaques.

[88] Shakourzadeh Bolouri H. (1994). Modélisation des structures-poutres tridimensionnelles à parois minces et simulation du comportement non linéaire géométrique et élasto-plastique (Doctoral dissertation, Compiègne).

[89] Bo-Zhen C. and Yu-Ren H. (1988). The torsional stiffness matrix of a thin-walled beam and its application to beams under combined loading. *Computers and structures*, *28*(3), 421-431.

[90] Conci A. and Gattass M. (1990). Natural approach for geometric non-linear analysis of thin-walled frames. *International Journal for Numerical Methods in Engineering*, *30*(2), 207-231.

[91] Kolbrunner C. F. and Basler K. (1969). *Torsion in Structures: An Engineering Approach*. Springer Verlag.

[92] Tralli A. M. (1986). A simple hybrid model for torsion and flexure of thin-walled beams.

[93] Liu G. R. and Quek S. S. (2013). The finite element method: a practical course. *Butterworth-Heinemann.*

[94] Clough R. W. and Penzien J. (1975). Dynamics of structures. *Journal of Structures, New York, McGraw-Hill Companies*.

[95] Hurty W. C. and Rubinstein M. F. (1964). Dynamics of structures. *Prentice-Hall Series in Engineering of the Physical Sciences, Englewood Cliffs: Prentice-Hall*.

[96] Thompson C. J. (1988). Classical equilibrium statistical mechanics. *Oxford University Press, USA.*

[97] Ewins D. (2000). Modal Testing: Theory, Practice, and Application. 2nd ed. Research Studies Press Ltd.

[98] Yura J. A. (2001). Fundamentals of beam bracing. *Engineering Journal. American institute of steel construction*, *38*(1), 11-26.

[99] Flint A. R. (1951). The influence of restraints on the stability of beams. *The Structural Engineer*, *29*(9), 235-246.

[100] Winter G. (1960). Lateral bracing of beams and columns. *ASCE Transactions, Paper*, (3044).

[101] Taylor A.C and Ojalvo M. (1966). Torsional restraint of lateral buckling. *J. Struct. Div*. 92(2), 115–130.

[102] Kitipornchai S. and NJ R. (1978). Elastic lateral buckling of I-beams with discrete intermediate restraints. *Transactions of the Institution of Engineers, Australia. Civil engineering*, (2), 105-111.

[103] Yura J. A. (1996). Winter's bracing approach revisited. *Engineering structures*, *18*(10), 821-825.

[104] Nguyen C. T., Moon J. and Lee H. E. (2010). Lateral–torsional buckling of I-girders with discrete torsional bracings. *Journal of Constructional Steel Research*, *66*(2), 170-177.

[105] McCann F., Gardner L., and Wadee M. A. (2013). Design of steel beams with discrete lateral restraints. *Journal of Constructional Steel Research*, *80*, 82-90.

[106] Agüero A., Pallarés F. J. and Pallarés L. (2015). Equivalent geometric imperfection definition in steel structures sensitive to lateral torsional buckling due to bending moment. *Engineering Structures*, *96*, 41-55.

[107] Zhang W. F., Liu Y. C., Hou G. L., Chen K. S., Ji J., Deng Y. and Deng S. L. (2016). Lateral-torsional buckling analysis of cantilever beam with tip lateral elastic brace under uniform and concentrated load. *International Journal of Steel Structures*, *16*(4), 1161-1173.

[108] Pezeshky P., Sahraei A. and Mohareb M. (2017). Effect of bracing heights on lateral torsional buckling resistance of steel beams. In *Proc., 6th Int. Conf. on Engineering Mechanics and Materials CSCE. Montreal, QC, Canada: Canadian Society for Civil Engineering*.

[109] Olhoff N. (1988). Minimum stiffness of optimally located supports for maximum value of beam eigenfrequencies. *Journal of Sound Vibration*, *120*, 457-463.

[110] Rao C. K. (1989). Frequency analysis of clamped-clamped uniform beams with intermediate elastic support. *Journal of Sound and Vibration*, *133*(3), 502-509.

[111] Abramovich H., and Hamburger O. (1992). Vibration of a uniform cantilever Timoshenko beam with translational and rotational springs and with a tip mass. *Journal of Sound and Vibration*, *154*(1), 67-80.

[112] Wu J. S. and Chou H. M. (1998). Free vibration analysis of a cantilever beam carrying any number of elastically mounted point masses with the analytical-and-numerical-combined method. *Journal of Sound and Vibration*, *213*(2), 317-332.

[113] Wang C. Y. (2003). Minimum stiffness of an internal elastic support to maximize the fundamental frequency of a vibrating beam. *Journal of sound and vibration*, *259*(1), 229-232.

[114] Wang D., Jiang J. S. and Zhang W. H. (2004). Optimization of support positions to maximize the fundamental frequency of structures. *International journal for numerical methods in engineering*, *61*(10), 1584-1602.

[115] Albarracín C. M., Zannier L. and Grossi R. O. (2004). Some observations in the dynamics of beams with intermediate supports. *Journal of Sound and Vibration*, *1*(271), 475-480.

[116] Maurizi M. J., Bambill D. V., Bellés P. M. and De Rosa M. A. (2005). Free vibrations of Bernoulli-Euler beams with intermediate elastic support: a concise thematic recension. *Journal of Sound Vibration*, *281*, 1238-1239.

[117] Wang D., Friswell M. I. and Lei Y. (2006). Maximizing the natural frequency of a beam with an intermediate elastic support. *Journal of sound and vibration*, *291*(3-5), 1229-1238.

[118] Gokdag H. and Kopmaz O. (2007). Natural frequencies of a bending-torsion coupled beam supported by in-span linear springs. *Structural Engineering and Mechanics*, *27*(2), 259-262.

[119] Zbirohowski-koscia. (1967). Thin-walled beams. First published By Crosby Lockwook and Son L td.

[120] Jrad W., Mohri F., Robin G., Daya E. M., and Al-Hajjar J. (2019). Analytical and finite element solutions of free and forced vibration of unrestrained and braced thin-walled beams. *Journal of Vibration and Control*, 1077546319878901.

Appendix A Free vibration analytical solutions for cantilever beams

In the section 2.2.3.2, closed form solutions for vibration modes for simply supported beam have been derived. In this part, the analogous modes for bi-symmetric, mono-symmetric and arbitrary thin-walled cross section beams with clamped-free boundary conditions are presented.
Let us remind that for bi-symmetric sections the angular velocities (eigenvalues) are given in the section 2.2.3.3 equations (2.88).

A.1 Cantilever beams with singly symmetric cross-sections:

Mono-symmetric sections z_c=0:

The angular velocities (eigenvalues) for mono-symmetric sections (z_c=0) like the channel sections are given by:

$$\Omega_1^2(n) = \Omega_z^2(n); \tag{A1}$$

$$\Omega_{2,3}^2(n) = \frac{(\Omega_y^2(n)+\Omega_\theta^2(n)) \pm \sqrt{(\Omega_y^2(n)-\Omega_\theta^2(n))^2+4\frac{{y_c}^2}{I_0}\Omega_y^2(n)\Omega_\theta^2(n)}}{2(1-\frac{{y_c}^2}{I_0})} \tag{A2}$$

With $\Omega_y^2(n)$, $\Omega_z^2(n)$ and $\Omega_\theta^2(n)$ are the angular velocities (eigenvalues) for bi-symmetric sections given in equations (2.88). It should be noted that Ω_1 is the pure bending angular velocities (eigenvalues) and Ω_2, Ω_3 are flexural-torsional coupled.

Mono-symmetric sections y_c=0:

The angular velocities (eigenvalues) for mono-symmetric sections (y_c=0) like the Tee sections are given by:

$$\Omega_1^2(n) = \Omega_y^2(n); \tag{A3}$$

$$\Omega_{2,3}^2(n) = \frac{(\Omega_z^2(n)+\Omega_\theta^2(n)) \pm \sqrt{(\Omega_z^2(n)-\Omega_\theta^2(n))^2+4\frac{{z_c}^2}{I_0}\Omega_z^2(n)\Omega_\theta^2(n)}}{2(1-\frac{{z_c}^2}{I_0})} \tag{A4}$$

With $\Omega_y^2(n)$, $\Omega_z^2(n)$ and $\Omega_\theta^2(n)$ are the angular velocities (eigenvalues) for bi-symmetric sections given in equations (2.88). It should be noted that Ω_1 is the pure bending angular velocities (eigenvalues) and Ω_2, Ω_3 are coupled flexural-torsional angular velocities.

A.2 Cantilever beams with arbitrary cross-sections

The angular velocities (eigenvalues) for no-symmetric sections are approximated by:

$$\Omega^2 = (\Omega_1^2(n), \Omega_2^2(n), \Omega_3^2(n)) \tag{A5}$$

The angular velocities (eigenvalues) of the beam are obtained by solving the following cubic equation:

$$aX^3 + bX^2 + cX + d = 0 \tag{A6}$$

With: $X = \Omega^2$,

$$\text{a}=[-I_0 + {y_c}^2 + {z_c}^2]$$

$$\text{b}=\left[I_0\Omega_y^2(n) + I_0\Omega_\theta^2(n) + \Omega_Z^2(n)I_0 - \Omega_Z^2(n){y_c}^2 - \Omega_y^2(n){z_c}^2\right]$$

$$\text{c}=\left[-I_0\Omega_y^2(n)\Omega_\theta^2(n) - \Omega_Z^2(n)I_0\Omega_y^2(n) - \Omega_Z^2(n)I_0\Omega_\theta^2(n)\right]$$

$$\text{d}=\left[\Omega_Z^2(n)I_0\Omega_y^2(n)\Omega_\theta^2(n)\right] \tag{A7}$$

$\Omega_y^2(n)$, $\Omega_z^2(n)$ and $\Omega_\theta^2(n)$ are the angular velocities (eigenvalues) for bi-symmetric sections given in equations (2.88).This leads to 3 solutions:

$X_1 = \Omega_1^2(n)$, $X_2 = \Omega_2^2(n)$, $X_3 = \Omega_3^2(n)$.

In this case, all the angular velocities (A6) are for fully flexural-torsional vibration modes. This problem is called the triply coupled free vibration problem. It should be noted that, for arbitrary cross-section shapes the numerical FEM are straightforward and more accurate.

Appendix B Free vibration analytical solutions for doubly clamped beams

In the section 2.2.3.2, closed form solutions for vibration modes for simply supported beam have been derived. In this part, the analogous modes for bi-symmetric, mono-symmetric and arbitrary thin-walled cross section beams with clamped-clamped boundary conditions are presented. Let us remind that for bi-symmetric sections the angular velocities (eigenvalues) for are given in the section 2.2.3.3 equations (2.94).

B.1 Doubly clamped beams with singly symmetric cross-sections

The angular velocities (eigenvalues) for mono-symmetric sections (z_c=0) like the channel sections are given by:

Mono-symmetric sections z_c=0:

$$\Omega_1^2(n) = \Omega_z^2(n); \tag{B1}$$

$$\Omega_{2,3}^2(n) = \frac{(\Omega_y^2(n)+\Omega_\theta^2(n)) \pm \sqrt{(\Omega_y^2(n)-\Omega_\theta^2(n))^2+4\frac{{y_c}^2}{I_0}\Omega_y^2(n)\Omega_\theta^2(n)}}{2(1-\frac{{y_c}^2}{I_0})} \tag{B2}$$

With $\Omega_y^2(n)$, $\Omega_z^2(n)$ and $\Omega_\theta^2(n)$ are the angular velocities (eigenvalues) for bi-symmetric sections given in equations (2.94). It should be noted that Ω_1 is the pure bending angular velocities (eigenvalues) and Ω_2, Ω_3 are flexural-torsional coupled.

Mono-symmetric sections y_c=0:

The angular velocities (eigenvalues) for mono-symmetric sections (y_c=0) like the Tee sections are given by

$$\Omega_1^2(n) = \Omega_y^2(n); \tag{B3}$$

$$\Omega_{2,3}^2(n) = \frac{(\Omega_z^2(n)+\Omega_\theta^2(n)) \pm \sqrt{(\Omega_z^2(n)-\Omega_\theta^2(n))^2+4\frac{{z_c}^2}{I_0}\Omega_z^2(n)\Omega_\theta^2(n)}}{2(1-\frac{{z_c}^2}{I_0})} \tag{B4}$$

With $\Omega_y^2(n)$, $\Omega_z^2(n)$ and $\Omega_\theta^2(n)$ are the angular velocities (eigenvalues) for bi-symmetric sections given in equations (2.94). It should be noted that Ω_1 is the pure bending angular velocities (eigenvalues) and Ω_2, Ω_3 are angular velocities for flexural-torsional coupled modes.

B.1 Doubly clamped beams with arbitrary cross-sections

The angular velocities (eigenvalues) for no-symmetric sections are approximated by:

$$\Omega^2 = (\Omega_1^2(n), \Omega_2^2(n), \Omega_3^2(n)) \tag{B5}$$

The angular velocities (eigenvalues) of the beam are obtained by solving the following cubic equation:

$$aX^3 + bX^2 + cX + d = 0 \tag{B6}$$

With: $X = \Omega^2$

$$a = [-I_0 + {y_c}^2 + {z_c}^2]$$

$$b = \left[I_0\Omega_y^2(n) + I_0\Omega_\theta^2(n) + \Omega_Z^2(n)I_0 - \Omega_Z^2(n){y_c}^2 - \Omega_y^2(n){z_c}^2\right]$$

$$c = \left[-I_0\Omega_y^2(n)\Omega_\theta^2(n) - \Omega_Z^2(n)I_0\Omega_y^2(n) - \Omega_Z^2(n)I_0\Omega_\theta^2(n)\right]$$

$$d = \left[\Omega_Z^2(n)I_0\Omega_y^2(n)\Omega_\theta^2(n)\right] \tag{B7}$$

$\Omega_y^2(n)$, $\Omega_z^2(n)$ and $\Omega_\theta^2(n)$ are the angular velocities (eigenvalues) for bi-symmetric sections given in equations (2.94). This leads to 3 solutions:

$X_1 = \Omega_1^2(n)$, $X_2 = \Omega_2^2(n)$, $X_3 = \Omega_3^2(n)$.

In this case, all the angular velocities (B6) are for fully flexural-torsional coupled modes. This problem is called the triply coupled free vibration problem. It should be noted that, for arbitrary cross-section shapes the numerical FEM are straightforward and more accurate.